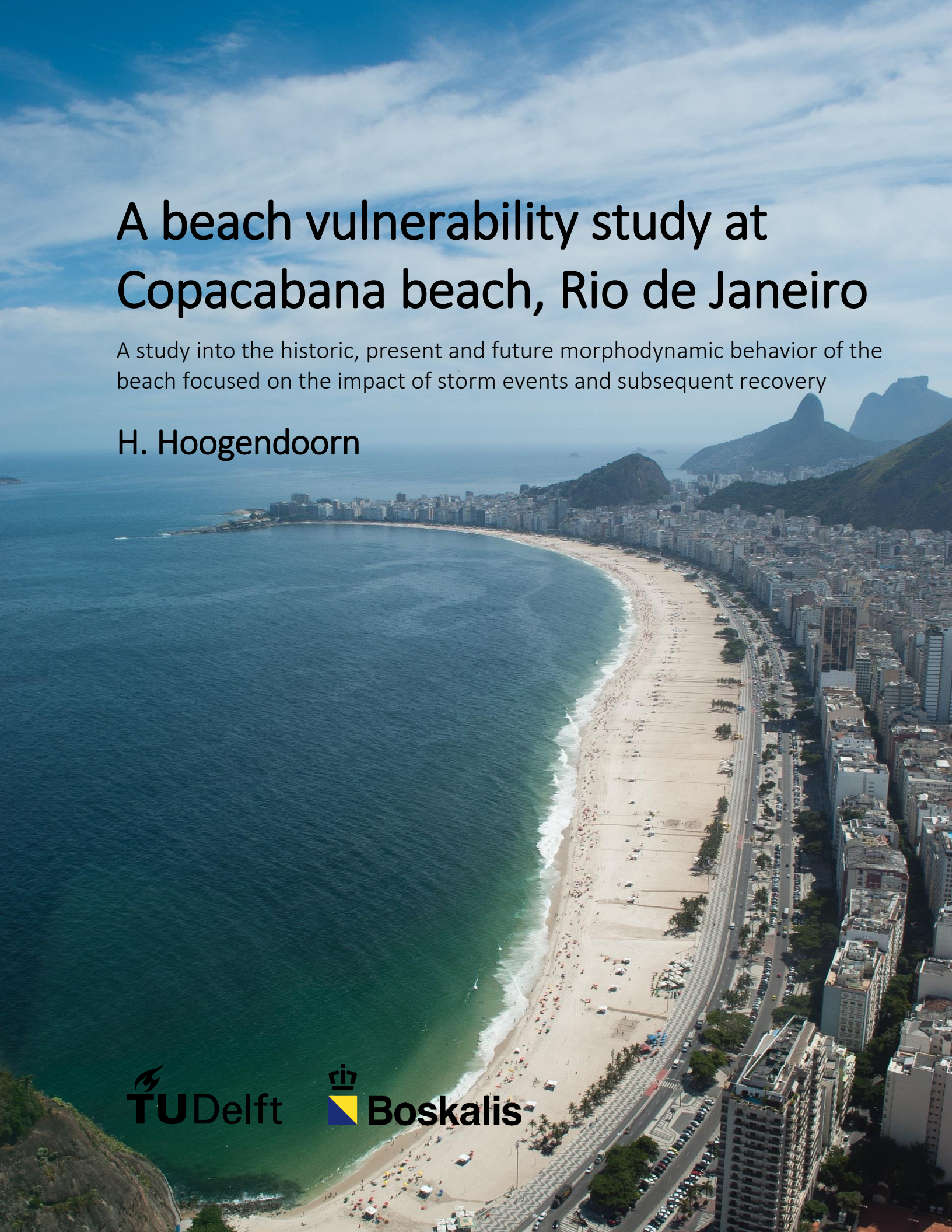

A beach vulnerability study at Copacabana beach, Rio de Janeiro

A study into the historic, present and future morphodynamic behavior of the beach focused on the impact of storm events and subsequent recovery

H. Hoogendoorn

TU Delft

Boskalis

A beach vulnerability study at Copacabana beach, Rio de Janeiro

A study into the historic, present and future morphodynamic behavior of the beach focused on the impact of storm events and subsequent recovery

By

H. Hoogendoorn

in partial fulfilment of the requirements for the degree of

Master of Science

in Civil Engineering

at the Delft University of Technology,

Thesis committee:	Prof. Dr. Ir. S. G. J. Aarninkhof,	TU Delft, Chairman
	Dr. Ir. J. A. Hopkins,	TU Delft
	Dr. M.F.S. Tissier	TU Delft
	Prof. Dr. Ir. J.C. Winterwerp	TU Delft, Advisor
	Ir. T.F. van der Biezen,	Boskalis
Version:	Final version	
Date:	22/01/2021	

TU Delft Boskalis

Summary

Sandy beaches can be found all over the world and are on the interface between the sea and the land. Important functions of beaches are the protection of the inland to the forces of the sea and providing local opportunities in recreation. The impact of storm events on the beach is therefore an important topic of research especially with future climate change predicting more extreme events with the influence of Sea Level Rise expected to result in a worldwide decrease in beach area.

The famous Copacabana beach, located at the South-Atlantic ocean is one of the most popular tourist attractions in Rio de Janeiro with thousands of visitors per year. The beach is characterized by its parabolic shape with rocky headlands on either sides. In July 2019 a storm event occurred at the beach with a 7-day period of energetic waves. This resulted in significant erosion along the whole beach up to 40 meters leaving not more than 10 meters of beach width in the South part of the beach. The period of erosion was followed up by a period with year-round average wave conditions resulting in rapid natural recovery with the beach returning to its original beach width within a period of 4 weeks. The focus of this research is on the cycle of erosion with subsequent recover which is important in having a long-term sustainable beach cycle.

The history of Copacabana beach is marked by one major nourishment in 1970 which resulted in the 55 meter widening of the beach parallel avenue and an average widening of the beach of 35 meters. From 1970 onwards historically available satellite images show a stable beach behavior with the equilibrium profile of the beach showing smaller beach widths in the South compared to the North. A dataset of high resolution Sentinel 2 is analyzed in terms of beach width for a period of 4 years (see Figure 1). This clearly shows the short-term variations in beach width of which most are the result of the impact of storm events. This highlights the impact of the July 2019 storm event showing rapid recovery in terms of beach width.

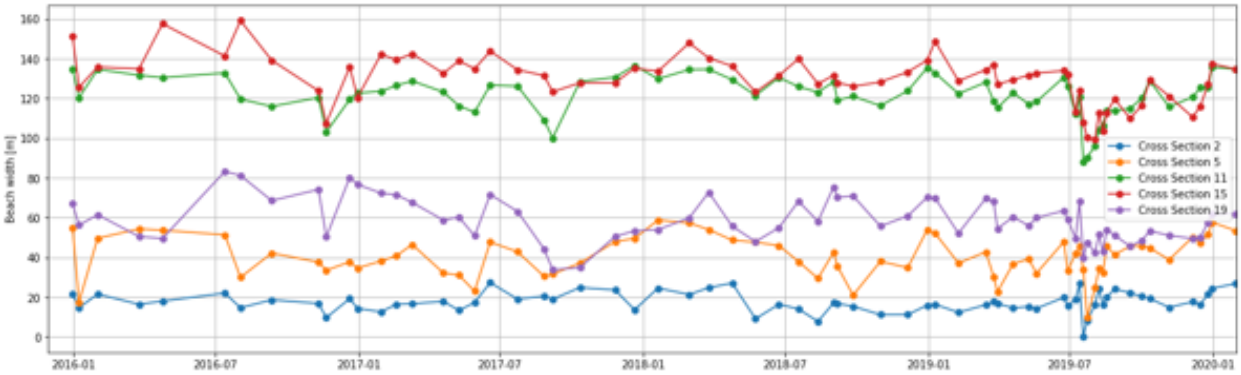

Figure 1: Beach width dynamics from 2016 until 2019 extracted from Sentinel 2 satellite images. The beach width is given for 5 different cross sections from South to North.

Storm events are characterized by a 2 to 7-day period of energetic swell-dominated waves often from in between the South and SSE. The maximum wave height during the July 2019 storm event was of a yearly return period in combination with an erosional impact which was of lower frequency according to locals. What caused the big erosional impact was the long 7-day duration of the storm in combination with an extraordinary wave direction from the SE. Under this wave direction the South part of the beach (near Cross Section 5 visible in Figure 1) is most vulnerable due to a convergence of wave energy as a result of bottom refraction. In combination with a lower

equilibrium width in this part of the beach due to the lack of sand placement during the 1970 nourishment this part of the beach is most vulnerable to storm impact. The subsequent beach recovery process shows rapid beach width recovery with recovery rates up to 1.4m/day. This is the result of mild wave steepness due to the swell-dominated wave climate in combination with the equilibrium beach state characterized by an attached sandbar. Both these system characteristics are positively related to the recovery rates (Phillips et al., 2017). However, structural erosion is visible in terms of backbeach elevation in the South part of the beach which as of 16 months after the July 2019 erosion event shows no signs of recovery.

To further test the beach vulnerability, the July 2019 storm and subsequent recovery period are modelled subsequentially with the XBeach Surfbeat and- stationary mode. With the use of scenario modelling an attempt is made to test the vulnerability related to wave characteristics, erosion/recovery duration and the frequency of storms. Judgement of the model performance resulted in good model applicability and realistic model results for the erosion simulation. The results confirm the highest impact is in the South part of the beach under a SE wave direction. Besides this, the impact of an increased wave height (resulting in a 21% increase in erosional volume with a 10% increase in wave height) is more significant along the whole beach compared to an increased extreme event duration (resulting in a 9% increase in erosional volume with a 20% longer duration). During periods of recovery the swash zone processes become more important. These processes are not well represented in XBeach. To compensate for these effects the Bermslope model can be used forcing the slope in the swash zone to a pre-defined value (Roelvink & Costas, 2017). The model results however still shows a limited interaction between the beachface and the sub-aquatic part of the beach resulting in accretion further offshore than is observed in reality. From this it is concluded that it is not possible to assess the beach vulnerability in relation to recovery rates with XBeach.

The third and last part of this research looks into the future changes in beach vulnerability taking into account the effect of climate change. Local long term climate trends are analyzed with the use of multiple data sources. This results in a clear positive trend showing a future increase of mean wave height. For the other climate parameters like the extreme wave height, storm frequency and wave direction a wide range of trends is found. This often shows both a positive and negative trend among the available data. Within the range of future climate trends there is a clear indication of a future increase in beach vulnerability. Both an increase in the mean wave height as a potential increase in extreme wave heights has significant implications on the erosional quantities judging from the model results. Where a 10% increase in extreme event wave heights results in a 22% increase in erosional quantities according to the model results. With a possible eastward change of mean wave direction chances of SE directed storm events increases resulting in increased beach vulnerability in the South under convergence of wave energy. For Sea Level Rise the impact is relatively highest in the South of the beach with beach decay predictions being approximated at a maximum of 8.4 meters as of 2070 with the use of the Bruun rule (Bruun, 1962). From this it is concluded that the vulnerability of the South part of the beach is bound to increase the most in the future with also taking into account the structural backbeach erosion as a consequence of the July 2019 erosion event. Future interventions with the goal decreasing beach vulnerability should focus on either widening or further protecting the South part of the beach.

Preface

This report is written to finish my master studies in Hydraulic Engineering at the Delft University of Technology. In the past months I have been working on this thesis as a graduate intern at Boskalis and have been lucky to have spent the first months of my thesis working at the Boskalis office and getting to know the company. I am very grateful with the opportunity Boskalis gave me of tackling such an interesting topic and the opportunities that came with it. With the highlight being my site visit to Rio de Janeiro where I felt very welcome at the Boskalis office with a special thanks to Leticia Silva Mendes for the help and support in advance and during the trip.

Furthermore, a special thanks goes out to Han Winterwerp for initially proposing this thesis topic after your interesting observations at the beach and additional opportunities that opened up for me with the support of the people from the Universidade Federal do Rio de Janeiro. I want to thank both Marcos Gallo and Susana Vinzon for allowing me to spend some time at the university and being able to use the facilities. As well as the students of the UFRJ for showing me around and helping me with carrying out the measurements and beach survey.

Furthermore, I want to express my gratitude towards my thesis committee for their continuous support during the thesis. Special thanks goes out to my daily supervisor at Boskalis, Tim van der Biezen, you always made the time for discussion and repeatedly me gave helpful feedback on the thesis progress and helped me steering the thesis in the right direction.

Lastly, I would like to thank all my friends for the fun times and support during my entire student life. And of course thanks to my family, and in special my mom and dad, for always supporting me, also during the times where the progress was slow.

Hugo Hoogendoorn
Delft, January 2021

Table of contents

List of Figures

List of Tables

1 Introduction

1.1 Background

Copacabana beach is a famous sandy beach located in Rio de Janeiro on the Atlantic east coast of Brazil. It is about 3.8 km in length with an average width of 100 meters. The beach is very popular among tourists and gets visited by thousands of people every year. Besides recreation purposes, an important functionality of the beach is coastal protection, where Copacabana beach is on the interface between the ocean and the densely populated rural neighborhoods of Copacabana and Leme.

Figure 2: Overview of the location of Copacabana beach. Courtesy of Worldatlas and Google Earth.

The beach is embayed by rocky headlands on both sides. On the west side the Punta de Copacabana and on the east side the Punta do Leme. This type of beach is also called an embayed beach. About half of the worlds beaches is 'embayed' by hard rocky headlands (Short, 1999). The shape of these beaches is generally curved, which is also the case at Copacabana beach. Furthermore, it is visible that the width of the beach varies over its length, the western end of the beach is about half the width compared to the eastern side of the beach (which covers the biggest part of the beach length) in its equilibrium state, which is not a typical feature of an embayed beach.

In July 2019 an erosion event occurred on the coast of Rio de Janeiro which was characterized by a 7-day period of high swell waves originating from the South-Atlantic ocean. This caused significant erosion on the beach leaving not more than 10 meters of beach width at some locations along the beach. However, when observing the beach state the weeks after the erosion event the beach shows the natural ability to recover in terms of beach width. This is clearly visible in the image below where a picture is shown respectively directly after the erosion 4 months after the erosion event at the same location along the beach. This event had an extraordinary impact according to locals who have never seen such erosion before.

Figure 3: Pictures taken at the same location along the beach in the South part directly after the July 2019 erosion event and 4 months after the erosion event. Courtesy of Han Winterwerp.

This recent erosion event raised questions about the health of the beach and if similar erosion events are more likely to occur due to possible changes in beach shape, beach width or due to the effects of climate change. The graph below shows the number of storms as per news publications of the local newspaper O'Globo from 1979 to 2013 in the state of Rio de Janeiro. In 29 of the news reports Copacabana beach was cited. This confirms that there is an on average yearly storm that notably impacts the beach. Most of the news articles are related to damage on streets, boardwalks, bars and houses along the beaches (Lins-de-barros & Klumb-oliveira, 2018).

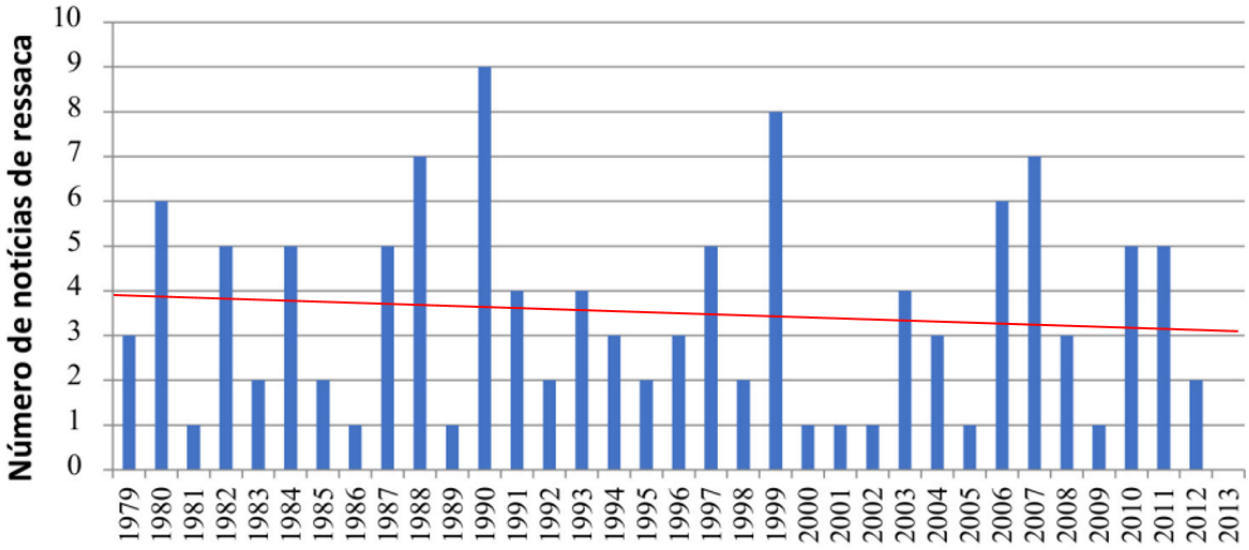

Figure 4: Number of storm news per year in the state of Rio de Janeiro as per survey of the news articles published by O'Globo (Lins-de-barros & Klumb-oliveira, 2018).

The history of Copacabana beach is marked by one significant human intervention in 1970, where a sand nourishment was done to widen the beach and the beach parallel avenue. A total of 3.5

million cubic meters of sand was nourished and resulted in a widening of the beach of about 35 meters. The recent high impact of the July 2019 erosion event raises questions about the current 'health' of the beach. Could it be that the nourishment in 1970 reached its lifetime, or that possible changes in wave climate due to climate change negatively affect the beach? This research aims to investigate the present and future behavior of the beach to be able to draw conclusions about the possible changes in beach behavior and if there is a possible need for human interventions.

1.2 Problem Description

The beach is directly exposed to waves in the range of SSE to ESE, these waves can cause changes in the state of the beach morphology in the timespan of days in extreme cases. The erosion event of July 2019 shows that a high variability in the state of the beach under the influence of energetic waves can cause the beach to lose part of its main functions. Dangerous situations can occur where the waves almost reach the promenade and in some cases beach scarps, as visible in Figure 3, can impact the safety of beach users.

When quantifying the magnitude of the problems, the reinstatement/accretion of the beach after the erosion is an important process to understand. This reinstatement process determines the amount of time the beach is in an erosive state and gives insight into whether the beach fully recovers to its original state or if there is a structural loss of sediment due to the erosion events. The problem analysis results in the two following problem statements:

> ***Problem statement 1:*** *Episodic beach erosion events lead to short-term undesirable situations related to coastal protection and recreation (e.g. narrow beach, beach scarps, promenade flooding and beach front property being at risk).*
>
> ***Problem statement 2:*** *The beach reinstates itself after an erosion event, this process is not well understood and it is unknown whether the long-term (10's of years) trend shows full reinstatement or structural losses of sediment.*

To understand the specifics of the problems arising on the beach, first the context needs to be understood. With context is meant: the analysis of the physical coastal system of Copacabana beach with respect to the important coastal processes and hydraulic forcing. The focus of this analysis is on the cycle of episodic beach erosion and the successive reinstatement of the beach. Extension and gathering of the current system knowledge is needed because the currently available information seems not to be giving the full system context of the Copacabana bay in order to identify the vulnerability of the beach. This gives the third problem statement:

> ***Problem statement 3:*** *Analyses into the morphological behavior of the Copacabana beach with the focus on the extreme erosion events and successive recovery are not available.*

There is one available research looking into the hydraulic and morphological behavior of the Copacabana bay system. This is carried out in and around 1970 by a Portuguese engineering firm called LNEC. The reason for that study was the nourishment of Copacabana beach in 1970. The information available on this research is limited and focuses on the original Copacabana beach without the nourishment (Vera-cruz, 1972).

1.3 Research Objectives and Methodology

The overall objective of this thesis is to gain an overall understanding of the morphodynamic system behavior of Copacabana beach both for the present-day behavior and the future behavior under the influence of climate change. This results in the following main research question:

What are the current morphodynamic system characteristics of Copacabana beach and how is this possibly changing in the future under the influence of climate change?

The research objective consists of 3 parts. At first, the natural dynamics of the Copacabana beach morphological system are discussed. This part of the research focuses on the historic evolution of the beach up to the present-day looking into both the long-term (10's of years) and short term beach dynamics. The focus of this part is on the morphological impact of erosion events and the subsequent recovery of the beach.

In the next part of the research a numerical model is used to look into the vulnerability of the beach under different conditions. And lastly a future outlook is made including the effects of climate change. An overview of the sub-questions is shown below including the methodology:

1. **What are the natural dynamics of the Copacabana beach?**
    a. **What are the typical characteristics of storm events and how do these relate to the July 2019 erosion event?**

As the storm events seem to be responsible for the biggest part of shoreline changes along the beach, the typical characteristics of these events are looked into. This is done using both nearshore wave buoy measurements and longer term offshore hindcast wave data. Storm events are characterized by periods of increased and energetic wave heights for a multiple day period. The nearshore wave buoy measurements are used to identify the storm events and compare their typical characteristics in terms of wave direction, wave height, duration and total wave energy. The offshore hindcast wave data is more suitable for a statistical approach to determine the return period of extreme events judging on maximum wave height.

After this the wave characteristics of the storm events are compared with the morphological impact/damage on the beach. This is primarily done using satellite images from multiple sources. From these images the coastline position is derived making it possible to estimate erosional impact in terms of beach width decrease after the storm events.

With this information the July 2019 erosion event can be put into perspective in terms of both wave characteristics and morphological impact. In addition to the use of wave- and beach width data, local perspectives are collected during a fieldtrip to Rio de Janeiro.

    b. **What causes the alongshore difference in storm impact and vulnerability within Copacabana bay?**

During storm events it can be observed that there is an alongshore difference in erosional impact on the beach. As part of the natural system dynamics the aim is to see if there is a relation between the wave characteristics of storm events and the alongshore differences in erosional impact on the beach. With alongshore differences the state of the beach prior to a storm event is looked into and the way that storm events impact the different parts of the beach. A conceptual visualization of the 2D wave patterns within the Copacabana bay under different wave directions is made using the available bathymetry measurements in combination with the wave characteristics. This takes into account the specific orientation of the beach including the effects of the both the headlands. With the effects of both diffraction and refraction taken into account, conclusions are drawn related to the alongshore differences in vulnerability during storm events with different characteristics.

    c. **What are the typical beach recovery timescales on Copacabana beach?**

It can be observed that the beach has the natural ability to recover from the impact of storm events in terms of beach width. An example is shown in Figure 3 where this natural recovery behavior is

clearly visible. A literature study is performed focusing on beach recovery and the relation between recovery rates, the state of the beach and wave parameters like wave height and wave period. With the information from the available wave records in combination with the satellite images different cases of beach recovery are observed at Copacabana beach where an increase in beach width occurs over time. The combination of the insights from the literature study and the data from Copacabana beach gives an explanation for the high recovery rates.

2. **Can a numerical model be used to assess the current vulnerability of the beach?**

Due to the limited information related to the storm events at Copacabana beach this part of the research tests the use of a numerical model in order to assess the current vulnerability of the beach. For this cause a 2DH XBeach model is setup to simulate the July 2019 extreme wave event and the subsequent recovery (D. Roelvink et al., 2009). A literature study related to the relevant nearshore processes during erosive and recovery conditions is performed with the goal to understand how these nearshore processes are (or are not) included in the formulations of the XBeach model. With these insights the XBeach results are interpreted with regards to beach recovery and beach erosion.

With scenario modelling the vulnerability of the beach is tested. The scenarios are based on the simulation of the July 2019 extreme wave event and subsequent recovery because of the high availability of data of this event. Taking into account the model performance related to the data availability, model applicability, model validation and the model sensitivity this sub-question can be answered for both the erosion as the recovery simulation.

3. **What are the potential likely effects of climate change on the future vulnerability of the beach?**

The previous research questions deal with the historic and present behavior of the beach. The last part of the research looks into the possible effects of climate change on the future vulnerability of the beach. At first, an overall collection is made of long-term climate trends for the relevant parameters. These parameters include the average- and extreme wave heights, wave direction, storm frequency and Sea Level Rise. The main sources for deriving the long-term statistics are the COWCLIP 2.0 global multivariate hindcast dataset, ERA5 hindcast data and the IPCC reports (Morim et al., 2020; Hennerrmann, 2016; Barcena et al., 2015).

The future climate trends that result from the data sources are compared with the modelling scenarios under the previous research question and the results from the natural system dynamics. This gives insight into future changes in beach vulnerability. This is an explorative assessment where with the current system knowledge an extrapolation is made to the future.

1.4 Thesis outline

The thesis is subdivided into 3 main parts. The first part consists of the natural system dynamics of the system with the use of observations and data analysis. Chapter 2 shows an overview of the history of Copacabana including the observations of the July 2019 erosion event and the short-term beach dynamics. Hereafter, Chapter 3 includes an in-depth data analysis related to the erosion and subsequent recovery process. Both these chapters are summarized in Chapter 4 showing an overview of the natural system dynamics of Copacabana beach. The second part of the thesis tests the use of a numerical model for further assessment of the beach vulnerability, this can be found in Chapter 5. Lastly, part 3 (Chapter 6) of the thesis discusses the future changes in beach vulnerability under the influence of climate change and what possible intervention strategies could be implemented. At last, Chapter 7 includes the final conclusions and recommendations.

Part 1: Natural system dynamics: observations and data analysis

2 History of Copacabana

This chapter starts with an overview of the data sources which are used in the first part of this thesis. Thereafter, the history of Copacabana beach is discussed starting from before 1970 up to the present-day situation. This includes details about the one major human intervention in 1970 and its implications for the beach. From 1970 onwards the long term movement of the shoreline is analyzed and next to that the recent erosion event in July 2019 is discussed showing more of the short-term behavior of the beach.

2.1 Data sources

This section gives an overview of the data which is used in this study. This data consists of long-term (10's of years) satellite images from multiple sources, nearshore and offshore wave datasets and details on the July 2019 extreme wave event in terms of pictures and local perspectives. Besides this data there is one available research that looks into the morphological behavior of the beach which is performed in 1970 before the nourishment by an institute called LNEC.

Satellite images:

The table below shows an overview of the available satellite image resources and their characteristics:

Table 1: Overview of the available satellite image data sources.

	Resolution [m]	Period	Frequency
Landsat 5	30	1985 to 2011	1-2 months
Landsat 7	15	1999 to present	1 month
Landsat 8	15	2013 to present	1 month
Sentinel 2	10	2016 to present	5 days
Google Earth commercial images	<10	2002 to present	Variable

The Landsat imagery has a lower resolution than the more recent Sentinel images, this makes the Landsat image not suitable for derivation of beach width because the uncertainty is too high. However, these images, besides some historical pictures, provide the only available information with regards to the state of the beach in the past 10's of years. This is important information when looking at the long-term morphodynamic stability of the beach. The Sentinel images have a higher frequency and higher resolution making these images suitable for investigating the short-term (e.g. storm impact) behavior.

Wave data:

For the analysis of the wave data there are various available data sources giving both nearshore and offshore wave time series. The offshore data is available in the form of hindcast data from the ERA5 dataset in two different offshore points. This data is generated using the Copernicus Climate Change Service Information. The wave data output points are respectively located 60km to the South and 90 km to the SE of Copacabana beach.

Nearshore there are 2 physical wave buoys which are part of the SIMCosta shoreline monitoring program (Garcia et al., 2016). The buoys are named RJ-3 and RJ-4. The locations of these buoys are shown in the image below in combination with the local bathymetry.

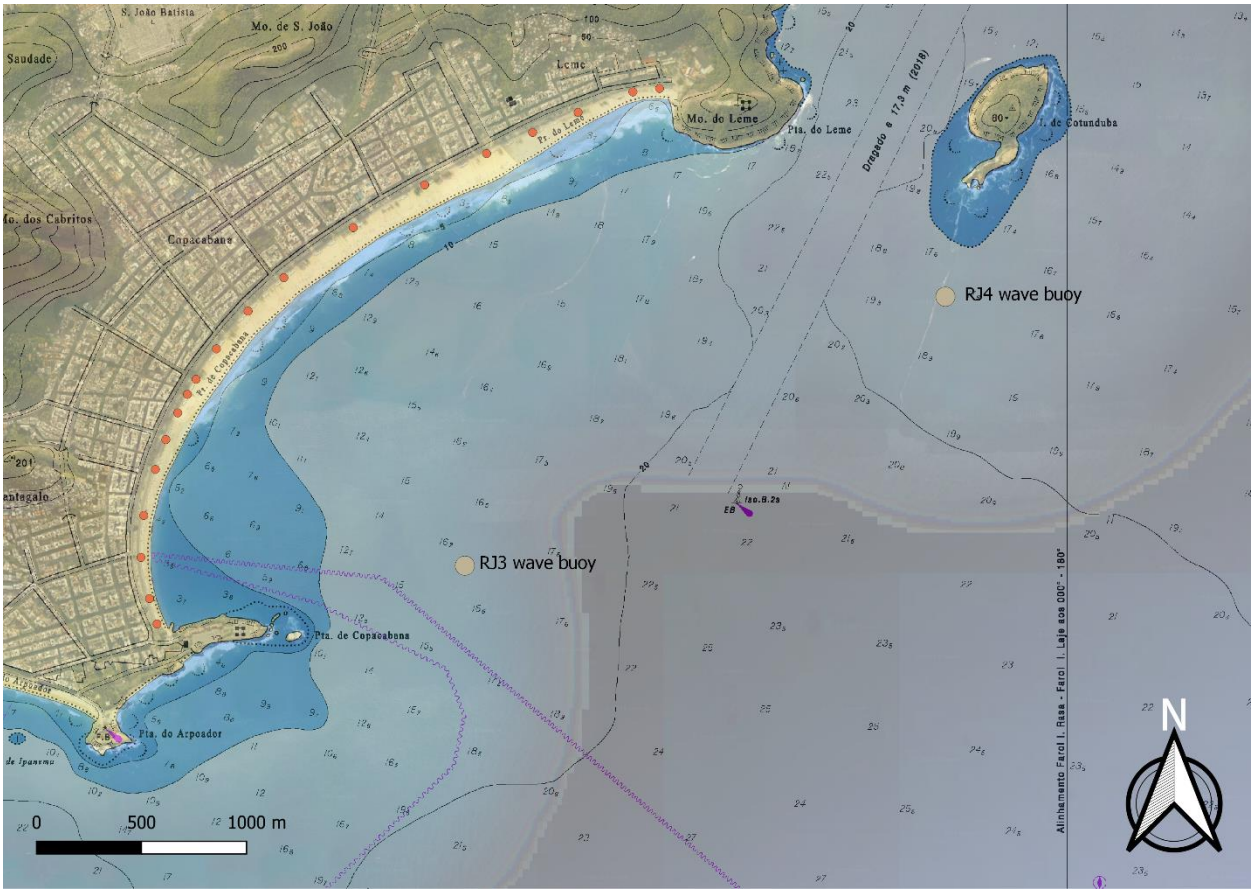

Figure 5: Overview of the locations of the nearshore SIMCosta wave buoys.

The table below shows an overview of the available offshore and nearshore wave data.

Table 2: Information on the wave data points

	Longitude	Latitude	Water depth [m]	Measurement frequency [min]	Data availability
RJ-3	-43.174472°	-22.983083°	17	30	15-07-2016 to 25-08-2017 and 30-01-2018 to 12-09-2019
RJ-4	-43.152166°	-22.971553°	18	30	28-08-2017 to present
Offshore ERA5 hindcast data	-43°	-23.5°	~120	60	01-01-1979 to 31-12-2019
Offshore ERA5 hindcast data	-42.5°	-23.5°	~120	60	01-01-1979 to 31-12-2019

2.2 Historical timeline

The focus of this chapter is on the long-term (10's of years) evolution and movement of the shoreline in the past. An important change of the Copacabana beach occurred in 1970 where a 3.5 million cubic meters sand nourishment was done to widen the beach by 35 meters and the shoreline parallel avenue with 55 meters. First, the characteristics of the beach before the nourishment are described and analyzed, using both historic photos and studies done before the nourishment. After that, the nourishment strategies and the changes within the system due to the

nourishment are analyzed and described. In the last part of this section the beach dynamics from 1970 to present are analyzed using satellite images.

2.2.1 Before 1970

Photos aging back to the beginning of the 20th century show a fishing community active in Copacabana beach where it is clearly visible that the Copacabana neighborhood was still in an early phase of urbanization. After construction of a tunnel in 1892, which connected the Botafogo neighborhood with Copacabana, the city of Rio de Janeiro began to spread towards Copacabana. In the picture shown below the first construction is visible along the beach on top of the (former) natural widespread dune area.

Figure 6: Picture of the Copacabana neighborhood in the beginning of the 20th century where the first urbanization is visible mixed with the natural dunes reaching hundreds of meters land inwards (Lins-de-Barros et al., 2019)

This is also the time the first buildings where constructed right next to the beach and there were the first notices of damage due to storm impact. This is confirmed by some examples shown below of storm impact on Copacabana beach in the 1920s. In extreme cases the waves reached the road along the beach and caused damage to the infrastructure (see Figure 7 below).

Figure 7: Two historical pictures showing damage due to wave impact on Copacabana beach in the 1920s (Lins-de-Barros et al., 2019).

The picture below shows Copacabana beach before 1970 on the left and the present-day Copacabana beach on the right. Before 1970 the beach had an average width of 55 meters which is a lot smaller than the present-day average width which is estimated at 90 meters on average. Also the beach parallel avenue was less wide and didn't have much traffic capacity. This meant that the protection of the road and buildings against the sea was not sufficient.

Figure 8: A picture of Copacabana beach before 1970 on the left and a picture of the present day Copacabana beach on the right (van Dijken, 2012)

In 1970, measurements were done by Kowsmann (1970) to capture the state of the beach before the nourishment. Kowsmann performed profile measurements at one location along the beach. This analysis resulted in an average beach width of 55 meters at the point of the beach shown in the figure below. This is the only available information on beach width before 1970.

2.2.2 Beach nourishment 1970

In 1970 a big artificial nourishment of Copacabana beach was carried out. The main goal of the project was to increase coastal defense and create a bigger beach area to accommodate more people for recreation purposes. Besides this, the beach parallel avenue was widened to increase traffic capacity. The project was instigated by the ministry of public works the SURSAN (Veracruz, 1972).

Two methods were used to nourish the beach: direct placement of sand on the beach and offshore placement of sand using a dredging vessel. The source of sand for the direct placement was the Botafogo bay to the North of Copacabana. With a 5 km long pipeline the sand was transported to Copacabana beach and distributed by auxiliary equipment. Offshore placement of the sand was done using a hopper boat of the Dutch dredging firm Boltje. The hopper picked up the material

4.5 kms from Copacabana beach and dropped it between the -4 and -6m contour of the beach for the sand to be naturally transported to the beach. See Figure 9 for an overview of the sand sources.

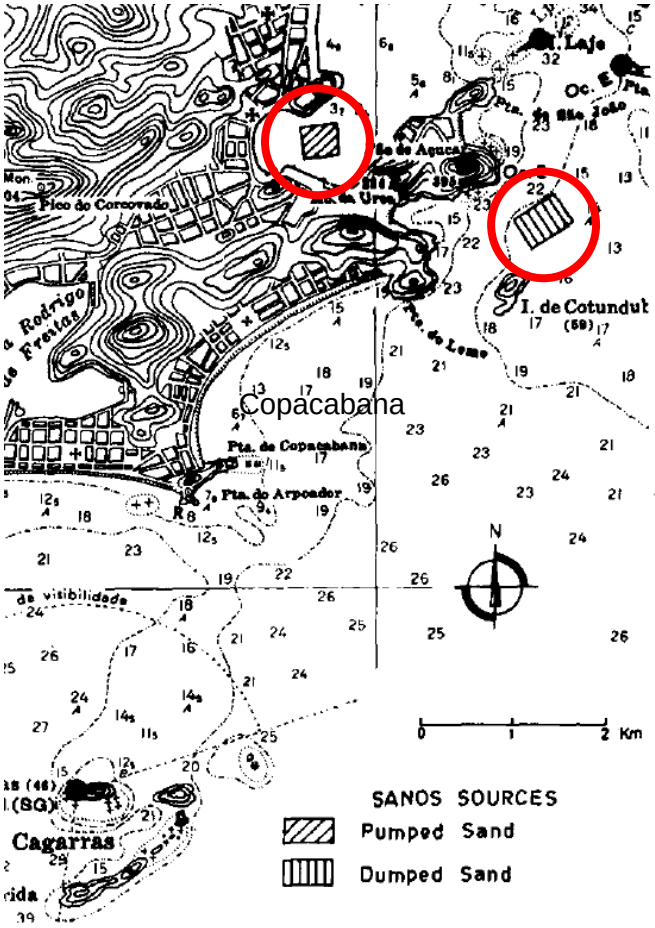

Figure 9: Overview of the sand sources (indicated with the red circles) for the direct placement and offshore dumping of the nourished sand in 1970 (Vera-cruz, 1972).

Sand samples taken from both sand sources showed different mean diameters. The mean diameter of the sand placed directly on the beach was 300 μm and the mean diameter of the offshore placed sand was greater than 400 μm and frequently greater than 500 μm. The nourished sand was coarser than the original sand at Copacabana beach before the nourishment which had a diameter in between 300 and 400 μm. A total volume of 3.5 million cubic meters of sand was nourished, 2 million cubic meters by offshore dumping and 1.5 million cubic meters by direct placement on the beach. This results in 920 m^3 per meters length of beach. The nourishment caused a mean increase in beach width from 55 meters to 90 meters. The width of the shoreline parallel avenue increased from 20 meters to 75 meters, so the shoreline moved a total amount of 90 meters in the seaward direction. In the figure below a concept sketch is made of a typical cross-section of the beach and promenade horizontally scaled before and after the nourishment (Vera-cruz, 1972).

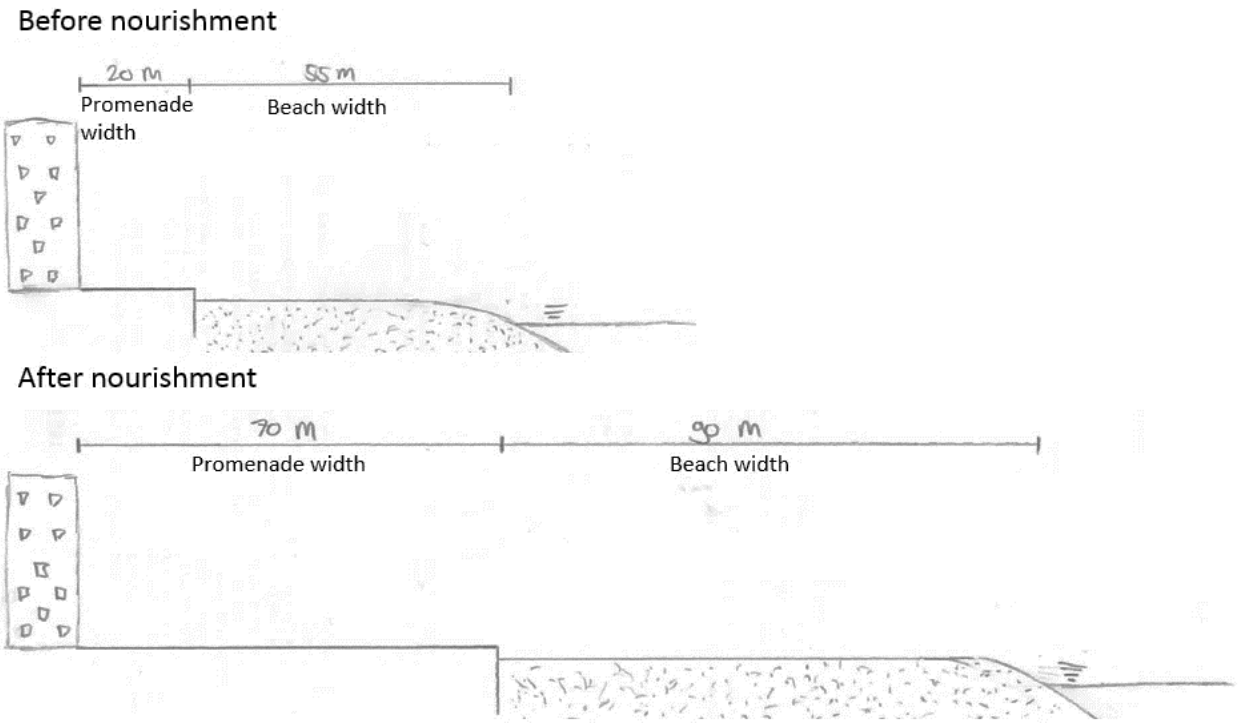

Figure 10 Horizontally scaled sketch of a typical cross-section of Copacabana beach before and after the nourishment in 1970.

The studies for the beach nourishment were carried out by Portuguese engineering firm LNEC. A 2-year long field observation program was carried out collecting physical data. Based on this data a small-scale physical model was designed in order to test the various nourishment strategies. The beach width during and after the nourishment was monitored every 15 days for 2 years across 14 different profiles. The location of the profiles is shown in Figure 11 below.

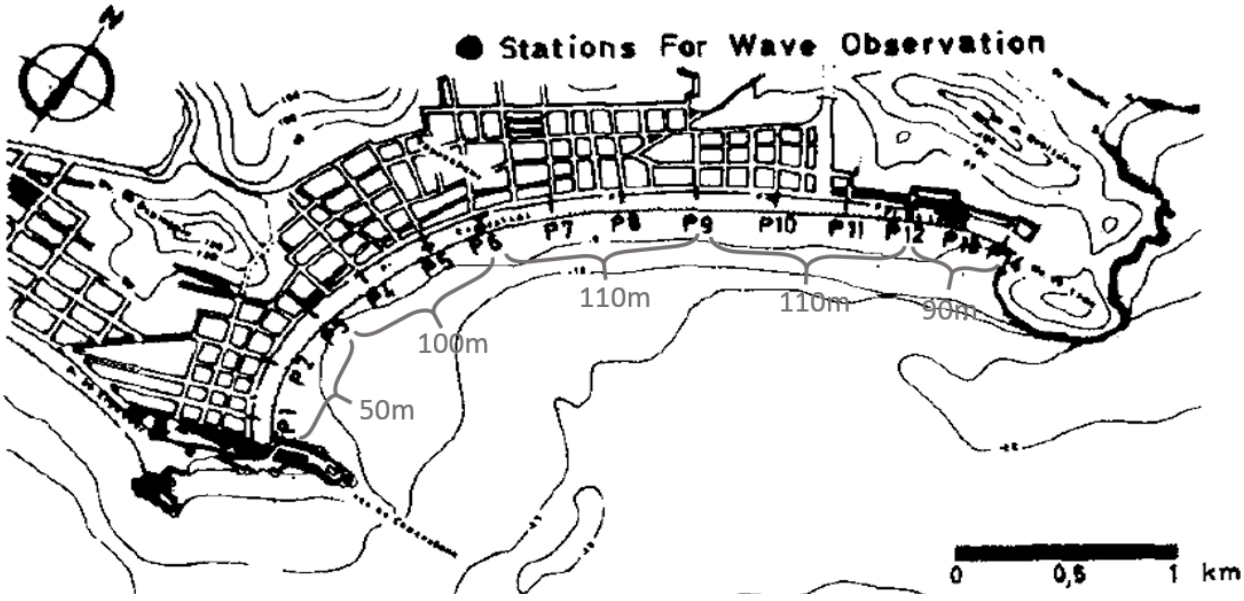

Figure 11: Map of Copacabana bay with the 14 locations of the profiles indicated as defined by LNEC including the average width of the beach sections after the nourishment was completed (Vera-cruz, 1972).

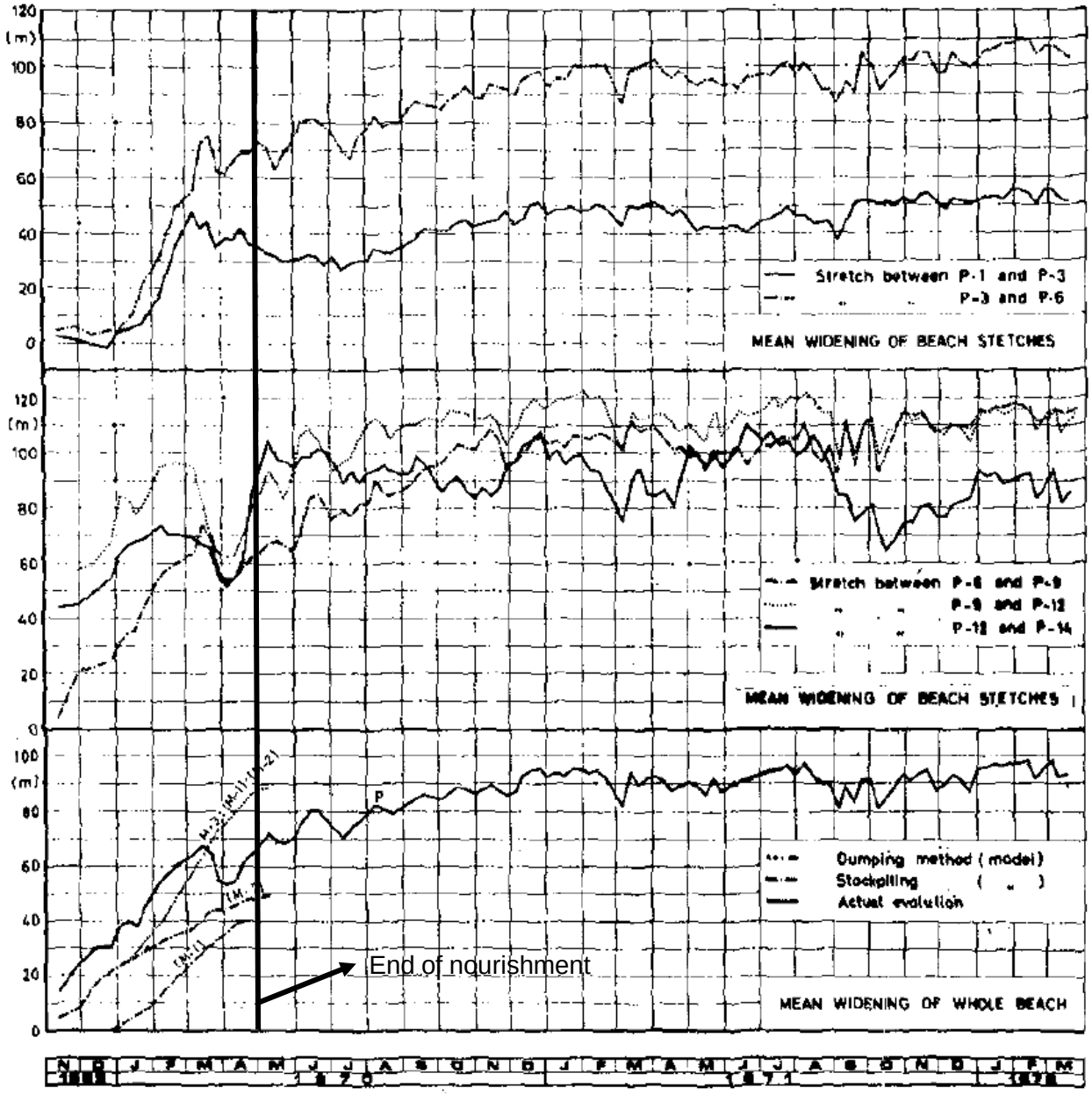

Figure 12: Beach width measurements from November 1969 to March 1972. The M1, M2 and M3 lines in the bottom plot show the predicted beach width resulting from the physical model tests. The nourishment was performed from November 1969 until the end of April 1970 (Vera-cruz, 1972).

The figure above shows the evolution of the total widening of the beach as a result of the beach nourishment. Approximately half a year after the nourishment ended, the average widening of the beach was 90 meters, this includes the 55m widening of the beach parallel avenue (see Figure 10). So after the end of the nourishment, natural processes caused an increase in beach width of another 20 meters after the nourishment was already finished (see Figure 12). This shows that the offshore placement of sand was successful in widening the beach with the help of natural processes.

The mean beach width of profile 1 to 3 (the Southern side of the beach) shows much lower values than the average beach width along the whole beach perimeter. According to Vera-Cruz (1972) this is partly due to the exceptional sheltered conditions in this part of the beach due to diffraction

around the Forte de Copacabana. The physical model used during the studies of LNEC could also not reproduce this phenomena. The amount of sand deposited on the foreshore and offshore part of the beach was minimal. The dredging vessel was not able to reach this part of the beach due to the shallow depth (see Figure 11) and the pipeline that transported the sand for the stockpiling was not long enough to reach this part of the beach.

2.2.3 1970 to present

In this section a distinction is made between the long-term and the short-term behavior of the beach. The long-term covers 10's of years and deals with the changes in coastline position and beach shape. The main data source used in determining the long-term health of the beach are the Landsat satellite images. The short-term behavior, which aims to cover the extreme event timescales, is in the order of days to months. For this purpose the Sentinel 2 images are used.

Landsat satellite images (1985-present):

The 4 different satellite images below show Copacabana beach in the years 1986, 1998, 2008 and 2019. When comparing the shape of the beach, the images show no distinct differences. It must be noted that these images have a large pixel size of up to 30 meters which makes it not possible to do an exact width comparison because of the large uncertainty compared to the width differences. This conclusion is based on visual judgement of the satellite images.

Similar beach shape can be observed in all of the pictures where in the Southern part of the beach there is a smaller equilibrium beach width. Besides, the eastern part of the beach is somewhat smaller than the middle part of the beach. The measurements after the nourishment show similar patterns (see Figure 12). What can be concluded from this analysis of satellite imagery is that since the nourishment in 1970 the beach shows a stable equilibrium profile on the long-term, and from this analysis there is no indication of any sediment losses or structural erosion of the beach from 1970 to present. This is an assumption based on limited information and needs to be verified in further analysis. When making an animation of all the available Landsat 5 images from 1986 to 2011, there is no trend visible in shoreline movement that confirms erosive trends, accretive trends or long-term redistribution of sediment within the bay.

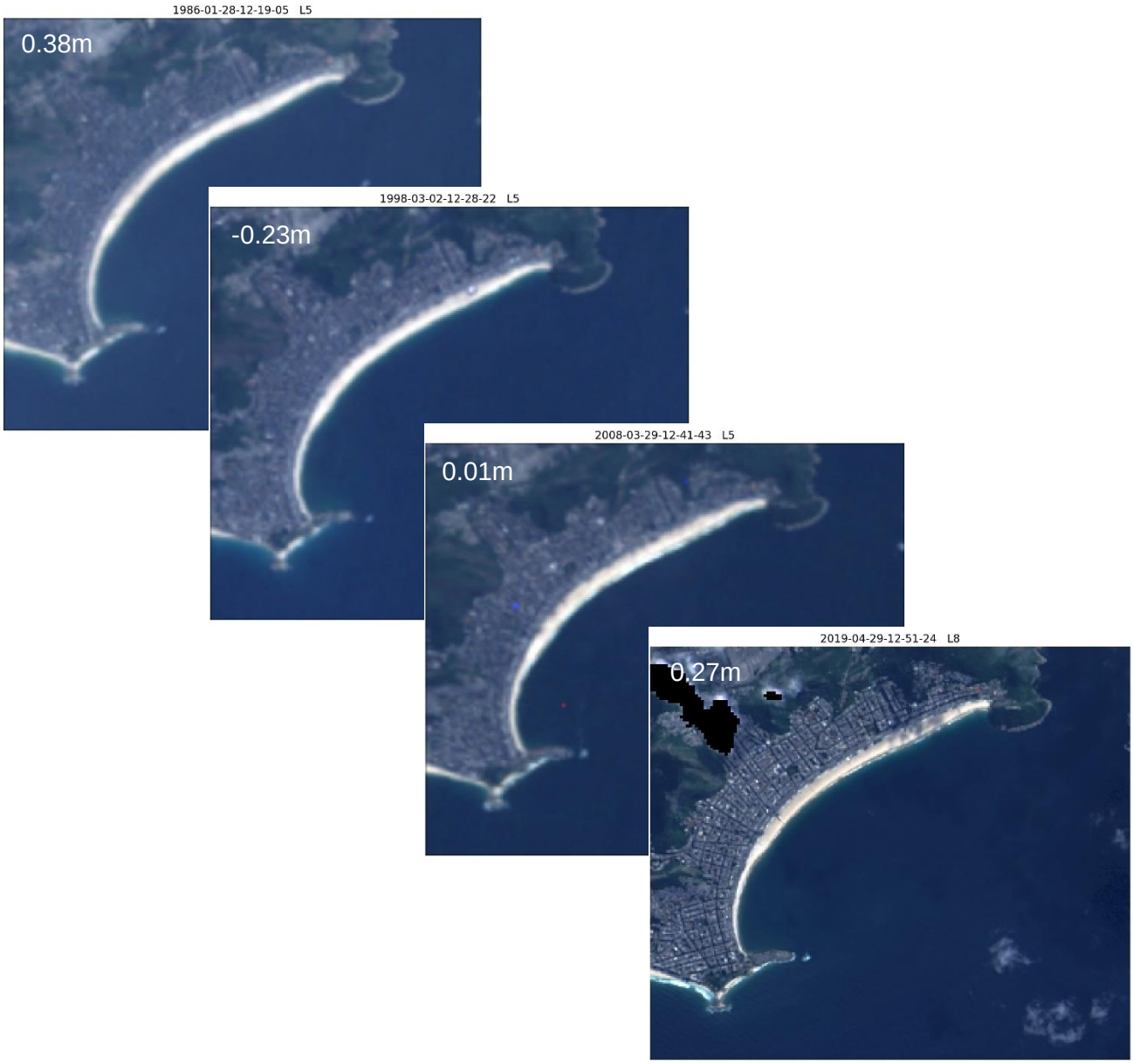

Figure 13: Four satellite images showing Copacabana beach from 01-1986, 03-1998, 03-2008 and 04-2019. For every image the tidal level is shown.

The Deltares shoreline monitoring tool tracks the position of coastlines using 30 meter resolution Landsat images from 1985 until 2016 (Luijendijk et al., 2018). The measurements are not individually corrected for the tidal elevations which increases the uncertainty. Still the results of this analysis can help in defining a long-term trend in coastline position.

Figure 14 Average yearly change in shoreline position over the period of 1984-2016 from the Deltares Shoreline monitoring application (data obtained from Luijendijk et al., 2018).

The analysis results in an erosive trend in the southern part of the beach at datapoint 1 and 2 and for the rest of the beach the trend shows accretion. Take for example point 2 of the beach, this trend is the result of 33 years of data. It indicates a total change of coastline position of 16.5 meters in shoreward direction within the 33 years. Including the influence of the tide, which can cause a change in coastline position in the order of 10 meters and the resolution of the satellite image which is equal to 30 meters this erosion value has a high uncertainty.

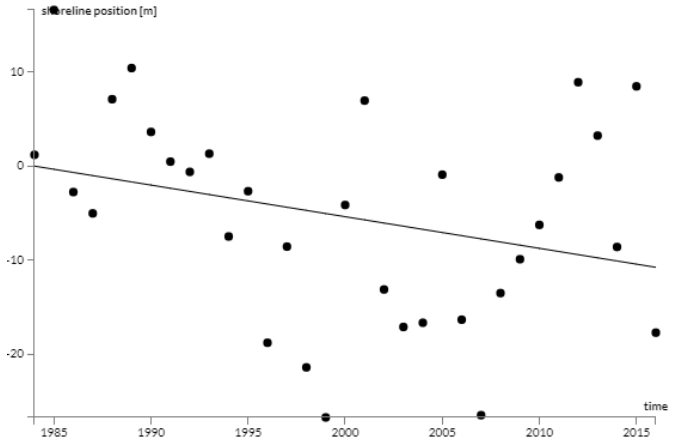

Figure 15 Yearly shoreline position of point 2 of Copacabana beach from 1984 to 2016 (Luijendijk et al., 2018)

From the yearly average shoreline positions plotted in the figure shown above, the shoreline position trend is not distinct and the data shows high variability per year. From this shoreline monitoring analysis it can be concluded that due to high uncertainty and variability in the data the erosive trend of the Southern part of the beach on the long-term cannot be confirmed.

Sentinel satellite images (2016-2019):

To analyze the evolution of the beach over time, historical Sentinel 2 satellite images are used. The images are available from January 2016 to January 2020 with a frequency of 5 days. Due to cloud cover the actual frequency is lower than 5 days. The spatial resolution of the satellite images is 10 meters. The width measurements are performed manually and corrected for the tides using an average beach slope of 1:12.5 (see appendix C.3 for the cross shore profile measurements from which the average beach slope is derived). With a fortnightly mean spring tidal range equal to 1.1 meters the tidal correction of the beach width is in the range of +-7m. The coastline is defined as the interface between saturated and non-saturated sand. This coincides with point of maximum uprush of waves. So the wave height at the moment the satellite image is made influences the measured beach width. The beach widths are manually extracted for 5 cross sections (see Figure 17 for the location of the cross sections) along the beach from the satellite images with the use of GIS software. The results are shown in the figure below:

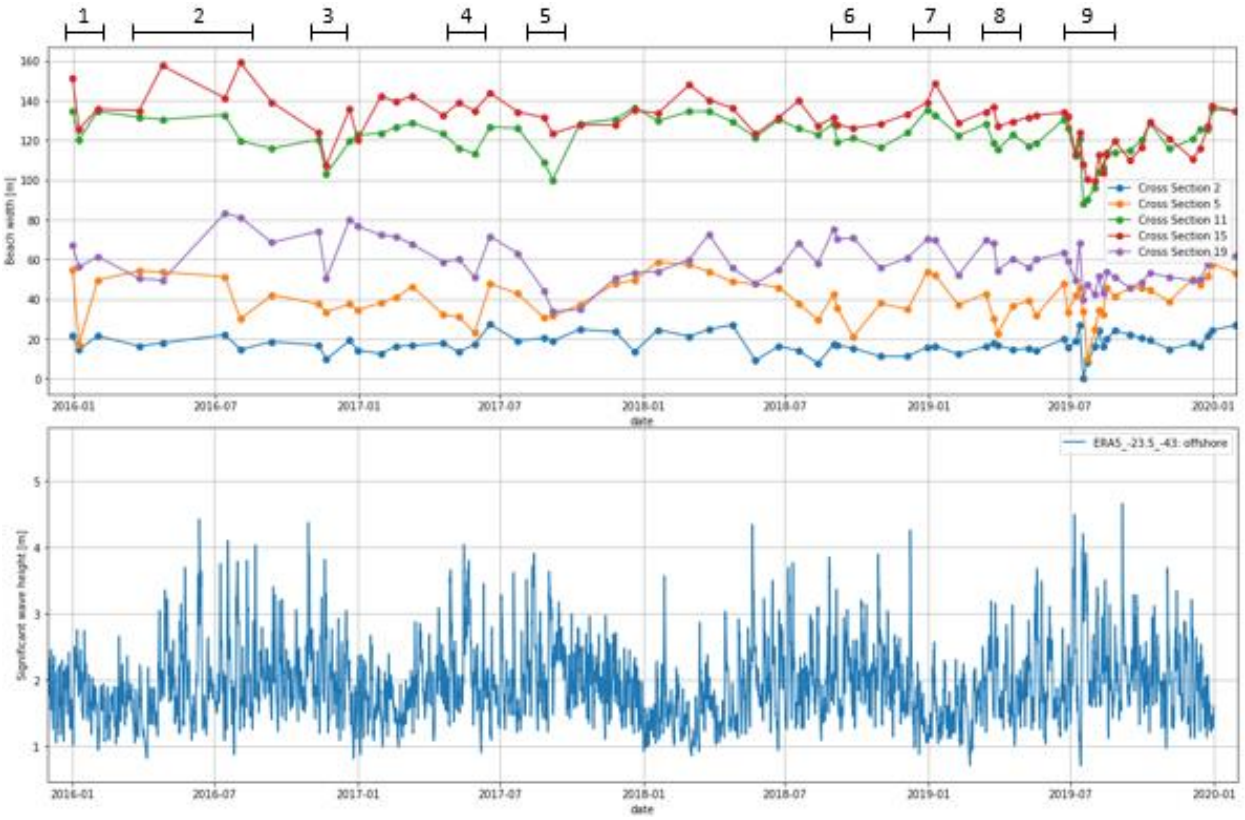

Figure 16: Beach width dynamics from 2016 until 2019 including a plot of the wave height from the ERA5 hindcast dataset over the same time period. The location of the 5 different cross sections are shown in Figure 17. The numbers 1 until 9 above the figure denote morphological behavior of the beach which is explained after this figure.

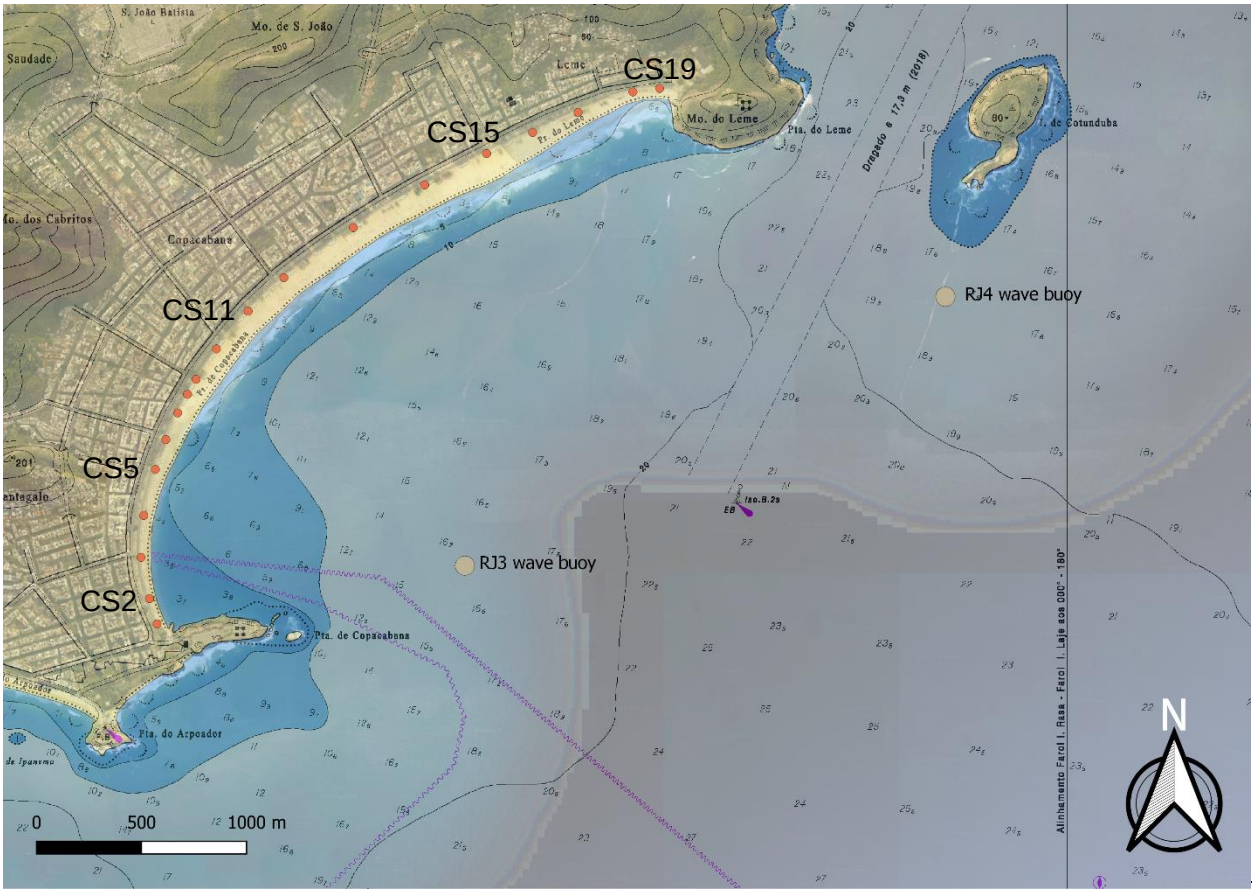

Figure 17: An overview of Copacabana bay with the different cross sections pointed out.

The numbers 1 to 9 in Figure 16 each denote different morphological behavior/features of the beach which are briefly explained below and elaborated upon in more detail later in this chapter.

Extreme event beach erosion: 1, 3, 4, 5, 6, 8 and 9:

Short-term erosion events are visible where a sudden decrease in beach width at a specific part of the beach or along the whole beach is visible. This sudden decrease in beach width coincides with periods of energetic wave heights. The impact of the July 2019 erosion event, as shown in the previous section of this chapter, is clearly visible where all cross-sections show a decrease in beach width of up to 40 meters.

Alongshore redistribution of sediment: 2:

From all the satellite images this is the only one clear indication of an alongshore redistribution of sediment which is visible in Figure 18 below zoomed in on the Northern part of the beach. A change of beach shape is visible where the right part next to the headland has an increase in width against a decrease in width on the left side of the image. This indicates an alongshore transport direction in the eastern direction during 3 months. What is interesting to note is the sudden increase in beach width at cross section 15 between 13-07-2016 and 02-08-2016 and the sudden transition in beach width which is visible only on the satellite image of 02-08-2016 (denoted with the white circle in Figure 18). During this time the Olympics took place in Rio de Janeiro and the volleyball stadium was placed on the beach near Cross Section 15. During periods of high waves hindrance was caused during construction due to the uprush of waves on the beach. With the construction of a big barrier of sand along the coastline they solved these

problems (Rangel, 2016). It is very likely that this human intervention is visible in the form of a wider beach in the satellite image taken on 02-08-2016.

Figure 18: Three satellite images showing an alongshore redistribution of sediment in the Northern part of the beach. The transport direction is denoted with the white arrow.

Increase in beach width due to low wave energy: 7:

An overall increase in beach width coincides with longer periods of low wave energy. These periods occur in the summer months where the average wave heights are significantly lower compared to the winter months.

2.3 July 2019 erosion event

From the 17th of July until the 23th of July 2019 large swell waves hit the coast of Rio de Janeiro largely impacting the state of Copacabana beach. The following pictures show the state of the beach before the event and directly after the event. The pictures are all taken near the same beach kiosk which is visible in both images.

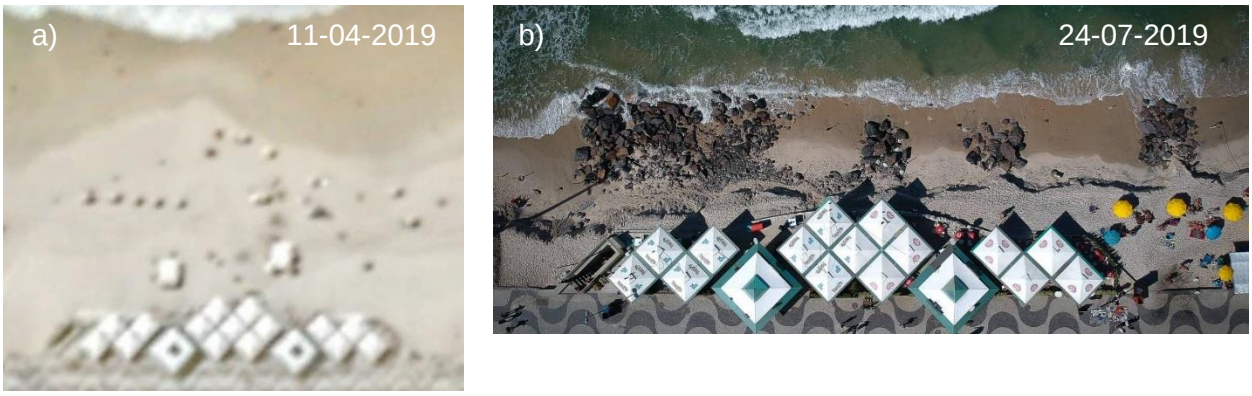

Figure 19: Pictures taken before the erosion event and directly after in July 2019. Courtesy of a) Google Earth, b) O'Globo.

The big difference in the state of the beach is clearly visible in the images shown above. Figure 19a shows a more stable beach state resembling the equilibrium beach state observed on the long-term in the previous chapter. However, directly after the extreme wave event the beach is in an extreme erosive state where there is almost no beach area left and a decrease in beach width in the order of 40 meters occurred. This leaves the beach in a very vulnerable state where further erosion could cause significant damage to beach infrastructure. This erosion occurred on the timescale of days due to the 7-day long period of high waves.

During a fieldtrip to Copacabana some interviews where performed. Renato, who works at the kiosk visible in the Figure 19, has already 14 years of experience working at Copacabana beach and mentioned that he had never seen such an erosion of the beach before. This is still no assurance that such erosion never took place since the nourishment in 1970, but it shows that an erosion event with this impact is rare.

The stones which are visible in Figure 19b are placed at the beach before the nourishment in 1970 according to local sources. This confirms that before the nourishment there were also erosion problems at this part of the beach that needed some local reinforcement of the beach using perpendicular groins to capture the sediment and prevent erosion. During the nourishment in 1970 the sand was placed on top of this structure and as of known the stones never surfaced before.

The satellite images in the figure below show the same pattern as observed in the images in Figure 19 where the beach shows erosion in the order of 40 meters due to the extreme waves. It is visible that the beach seems to recover to its original beach width within 4 weeks after the extreme event.

Figure 20: Sentinel 2 satellite images before, directly after and 4 weeks after the July 2019 extreme wave event showing the beach width at the Southern part of the beach.

In the images below the same trend is visible where the beach reached its original state in terms of beach width. However, when looking at the vertical elevation of the beach a clear difference is visible. This can be observed when looking at the steps that access the beach kiosk visible on the right side of both images. The left image is taken directly after the erosion occurred and shows a big beach scarp. It is assumed that the part of the beach in the onshore direction starting from the beach scarp (to the right of the beach scarp in Figure 21) is not affected by the erosion event at the moment the picture is taken. From this, the conclusion can be drawn that the original level of sand on the beach exposed 1.5 steps as is visible in Figure 21a. When looking at the state of the beach 4 months after the erosion event, 7 steps are exposed. The reason for this exposure is the steep slope of the beach scarp which apparently was not able to be sustained. Next to that the natural processes are not able to recover this part of the beach up to its original level. This indicates that full recovery of the beach has not taken place yet in terms of vertical beach elevation, especially on the back of the beach near the kiosk.

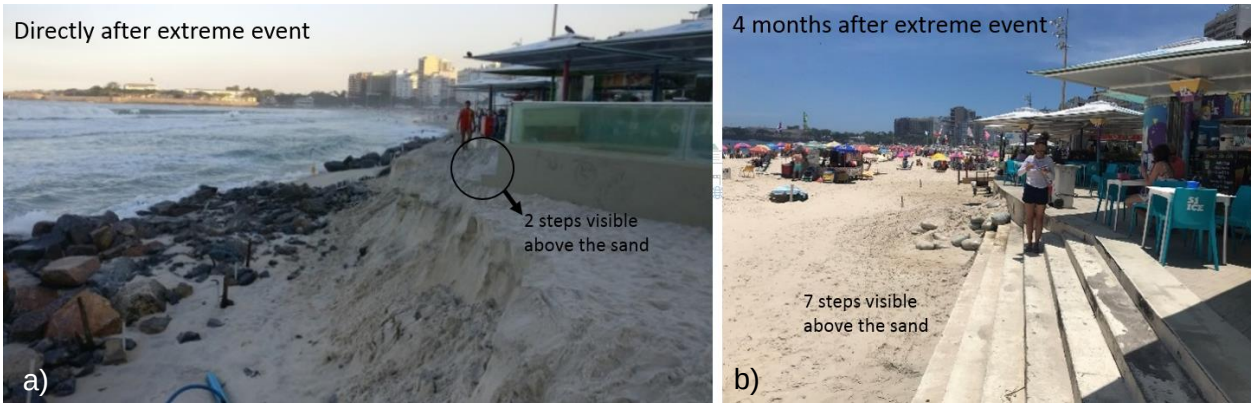

Figure 21: A picture taken at a similar location along the beach: a) directly after the erosion event on 24-07-2019 and b) 4 months after the erosion event on 07-12-2019.

Besides the more recent example of the erosion event in July 2019, there are other examples of storm events having a short-term impact on the beach. The images below show the impact of various storm events in the history of Copacabana beach. It can be concluded that most of the storm events focus around the local winter period.

Figure 22: a) Erosion of the beach near cross section 2 of the beach at 12-06-2016 where the waves reach the kiosk along the beach. Courtesy of Flavia Lins-de-Barros. b) Picture taken during a storm event in April 2011 where the waves reach the promenade 200 meters North of cross section 5. Courtesy of surfguru. c) The overwash of waves on 29-05-2011 caused part of the promenade to be flooded. Courtesy of iG. d) Picture taken during the Olympics in July 2016 where clear erosion is visible. Courtesy of O'Globo.

Different kinds of short-term beach states can be observed in the collection of historical images shown in the figure above. The Southern part of the beach, where the equilibrium beach width is smallest, seems to be the location where the most problems related to storm events occur. In some cases it can be seen that the beach completely disappears and the foundation of the beach kiosks is impacted (see Figure 22a). This part of the beach has more sheltered and less energetic wave conditions compared to the Northern part but due to the smaller beach width problems seems to occur.

The images in Figure 19 and Figure 22 b,d are from a very similar location along the beach about 800 meters from the Southern headland. When energetic waves reach the coast there have been multiple cases where erosion caused flooding of the promenade. The image in Figure 22d is taken during the Olympics in Rio de Janeiro in 2016 where a temporary TV station was constructed on the beach. During a period of extreme waves the coastline shifted in landward direction due to erosion processes which endangered the stability of the TV station. No cases of erosional damage seem to exist in the Northern part of the beach. This is partly due to the bigger beach width in this area. However, like Figure 22c shows, overwash of waves on the beach can cause flooding of the boardwalk along the beach.

2.4 Summary

An overview of the most important findings and conclusion drawn from this chapter are listed below:

- In the history of Copacabana beach there has been one major human intervention. This is the artificial nourishment of the beach in 1970 where 3.5 million cubic meters of sand was placed at the beach. This lead to a widening of the beach of 35 meters on average and a movement of the shoreline in the shoreward direction of 90 meters because of the widening of the shoreline parallel avenue. This has been the only human intervention at Copacabana beach in the last 10's of years.
- After the nourishment the equilibrium shape of the beach showed a smaller beach width in the Southern part of the beach. An explanation for this smaller beach width can be found in the fact that during the nourishment less sand was placed due to the inability of the dredging equipment to reach this part of the beach. The typical equilibrium beach shape has not changed since the nourishment in 1970 and present-day this shape is still observed.
- Analysis of the shoreline position from the nourishment in 1970 to present-day show no observable erosion or accretion trends. Data for this analysis is available in the form of Landsat satellite images with a resolution of 15 to 30 meters from 1985 to present. These Landsat images are used by the Deltares shoreline monitoring tool to track the shoreline position. Taking into account the uncertainty in this analysis related to tidal range and image resolution, it is concluded that from this analysis there is no observable trend and the beach shows stable behavior on the long term.
- Short-term dynamics of the beach are mainly related to erosion due to storm events which occur multiple times a year during the local winter period. From 2016 until 2019 multiple erosion events are visible with erosion up to 40 meters in some cases of which the July 2019 erosion event clearly had the biggest impact.
- During the July 2019 erosion event the Southern part of the beach almost completely disappeared leaving limited beach area and a beach scarp along the beach. A set of big stones surfaced due to the erosion which were apparently placed on the beach before the nourishment in 1970 for local reinforcement. Locals state that the stones never surfaced before, which confirms the unique and extreme impact of the July 2019 extreme wave event. Judging from the satellite images, the beach width fully recovered 4 weeks after the extreme event. However the vertical elevation of the backbeach has not reached its original level yet.

3 In-depth data analysis

From the previous chapter the conclusion was drawn that especially the storm event impact and subsequent recovery are important factors in determining the health of Copacabana beach. This chapter includes a more in-depth analysis of these processes starting with a detailed description of the local wave climate including the 2D wave patterns. Hereafter the focus is on the characteristics of storm events where, among other things, the July 2019 erosion event is put into a larger perspective. This is followed by details on the response of the beach under the influence of storm. The last part of this chapter deals with the characteristics of the post-storm recovery of the beach.

3.1 Wave climate

The nearshore wave statistics are shown in the figures below for the 2 different nearshore wave buoys RJ3 and RJ4. The wave spectrum is very unidirectional. This can be explained by the sheltered location of the Copacabana bay between the headlands and the eastern edge of the Guanabara bay. When comparing the data from both buoys, the relation between the significant wave height and the peak period shows high similarity and wave heights in both points are of similar magnitude. There is however, a small difference in the mean direction of the waves. The average wave direction at buoy RJ3 is approximately 150 degrees. And the average wave direction at buoy RJ4 is approximately 160 degrees. This shows that the local bathymetry is influencing the wave direction and refraction has already taken place when waves from the offshore direction reach the location of the nearshore buoys. In the nearshore wave data there is clear dominance of swell waves with wave heights of 0.5 to 1.5 meters and a peak period between 10 and 15 seconds.

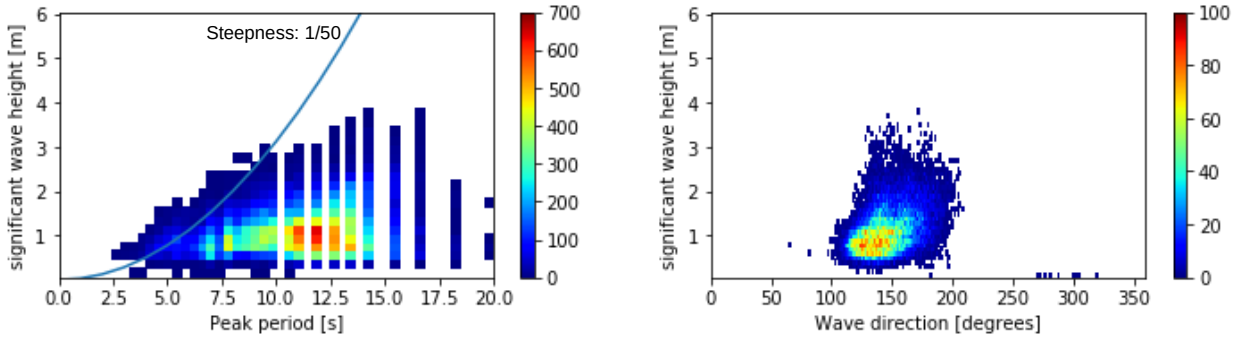

Figure 23: RJ3 nearshore wave characteristics

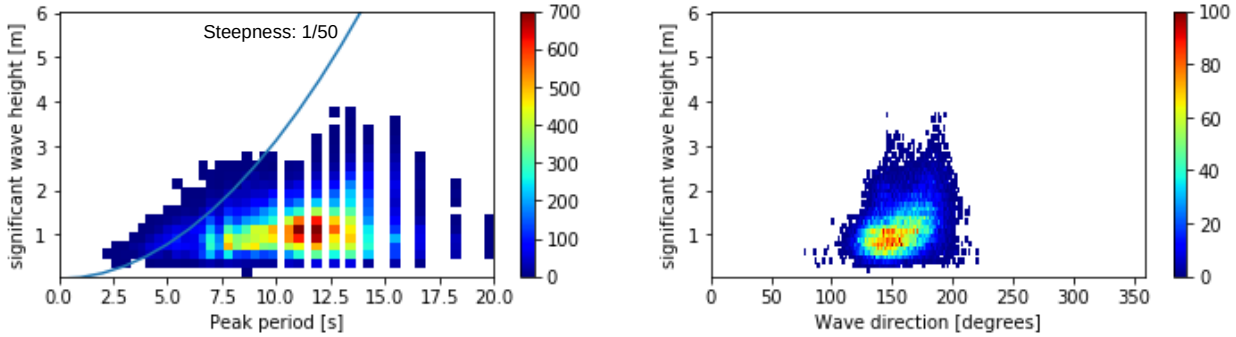

Figure 24: Nearshore wave characteristics from the RJ4 nearshore wave buoy.

No clear distinction between swell waves and wind waves can be made in the nearshore dataset because there is just a single significant wave height given which most of the times consists of a wind and a swell part. An assumed wave steepness curve with steepness 1/50 is plotted in both Figure 23 and Figure 24. It is clearly visible that only a very small part of the wave spectrum can be possibly classified as wind waves and do not including the more extreme wave heights. When splitting the dataset on wave steepness there was no match between the steeper waves and the wind records of the nearshore wave buoys. From this the conclusion is drawn that the wave climate does dominantly consist of swell waves.

The wave roses are shown below for both wave buoys. This shows that the mean wave direction is from the SE/SSE. Also wave roses for waves higher than 2 meters are shown. From this it can be concluded that the extreme wave direction is more directed towards the South.

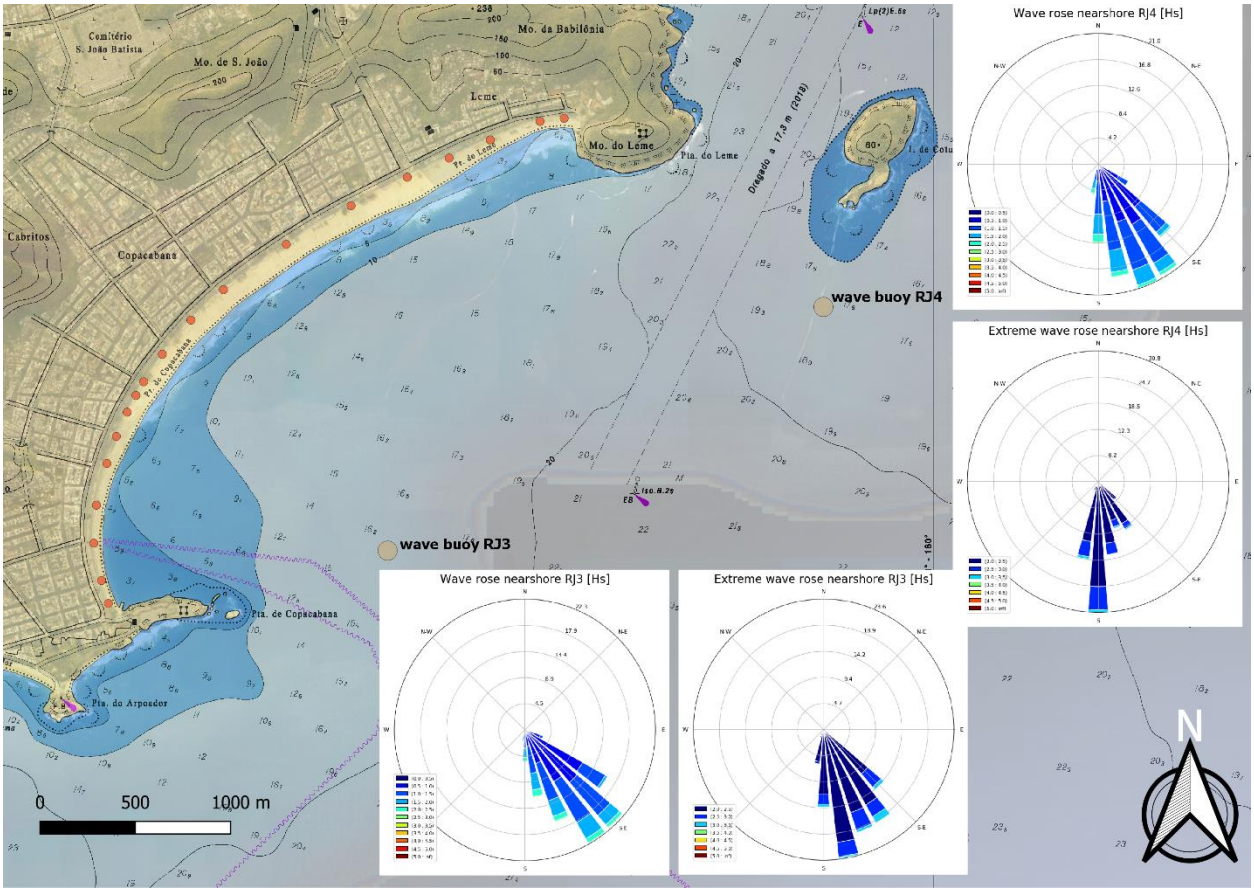

Figure 25: Normal and extreme nearshore wave roses for buoy RJ3 and RJ4. The percentages shown in the various wave roses are normalized.

The wave climate near Copacabana beach shows very clear seasonality. The figure below shows the average wave height for every month and the average hours per month the significant wave height of 2.5 meters is exceeded. From May until September there is a higher probability of extreme wave heights. This period is in the local winter period where more cold fronts form above the South-Atlantic. During and around the summer period the average wave height decreases and the occurrence of extreme wave events is lower. This period is from October to April.

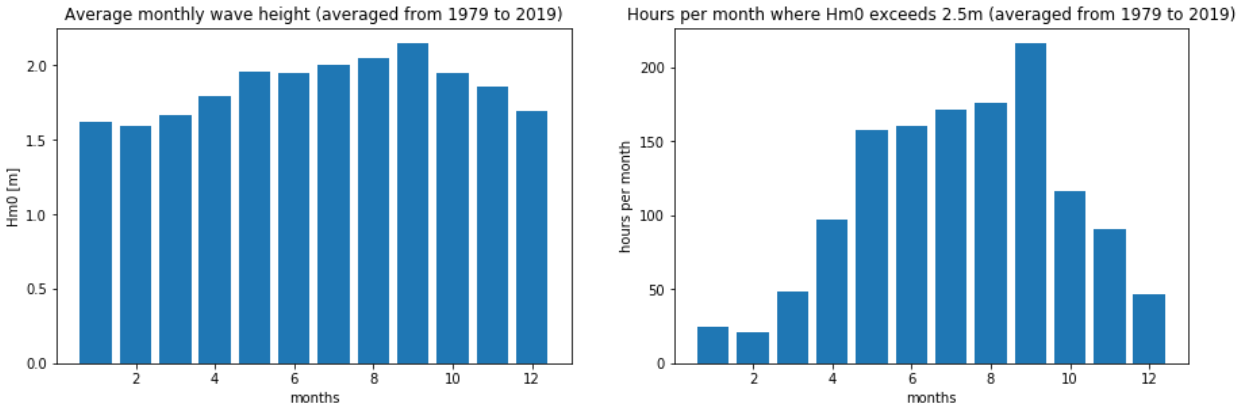

Figure 26: Monthly variations in offshore wave height.

Due to the specific shape and orientation of the beach different wave directions cause different wave patterns within the bay. The Southern headland causes the Southern part of the beach to be sheltered dependent on the incoming direction of the waves. As discussed before, the mean direction of waves is in between the SSE and SE, where more extreme waves are originating more from the South. The two sketches in Figure 27 show the refraction pattern in the bay under SE and SSE directed waves. The lines indicate the direction of propagation of waves from offshore to nearshore. Refraction is caused by depth variation along the wave crests causing a difference in phase speed along the crest resulting in change of wave direction. This change in direction can be estimated using Snell's law:

$$\frac{\sin(\varphi_2)}{c_2} = \frac{\sin(\varphi_1)}{c_1}$$

With:

- φ = angle between the local wave direction relative to the local bathymetry contours [degrees]
- c = wave phase speed [m/s]

The bathymetry map reveals that in the Southern part of the bay there is an accumulation of sand causing shallow water depths compared to the Northern side. This sand accumulation is also visible in the historic bathymetry map from Vera-cruz (1972) in Figure 11. This significantly influences the wave patterns in the Southern part of the bay which results in a divergence and convergence of wave energy when waves origin from the SE (see Figure 27a).

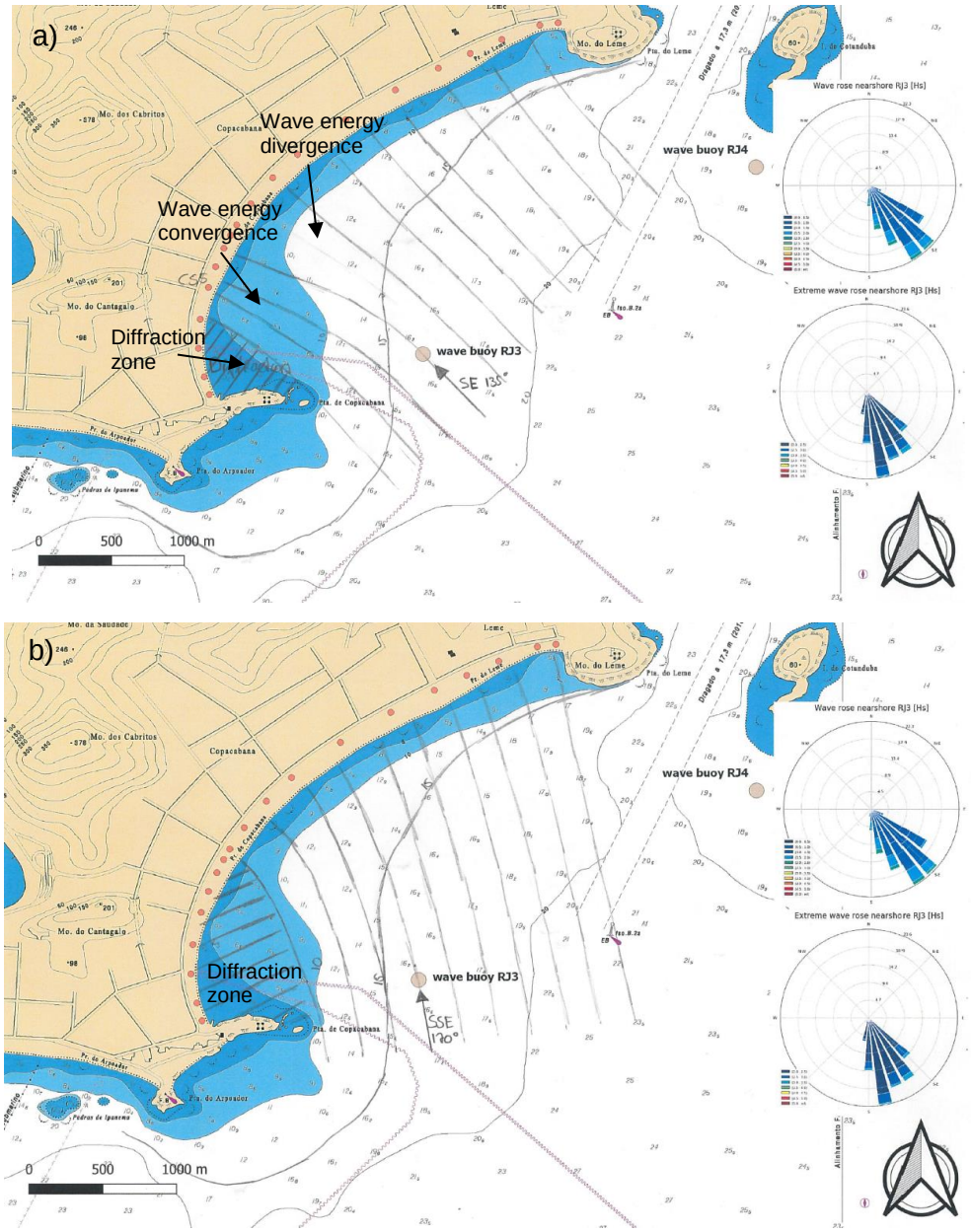

Figure 27: Wave refraction diagram based on Snell's law for a nearshore wave direction of a) 135 degrees and b) 170 degrees.

Besides the refraction pattern, the approximated diffraction zone is sketched. This is the area of the beach that is sheltered from direct wave impact due to the Southern headland. Diffraction is characterized by a transfer of wave energy along the wave crests, which forms a circular arc with a decreasing wave height along the wave crest. The area of the diffraction zone increases when waves origin more from the South.

More information on the wave characteristics, especially with regards to the offshore wave climate, can be found in Appendix B.

3.2 Extreme event characteristics

In the figure shown below, 6 different storm events are plotted with their nearshore significant wave height, wave direction and peak period over time. The events shown below are the only

recorded storm events in the nearshore dataset (containing wave data from 2016 until 2019) with a maximum wave height above 3 meters. Typical patterns that arise from the storm events are as followed:

- Extreme significant wave heights occur with a peak period of about 15 seconds which confirms that the storm events are swell dominated. This is also confirmed by the nearshore wave buoy analysis which does not show any relation between local wind records and the occurrence of extreme waves. Locals confirm that during periods of extreme waves the weather is often 'non-stormy' with blue skies and minimal wind.
- Wave heights above 3 meters origin from the South in most cases. An exception is the storm event in July 2019 where waves above and around 3 meters origin from the SE. Furthermore, wave heights above 2 meters origin from in between 150 and 180 degrees for the most part. This is also confirmed by the nearshore extreme wave roses shown in Figure 25.
- The wave direction at the start of storm events is directed from the South in most cases and moves counterclockwise with time towards the SE.
- The duration of storm events differs from 2 days to a maximum of 7 days.

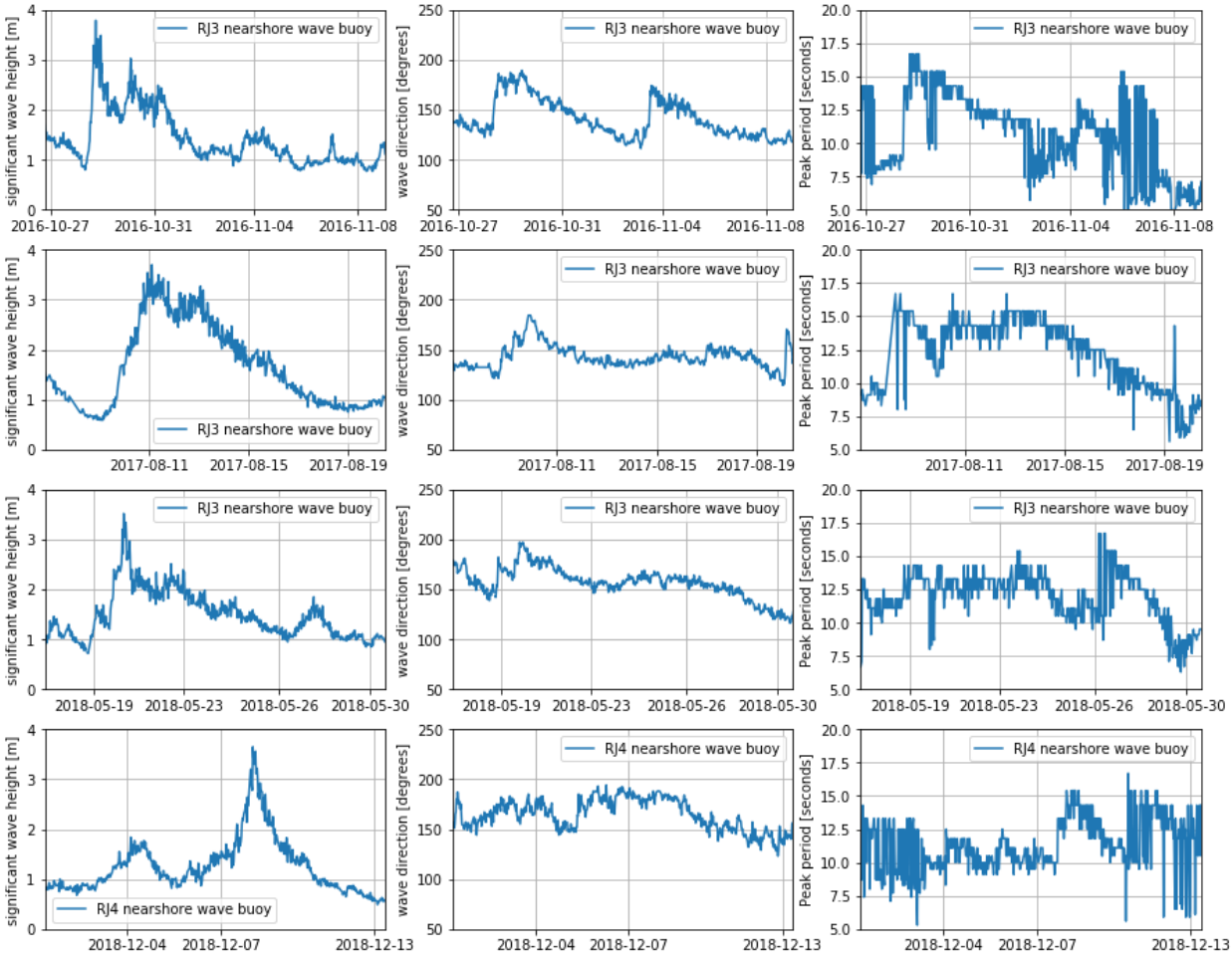

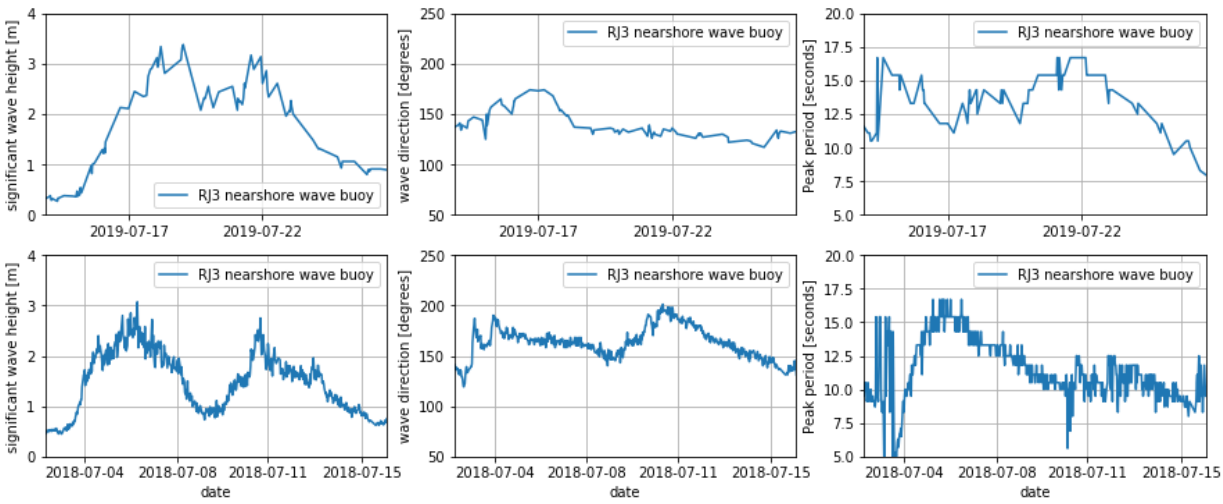

Figure 28: Characteristics of multiple storm events from 2016 until 2019.

A study by Parise et al (2009) looked into the relation between sea waves off the coast of Brazil and extratropical cyclones in the South Atlantic ocean. Judging from wave hindcast data the cyclones cause significant wave heights often higher than 4 meters multiple times a year (as recorded from hindcast data approximately 100kms off the shore of Rio de Janeiro). The path of the cyclones is most often from west to east originating from Uruguay at a latitude of about 33 degrees South. This is confirmed by research by Gan & Rao (1990) who looked into the cyclogenesis over the whole continent of South-America from which a frequent center of cyclogenesis is found around Uruguay. An example of the path of a typical cyclone is given in Figure 29 below. The pattern where most often the storm events initially cause Southward directed waves and with time this direction changes eastward matches with the typical path of the cyclones from west to east.

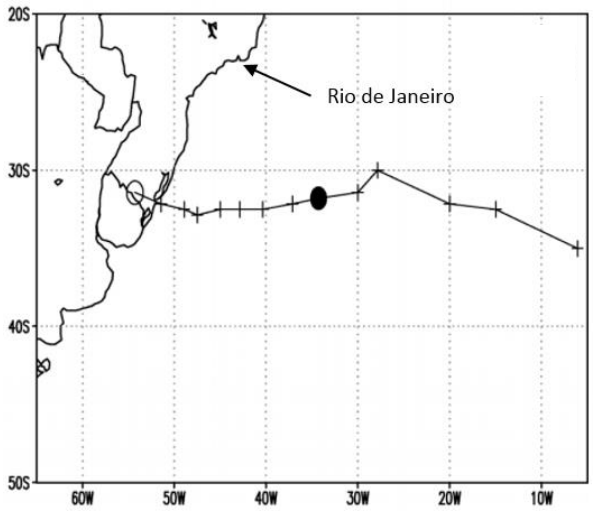

Figure 29: Typical path of an extratropical cyclone above the Southern Atlantic ocean where the open circle denotes the initial position of the cyclone and the filled circle denotes the most mature state of the cyclone (Parise et al., 2009).

3.2.1 Erosion event July 2019

The erosion in this event resulted from 7 consecutive days where the significant wave height was above 2 meters with a maximum nearshore significant wave height equal to 3.4 meters. The primary wave direction of the waves was from SE (see Figure 30 below). This wave direction

matches with the wave patterns shown in Figure 27 where there is a local convergence of wave energy in the Southern part of the bay. This caused erosion of about 35 to 40 meters at cross section 5 of the beach. However, 1 month after the extreme wave event, the beach width, as observed on satellite images, seems to have recovered. This is however not the case for the vertical elevation of the backbeach at certain parts of the beach.

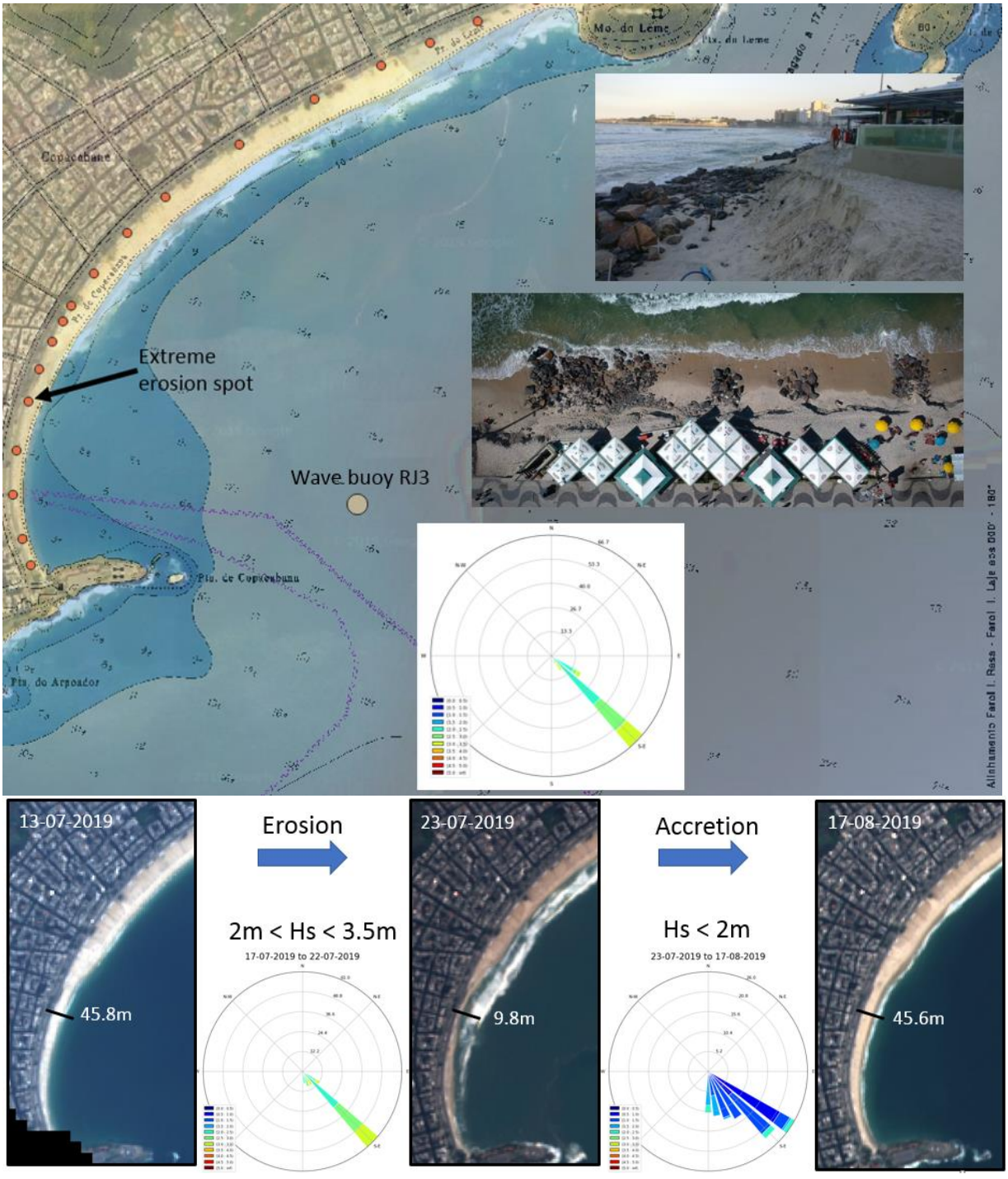

Figure 30: Overview map of the Copacabana beach with the point of extreme erosion and the wave rose for the period of the extreme wave event (17-07-2019 until 22-07-2019). Courtesy of Han Winterwerp, O'Globo,and Coastsat.

The maximum recorded significant wave height in the offshore dataset was equal to 4.2 meters during the July 2019 storm event. Performing an extreme value analysis using the offshore wave data from 1979 to present gives a return period of a storm with this maximum wave height of 1 year (for more details on the Extreme Value Analysis see Appendix B.4). In terms of erosional impact this event is clearly not of yearly occurrence so besides the maximum wave height other characteristics need to be considered.

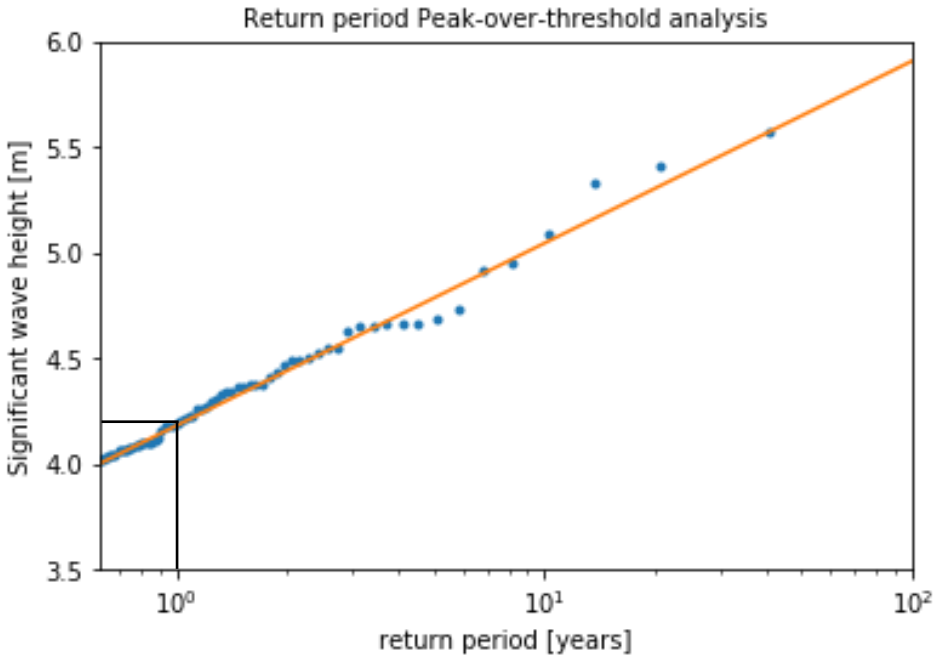

Figure 31: The long term distribution of the peak-over-threshold significant wave height with a threshold of 4 meters fitted by a shifted exponential distribution with A=4 and B=0.375. The data used for this analysis is the ERA5 offshore wave dataset from 1979 until 2019.

The mean wave direction of this storm event is from the SE. This wave direction is not common for extreme wave heights. This is also visible in the analysis of the different storm events which are captured by the nearshore wave buoys in the last 3 years (see Figure 28), from which is concluded that the common wave direction of extreme waves is in between 150 and 180 degrees. The histograms below confirm the extraordinary direction of the July 2019 wave event.

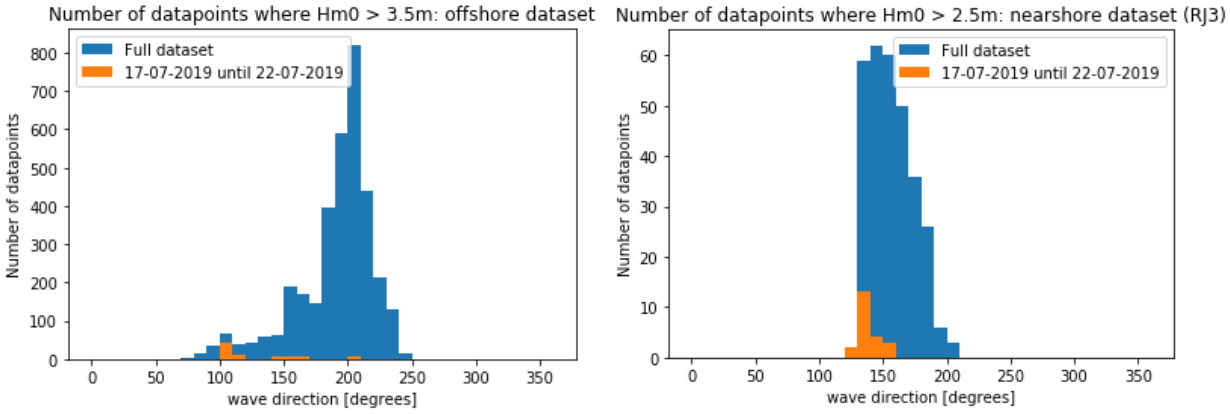

Figure 32: Distribution of the wave direction for extreme waves for the offshore and nearshore dataset (buoy RJ3).

The wave pattern in the Copacabana bay changes with wave direction. The wave directions during the storm event caused the part of the beach with the extreme erosion to be directly exposed to the waves (see Figure 30). The waves were able to propagate around the Forte de Copacabana at the South of the bay and causing local wave energy convergence in the South as visible in Figure 27a. The extraordinary wave direction together with an above average duration of 7 days caused the high impact of this erosion event.

3.3 Beach response during extreme events

Besides the erosion event of July 2019, other erosion events due to period of high waves are captured in the beach width analysis over the last 4 years. When looking at cross section 5 of the beach, the events pointed out in Figure 16 with numbers 1, 4, 6, 8 and 9 show significant erosion at this point of the beach. All of these events show an above average decrease in beach width of Cross Section 5 in comparison with the other cross sections of the beach. The detailed characteristics of these storm events are shown in Appendix D, where the satellite images before and after the erosion are shown with corresponding wave conditions. Besides this, wave characteristics during accretion and recovery of the beach are shown. The table below shows an overview of the characteristics of the storm events:

Table 3: Overview of the main characteristics of 6 different selected erosion events. The wave data used in this analysis is obtained from the nearshore wave buoys.

	Duration [days]	Max Hs [m]	Wave direction during erosion	Wave direction during recovery	Erosion Cross Section 5 [m]	Total Wave energy [*10^8]
Jan-2016*	5	2.8	ESE	SSE	37	-
May-2017	8	2.9	SE	SSE	8	20.4
Aug-2017	5	3.6	SE	SE	12	17.4
Sep-2018	4	2.4	SSE	SSE	22	6.3
Mar-2019	4	2.6	SE	SE	20	9.9
Jul-2019	7	3.4	SE	SSE	36	25.7
*Wave data from the offshore ERA5 hindcast is used						

After analyzing this data the following recurring patterns are identified by linking the wave data with the coastal impact in terms of both erosion and accretion (beach recovery):

- At the location of Cross Section 5 of the beach higher erosion rates are found compared to other parts of the beach. This part of the beach has a smaller beach width on average from which it can be concluded that this part of the beach is most vulnerable to erosion. This is confirmed in the previous section where the impact of the July 2019 extreme wave event is clearly highest at this part of the beach.
- Periods of high waves with SE origin have the most impact on the beach, especially at cross section 5 of the beach. When waves origin more from the east this part of the beach is less protected by the Southern headland and this results in local wave convergence.
- The erosion is caused by a period of waves around and most of the times higher than 2 meters in combination with a SE orientated average wave direction. In the studies done before the nourishment in 1970 it was concluded that waves higher than 2 meters cause recession and waves lower than 2 meters rebuild the beach to its equilibrium state (Vera-cruz, 1972). This is in accordance with the patterns that arise from the data in this chapter.
- The duration of the wave events varies from in between 4 and 8 days. This duration is determined as the period of time where the waves frequently exceed 2 meters.

3.4 Post-storm beach recovery

With regards to the health of the beach, recovery is an essential process in keeping a long-term sustainable beach state. As concluded in previous chapters, there is a clear cyclic behavior of Copacabana beach where frequent storm events in the winter months cause coastal erosion and afterwards, on the timescale of weeks, the beach shows full recovery in terms of coastline position. The long-term stability of the beach shows minor indication of structural beach losses or decay, which indicates that structural losses due to extreme events are minimal and the beach often fully recovers (see Chapter 2.2 for the full background on long-term beach dynamics). A clear example showing the beach recovery is the July 2019 erosion event where beach width erosion of up to 40 meters was recovered within the period of a month. In Figure 33 one can clearly see that the period of high waves caused the erosion of the beach. The period of recovery is characterized by smaller sized waves in the range of 0.5 to 2.5 meters. The peak period of the waves is considered to be higher than 10 seconds for the largest part of the recovery period.

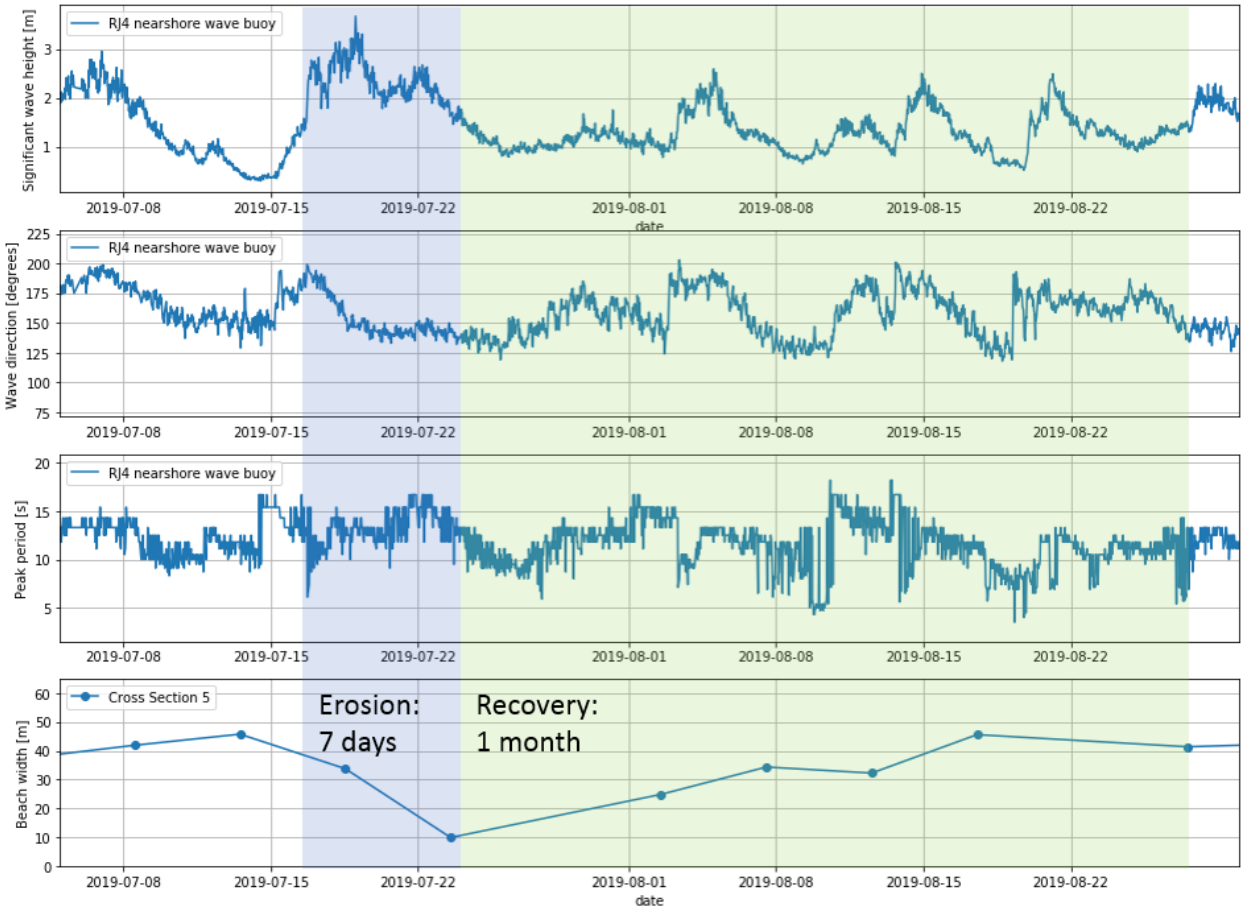

Figure 33: Wave characteristics and beach width of cross section 5 during and after the July 2019 extreme wave event. With the period of erosion marked in blue and the period of recovery marked in green.

The images below, all taken within a period of 4 years show the same location along the beach. In the previous chapter, it was already discussed that the July 2019 erosion event eventually caused a lowering of the beach level (equal to 5 steps) on the backbeach which is visible when observing the amount of steps that access the kiosk. From this it can be concluded that recovery of the backbeach after the erosion has not taken place yet as of 16 months after the erosion occurred. A photo taken approximately 16 months after the erosion event shows a similar picture where there is still a structural loss of sediment on the backbeach. From previous available images

accessed with the use of Google Earth it can be concluded that the level of the backbeach shows stable behavior in the years before the erosion event in July 2019. In Figure 34 a) and b) both show a comparable backbeach elevation judging from the kiosk steps. From the picture taken directly after the July 2019 erosion event it can be observed that the original beach level before the erosion exposed 2 steps. Due to the steep beach scarp not able to be sustained this eventually resulted in a reduction of the vertical sand level on the backbeach equal to 5 steps, which is assumed to be about 0.8 meters.

Figure 34: The set of pictures are taken of the same beach kiosk along Copacabana beach showing variations in backbeach elevation. Number of steps visible above the vertical beach level for every image: a) 2.5, b) 2, c) 7 and d) 6/7. Courtesy of Google maps and Han Winterwerp.

3.4.1 Stages of beach recovery

Different stages of beach recovery were defined by Morton et al. (1994) which are forebeach accretion, backbeach aggradation, dune restoration and revegetation. The stages that apply to Copacabana beach are the first and second stage of recovery because of the absence of a dune system. The first stage, forebeach accretion, which in the remainder of this thesis is called beachface accretion (as in Figure 73), is characterized by the onshore directed movement of sand which causes the deposition of sand on the frequently saturated part of the beachface (see Figure 35). This onshore movement causes steepening of the beach in most cases and overall widening of the beach. In the case that the erosion reaches the backbeach, the sand levels on this part of the beach are often not able to reach its original levels during the beachface accretion phase of the recovery. The second stage of the recovery, aggradation of the backbeach, occurs on a much higher timescale than beachface accretion and is predominantly the result of minor flooding of the beach due to the overflow of waves or aeolian transport. In the case of minor flooding of the beach this most often occurs in the next post-storm winter at the earliest. This can result in transport of

sediment both in the offshore (transport from the beachface in the offshore direction) and onshore direction (transport from the beachface to the backbeach) as is visible in Figure 35.

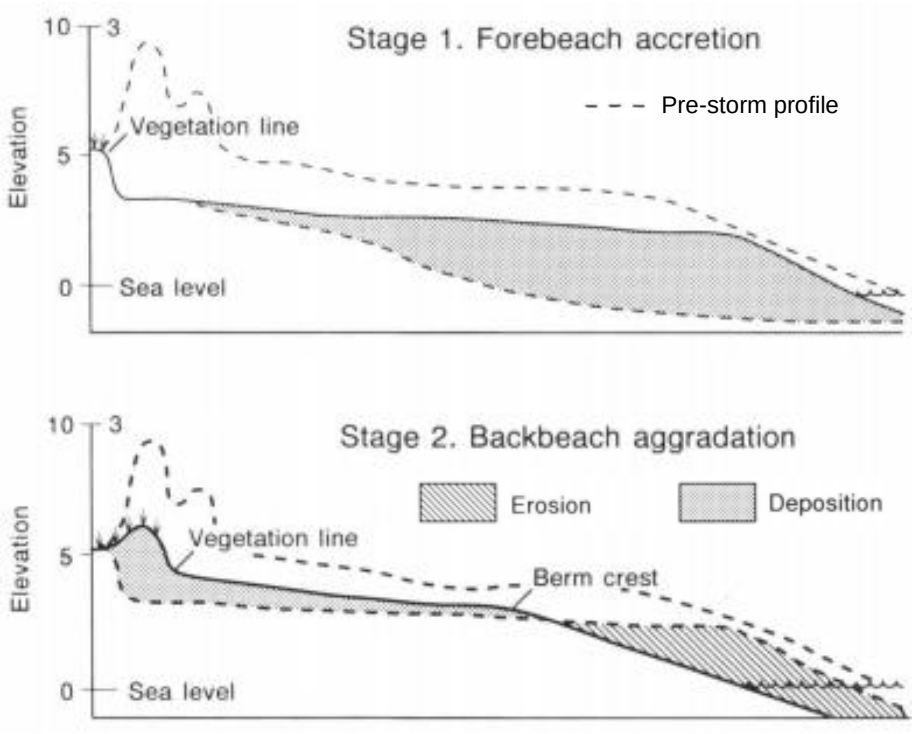

Figure 35: The first two stages of beach recovery (Morton et al., 1994).

Especially the second recovery stage, backbeach aggradation, is not very well understood. An example of such behavior is shown by Otvos (2004) whose research focused on the more frequent occurring hurricanes in the Gulf of New Mexico especially after a major hurricane. This showed that in terms of backbeach recovery the more frequently occurring hurricanes (with lower duration and smaller wave heights) happening after a major hurricane resulted in aggradation of up to 0.9 meters on the backbeach. This supports the theory of Morton et al. (1994) who concluded that flooding of the beach due to wave impact can result in backbeach aggradation. The waves that cause flooding often can be classified as part of a storm (or period of high waves).

When projecting the two different recovery phases on Copacabana beach it is clear that the beachface accretion is very effective and causes rapid recovery in terms of beach width after erosion events. In terms of backbeach aggradation it gets more complicated because of the limited data that is available to show the behavior of the backbeach in terms of vertical elevation levels. There is however no available evidence showing a natural recovery of the backbeach and as of 16 months after the July 2019 erosion event backbeach levels do not show any signs of recovery.

Accretion of the backbeach at Copacabana is likely not to be caused by aeolian transport. The swell-dominated wave climate shows that the influence of local wind on the waves is minimal which makes it unlikely that this is able to cause significant sediment transport on the beach. The second process that could be responsible for backbeach aggradation is minor flooding of the beach as a result of higher waves overflowing the beach. These higher waves can be responsible for erosion but in some cases can cause an accumulation of sand on the backbeach. Take for example Figure 22b, where it is clearly visible that there is an overflow of waves on the beach resulting in deposition of sediment on the backbeach and even on the beach parallel promenade. Under these conditions there is a clear erosion of the beachface in contrary to the accretion on

the backbeach. The occurrence of such conditions is however not common which results in very high timescales for possible recovery of the backbeach. Referring back to Figure 6, which shows a picture of Copacabana beach dating back from the beginning of the 20th century. In this picture part of a dune system can be visible which in the present-day has fully disappeared due to infrastructure. This makes it not possible for the beach to interact with a dune system which often allows for backbeach recovery.

3.4.2 Beach recovery timescales

Timescales of beach recovery can be very different and display strong variations for different field sites. An overview of different field investigations was made by Phillips et al. (2017) showing that the timescale of full beach width recovery ranges from several weeks to years with an average advance of the coastline of 0.04 to 0.16 m/day. The research by Philips et al. focuses on the first stage of beach recovery: beachface recovery. The timescale of recovery is important and influences the vulnerability of a beach. When sequential storms hit the beach the degree of beach recovery is very important in determining the vulnerability of the beach. When the beach is not yet fully recovered from the previous storm the next storm can have an even bigger impact.

At Copacabana beach the erosion timescale is observed to be very low and in the case of the July 2019 extreme wave event the recovery time was equal to a month with a rapid recovery rate up to 1.4 m/day in some locations along the beach, which is almost a factor 10 higher than the average recovery rates found by Phillips et al. (2017). There are few examples that can be found of beaches that show similar average recovery rates. Recovery rates in the same order of magnitude (but somewhat lower) are found in Biscarosse, France where typical recovery rates are 0.3 to 0.5 m/day with recovery rates observed immediately within the days following a storm of up to 3.7 m/day. Next to that, on the east coast of the US two so-called ‘reversing storm hotspots’ are identified that show recovery rates in the order of 1 m/day. Both the examples from the USA and France are located on a part of open uninterrupted sandy coastline with minimal human interventions (Senechal et al., 2015; List et al., 2006). This is significantly different than the embayed Copacabana beach which makes the different cases difficult to compare. Examples of sites with comparable characteristics (embayed beach) as Copacabana beach showing similar recovery behavior can’t be found in the available research. This shows the unique behavior of Copacabana beach with rapid recovery rates.

Phillips et al. (2017) looked into the relation between the rate of recovery and both nearshore wave parameters and sandbar morphodynamics. This research focuses on Narrabeen beach in Australia where a 10-year dataset of daily shoreline and sandbar positions is used. The beach is a 3600 meter long wave-dominated embayed beach which is somewhat comparable to Copacabana beach. The main outcomes of this research was the influence of the cross-shore proximity of the sand bar located at Narrabeen beach. With the sandbar being in close proximity of the waterline, also called an attached sandbar, the beach shows a much higher beach recovery rates compared to a detached sandbar. The figure below shows a conceptual model describing different rates of shoreline recovery under different offshore locations of the sandbar. The sand-bar locations are closely related to the so-called beach states by Wright & Short (1984) whom defined six beach states ranging from fully dissipative to fully reflective beaches (see Appendix A.5 for more information on beach states).

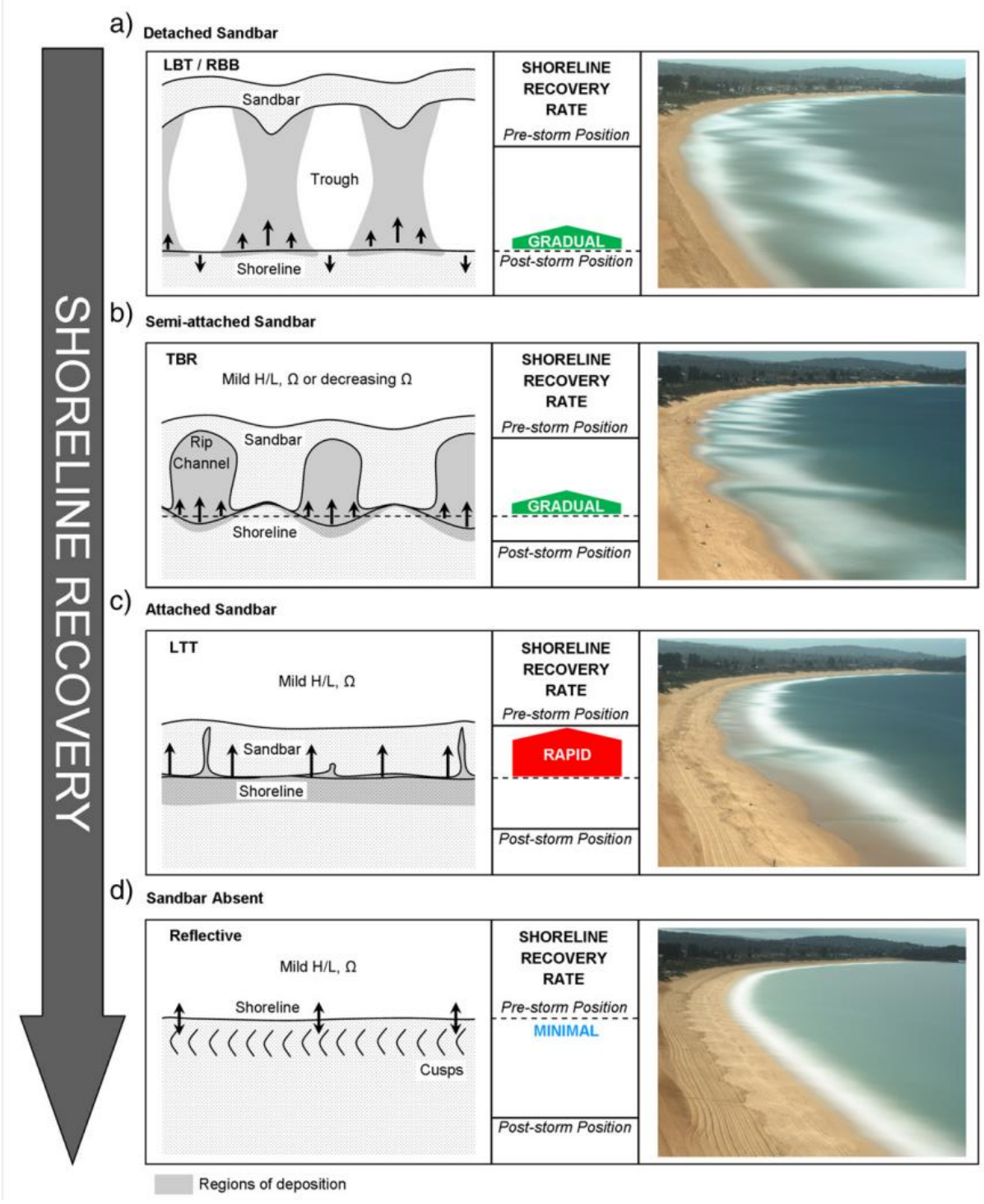

Figure 36: Conceptual model created by Phillips et al. (2017) describing different beach states in combination with shoreline recovery rates. The beach states correspond to the beach states as defined by Wright & Short (1984): LBT / RBB (Longshore Bar-Trough / Rhythmic Bar and Beach), TBR (Transverse Bar and Rip), LTT (Low Tide Terrace).

The correlation of the recovery rates with the dimensionless fall velocity (Ω) is found to be negative. The dimensionless fall velocity is defined as,

$$\Omega = \frac{H_s}{w_s * T_p}$$

With:

- w_s = Sediment fall velocity [m/s]
- D_{50} = Median sediment diameter [m]
- s = Relative density [-]
- ν = kinematic viscosity of water [m^2/s]

The dimensionless fall velocity is related to different morphological states of the beach by Wright & Short (1984). Beaches are defined to be reflective where $\Omega < 1$ and dissipative when $\Omega > 6$. So when the beach is in a more reflective state (low value of Ω) the recovery rates are higher (Phillips et al., 2017). Similar results were found with the investigation of the recovery behavior of 3 beaches in South-Portugal and a beach near Biscarosse, France where more reflective beaches (or closer sandbar proximity) showed higher recovery rates compared to the more dissipative beaches (Sá-Pires et al., 2003; Senechal et al., 2015).

The equilibrium profile of the beach can be approximated using the dimensionless fall velocity with year-round averaged wave conditions. The wave records from the RJ4 nearshore wave buoy are used, because of a higher data frequency compared to the RJ3 wave buoy, and the significant wave height and peak period averaged over the full data range is calculated. By using the sediment fall velocity formula from van Rijn (1993) the following equilibrium dimensionless fall velocity is found for Copacabana beach:

$$\Omega_{eq} = \frac{\bar{H}_s}{w_s * \bar{T}_p} = \frac{1.135}{0.058 * 10.61} = 1.84$$

With:

- w_s $= \frac{10*\nu}{D_{50}} * \left(\sqrt{1 + \frac{0.01*(s-1)*g*D_{50}^3}{\nu^2}}\right) - 1 \ = 0.058 \ m/s$
- D_{50} = Median sediment diameter = $400 \ \mu m$ (Vera-cruz, 1972)
- s = Relative density $\rho_s/\rho_w = \frac{2600}{1020} = 2.55$
- ν = kinematic viscosity of water = $0.000001 \ m^2/s$

According to the relation between different beach states and the dimensionless fall velocity by Wright & Short (1984), the equilibrium profile of Copacabana beach is in the intermediate range where the Low Tide Terrace beach state is most likely to occur (see a full overview of the different beach states in Appendix A.5). This corresponds to an attached sandbar as defined in the conceptual model by Phillips et al. (2017) shown in Figure 36. A picture made during a site visit in December 2019 (see Figure 47) shows a tidal terrace during low tide that matches the beach state description as provided by Wright & Short (1984). The equilibrium beach state at Copacabana beach results in high rates of recovery according to the conceptual model shown in Figure 36.

Next to a clear correlation between the beach state and the rate of recovery, the wave steepness shows clear correlation with the recovery rates. The wave steepness is negatively correlated to the recovery rates. So minor wave steepness causes higher beach recovery rates compared to high wave steepness (Phillips et al., 2017). Overall, swell waves are characterized as high period waves with a mild wave steepness when comparing to wind waves. The wave climate at Copacabana beach is very much swell dominated which is also visible during the recovery period

of the July 2019 extreme wave event. The average peak wave period during the recovery period is equal to 11.5 seconds with an average significant wave height of 1.3 meters.

3.5 Summary

An overview of the main outcomes of this chapter is listed below:

Wave climate:

- The wave climate is swell-dominated with an average significant wave height of 1.14m and an average peak period of 10.6s. The average wave direction is from the SE/SSE where higher wave heights origin more from the South and are focused around the local winter period.
- The wave patterns within Copacabana bay reveal a clear convergence of wave energy in the South of the beach under waves from the SE due to refraction of the waves around a big sand bank in the Southern part of Copacabana bay. For wave originating from the S there is no local convergence and the sheltered diffraction zone in the Southern part of the bay gets bigger.

Storm event characteristics:

- Storms often origin from in between the South and SSE with a duration of 2 to 6 days and are most often swell-dominated with non-significant local winds. Longer periods of extreme waves are often caused by extratropical cyclones moving from west to east over the South-Atlantic ocean.
- The July 2019 erosion event was caused by a 7-day period of extreme waves from the SE with a maximum significant wave height in the offshore dataset of 4.2 meters. With an extreme value analysis it is concluded that storms with this maximum wave height have a return period of 1 year. This return period however does not match the erosional impact of the storm which is less frequently occurring than 1 year according to local perspectives and satellite images. The long duration in combination with the extraordinary wave direction from the SE (resulting in a local convergence of wave energy in the South of the bay) were primarily responsible for the extreme erosional impact.

Beach response during extreme events:

- The biggest erosional impact due to storm events is caused in the Southern part of the beach near cross section 5 (see Figure 17) when extreme waves origin from the SE (erosion event July 2019). Erosion occurs up to 40 meters in this part of the beach.
- The duration of extreme wave events (period where waves frequently exceed a significant wave height of 2 meters) causing significant erosional impact is in between 4 and 8 days.

Post-storm beach recovery:

- A clear example of beachface recovery, which is considered as the first stage of recovery according to Morton et al., (1994), is visible after the July 2019 erosion event where within 25 days the beach reached its original width and the coastline advanced with a total of 35 meters (1.4 m/day).
- The second stage of recovery according to Morton et al., (1994) is the aggradation of the backbeach which did not fully occur as of 16 months after the July 2019 erosion event. Historic pictures show stable behavior of the backbeach in the years before the erosion event. Possible processes that could result in backbeach recovery at Copacabana beach is the overflowing of waves reaching the backbeach (see Figure 22b).

- On average, timescales of beach recovery range from 0.04 to 0.16 m/day. Similar rapid recovery rates as Copacabana beach (1.4 m/day) can occasionally be observed at other beach sites. These however do not have similar characteristics as Copacabana beach. This confirms the above average and unique recovery rates at Copacabana beach.
- The rapid recovery rates can be explained by means of the proximity of the sandbar, which in the case of Copacabana is part of the equilibrium beach state (also called Low Tide Terrace according to the beach states by Wright & Short, (1984)). According to the conceptual model of Phillips et al. (2017) this results in rapid recovery in contrast to a beach state with a detached bar. The same holds for the wave steepness where mild wave steepness results in a faster recovery time in comparison to high wave steepness. With the swell-dominated wave climate at Copacabana beach, insisting a mild wave steepness, this is another reason for the rapid recovery rates.

4 Summary and conclusions: Natural system dynamics

The history of Copacabana beach is marked by on major human intervention which occurred in 1970. This included both a widening of the beach parallel avenue of 55 meters and the widening of the beach by an average of 35 meters. From 1970 onwards the equilibrium profile of the beach shows very stable behavior and a collection of available Landsat satellite images dating back to 1985 do not show any accretive or erosive trends on the beach. The beach is characterized by a more narrow stretch in the South where the average width is around 50 meters in contrast to the North where the beach reaches widths of up to 120 meters. The smaller beach width in the South can be explained by the lack of sand placement in this part of the beach during the nourishment in 1970 (Vera-cruz, 1972).

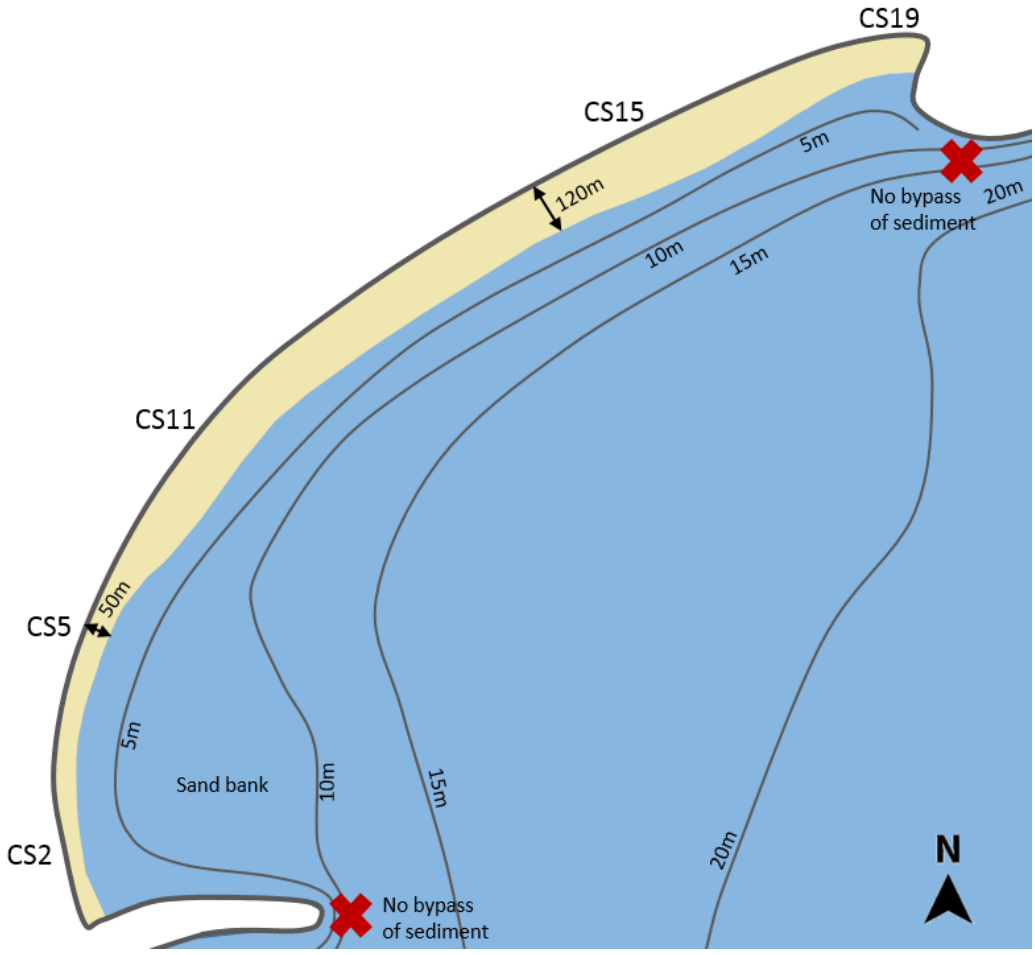

Figure 37: Overview picture showing the long-term equilibrium of Copacabana beach.

Overall it can be concluded that the nourishment in 1970 has been very effective in maintaining sufficient and stable beach area on the long-term. There is no indication of structural loss of sediment and the conclusion can be drawn that the Copacabana bay system is a closed sediment cell with no bypass of sediment around both of the headlands.

In contrast to the long-term stable trend, on the shorter term there are still a lot of fluctuations in coastline position mainly due to erosion related to storm events. This study was initiated after seeing the impact of a recent erosion event which occurred in July 2019 where a 7-day period of high waves caused significant erosion along the beach leaving not more than 10 meters of beach width in some places along the beach as a result of up to 40 meters. Figure 38 below shows the beach width at 5 difference cross sections (see Figure 37 for the locations of the cross-sections) along the beach from 2016 until 2019 extracted from Sentinel 2 satellite images. The sections in the figure denoted with the numbers 1, 3, 4, 5, 6, 8 and 9 are all related to erosion due to storm events. In most cases of erosion there is a rapid recovery where the beach reaches its equilibrium width on the timescale of weeks. The best example of this can be found when looking at the impact of the July 2019 erosion event (see Figure 38).

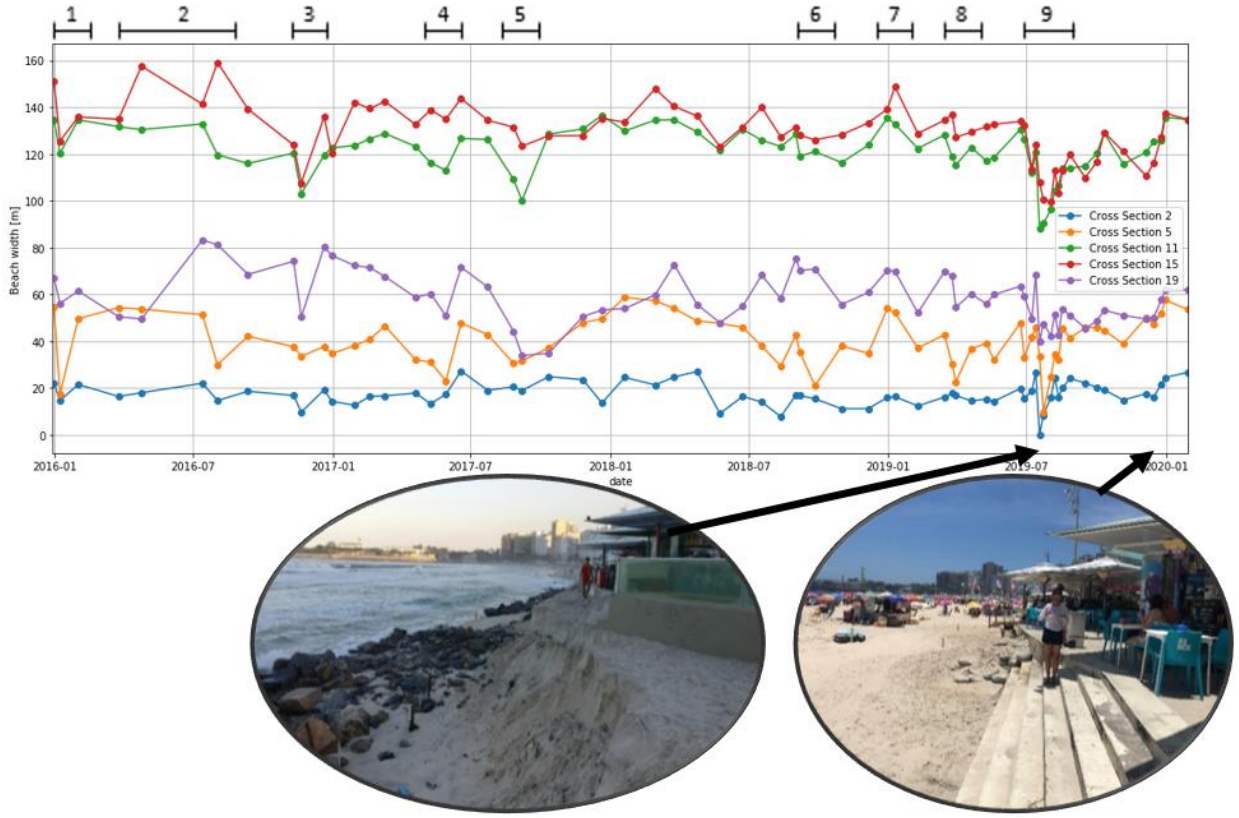

Figure 38: Beach width measurements from 2016 until 2019 derived from Sentinel 2 satellite images for 5 different cross sections along the beach. The numbers 1 until 9 above the figure denote different morphological behavior of the beach.

The wave patterns within Copacabana bay reveal a clear convergence of wave energy in the South of the beach under waves from the SE due to refraction of the waves around a big sand bank in the Southern part of Copacabana bay (see Figure 39). For waves originating from the South there is no local convergence and a bigger sheltered diffraction zone in the Southern part of the bay.

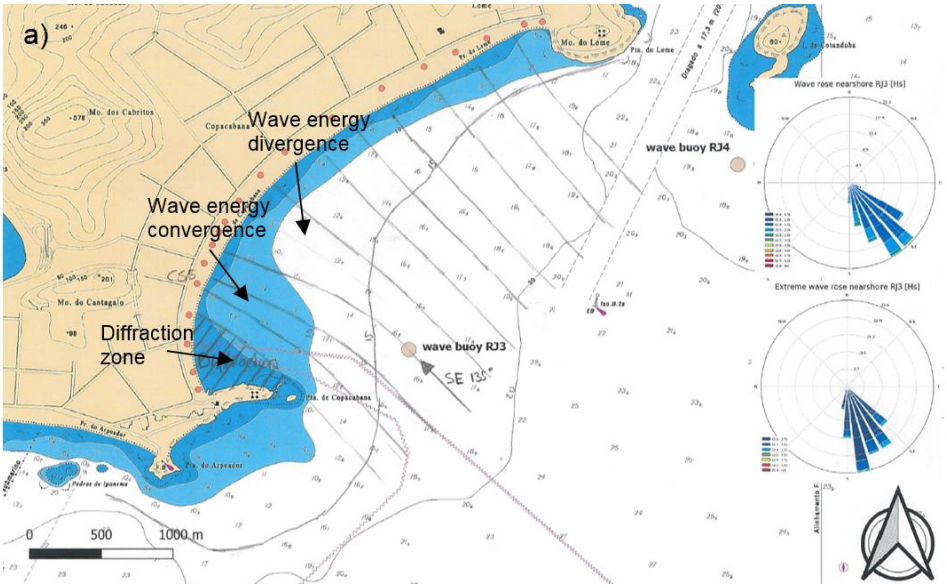

Figure 39: Wave refraction diagram based on Snell's law for a nearshore wave direction of 135 degrees (SE).

From here onwards the 3 research questions are answered which belong to part one of this research looking into the natural system dynamics with use of observations and data analysis.

What are the typical characteristics of storm events and how does this relate to the July 2019 erosion event?

Storm events are characterized by 2 to 7 day periods of swell-dominated waves. The wave direction for these events is often in between the South and SSE. Storm events are often caused by cyclones moving over the South-Atlantic ocean from west to east which at the start of the extreme event causes the highest waves at Copacabana beach to come from the South and with time the wave direction moves towards the SE with decreasing wave heights.

The 40 year long hindcast wave dataset is used for an extreme value analysis. This resulted in a return period of 1 year for the July 2019 extreme wave event judging on the maximum significant wave height (see Figure 40a). The erosional impact was however not of yearly occurrence. Locals indicate that they never seen such erosion before along the beach and the stones which are visible in Figure 40b, which are placed somewhere before the nourishment in 1970 according to local resources, have never surfaced before. The two reasons that this extreme event had such a high erosional impact is related to the duration and the average direction. Especially the direction of the extreme wave event, which origins more from the SE than on average (see Figure 40c), caused Southern part of the beach to be exposed to more wave energy due to the convergence of wave energy as is visible in Figure 39. Next to that, the duration of the extreme wave event was 7 days which high compared to other events with similar maximum wave heights (see Figure 40d).

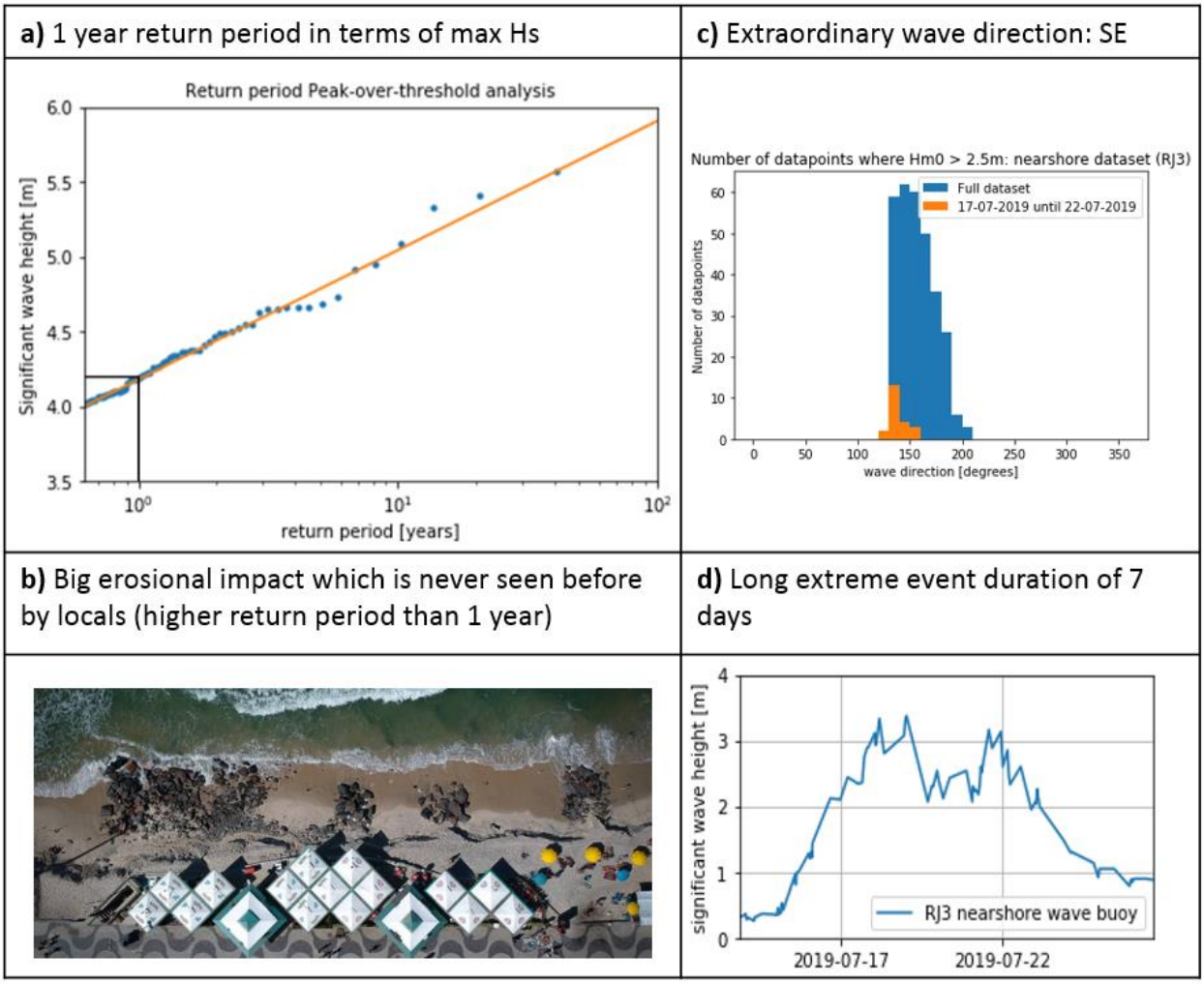

Figure 40: Overview of the characteristics of the July 2019 storm event which caused significant erosion quantities at the beach.

What causes the alongshore difference in storm impact and vulnerability within Copacabana bay?

With the specific orientation of Copacabana beach there is an alongshore difference in wave impact due to refraction patterns caused by local bottom contours and the Southern headland causing a sheltered diffraction zone in the South. Figure 41 below shows the alongshore difference in wave energy under 2 different extreme wave directions: SE and South. From this it can be concluded that especially the Southern part of the beach near Cross Section 5 is most vulnerable to extreme event impact under a SE wave direction. The two important factors in determining the alongshore difference in vulnerability are listed below:

- During the nourishment in 1970 there was relatively low placement of sand in the Southern part of the beach which is the reason for the low equilibrium beach width in this part of the beach. Under extreme wave impact this sooner results in the loss of functionality of the beach as a place of recreation and coastal protection.
- Refraction patterns caused by the local bottom contours results in the local convergence of wave energy in the Southern part of the beach under extreme waves from the SE (see

Figure 41a). This results in higher variability in coastline position relative to the other parts of the beach. The extreme erosion event in July 2019 is a good example of this.

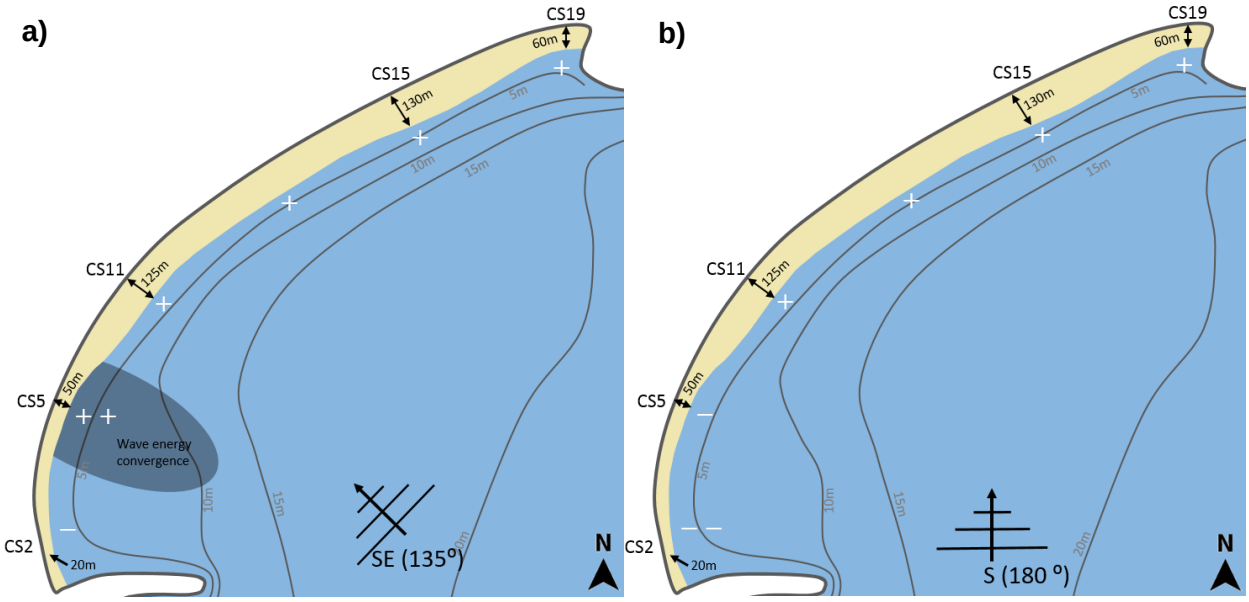

Figure 41: The two pictures above show the equilibrium state of the beach and the alongshore difference in local wave energy levels (where ++ indicates a high local wave energy and - - indicates a low local wave energy) for two different storm event wave directions: a) SE and b) South.

What are the typical beach recovery timescales on Copacabana beach and does the beach show full recovery?

A distinction is made between two different stages of recovery: beachface accretion and backbeach aggradation. Both these processes occur on different timescales. After erosion events there is a clear observation of beachface recovery, which results in widening of the beach as a result of accretion on the beachface on the timescale of weeks with recovery rates up to 1.4 m/day. This is a very rapid rate of recovery and examples show that in most cases this results in a full recovery in terms of beach width after extreme event erosion. The low recovery timescale limits the vulnerability of the beach and the impact of successive extreme wave events. The reason for this rapid recovery of the beachface is the positive relation between the rate of recovery and the equilibrium beach state at Copacabana beach, which is characterized by an attached sandbar. Besides this, mild wave steepness results in high recovery rates, which is the case at Copacabana with a swell dominated wave climate (Phillips et al., 2017).

In terms of backbeach recovery there is less available data to give exact details about the recovery timescale. With observations and insights from literature it can be concluded that the process of backbeach aggradation usually occurs on the timescale of years or does not eventually lead to full recovery (Morton et al., 1994). As of 16 months after the occurrence of the July 2019 erosion event no recovery of the backbeach has taken place yet judging from photos at Copacabana beach. This leaves the Southern part of the beach in a vulnerable state in the case an event occurs with comparable wave direction and severeness as the July 2019 erosion event.

Part 2: The use of a numerical model to assess the vulnerability of the beach

5 Beach vulnerability assessment: XBeach model

This goal of this chapter is to see if a numerical model can be used to assess the vulnerability of the beach. After the definition of the term beach vulnerability the modelling approach is explained which uses scenario modelling. XBeach is used to simulation the July 2019 storm event with subsequent recovery period which is chosen because most data is available related to this storm event. Important factors when judging about the possible vulnerability assessment with use of a numerical model is dependent on factors like data availability, model applicability, model validation and the sensitivity of the model. Details on all these factors and their shortcomings are extensively discussed and explained to eventually be able to answer the question if a numerical model can be used for a vulnerability assessment.

5.1 What is beach vulnerability?

Coco et al. (2014) defined the vulnerability of the beach to be: 'The potential of the beach to be affected by a major storm'. This definition confirms that an important factor in the behavior of the beach is the impact of storm events and the way they affect the beach. This definition of beach vulnerability is also used in this thesis as the storm events are the main reason for increased beach vulnerability and problems on the beach. The beach can be affected in multiple ways. In the case of Copacabana beach, storm events can have the following effects on the main functions of the beach:

- Copacabana beach is a popular tourist attraction and income is generated by local residents for example by restaurants and bars on and around the beach, the rental of beach equipment and recreational activities. This can be highly affected by the impact of storm events which causes a decrease in beach area leaving less room for beach usage. Besides this, beach features like beach scarps can be dangerous for beach users. Referring back to the impact of the July 2019 extreme erosion event, which is visible in Figure 30, it is clearly visible that on this part of the beach there is less room for recreational activities. When speaking to the people working at the kiosk visible in this image, the kiosk had to go out of service for 4 days because the possible danger of the beach erosion to the kiosk infrastructure.
- Besides the beach being a big source of income for the city of Rio de Janeiro and especially the Copacabana neighborhood, one of the main functions of the beach is coastal safety. Simply said, the ability of the beach to protect the inland against the force of the ocean. In the case of Copacabana beach the main infrastructure that can possibly be affected by the impact of storm events are the beach kiosks, promenade and road along the beach.

Altogether, the storm impact on Copacabana beach can cause significant negative economic impact on the beach. Both the recreational use of the beach together with the coastal safety can be negatively affected. These two beach functions are considered to be the main indicators for beach vulnerability. The two main parameters which influence these vulnerability indicators are the volume and the width of the beach. These two parameters are used in the remainder of this thesis when drawing conclusions about beach vulnerability.

The impact of a storm and its influence on the vulnerability of the beach depends on multiple factors related to both beach morphodynamics and- hydronamics. In Figure 42 an overview is shown of factors that influence the vulnerability of the beach created by Eichentopf et al. (2019).

Figure 42 Key factors in determining the vulnerability of the beach (Eichentopf et al., 2019).

Each of these factors is discussed below:

Wave conditions during storm and recovery:

In previous chapters the hydrodynamic characteristics during both storm and recovery were already discussed in terms of wave height, wave direction and wave period. In this analysis especially the wave direction is of high importance during storms. Wave conditions during recovery consist of year-round average wave conditions which seems to cause a high recovery rate.

Duration of storms and recovery:

The longer the storm duration, the higher the impact on the beach is expected to be. After storms, recovery often occurs. The duration of this recovery is important because this influences the period of time that the beach is in a more exposed condition.

Storm frequency:

Again, in relation to the cyclic behavior of the beach where storms are followed up by periods of recovery, the frequency of storms is an important factor. When two major storms occur in close sequence the beach could not have had sufficient time to recover which could lead to an increased storm impact.

Beach state prior to storms:

The beach state prior to storms depends on all 3 of the previously mentioned factors. When the beach state prior to a storm has a ‘smaller than average’ beach width for example due to a sequence of storms or a not yet full beach recovery after the prevailing storm this causes a significant increase in beach vulnerability.

5.2 Modelling approach

In the previous section it was concluded that the main factors that affect the beach and its vulnerability are related to the storm impact and subsequent recovery. This is also concluded in chapter 3 where the main dynamics of the beach are related to the subsequent erosion and

recovery during and after storm events. To test the vulnerability of the beach to changing conditions during storm and recovery one storm and recovery cycle is modelled.

The storm of July 2019 was a recent example of a high impact erosion event. Information on this extreme event is available in the form of pictures, satellite images (before, during and after the extreme events), two nearshore wave buoy records and a beach survey approximately 4 months after the extreme events. Besides, it was concluded before that the storm events which origin from the SE cause the highest impact on the beach, especially when comparing to the Southern wave direction. Where in terms of wave characteristics the biggest part of energetic waves origin from the South these waves are not responsible for the most significant impact on the beach. Large variations in beach width can for the largest part be coupled to a period of high waves from the SE which can be observed on a yearly basis (see Table 3). The recent July 2019 extreme erosion event is a clear example resulting in significant impact on the beach. With regards to validation of the model and the representative conditions that cause the large part of beach width variations, this recent erosion event is chosen as the main focus for the modelling because of the higher availability of data during and around this extreme event.

The wave conditions during both the July 2019 storm event and recovery period are shown in Figure 43 below. Timescales of modelling are a total of 7 days of erosive conditions and 30 days for the recovery period with year-round averaged conditions.

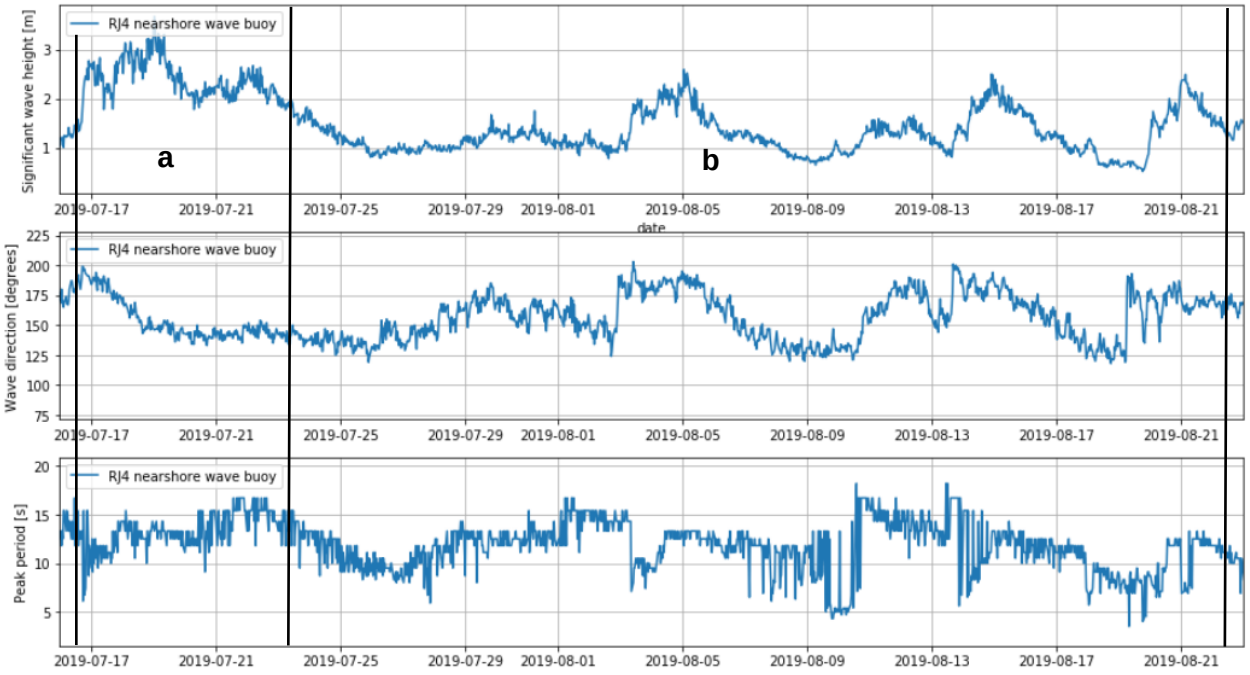

Figure 43: Wave conditions used in the XBeach simulation for both the July 2019 storm event (a) and subsequent recovery period (b).

Using the July 2019 erosion event as the base case the following model runs are performed in the remainder of this chapter to test the vulnerability of the beach:

Table 4: Different model scenarios for testing beach vulnerability.

Goal	Model run
Test the influence of storm frequency	July 2019 storm: - Run similar storm while taking the initial beach profile after 4 weeks of recovery.
Test the influence of different wave conditions during storm (storm severeness)	July 2019 storm: - Increase in Hs - Changes in wave direction - Increased storm duration
Test the influence of different wave conditions on recovery rates/timescales	Post-storm recovery: - Increase/decrease in Hs - Varying wave steepness - Decreased recovery duration

Analysis and comparison of the model results for the different scenarios is performed using the following model output:

- *Beach width:* Comparing the coastline position for the different runs gives information about the erosion quantities at Copacabana beach including alongshore differences.
- *Beach volume:* To get a clear indication of the total eroded/accreted volume. The beach volume is taken equal to the volume of sand which is above the MSL and considered to be part of the beach.
- *Alongshore transport quantities:* By defining different alongshore cells, the difference in alongshore transport of sediment can be compared for the different scenarios.

The beach width and beach volume both before and after the erosion and recovery are used to be able to draw conclusions about beach vulnerability. As discussed in the previous section, these two parameters have a direct relation with the two main functions of the beach: area for recreation and coastal protection. For this cause the beach is sub-divided into multiple sections in order to differentiate in the alongshore direction.

5.3 Choice of model

The goal of the use of a model is to be able to obtain more details about the vulnerability of the beach under various conditions, these conditions are based on the July 2019 storm event and subsequent recovery. From part one of this study it became apparent that the storm erosion and subsequent recovery cycle are an essential in defining beach vulnerability at Copacabana beach. With the help of scenario modelling the relative influence of various key vulnerability factors (as shown in Figure 42) can be further studied and defined. In the case of Copacabana beach there are some important requirements for the choice of the model related to the methodology. These are summarized below:

- In part one of this study it became apparent that there is a clear alongshore difference in equilibrium beach state and the impact of storm events. This is mainly the result of the specific orientation and shape of the beach with for example the sheltered diffraction zone in the South. For this cause it is required to apply a 2D model approach with realistic 2D wave patterns including processes like bottom refraction, wave transformation and diffraction. This allows for realistic 2D model hydronamics and for example the local wave convergence due to bottom refraction to be included (as visible in Figure 27).
- Besides the model hydronamics, the morphodynamics are important related to the storm erosion and subsequent recovery of the beach. in order to draw conclusions about the beach vulnerability the changes in the morphodynamic state of the beach need to be taken into account. With the focus on storm erosion and recovery especially the nearshore

sediment transport processes are important. This implies that the important processes related to nearshore sediment transport processes need to be included in the model.
- The timescales of modelling are in the order of weeks. With scenario modelling multiple model runs need to be performed. This requires manageable runtimes which preferably are below 24 hours.

Examples of common process-based numerical models which are used in coastal applications are Delft3D and XBeach. Both models have a different approach and range of applicability. Delft3D has a very wide range of application in for example the simulation of flow, sediment transport and waves. The model can be applied in multiple dimensions (2D or 3D). In the area of nearshore coastal processes Delft3D is less validated and applicable. The XBeach model is originally made to simulate nearshore processes and its primary application is simulation of the coastal response to storm and hurricane conditions. XBeach can be applied in both 1D and 2D.

As the XBeach model mainly deals with nearshore processes, can be applied in 2D and is designed for erosive conditions, this model was chosen to be used in this study. Especially in 2DH computations with a high amount of grid cells the runtime of XBeach can be high. The modelling timescales used in this study are in the order of weeks. With this relatively short modelling timescale the application of XBeach is possible with acceptable model runtimes. The amount of applications of XBeach related to the modelling of recovery conditions is limited, which is also the case for other numerical models. There are however recent examples of successful applications with the use of additional model parameters which shows that there is a possibility of using XBeach for beach recovery simulations (Roelvink & Costas, 2019).

5.3.1 Introduction XBeach

XBeach is an open-source numerical modelling tool which was first introduced by Roelvink et al. in 2009. The model was developed following the extreme occurrences of hurricanes especially during the 2004 and 2005 season in Northern America which raised the need for further analysis and assessment of the impact of such events on the coast. XBeach focuses on nearshore processes and the model includes things like dune erosion, overwashing, wave breaking and surf and swash zone processes. The aim of the model is to simulate processes in different regimes as described by Sallenger (2000), which are the swash, collision, overwash, and inundation regime. XBeach consists of 3 different modes which all use different approaches towards solving the model hydronamics:

- *Surfbeat mode:* In this mode the variation of the short-wave envelope is solved on the wave group scale including the infra-gravity motions. When the focus is on swash zone processes instead of time-averaged currents and setup this mode can best be used.
- *Stationary mode:* This mode solves the wave-averaged equations but neglects all infra-gravity motions. This mode can be applied under moderate wave conditions where the infra-gravity motions are less important.
- *Non-hydrostatic mode:* In this mode individual waves are modelled using the combination of non-linear shallow water equations with a pressure correction term. This mode is able to resolve complex patterns like diffraction around structures but comes with a higher computation time and lower numerical stability compared to the Surfbeat and stationary mode.

In the last years the XBeach model has been used in a lot of different applications and has been validated multiple times using both laboratory experiments and field experiments (e.g. McCall et al., 2010 and Roelvink et al., 2018). Validation of the morphological response for the non-hydrostatic mode hasn't been done as extensively compared to the other two modes. A recent

example shows that the non-hydrostatic model overestimates the bed level changes due to sediment transport (Jongedijk, 2017).

5.3.2 Conclusion

XBeach is used as the main numerical model in this study. The modelling consists of 2 parts: the modelling of an extreme event and the modelling of the subsequent recovery period which is under moderate conditions. Due to the importance of long waves in extreme conditions (see Appendix A.2.8) the Surfbeat mode is used during the extreme conditions. It is chosen not to use the non-hydrostatic mode because it is computationally more expensive and not as well validated as the Surfbeat mode with regards to sediment transport. For the recovery period, the stationary mode is chosen to be used because it is computationally less expensive than the Surfbeat mode. The stationary mode does not include the long waves which, under moderate conditions does not have a significant influence.

5.4 XBeach: processes and model formulations

In the literature study in Appendix A, an overview is made of the main nearshore processes in the coastal zone and how they influence the cross-shore transport. In this section an overview is made of how these processes are included in XBeach to eventually be able to judge about the model applicability for both erosion and recovery.

5.4.1 Wave action balance

As concluded in the previous section both the Surfbeat as the stationary mode are used, where the stationary mode differs from the Surfbeat mode because it does not include the long waves. The short wave action balance is given below. This equation is based on the TU Delft HISWA model (Holthuijsen et al., 1989):

$$\frac{\partial A}{\partial t} + \frac{\partial c_x A}{\partial x} + \frac{\partial c_y A}{\partial y} + \frac{\partial c_\theta A}{\partial \theta} = \frac{D_w + D_f + D_v}{\sigma}$$

With:

- A = Wave action term
- c_x = Wave action propagation speed in x-direction
- c_y = Wave action propagation speed in y-direction
- c_θ = Wave action propagation in the directional space
- σ = Intrinsic wave frequency
- D_w = Wave breaking dissipation term
- D_f = Bottom friction dissipation term
- D_v = Vegetation dissipation term

This equation solves the short-wave envelope on the wave group timescale. This means that the wave height variations within the model vary with the wave group, also considered the short-wave averaged approach. Due to the short-wave averaging the diffraction process is not included in the model because this is a process that occurs on the short-wave timescale. Included in this wave action balance are the processes of shoaling and directional spreading. The wave dissipation terms used in the model are for wave breaking (D_w), bottom friction (D_f) and vegetation (D_v). The propagation speed in the directional space (c_θ) is included in the wave action balance as follows:

$$c_\theta(x,y,t,\theta) = \frac{\sigma}{\sinh(2kh)}\left(\frac{\partial h}{\partial x}sin\theta - \frac{\partial h}{\partial y}cos\theta\right) + cos\theta\left(\frac{\partial u}{\partial x}sin\theta - \frac{\partial u}{\partial y}cos\theta\right) + sin\theta\left(\frac{\partial v}{\partial x}sin\theta - \frac{\partial v}{\partial y}cos\theta\right)$$

With:

- c_θ = Propagation speed in the directional space
- σ = Intrinsic wave frequency
- k = Wave number
- h = Local water depth
- θ = Angle of incidence with respect to the x-axis

This equation includes both wave refraction due to differences in bottom depth (first term) and wave refraction due to currents (second and third term).

5.4.2 Dissipation

Wave breaking:

The wave breaking formulation by Roelvink (1993) is used to account for the variations in wave energy due to wave breaking. The approach of this wave breaking formulation is the use of the fraction of breaking waves (Q_b) multiplied by the dissipation per breaking event. The fraction of breaking wave is calculated using the ratio between the root mean squared error wave height (H_{rms}) and the maximum wave height (H_{max}). The maximum wave height is defined as the wave height where wave breaking starts to occur. For defining this maximum wave height a breaker index γ is used.

$$\bar{D}_w = 2 * \left(\frac{\alpha}{T_{rep}}\right) * Q_b * E_w \; and \; Q_b = 1 - \exp\left(-\left(\frac{H_{rms}}{H_{max}}\right)^n\right)$$

With:

- $\bar{D}_w$ = Wave breaking dissipation term
- α = Wave dissipation coefficient
- T_{rep} = Representative wave period
- Q_b = Fraction of breaking waves
- E_w = Energy of the wave
- H_{rms} = Root-mean-square wave height
- H_{max} = Maximum wave height
- n = Ratio of group velocity and phase velocity

Roller model:

After waves start breaking there is temporal storage of shoreward directed momentum in the so-called surface rollers. Including of the effect of surface rollers is important to include the often found delay between the location of the waves breaking and the point where the longshore current and wave set-up starts to build. This roller model is basically an addition to the radiation stress in the breaker zone.

Turbulence:

When waves break there is a high amount of turbulence within the water column. This can cause an increased amount of suspended sediment when this turbulence reaches the bed. This is

accounted for in XBeach with the use of a turbulence model. This allows transport of the turbulence from the water surface (where the waves break) to the bed which causes the stirring up of sediment. The model uses an exponential decay from the water surface to the bed to determine the turbulence near the bed:

$$k_b = \frac{\overline{k_s}}{\exp\left(\frac{h}{L_{mix}}\right) - 1}$$

With:

- k_b = Turbulence variance at the bed
- $\overline{k_s}$ = Wave-averaged turbulence energy
- h = Local water depth
- L_{mix} = Mixing length

Bottom friction:

The short wave dissipation due to bottom friction is included in the model as follows:

$$D_f = \frac{2}{3\pi} * \rho f_w \left(\frac{\pi H_{rms}}{T_{m01} \sinh(kh)}\right)^3$$

With:

- D_f = Short wave dissipation by bottom friction
- ρ = Density
- f_w = Short-wave friction coefficient
- H_{rms} = Root-mean-square wave height
- T_{m01} = Mean wave period
- k = Wave number
- h = Local water depth

In this formulation f_w is the short-wave friction coefficient, this coefficient is not related to the bed friction in the flow equations.

5.4.3 Radiation stresses

The radiation stresses in the model are defined as the following:

$$S_{xx,r}(x,y,t) = \int \cos^2\theta S_r d\theta$$
$$S_{xy,r}(x,y,t) = S_{yx,r}(x,y,t) = \int sin\theta cos\theta S_r d\theta$$
$$S_{yy,r}(x,y,t) = \int \sin^2\theta S_r d\theta$$

With:

- $S_{xx,r}$ = Radiation stress, x-component
- $S_{xy,r}$ = Radiation stress shear component
- $S_{yy,r}$ = Radiation stress, y-component
- θ = Angle of incidence with respect to the x-axis
- S_r = Radiation stress

The radiation stress can also be considered as the variation in wave energy in the model domain. The radiation stress, among other things, is influenced by the bottom friction, wave height, wave breaking and the surface rollers. The gradients in radiation stress drive wave-driven currents like longshore currents, rip currents and undertow. These gradients also drive the long wave motions (bound and free) including the runup and rundown of the long waves in the swash zone. These motions are solved by the shallow water equations which are discussed in the next section.

5.4.4 Shallow water equations

The shallow water equations translate the forcing due to wave into mean flow components. This includes undertow, long waves and wave set-up and set-down. The depth-averaged Generalised Lagrangian Mean formulation are used for this purpose. The GLM-momentum equations are given below:

$$\frac{\partial u^L}{\partial t} + u^L * \frac{\partial u^L}{\partial y} + v^L * \frac{\partial u^L}{\partial y} - f v^L - v_h \left(\frac{\partial^2 u^L}{\partial x^2} + \frac{\partial^2 u^L}{\partial y^2} \right) = \frac{\tau_{sx}}{\rho h} - \frac{\tau_{bx}^E}{\rho h} - g * \frac{\partial \eta}{\partial x} + \frac{F_x}{\rho h} + \frac{F_{v,x}}{\rho h}$$

$$\frac{\partial v^L}{\partial t} + u^L * \frac{\partial v^L}{\partial y} + v^L * \frac{\partial v^L}{\partial y} - f u^L - v_h \left(\frac{\partial^2 v^L}{\partial x^2} + \frac{\partial^2 v^L}{\partial y^2} \right) = \frac{\tau_{sy}}{\rho h} - \frac{\tau_{by}^E}{\rho h} - g * \frac{\partial \eta}{\partial y} + \frac{F_y}{\rho h} + \frac{F_{v,y}}{\rho h}$$

$$\frac{\partial \eta}{\partial t} + \frac{\partial h u^L}{\partial x} + \frac{\partial h v^L}{\partial y} = 0$$

With:

- u^L, v^L = Langrangian velocities
- f = Coriolis coefficient
- τ_{sx}, τ_{sy} = Wind shear stresses
- τ_{bx}, τ_{by} = Bed shear stresses
- F_x, F_y = Wave-induced stresses
- $F_{v,x}, F_{v,y}$ = Stresses induced by vegetation
- ρ = Density
- g = Gravitational acceleration
- h = Local water depth

In these equations the u^L and v^L are the Lagrangian velocities consisting of the Eulerian velocity in combination with the Stokes drift velocity. Furthermore, τ_{bx} and τ_{by} are the bed shear stresses, F_x and F_y are the wave induced stresses related to the gradients in radiation stresses, v_h is the horizontal viscosity and f is the effect of Coriolis.

5.4.5 Sediment transport

Modelling of the sediment concentrations in the water is performed using the depth-averaged advection-diffusion equations. In this formulation the entrainment and deposition of sediment is determined by the difference between the equilibrium sediment concentration (C_{eq}) and the actual sediment concentration (C).

$$\frac{\partial hC}{\partial t} + \frac{\partial hC(u^E - u_a \sin\theta_m)}{\partial x} + \frac{\partial hC(v^E - u_a cos\theta_m)}{\partial y} + \frac{\partial}{\partial x}\left[D_h h * \frac{\partial C}{\partial x} \right] + \frac{\partial}{\partial y}\left[D_h h * \frac{\partial C}{\partial y} \right] = \frac{hC_{eq} - hC}{T_s}$$

With:

- C = Depth-averaged sediment concentration

- D_h = Sediment diffusion coefficient
- T_s = Adaptation time
- h = Local water depth
- w_s = Sediment fall velocity
- u^E, v^E = Eulerian velocities
- u_a = onshore directed velocity

Effects of wave non-linearity:

As the hydronamics of the model are solved on the wave group timescale, the short-wave motions are not included in the model. The wave energy is therefore averaged over the wave length. To include the effects on sediment transport of the non-linearity (both skewness and asymmetry) of waves, an extra onshore sediment transport term is added. Wave non-linearity causes an onshore directed cross-shore sediment transport component (see Appendix A.3). This is taken into account within the model as an cross-shore velocity component which is included in the advection diffusion equation shown above.

A discretization for the skewness and asymmetry was introduced by van Thiel de Vries (2009). In this function the u_a is calculated based on both the wave skewness (S_k) and wave asymmetry (A_s) multiplied by the mean root squared velocity (u_{rms}) and the calibration factors f_{Sk} and fac_{As}. The two calibration factors can be set using the keyword *facua* in XBeach.

$$u_a = (f_{Sk}S_k - f_{As}A_s)u_{rms}$$

Bed slope effect:

The influence of the bed slope on the local hydronamics is not considered in XBeach. For this purpose the Bermslope model was introduced by Roelvink & Costas (2017). This model forces the cross-shore slope in the swash zone to be forces to a pre-defined equilibrium bed slope. In Surfbeat this is applied where H/h < 1 and in stationary mode for h < 1m. This mode has been tested. Van Dam (2019) found that the Bermslope model significantly improves the prediction of berm growth during periods of recovery. However, during episodic erosion events the Bermslope model resulted in onshore transport which caused the erosion not to be captured in the model. The Bermslope model has also been tested by Roelvink & Costas (2019) on a case study at Praia de Faro in Portugal, resulting in good reproduction of erosion and accretion processes and showed the importance of the beach berm.

$$q_{bermslope,x} = f_{bermslope}Cv_{mag}h\left(\frac{dz_b}{dx} - bermslope\right)$$

The Bermslope model gives an additional cross-shore transport component ($q_{bermslope,x}$) dependent on an calibration factor $f_{bermslope}$, the sediment concentration (C), the velocity magnitude (v_{mag}), the water depth (h) and the instantaneous local bed slope ($\frac{dz_b}{dx}$).

5.5 XBeach: applicability of the model

Within the model formulations there are some limitations with regards to the simulation of the essential coastal processes during erosion and recovery. In this section a comparison is made between the model formulations in the previous section and the literature study in Appendix A to be able to draw conclusions for the applicability of the model for the simulation of erosion and recovery.

Wave transformation:

With regards to the transformation of waves from offshore to the nearshore the refraction due to both currents and bottom depth is included in the model. Diffraction is however not included in the Surfbeat and stationary mode of XBeach. This calls for a short-wave resolving model setup (e.g. XBeach non-hydrostatic mode) which is too computationally expensive and not yet fully validated. This is thus a shortcoming of the model which especially influences the wave patterns in the Southern part of the bay where the waves in reality diffract around the Southern headland.

Changes in the wave shape are not fully included in XBeach where only the short-wave envelope is solved which includes an increase in wave height due to the shoaling of waves. Due to the short-wave averaged formulations the hydronamics in XBeach does not include the non-linearity of waves (both asymmetry and skewness). This sediment transport component is included in XBeach in the form of an additional onshore directed mean current which can be calibrated with the *facua* parameter. This factor is considered as one of the more important model calibration factor which has the most significant impact on both the accretion (during recovery) and erosion amounts in the model (Bugajny et al., 2013). This is in line with Appendix A.3, where the wave non-linearity is found to be the main forcing that causes significant onshore transport which balances the offshore directed cross-shore transport mainly due to undertow. Recent studies show a relationship of the *facua* parameter with the bed slope (Elsayed & Oumeraci, 2017). This improves the calibration process of the onshore transport component due to wave non-linearity. It must however be said that the *facua* term is based on a single onshore direct velocity component which in then multiplied by both wave skewness and asymmetry. As shown in Appendix A.3, there are clear cross-shore differences in the dominance of both the velocity skewness and acceleration skewness which results in either transport due to bed shear stresses or pressure gradients. These processes are considered to be essential in the accurate modelling of onshore directed transport (Fernández-Mora et al., 2015). These physical processes having a clear impact on especially the onshore movement of sediment are not included in the XBeach model formulations. It must be noted that the *facua* model is a simplified onshore directed transport term that does not include the physics as just discussed related to the orbital wave motions in combination with both velocity and acceleration skewness.

Wave breaking is applied in the model with the Roelvink (1993) formula in combination with a roller model for the modelling of the dissipation due to wave breaking and taking into account the energy transport by the wave rollers.

In the nearshore zone, the return flow of the waves is very important especially during the erosion, this phenomena is also called undertow. This process is included the XBeach model within the Surfbeat mode.

Swash zone processes:

The main point of notice with regards of the swash zone processes is that short wave run-up and run-down is not included in the XBeach model. This is due to the short-wave averaged approach. What is included in the Surfbeat mode is the run-up and run-down of the long waves. In the case of dissipative beaches this approach is fully valid because of the almost fully dissipated short wave energy in the swash zone. In the case of more intermediate beaches, which is the case for Copacabana beach, short-wave run-up is more important but these motions are mostly within the range of the long wave run-up and run-down during erosive conditions. The stationary mode does not include any wave run-up processes but does include wave set-up and set-down.

Table 5: Overview of the important processes in the nearshore zone related to both beach recovery and erosion and how they are included in the XBeach model.

	Model applicability	Details
Wave transformation		
Refraction	++	Included in the wave-action balance (both refraction due to currents and bottom contours).
Diffraction	- -	Not included in both the stationary and Surfbeat mode.
Shoaling	++	Included in the wave-action balance.
Wave non-linearity	+-	Not included in the model hydronamics. Effects on sediment transport included as an onshore directed cross-shore current included in the advection-diffusion equation (*facua*).
Wave breaking	++	Dissipation due to wave breaking is included using the well-validated breaking formulation by Roelvink (1993).
Undertow	++	Included in the shallow water equations where the wave forcing is translated into flow components.
Long waves		
Long waves (stationary mode)	- -	Not included.
Long waves (Surfbeat mode)	++	Both bound and free long waves are included in the Surfbeat. These motions are solved by the shallow water equations.
Swash zone processes		
Long wave run-up	++	In the Surfbeat mode long wave run-up is included and solved by the non-linear shallow water equations.
Short wave run-up*	- -	With the short-wave averaged Surfbeat and stationary mode the short-wave run-up is not included.
Bore turbulence*	+-	The translation of the turbulence from the surface to the bottom to account for increase stirring up of sediment is taken into account using an exponential turbulence model. This effect is however still limited in the swash zone due to the short wave run-up not being taken into account.
In- and exfiltration*	+-	In- and exfiltration of water in and out of the bed can be computed by XBeach. This effect is however still limited in the swash zone due to the short wave run-up not being taken into account.
Settling and scouring lag*	+-	Settling lag is included using the sediment fall velocity in the water column. Scouring lag, which is related to differences in flow acceleration during run-up and run-down is not included in the model.
***The Bermslope model can be used to account for the missing onshore transport components (process-base) in the swash zone.**		

The final judgement with regards to the applicability of XBeach can be made for both the modelling of beach erosion and beach recovery. As explained in previous sections, the modelling approach consists of 2 different setups where the Surfbeat mode is used for extreme erosive conditions (extreme event July 2019) and the stationary mode is used for the modelling of the prevailing recovery period under moderate wave conditions.

The applications of XBeach with regards to extreme/erosive conditions are very widespread and validation of the model with regards to extreme conditions is performed for many different case studies over the last years (e.g. McCall et al., 2010 and van Thiel de Vries, 2009). With the forcing of the free and bound long waves, which is an important factor with regards to beach and dune erosion, the extreme event erosion is able to be well predicted by XBeach. The run-up and run-down of the short waves, which is not included in the model, is mostly within the ranges of the run-up and run-down of long waves. With this given, the long waves are important with regards to beach and dune erosion and are able to reproduce realistic erosion patterns (van Thiel de Vries, 2009). Important coastal processes like undertow are very important during beach erosion and are well included in the XBeach model.

In Appendix A.4 it was concluded that the most important processes related to beach recovery, or onshore directed sediment transport, are the bore turbulence, in- and exfiltration, settling and scouring lag and sediment advection. These processes are all related to the wave run-up and run-down cycle and pinpoint the importance of the interaction between the swash zone and the subaquatic part of the beach profile during beach recovery. As said before, in both the stationary and the Surfbeat mode the wave run-up is not included. This causes limited interaction between the beach face and the sub-aquatic part of the profile. The stationary mode is chosen for the recovery part of the simulation because the long waves are of less importance during moderate wave conditions. XBeach was originally designed to simulate the impact of extreme events which did not take into account the recovery process. Only few applications can be found where XBeach is used to simulate recovery conditions. In a recent study van Dam (2019) concluded that the standard XBeach model is not able to reproduce the effects of beach recovery. The same conclusion is drawn by Roelvink & Costas (2019), who concluded that due to a lack of representation of the complex swash processes in the model the beach recovery often resulted in a profile with a mild, dissipative slope. A solution to the often found mismatch of the cross-shore profile is found in the Bermslope model as explained in the previous section. This forces the beach slope in the swash zone to a predefined slope to compensate for the effects of the non-included complex swash zone processes. This method is shown to be effective in reproducing a more realistic cross-shore profile with a more reflective/intermediate beach slope (van Dam, 2019 and Roelvink & Costas, 2019).

5.6 Model setup

Grid and bathymetry:

The figure below shows the model domain. The grid is a rectangular grid with varying grid size in both x and y direction varying from 5x5m to 20x40m making it a 2DH model. The finer grid cells are located in the Southern part of the beach and around the Southern headland. This is done to increase numerical stability where wave patterns are more complicated and the bottom gradients are larger. Besides this, the main interest lies with the Southern part of the beach where the erosion hotspot is located. A coarser grid in the offshore area results in a decrease in computation time. The grid extends some distance beyond the headlands to avoid any influence of disturbance at the boundary influencing the wave patterns within the bay. For the recovery simulation the grid is coarsened with a factor 2 to limit the runtime.

Figure 44: XBeach model domain.

The initial bathymetry and beach topography which is used in the model is derived from 2 different field surveys performed at Copacabana beach. The bathymetry was measured on 13-12-2019 using a single beam sonar transducer. The bathymetry was able to be measured for depth contours lower than approximately -3.5m because of the depth limitations of the boat. The path of the point measurements and the measurement equipment is shown in the figure below:

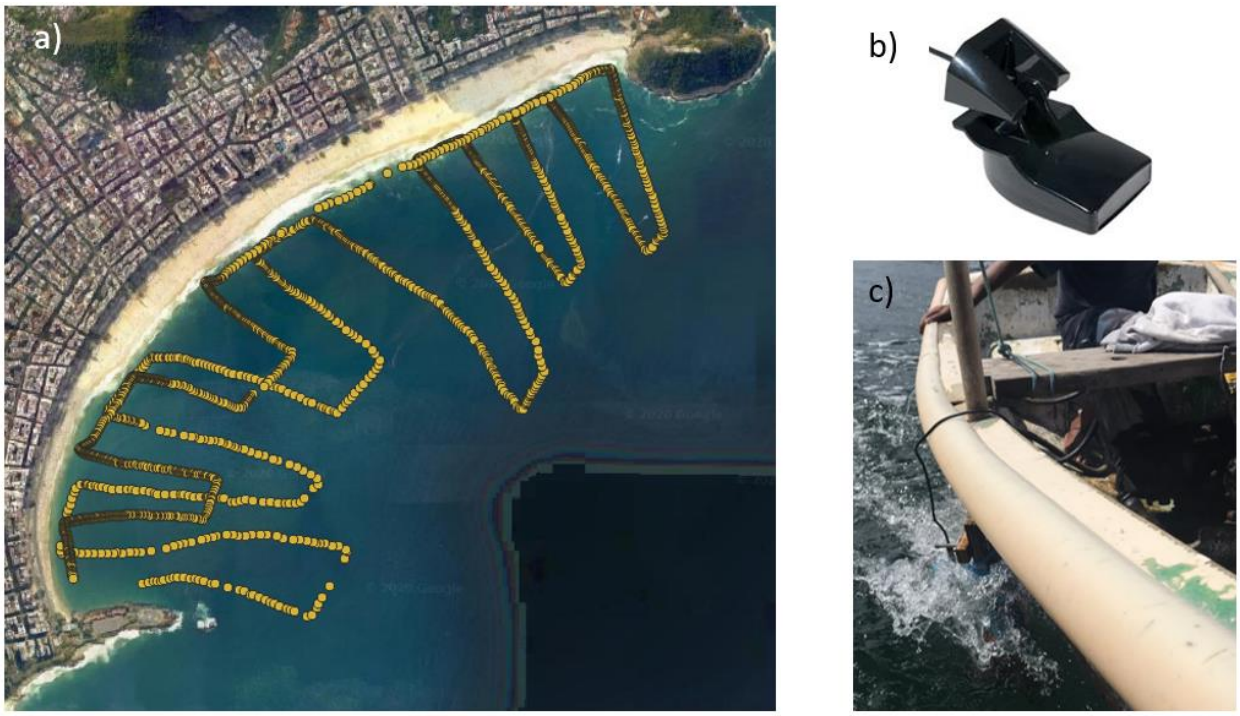

Figure 45: a) The measurement path of the bathymetry measurements. b) The sonar transducer used during the measurements. c) The sonar transducer mounted to the side of the boat at approximately 15 cm under the waterline.

The bathymetry measurements were corrected for the tidal levels at the time of measuring and for the distance of the instrument under the water surface. The measurement equipment was connected to the boat causing the local wave oscillations to be included in the measurements. During the measurements the significant wave height was around 0.7 meters which did not cause significant measuring errors because of the high frequency of point measurements.

Besides the bathymetry measurements, the beach topography for 19 different cross sections along the beach was measured. The cross sections were measured using 2 different kinds of equipment: a Digital GPS device mounted on a walking pole and a total station in combination with a prism. The measurements were performed from the edge of the beach promenade to the waterline. Because of the force of the waves no measurements could be performed of the intertidal part of the beach. The image below shows the locations of the different cross sections together with the measurement equipment.

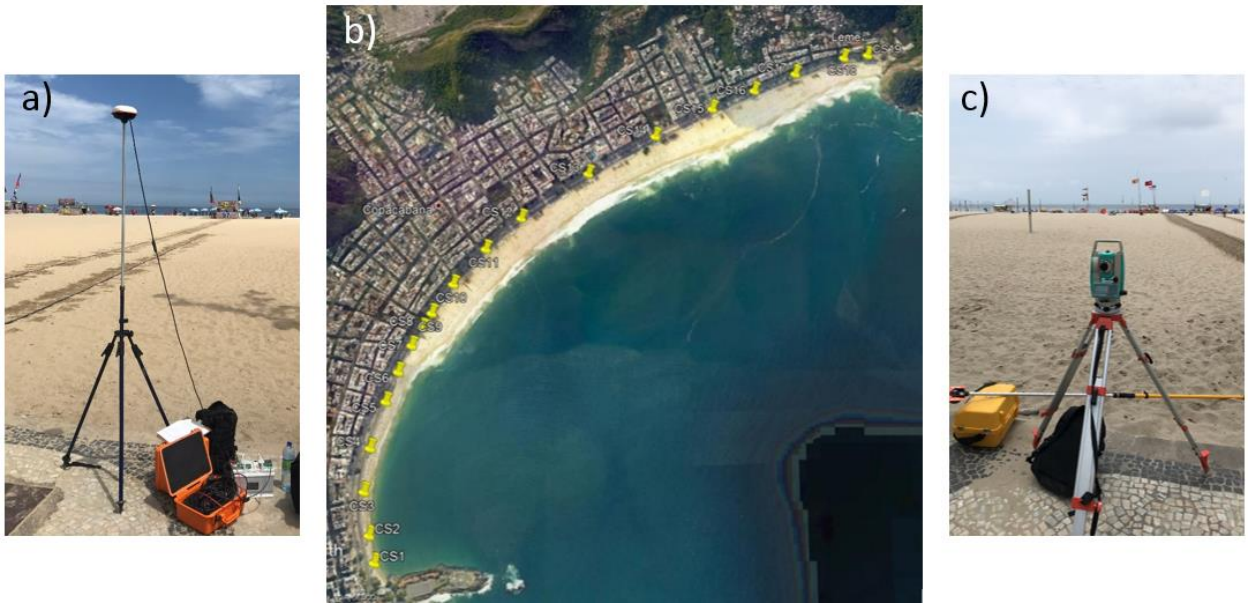

Figure 46: a) The DGPS mounted on a fixed stand. This DGPS functioned as a reference point for the other DGPS which was mounted on a walking pole and used for recording the profile elevations. b) The location of the 19 different profile measurements. c) The total station.

Both the bathymetry and beach topography measurements are vertically referenced to the MSL which is taken equal to 0m. Using QGIS, a geographical information system, contour lines were drawn following the point measurements from both the bathymetry and beach topography. Next to this a digital bathymetry is added with the use of C-MAP, which is a digital database of bathymetric data. Between the 0m contour and -3.5m contour there are no available measurements due to the inability of the available measurement equipment to measure in these water depths. The bathymetry here is approximated using local pictures and observations during the site visit. The clear identification of a tidal terrace along a the Northern part of the beach is included in this part of the bathymetry (visible in Figure 47 below).

Figure 47: Picture taken near the Punta do Leme on the Northern side of the beach during low tide revealing a tidal terrace.

The bottom contours at the outer sides of the headlands are modified from the bathymetry measurements to be alongshore uniform and perpendicular to the boundary. This is done to increase the numerical stability of the XBeach model at the boundary and is suspected not to cause any changes within the system. This is supported by the hypotheses made in Chapter 3 that the system is a closed system and there is no influence from the outside of the headlands.

Wave boundary conditions:

The wave boundary conditions are taken from the RJ4 nearshore wave buoy measurements (see Figure 5 for the location of the wave buoy). The buoy records 30 minutes averaged measurements of the most important wave parameters: significant wave height, peak period and wave direction. The RJ4 wave buoy is chosen above the RJ3 wave buoy because the RJ3 wave buoy has a lower measurement interval due to missing data. This buoy is located near the Northern boundary of the model domain. The waves are forced at the offshore boundary of the model domain which has a water depth ranging from 20 to 25 meters where the RJ4 wave buoy is located at an approximated water depth of ~18m.

The wave boundary conditions are of the spectral type with the use of the JONSWAP spectrum. The shape of the spectrum is defined by the following two parameters:

- γ_{jsp} = Peak enhancement factor [-]
- s = Directional spreading coefficient [-]

The wave buoy measurement are not of the spectral type. That is why it is decided to use the default values for these two parameters in XBeach which are taken equal to 3.3 and 10.

Tides:

The tides are included into the model as a time-varying water level similar along all boundaries. The tidal data is derived from the Deltares Matlab tool: Delft Dashboard with the use of IHO tide model.

Sediment characteristics:

The sediment characteristics are taken from the measurements done before the nourishment in 1970 where the D50 was equal to 400 μm and the dry unit weight of the sand was equal to 2600 kg/m^3 (Vera-cruz, 1972). This is the only available information related to sediment characteristics.

5.7 Model validation

5.7.1 Hydronamics

To validate the hydronamics of the model 2 wave buoys are available within the model domain. The validation is performed separately for the extreme event simulation and the recovery simulation because of the use of different XBeach modes for each of the simulations. The validation process for the model hydronamics is summarized below:

1. The RJ4 wave buoy measurements are used as model input at the offshore model boundary with an average interval of 30 minutes.
2. The model run is performed.
3. The model point output at the location of the RJ3 wave buoy is compared with the physical RJ3 wave buoy data available at this location:
    a. If there is a good match between the model point output and the RJ3 wave buoy data the model is considered to be validated in terms of hydronamics.
    b. If there is not a good match, step 1 through 3 is repeated with an adaptation of the RJ4 wave buoy measurements, in terms of Hs and/or wave direction, which is again directly used as model input at the offshore model boundary. This process is repeated until step 3 results in a good match.

The model input for the significant wave height had to be multiplied by a factor of 1.1 for the first 80 hours of the simulation period and by a factor of 1.2 for the remainder of the simulation (see Figure 48 below). This shows that when waves origin more from the SE a loss of energy is occurring compared to when waves originate from the South. For the wave direction, there was no initial mismatch between the RJ3 buoy measurements and the model point output which shows good model performance in terms of wave refraction. The difference between the original RJ4 wave buoy input and the adapted input after validation is shown in

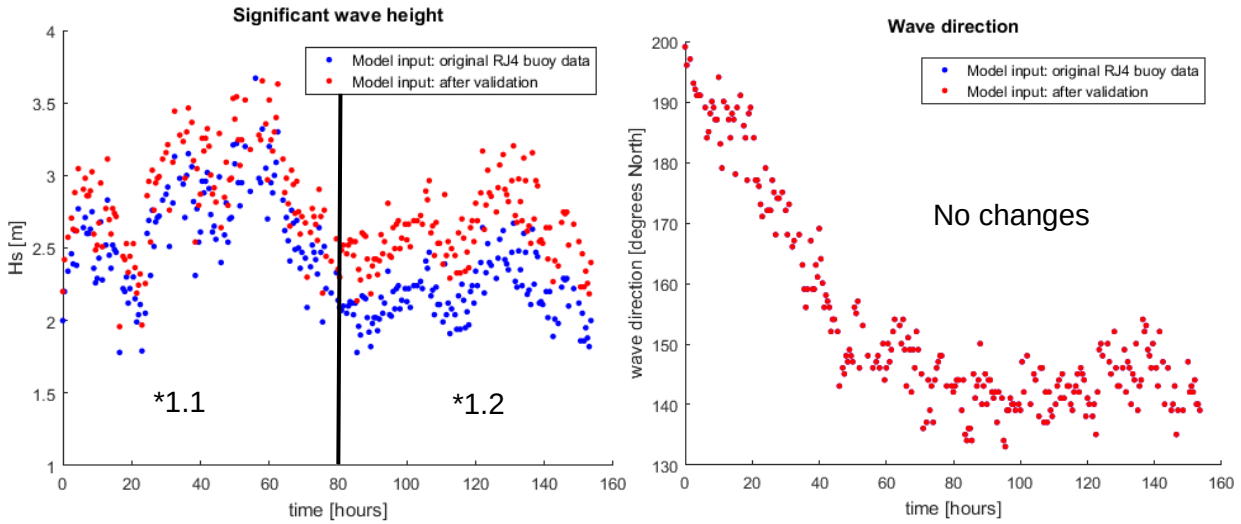

Figure 48: Overview of the model input showing the original input for the erosion simulation taken equal to the RJ4 wave buoy measurements and the input after the validation with different adaptation factors.

The figure below shows plots for the wave direction and significant wave height during the simulation time after the validation with the use of the model input. As said before, the RJ3 wave buoy has a high amount of missing data resulting in a measurement interval being higher than 30 minutes. The measurements are however still a 30 minutes averaged value which also holds for the model output making them well comparable.

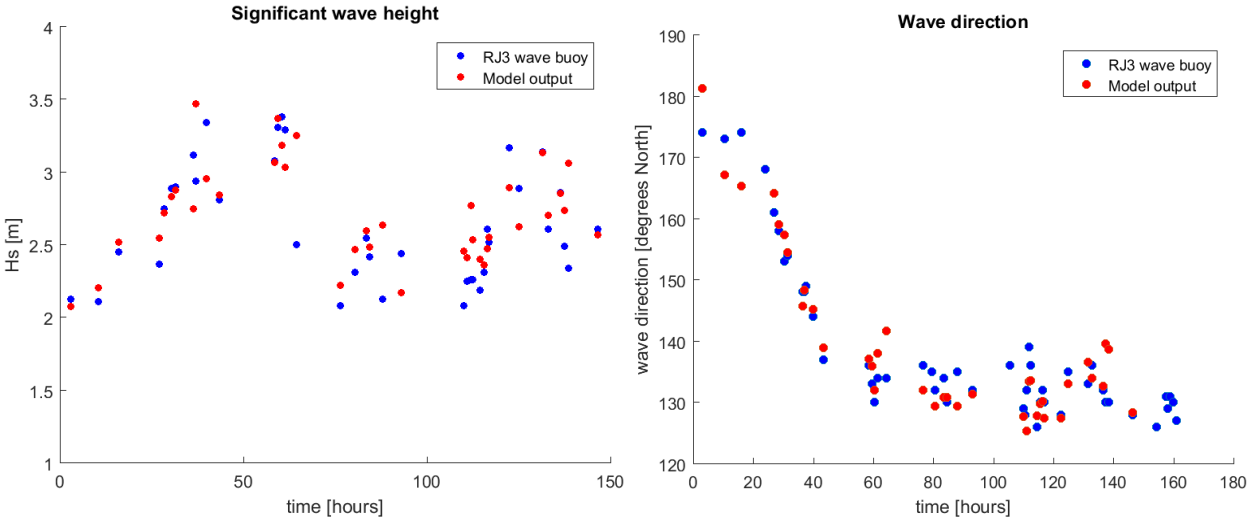

Figure 49: Validation of the hydronamics of the extreme event: July 2019 simulation showing both the significant wave height and wave direction for the model output at the location of the RJ3 physical wave buoy and the data from the wave buoy.

For the recovery simulation the stationary mode is used and the validation of the hydronamics shows different characteristics. The wave height for the whole simulation had to be increased by 4% to match the measurements. For the first 260 hours of the simulation the wave direction input is decreased with 7 degrees to be able to get the perfect match between the model output and the buoy measurements. This visible in the figure below:

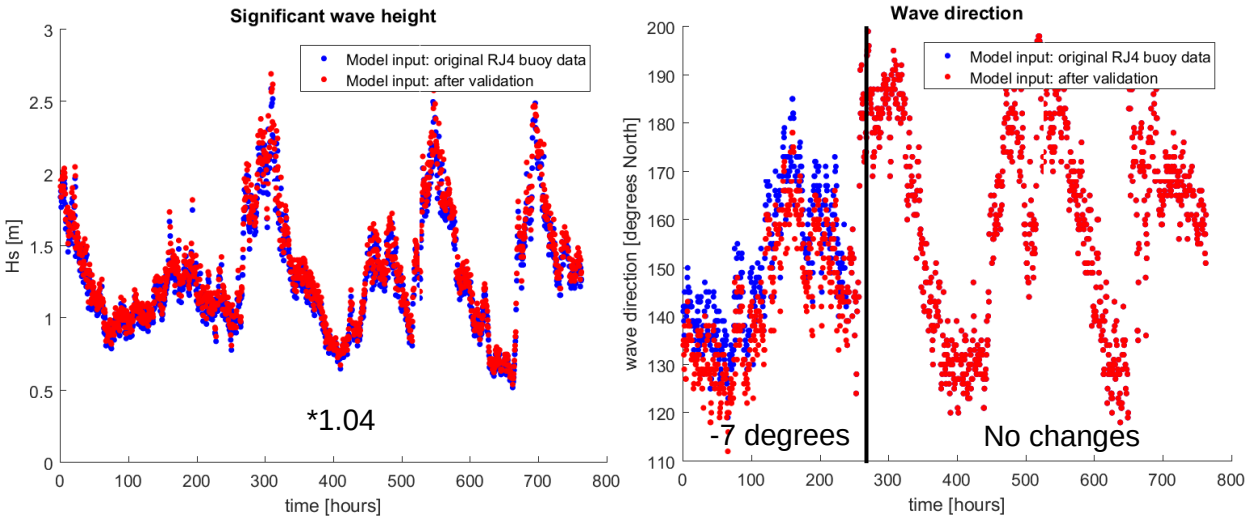

Figure 50: Overview of the model input of the model showing the original input for the recovery simulation taken equal to the RJ4 wave buoy measurements and the input after the validation with the different adaptation factors.

The figure below shows plots for the wave direction and significant wave height during the recovery simulation after the validation with the use of the model input:

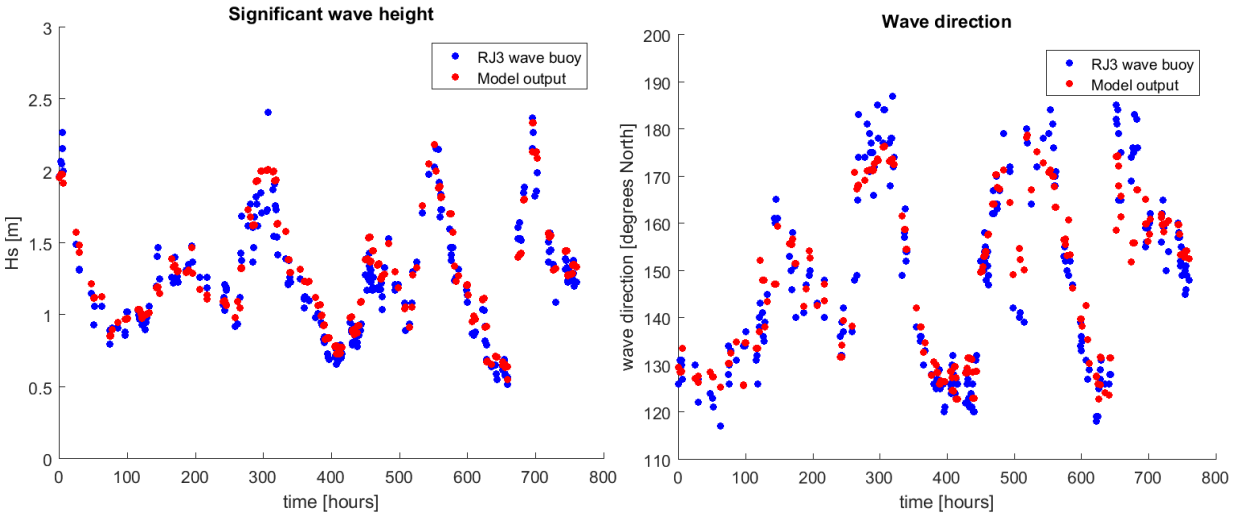

Figure 51: Validation of the hydronamics of the July 2019 recovery simulation showing both the significant wave height and wave direction for the model output at the location of the RJ3 physical wave buoy and the data from the wave buoy

5.7.2 Morphodynamics

For the validation of the morphodynamics of the model, the coastline position after the July 2019 storm event is used. This information is available in the form of satellite images. The main model parameter that is used for the tuning of the morphodynamics is the *facua* parameter. This is an important parameter in an XBeach model as it is the only parameter that directly influences the net cross-shore transport (Vousdoukas et al., 2012). This parameter influences the wave

asymmetry and skewness in the model domain using the following model by van Thiel de Vries (2009):

$$u_a = \gamma_{ua} * u_{rms}(S_k - A_s)$$

This formulation adds a net onshore directed velocity u_a to the depth averaged velocity adding an onshore sediment transport component. This onshore component depends on both the wave skewness (S_k) and wave asymmetry (A_s). In the case of linear waves, where the wave asymmetry is equal to the wave skewness the net velocity term equals to 0. The *facua* factor (γ_{ua}) has a standard value of 0.1 in XBeach. With higher values the onshore transport increases.

Elsayed & Oumeraci (2017) defined a relation between the *facua* parameter (degree of wave non-linearity) and the average seaward slope. Multiple previous researches reported that beaches of steeper slopes require higher values of *facua* in order to improve the model results and prevent an erosion overestimation (Vousdoukas et al., 2012; Nederhoff et al., 2015). This relation is defined based on different sensitivity analyses performed for different case studies in XBeach and shown in the figure below:

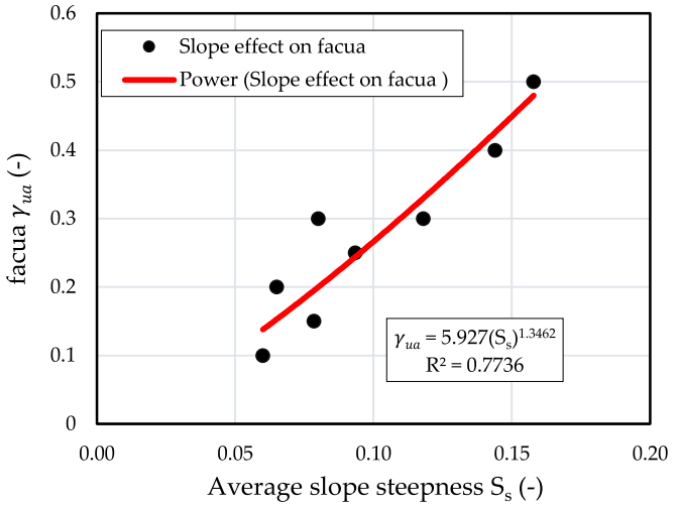

Figure 52: Relation between *facua* and the average slope steepness as defined by Elsayed & Oumeraci (2017).

Validation erosion simulation:

The relation shown in Figure 52 can be used to define the value of *facua,* taking into account the slope of the beach. This slope is calculated perpendicular to the beach from the location of the maximum wave run-up to the closure depth. The closure depth is estimated at the point in the offshore direction where minimal change is observed in the post storm beach profile after the July 2019 model simulation (see Figure 53). Furthermore, the point of maximum run-up is estimated at 1.5 meters above the waterline. The average slope of the beach can be derived from the cross sectional measurements performed at the beach visible in Appendix C.3 and is equal to 0.08. According to the relation shown in Figure 52 this slope steepness matches with a value of 0.2.

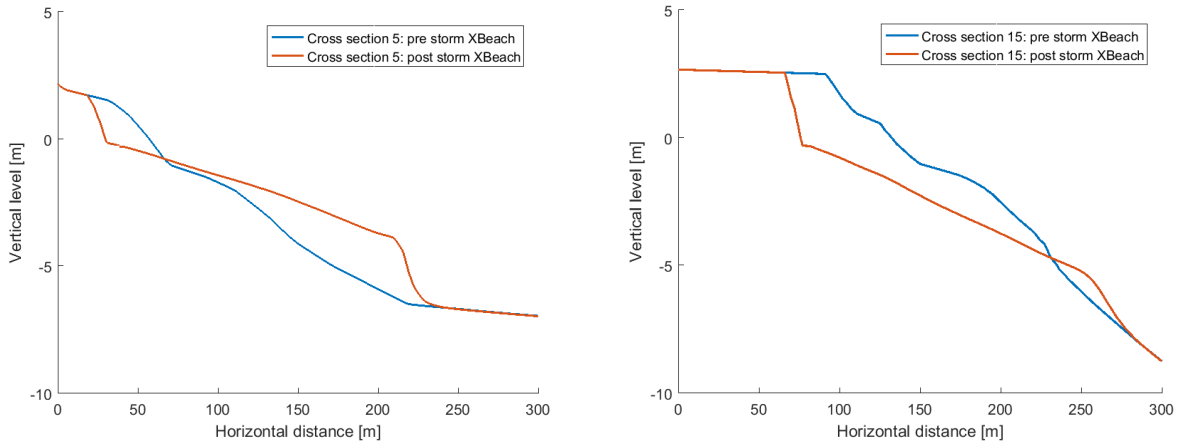

Figure 53 Cross shore profiles for cross section 5 and 15 (cross sections as defined in Figure 17) pre July 2019 storm and post July 2019 storm.

When running the model for the default *facua* value of 0.1 there is a clear overestimation of the erosion on the beach. This is especially in the Northern part of the beach. For this reason the *facua* parameter is increased to 0.15 which shows a decrease in beach erosion resulting in the closest match with the real post storm beach profile (see Figure 54 below). This is somewhat below the curve shown in Figure 52 but is within an acceptable range of variance taking into account the R-squared value of 0.77.

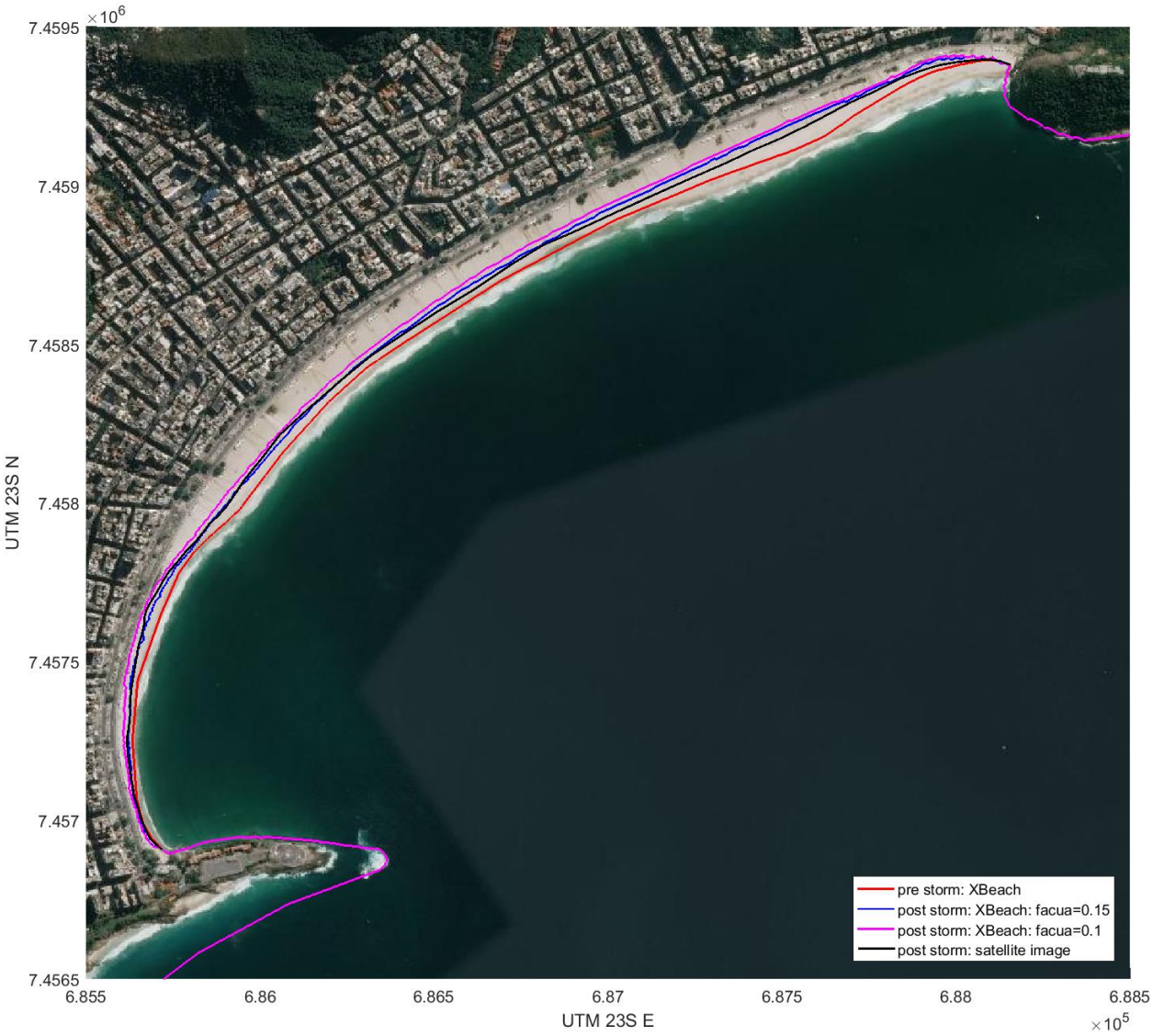

Figure 54: The post storm coastline position resulting from the XBeach model for facua=0.1 and facua=0.15.

When analyzing Figure 54, the beach width shows larger changes in the Northern side with a decrease in beach width of up to 65 meters where in the South the decrease in beach width is 35 meters at its maximum. This is a slight overestimation of the erosion in the Northern side and an underestimation of erosion in the Southern side. The reason for this alongshore difference in erosion rates not showing the best match with the real life coastline after the storm is the alongshore transport that occurs within the bay. This is clearly visible in Figure 55 below. It can be observed that directly on the beach there is erosion along the whole beach (the blue color) but when moving more offshore, high amounts of accretion (the red color) is visible, especially in the Southern side of the bay. It is clearly visible that the system is closed and there is no sediment transport around the headlands. This indicates a strong alongshore sediment transport component directed to the South which is responsible for an increase in erosion in the North and a decrease in erosion in the South of the bay.

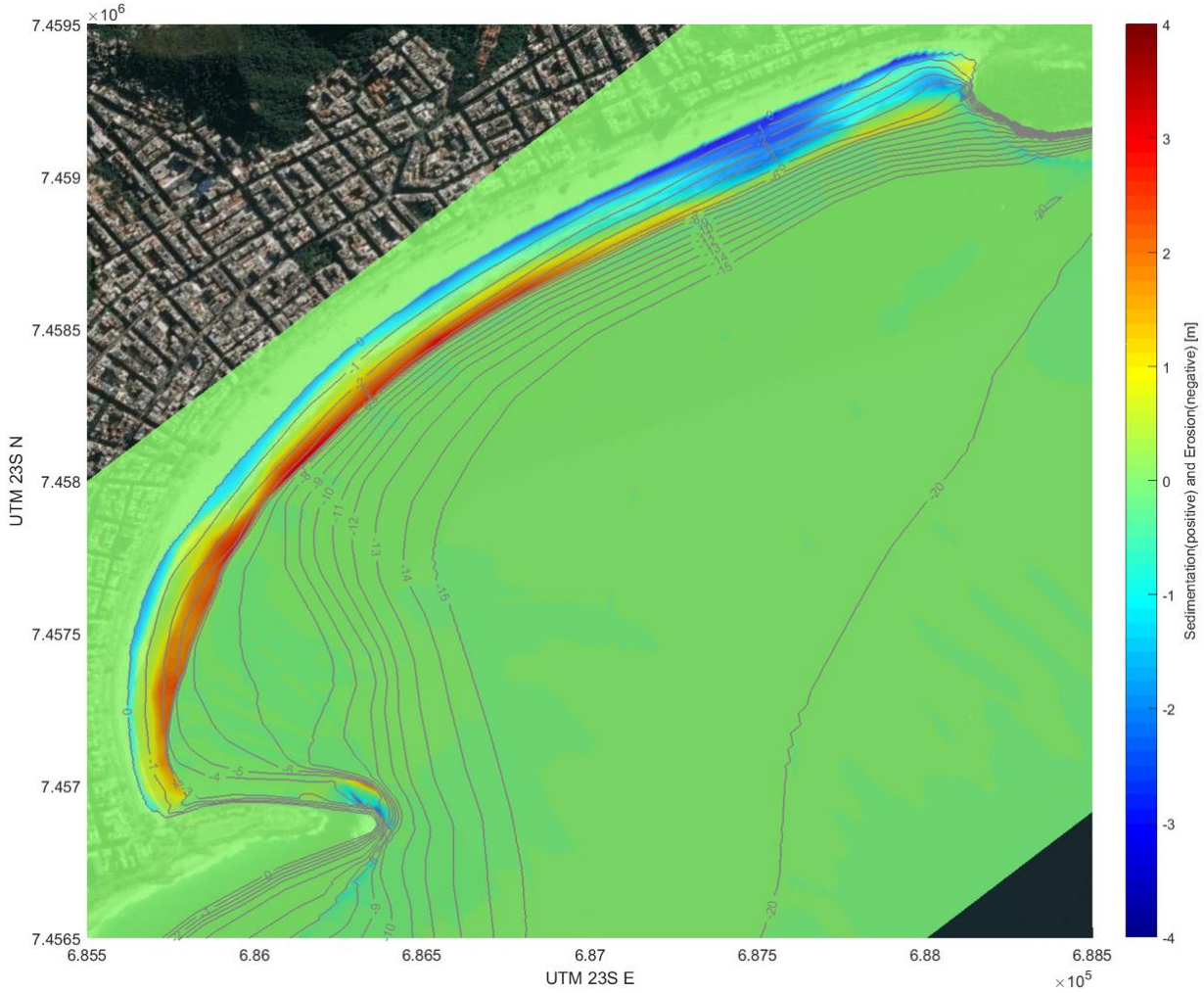

Figure 55: Total sedimentation (red) and erosion (blue) after the simulation of the July 2019 storm event.

Validation recovery simulation:

For the validation of the recovery simulation the following parameters are used: the *facua* parameter and the bermslope depth. The bermslope depth is the water depth at which the bermslope model, as described in section 5.4.5, is activated. The first run is made with the same value of *facua* as used in the extreme event simulation (0.15) and the default value for the bermslope depth (1m). For the recovery simulation the judgement of the model results is performed using the percentage of recovery in terms of both beach volume and beach width. This percentage is calculated using both the decrease in beach width and the decrease in beach volume during the extreme event simulation relative to the accretion during the recovery simulation. Besides this, 2 cross-sections in the North and South part of the beach are analyzed.

The results for first run (*facua* = 0.15 and bermslope depth = 1m) are visible in Figure 56 below. It can be observed that there is a high amount of advance in coastline position, especially in the South of the beach which is also observed on the satellite images. However, it is visible that the deposition of sand does not occur directly on the beachface but somewhat more offshore. This results in a sandbank, which is not fully submerged. This is not observed in reality when looking at the satellite images after 4 weeks of recovery. This confirms the limited applicability of XBeach with regards to the run-up of the short waves, which during more calm recovery conditions is an essential factor when simulating realistic interaction between the beachface and sub-aquatic part

of the beach (this is explained in more detail in section 5.5 of this chapter). The percentage of recovery in terms of beach width is equal to 82% on average but only 28% on average in terms of beach volume. This again confirms the limitations of the model to transport the eroded sediment higher up the beach. As said before, during the extreme event simulation there was significant alongshore transport to the South. This results in an overestimation of the beach recovery in terms of beach width in the Southern part of the beach and an underestimation in the Northern part.

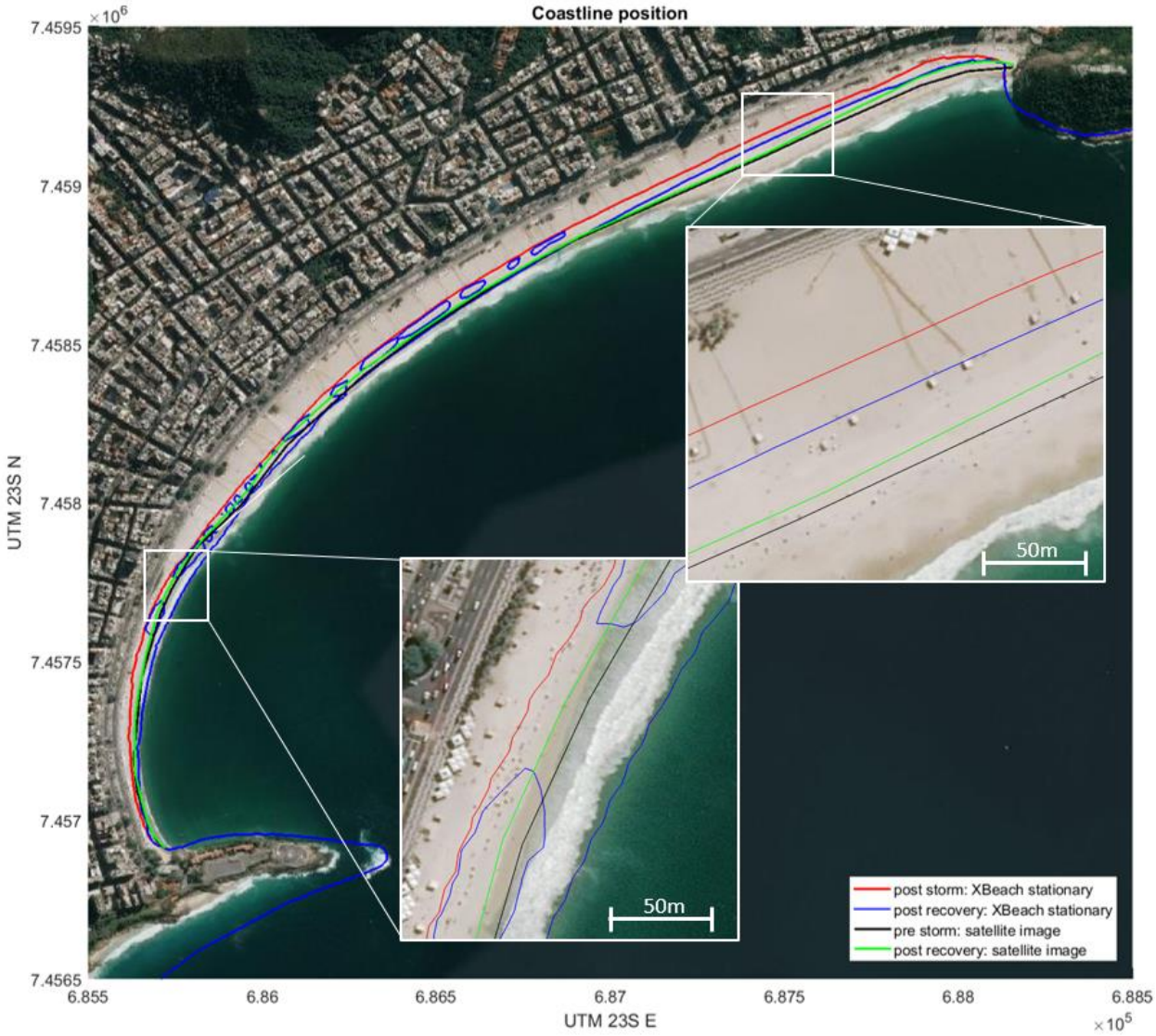

Figure 56: The coastline position of the XBeach model output is shown for the pre storm, post storm and post recovery. And next to this the coastline position derived from the satellite image post recovery. In the XBeach model setup the *facua* is equal to 0.15 and the bermslope depth equal to 1m.

In order to improve the model results the model runs are made for different values of *facua* and Bermslope depth with the goal of improving the performance in terms of accretion on the beachface. This results in the following values for the recovery percentages:

Table 6: The percentage of recovery resulting from the XBeach simulations in terms of both beach width and beach volume for different values of *facua* and the bermslope depth.

	% of recovery (beach volume)	% of recovery (beach width)
Run 1: *facua* = 0.15 & BS depth = 1m	28	82
Run 2: *facua* = 0.225 & BS depth = 1m	33	94
Run 3: *facua* = 0.3 & BS depth = 1m	38	105
Run 4: *facua* = 0.15 & BS depth = 0.5m	27	75
Run 5: *facua* = 0.15 & BS depth = 0.15m	23	63

As expected, an increase in *facua* results in an increased recovery rate for both the beach width and beach volume. It can however be observed that with a higher *facua* the placement of sand as a result of onshore transport results in a deposition further offshore and thus further from the beachface. This can be observed in the cross sections shown below where cross section 5 is located in the South of the beach and cross section 15 in the North of the beach. The increase in accretion with increasing *facua* is clearly visible. Especially at cross section 5 the 'sandbank' is clearly visible which in the case of a higher *facua* is located further offshore resulting in a limited interaction with the beachface (this is also visible when observing the coastline position for the different values of *facua* in Appendix E.1). Therefore *facua* is taken equal to 0.15.

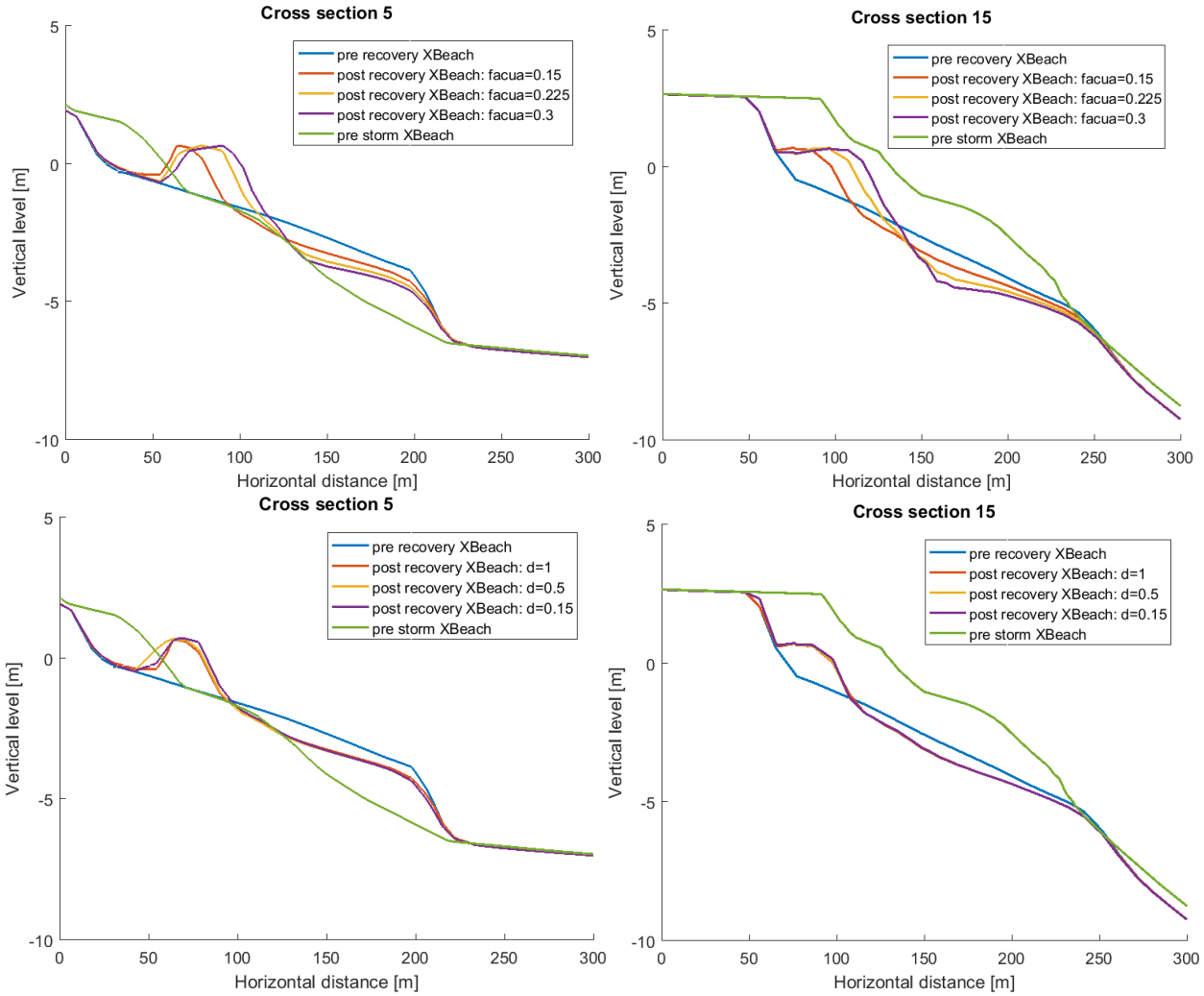

Figure 57: Cross section 5 (South of the beach) and cross section 15 (North of the beach) are plotted for different values of *facua* and the bermslope depth.

With decreasing bermslope depth, which is the depth at which the bermslope model is activated, there is a decrease in recovery percentage for both the beach width and beach volume. In terms of the placement of sand in the cross-shore direction there is no significant observable difference in the cross-shore profiles from which it is concluded that the default value for the bermslope depth equal to 1m is best to use.

The Bermslope model is used to compensate for the short-wave run-up not being included which is an important factor during beach recovery. With the standard model formulations and the use of stationary mode including the Bermslope model the results still show a limited interaction of the beachface with the sub-aquatic part of the beach. However, in terms of recovery rates, which are found to be very rapid for the beach width compared to other examples of beach recovery (see section 3.4.2) the model results show comparable recovery rates where in the 30-day period 82% of the beach width recovery has taken place.

5.7.3 Alongshore transport formulations

Besides the model results, various analytical alongshore transport formulations are used in this section to be able to compare to validate the outcomes of the model. This is done for the validation of the alongshore transport quantities during both the erosion and the recovery simulation. The first one is the Van Rijn (2014) formula given below. This formula has been validated against measurements of alongshore transport, the results are most often within a factor 2 of the measured values. The main dependencies of this formulation are the wave height and wave angle at the breaker line as well as the average slope of the surfzone and median sediment diameter. As the wave period is not part of the Van Rijn formula a swell correction factor(K_{swell}) is added to the formula. This is to add the effect of high-period swell waves with a wave height of 1 to 2 meters which produce significantly larger transport rates. In the case that these kind of wave do not occur this correction factor is taken equal to 1 (Van Rijn, 2014).

Next to the Van Rijn formulation, the remodified Kamphuis (1993) formulation for bulk longshore transport by Mil-Homens et al. (2013) is used. This formulation performs well in the case of short-term transport cases but comes with a slight overprediction at lower wave energy and a slight underprediction in the case of high wave energy (Van Rijn, 2014). Both formulations are given below:

Van Rijn (2014) formula:

$$Q_{t,mass} = 0.0006 * K_{swell} * \rho_s * (\tan\beta)^{0.4} * (D_{50})^{-0.6} * \left(H_{s,br}\right)^{2.6} * V_{wave}$$

$$V_{wave} = 0.3 * \left(g * H_{s,br}\right)^{0.5} * \sin(2 * \theta_{br})$$

Modified Kamphuis formula by Mil-Homens et al. (2013):

$$Q_{t,mass} = 17.5 * H_{s,br}^{2.75} * T_p^{0.89} * (tan\beta)^{0.86} * D_{50}^{-0.69} * \sin^{0.5}(2 * \theta_{br})$$

With:

- K_s = Swell correction factor [-]
- D_{50} = Median sediment diameter = $400\ \mu m$ (Vera-cruz, 1972)
- ρ_s = Sediment density = $2600\ kg/m^3$
- $tan\beta$ = Slope of the surfzone [-]
- $H_{s,br}$ = Significant wave height at breaker line [m]
- θ_{br} = Wave angle with respect to the local coastal orientation [degrees]
- T_p = Peak wave period [s]

The wave related parameters $H_{s,br}$, θ_{br} and T_p are extracted from the hydronamics of the XBeach model. At the location of the defined transects (visible in Figure 58) , the point of maximum wave height in the cross-shore direction is chosen as the breaking point. This is considered to be the point of maximum shoaling where the wave is starting to lose energy due to wave breaking. The slope of the surfzone $\tan\beta$ is also taken from the time varying bed level of the model and defined as the water depth at the breaker line divided by the horizontal distance between the shoreline and the breakerline. The local orientation of the coastline is also defined at the breakerline using the contours of constant bed level during the model run.

Figure 58: 9 different sections along the beach including the initial coastline position.

For both the recovery and the extreme event simulation the following changes in sediment volumes can be found due to alongshore transport for the 9 sections of the beach (as defined in Figure 58):

Table 7: Overview of the changes in sediment volumes [m^3*1000] due to alongshore transport for 9 sections along the beach using the XBeach storm event and recovery simulation output and the Kamphuis and Van Rijn formulation.

Section:	1	2	3	4	5	6	7	8	9
XBeach: extreme event	35.0	46.6	35.3	41.3	35.4	3.7	-48.4	-105.7	-48.9
Kamphuis: extreme event	6.7	-9.2	70.1	11.0	49.3	12.7	8.3	-22.6	-126.3
Van Rijn: extreme event	1.5	-5.0	190.3	53.9	232.0	38.0	23.3	-54.8	-479.2
XBeach: recovery	4.6	1.3	2.5	-7.3	-5.2	1.5	-1.4	-4.2	10.4
Kamphuis: recovery	-22.2	105.8	-89.3	20.9	-5.3	-5.7	13.6	1.9	-19.8
Van Rijn: recovery	-57.1	370.0	-326.4	49.8	19.6	-39.9	9.0	39.6	-64.6

It can be observed that there is a clear overestimation of alongshore transport volumes for the Van Rijn formulation. The Kamphuis formula results in volumes in the same order of magnitude as the XBeach model output. For the extreme event simulation comparable transport patterns are observed moving sediment from North to South. However, one big difference is observed in the fact that the Southern 2 sections of the beach (section 1 and 2) show minimal volume changes for both the Van Rijn and Kamphuis formulations. This could lead to an underestimation of the amount of erosion in the Southern part of the beach.

For the recovery simulation the XBeach model shows minimal alongshore redistribution of sediment which is confirmed by the results of the Kamphuis formulation. It can however be observed that there is a big exchange in sediment between section 2 and 3. These magnitudes of transport are expected not to be realistic to occur during calm conditions and are probably caused by a deviation in coastline position in this part of the beach as a results of the XBeach recovery simulation compared to the satellite images.

5.8 Parameter sensitivity

To test the robustness of the model a sensitivity analysis is performed for the following key parameters:

Median sediment diameter (D_{50}):

There is limited information available about the sediment characteristics at Copacabana beach. The only available information a sediment survey performed in 1970 (Vera-cruz, 1972). This is therefore an uncertainty within the model that can be quantified with the use of a sensitivity analysis which is shown in Figure 59 below. The changes in erosion rates are very minor and only subtle differences can be observed in the Northern part of the beach where the smaller sediment size causes more erosion. The model is thus not very sensitive to changes in median sediment diameter.

Figure 59: Sensitivity analysis of the July 2019 extreme event model run for different values of the median sediment diameter (D50).

JONSWAP spreading parameter (s):

The spreading parameter is used for the input of the wave boundary conditions at the offshore boundary. It determines the directional spreading of the wave field. The model sensitivity to changes in directional spreading parameter are visible in Figure 60 below. It is visible that the variation in erosion rates significantly differ in the case of a varying directional spreading parameter. Higher directional spreading causes more erosion along the whole beach perimeter compared to lower directional spreading. This difference can be up to ~15 meters of beach width erosion. When looking at the diffraction pattern around the Southern headland the spreading parameter influences the propagation of the waves around the headland.

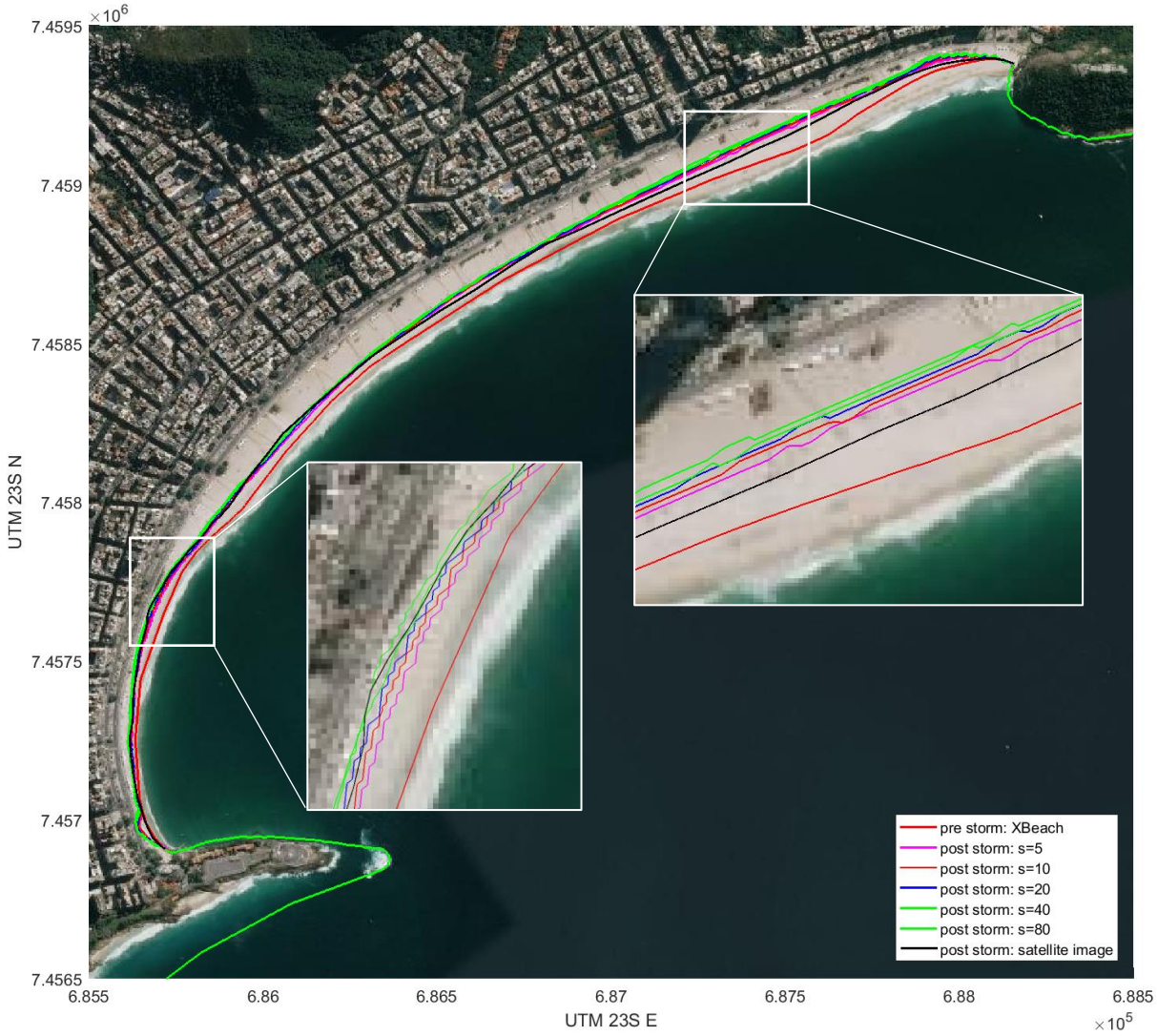

Figure 60: Sensitivity analysis of the July 2019 extreme event model run for the directional spreading parameter s.

5.9 Vulnerability assessment

This section starts with the results from both the erosion simulation and the recovery simulation with the modelling scenarios. After this an overall conclusion is drawn where the vulnerability of the beach is assessed with use of the model results. This is a preliminary assessment which in the next section is put into perspective taking into account things like model applicability, model sensitivity and the model validation to be able to eventually answer the corresponding research question: Can a numerical model be used to assess the current vulnerability of the beach?

5.9.1 Results: extreme event July 2019

In order to research the vulnerability of the beach during extreme events the July 2019 extreme wave event is simulated. First the extreme event base case is analyzed in more detail in terms of erosion quantities and alongshore transport. The results for each beach section (as visible in Figure 58) is given below:

Table 8: Overview of the model results for the 'base case' erosion event simulation for the different sections of the beach as shown in Figure 58.

Section:	1	2	3	4	5	6	7	8	9	Whole beach
Beach width erosion [m]	14.7	27.4	31.6	25.2	34.6	39.2	48.3	71.5	31.4	**35.9**
Beach width decrease [%]	-31.9	-45.9	-27.4	-19.6	-26.8	-30.7	-36.6	-51.8	-40.8	**-33.8**
Beach volume erosion [m^3*1000]	4.0	11.8	10.1	10.6	15.8	21.0	29.5	40.7	19.2	**162.8**
Beach volume decrease [%]	-17.1	-32.3	-11.4	-8.8	-13.4	-18.8	-25.9	-38.0	-29.6	**-20.8**
Alongshore transport [m^3*1000]	35.0	46.6	35.3	41.3	35.4	3.7	-48.4	-105.7	-48.9	-

As was identified in the previous part of this study, section 2 of the beach coincides with an area of wave energy convergence due to local bottom contours under SE directed waves. This results in more coastline fluctuations and erosion quantities which is observed on the satellite images. The extreme event of July 2019 was a clear example of where this part of the beach was largely impacted. The model results of this same event show a similar trend where, especially compared to the other beach sections in the South, section 2 of the beach shows relatively high variability with a beach width decrease of 45.9% (see Figure 61 for an overview of the beach width changes for the different beach sections) and a volumetric decrease in beach volume of 32.3%. Next to that a significant alongshore redistribution of sediment can be observed from North to South. Even though this causes an increase in sediment volume due to alongshore transport at section 2 there is still significant erosion.

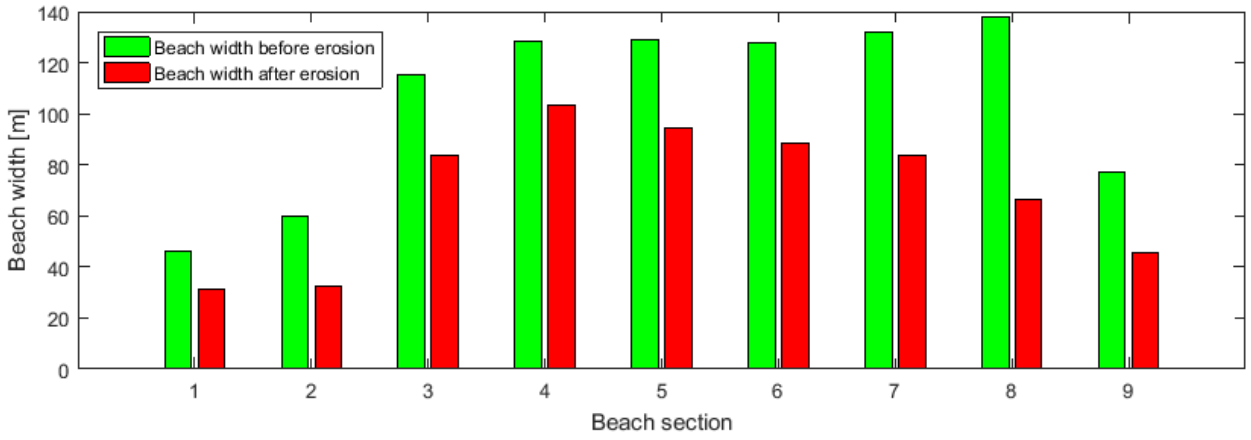

Figure 61: Beach width before and after the XBeach storm event simulation for the 9 different beach sections as defined in Figure 58.

With the use of scenario modelling the vulnerability of the beach during extreme events is tested. The scenarios include an increased average wave height, changes in average wave direction in both the eastward and Southward direction, an increase in storm duration of 20% and a sequential occurrence of storms. To test the influence of sequential storm the July 2019 storm event is run with the initial bathymetry taken equal to the final beach profile at the end of the recovery simulation. An overview of the scenarios is given in Table 9 below:

Table 9: Overview of the different modelling scenarios for the 2019 extreme erosion event with the average decrease in beach width and the total decrease in beach volume.

Scenario:	Details (applied to the whole simulation period)	Average beach width erosion [m]	Beach volume erosion [m^3 * 100000]
Base	-	35.9	1.63
1	Hs +5%	37.9	1.79
2	Hs +10%	40.3	1.98
3	Wave direction +10 degrees	33.9	1.44
4	Wave direction +20 degrees	30.9	1.20
5	Wave direction -10 degrees	37.4	1.79
6	Duration +20%	37.5	1.78
7	Sequential storms*	47.6	2.96
*The July 2019 extreme wave event was modelled for the second time with the 30 day recovery period in between.			

Erosion quantities are most sensitive (in terms of wave characteristics) to a change in the average significant wave height resulting in a significant increase in beach width- and beach volume erosion. In terms of wave direction, with the average wave direction moves towards the South (scenario 3 and 4) the total erosional impact on the beach decreases significantly. For scenario 5, where the average wave direction moves more towards the east, the impact on the beach increases. With an increased duration of the extreme event there is a clear increase in erosion. However this increase is considered to be limited. The biggest beach impact is the result of 2 sequential storms (including the effects of a one month-long recovery period) where especially the beach volume erosion shows an increase which is almost doubled compared to the base case.

Table 10: Percentual decrease in beach volume per beach section during the XBeach extreme event scenarios. The beach volume is taken as the volume of sand above the MSL.

Section:	1	2	3	4	5	6	7	8	9	Avg
Base	-17.1	-32.3	-11.4	-8.8	-13.4	-18.8	-25.9	-38	-29.6	-20.8
1) Hs +5%	-17.2	-32.2	-12.4	-10.0	-15.1	-20.6	-28.9	-40.9	-35.0	-22.8
2) Hs +10%	-19.4	-35.3	-14.6	-10.8	-17.1	-22.6	-31.6	-44.1	-40.3	-25.3
3) Wave direction +10 degrees	-13.0	-33.2	-11.5	-9.9	-14.5	-17.3	-21.9	-30.6	-19.9	-18.4
4) Wave direction +20 degrees	-9.8	-31.9	-10.8	-10.8	-12.7	-13.7	-17.6	-24.8	-10.5	-15.3
5) Wave direction -10 degrees	-22.3	-29.6	-10.3	-7.4	-14.1	-21.0	-29.7	-42.2	-39.6	-22.8
6) Duration +20%	-15.8	-31.1	-11.0	-9.3	-14.5	-20.5	-28.5	-42.3	-36.7	-22.7
7) Sequential storms	-5.9	-35.8	-20.6	-15.7	-23.2	-32.7	-51.4	-67.3	-76.6	-37.7

Table 10 shows the alongshore differences in beach volume erosion for the base case and the modelling scenarios. For an increase in the average wave height the alongshore differences in erosional impact are minor and equally distributed. The erosion quantities increase along the whole beach.

With changes in wave direction there are significant alongshore differences in erosional impact related to the following three processes:

1. Changes in wave direction cause a change in alongshore transport quantities where a Southward change of direction (scenario 3 and 4) results in a decrease in North to South sediment transport so an increased erosion in the South of the beach and a decrease in erosion in the North of the beach. The opposite occurs for an eastward change in wave direction (scenario 5).
2. With a Southward change in wave direction the sheltered area in the South of the beach gets bigger (see Figure 27) resulting in a decreased erosion rate in section 1 and 2 of the beach. The opposite occurs for an eastward change in wave direction.

3. The convergence of wave energy effect near section 2 (as visible in Figure 27) of the beach diminishes with a Southward change in direction resulting in a decreased erosion rate.

With changes in wave direction the dominant process is the change in alongshore transport quantities. This results in the largest relative changes in erosional volume in the North part of the beach (section 6 until 9). The effects in the South are smaller due to the combined effects of the three important processes as listed above. It can however be concluded that both a eastward and a Southward change in wave direction results in a decrease in erosional impact in the South of the beach. This confirms that the with the SE wave direction that occurred during the July 2019 erosion event causes is the wave direction having the biggest impact in the South of the beach.

With an increase in duration there is an increase of erosion in the North and a slight decrease in the South. This can be explained by the increase in Southward directed alongshore transport causing no further erosion in the South of the beach with an increased extreme event duration.

With a sequence of 2 storms there is a big increase in erosion volumes in the North but a decrease in erosion in the South compared to the erosion during a single extreme event. This can be explained by the higher recovery rates in the South of the beach and the increasing alongshore sediment imbalance which is not recovered during the one month-long recovery period resulting in an increase in sediment volume in the South of the beach opposed to the North.

5.9.2 Results: Recovery simulation

The recovery simulation is performed by modelling the conditions for the 30 days after the July 2019 extreme erosion event. Satellite images show a rapid recovery in terms of beach width, but according to local images there is still no full recovery of the backbeach in terms of beach volume as of 4 months after the erosion event. At first the recovery simulation without any alternations (also called 'base case') is analyzed in more detail from which the results are shown in Table 11 below.

Table 11: Overview of the model results for the 'base case' recovery simulation for the different section of the beach as shown in Figure 58. Beach volume is defined as the area of the beach that is above MSL.

Section:	1	2	3	4	5	6	7	8	9	Whole beach
Recovery rate [m/day]	0.89	1.25	1.08	0.97	0.78	1.08	0.93	0.70	0.68	**0.93**
Increase in beach width [m]	28.5	39.7	34.4	30.8	24.9	34.3	29.6	22.3	21.6	**29.5**
% of recovery (beach width)	193.7	145.0	108.8	122.0	71.8	87.5	61.3	31.3	68.7	**82.2**
Increase in beach volume [m^3*1000]	3.2	6.3	4.2	4.0	3.3	5.5	6.5	6.2	6.1	**45.3**
% of recovery (beach volume)	80.3	52.8	41.4	36.7	20.7	26.3	22.1	15.3	31.7	**27.7**
Alongshore transport [m^3*1000]	4.6	1.3	2.5	-7.3	-5.2	1.5	-1.4	-4.2	10.4	-

What can be concluded is that the rate of recovery, which is on average equal to 0.93 m/day is in the same order of magnitude as the observations from the satellite image (see section 3.4.2). Furthermore there is a clear difference in recovery rates between the South and the North part of the beach where the South part of the beach shows higher rates of recovery. This again matches the observations from the satellite images where this part of the beach shows the highest rates of recovery. Furthermore, in terms of beach width there is an almost complete recovery which is on average equal to 82.2%. In the South part of the beach the beach width exceeds the original

beach width before the erosion occurred. This is not observed in the satellite images. During the recovery simulation only small amounts of alongshore transport occurs showing that the recovery process occurs solely in the cross-shore direction.

In order to test the influence of different wave conditions on the recovery rates the following scenarios are made including the recovery percentages judging on both the beach width and the beach volume are visible in Table 12 below. It must be noted that the mild and steep waves simulation are performed with similar wave heights but with variations in wave period.

Table 12:Overview of the various scenarios for the recovery simulation including the recovery percentages for both the beach width and the beach volume.

Scenario:	Details (applied to the whole simulation period)	Recovery percentage (beach width) [%]	Recovery percentage (beach volume) [%]
Base	-	82.2	27.7
1	Milder wave steepness (Tp +10%)	83.1	29.2
2	Steeper waves (Tp -10%)	77.1	25.1
3	Hs +10%	85.6	29.1
4	Hs -10%	75.8	25.1
5	Duration -50%	70.9	20.8

In the graph below a plot is shown of the total recovered beach volume over the recovery period for the different model scenarios. The total recovered beach volume is defined as the increase in beach volume for the whole beach. The beach volume is the volume of sand above the MSL. It can be concluded that the effects of an increased wave height are most significant. Because in the case of an increased wave height the wave becomes steeper (which with similar wave heights results in a decreased recovery rate) but still shows a significant increase in recovery rates. Besides this, a clear correlation is visible between the wave height during the simulation and the recovery rates of all the scenarios. Wave heights around 2 meters results in more rapid recovery rates. Furthermore, the recovery rates at the start of the recovery period are higher and become more stable as time passes by.

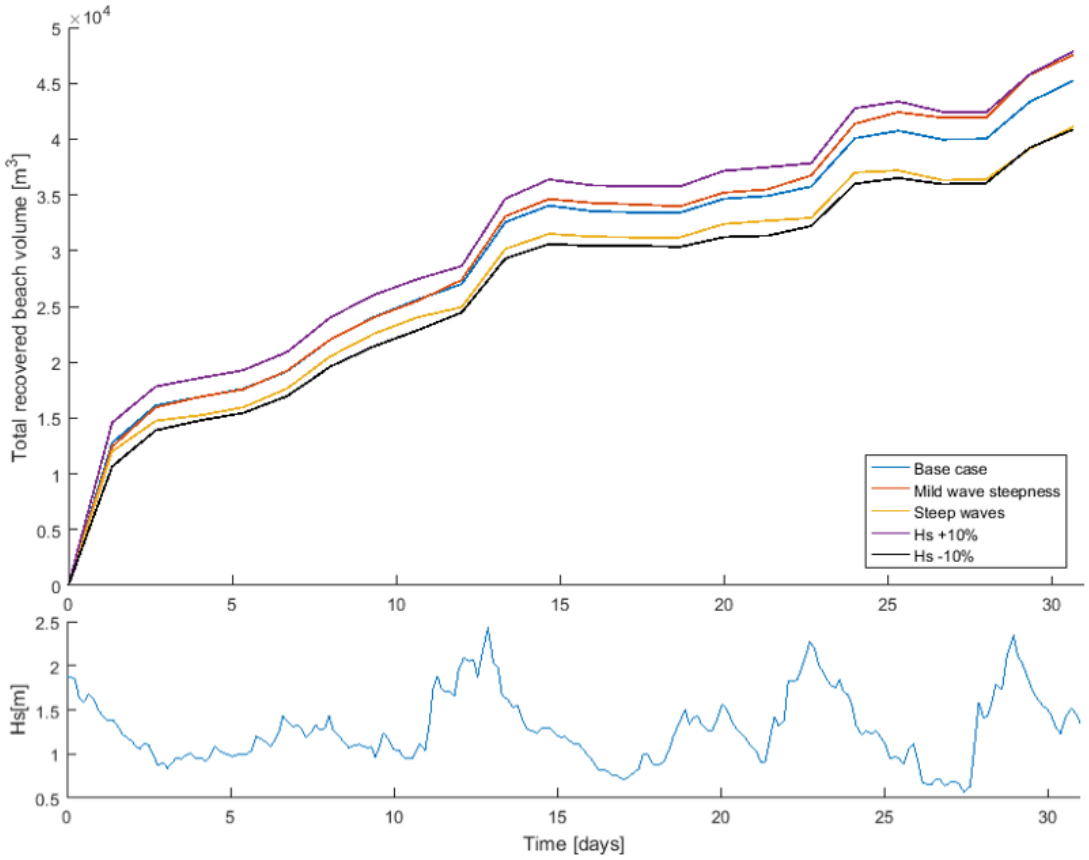

Figure 62: Total recovered beach volume over the full modelled recovery time for 5 different model scenarios. The graph below shows the significant wave height during the simulation period.

In order to compare the different scenarios based on the rate of recovery Table 13 below shows an overview of the rate of recovery for the different simulations.

Table 13: Overview of the recovery rates in m/day for the different recovery simulation scenarios.

Section:	1	2	3	4	5	6	7	8	9	Avg
Base	0.89	1.25	1.08	0.97	0.78	1.08	0.93	0.70	0.68	**0.93**
Milder wave steepness (Tp +10%)	1.03	1.26	1.06	0.82	0.75	0.98	0.99	0.80	0.78	**0.94**
Steeper waves (Tp -10%)	0.76	1.14	1.02	0.91	0.84	1.09	0.85	0.67	0.56	**0.87**
Hs +10%	0.95	1.28	1.07	0.92	0.91	1.05	0.99	0.78	0.76	**0.97**
Hs -10%	0.82	1.20	0.99	0.85	0.77	1.03	0.82	0.67	0.56	**0.86**
Duration -50%	1.76	2.35	1.84	1.66	1.55	1.83	1.53	1.00	0.90	**1.60**

Wave steepness:

The rate of recovery negatively related to the recovery rate where steeper waves result in a decrease in recovery and milder waves increase the recovery rate. This is also confirmed in the research by Phillips et al. (2017).

Average significant wave height:

The average significant wave height on average is equal to 1.29m during the base case recovery simulation. With an increase of the average Hs of 10% the recovery rate increases slightly. With a decrease in Hs there is an decrease in the rate of recovery.

Duration:

When running the recovery simulation for only the first half of time (duration -50%) it can be observed that the recovery rates during the first half of the whole simulation are significantly higher compared to the second part. The percentage of recovery in terms of beach width and beach volume are respectively equal to 70.9% and 20.8% compared to 82.2% and 27.7% for the full simulation. So during the first half of the recovery simulation most of the recovery takes place.

5.9.3 Conclusion

Beach vulnerability depends on 4 different main characteristics related to major storm impact. The following conclusions can be drawn for each of the characteristics using the results from the modelling scenarios for both the extreme event and recovery model simulations:

Beach state prior to storms:

The equilibrium beach shape is characterized by a smaller beach width in the South ranging in between 20 to 60 meters. In the North the beach width reaches widths of up to 130 meters. This causes the Southern part of the beach to be more vulnerable to erosion. This is shown in the base case where especially section 2 of the beach shows a large percentual decrease in beach area (see Table 8). Including the effects of the July 2019 erosion, there is a permanent loss of sediment on the backbeach near section 2 of the beach which as of now has not yet shown signs of recovery resulting in an increased vulnerability.

Wave conditions during storm and recovery:

With wave conditions a distinction is made between wave direction and wave height. Before taking into account the results for the modelling scenarios it can be concluded that under SE wave direction there is a clear convergence of wave energy resulting in increased erosion rates in the South of the beach (section 2 in Figure 58). The model scenarios show that with varying the average wave direction during the July 2019 extreme event there are higher fluctuations in erosional volumes in the North compared to the South. In the case of a more Southward wave direction (+20 degrees) this results in an overall decrease in erosion rates which is small in the South and more significant in the North. With a more eastward wave direction erosion rates increase in the North and decrease in the South. It can be concluded that the SE wave direction during the July 2019 erosion event leaves the South part of the beach in its most vulnerable state because both an eastward as a Southward change in wave direction does not result in increased erosional impact in this part of the beach.

An increase in wave height results in a significant increase in erosion rates along the whole of the beach which is more considerable than the effect of the wave direction. The rate of recovery increases with an increasing wave height which indicates that a smaller than average wave energy slows down the recovery process. The effect of wave steepness, which in the case of an increase in wave height results in steeper waves, results in a smaller rate of recovery. This effect is however much smaller compared to the increase in wave energy resulting in a higher rate of recovery. This shows that an increase in wave energy in the case of calm wave conditions is more effective in transporting sediment in the onshore direction. So overall an increased average wave height results in a higher rate of erosion but also a higher rate of recovery.

Duration of storms and recovery:

The duration of extreme events does not show a linear relation with the amount of erosion along the beach. In the case of a 20% increase in extreme event duration the erosion quantity increases with about 9%. This shows that also under extreme conditions the beach seems to reach a new equilibrium which with an increased duration shows minor additional changes in erosion rates. The recovery rate is highest directly after the erosion event and decreases with time until a new equilibrium is reached. About 80% of the recovery occurred in the first 2 weeks of the 1 month-long recovery period. This shows high initial recovery rates which has a positive effect on the beach vulnerability. From this it can be concluded that the beach is more vulnerable in the case of an increased storm intensity (in terms of an increase in wave height) compared to an increased duration. Similar results are found in the study of Hopkins (2018).

Storm sequence:

The biggest impact is caused when two storms occur in close sequence, even though the one month-long recovery period is included in between the two events. Recovery in terms of beach volume is far from complete (27.7%) at the end of the recovery period which causes the next storm to increase the erosion rates occurring relative to the first storm with about 80% and especially in the North having a large impact.

The table below shows an overview of the impact of both erosion and recovery characteristics on the beach vulnerability judging from the model results:

Table 14: Overview of the main characteristics of the erosion and subsequent recovery cycle with their influence on the beach vulnerability for the South (section 1,2), middle (section 3,4,5) and North (section 6,7,8,9) part of the beach. The results range from + + + meaning a very positive impact on the beach vulnerability and – – – meaning a very negative impact on the beach vulnerability.

Erosion/recovery characteristics	Section 1 and 2	Section 3, 4, 5	Section 6, 7, 8, 9
Equilibrium beach state	– – –	+ +	+ +
SE wave direction (erosion)	– – –	–	– –
Increased wave height (erosion)	– –	– –	– – –
Increased wave height (recovery)	+	+	+
Increased storm duration	–	–	–
Decreased recovery duration	–	–	–
Storm sequence	+	– – –	– – –

5.10 Discussion

Part one of the thesis shows that an important part in defining the vulnerability of the beach is taking into account the recovery process. Lots of studies are performed focusing on the erosional impact of storms leaving out the subsequent recovery of the beach. In this chapter an attempt is made to create an 2DH XBeach model that simulates a single erosion and recovery cycle. With the use of scenario modelling this single cycle is tested for various changes in wave conditions.

The previous section shows the results of the vulnerability assessment judging from the various modelling scenarios. The main vulnerability indicators at Copacabana beach were defined as:

- Decrease in beach area resulting in hindrance of recreative beach usage.
- Decrease in beach width/volume resulting in coastal damage and a decrease in the coastal protection function of the beach.

5.10.1 Model performance

The model performance is important when looking at the model results and needs to be taken account when drawing conclusions about beach vulnerability. The model performance is dependent on the following factors: data availability, model applicability, model validation and the model sensitivity. The main model findings related to these factors are discussed below:

Data availability:

The data available for the setup of the model consists of a bathymetry survey performed 4 months after the occurrence of the July 2019 extreme erosion event making it not completely accurate as the initial profile for the July 2019 erosion event simulation. This can result in slight deviation in the model results. It can however be concluded that this bathymetry is representative for the equilibrium state of the beach. Furthermore there are 2 physical wave buoys within the modelling domain having data available for both the extreme event and the recovery period. For validation of the model morphodynamics the main data source is the coastline position taken from Sentinel 2 satellite images with a maximum frequency of 5 days. There is no further data available related to sediment transport volumes or flow velocity measurements.

Model applicability;

For the model applicability a distinction is made between beach erosion and- recovery simulation which respectively uses the Surfbeat and stationary mode of XBeach. The main limitation of XBeach in terms of hydronamics is the diffraction process not being included which is important due to the sheltering of the Southern headland.

The applications of XBeach with regards to extreme/erosive conditions are very widespread and validation of the model with regards to extreme conditions is performed for many different case studies over the last years (e.g. McCall et al., 2010 and van Thiel de Vries, 2009). This is also the main reason for the use of XBeach. The run-up and run-down of the short waves, which is not included in the model, is mostly within the ranges of the run-up and run-down of long waves. With this given, the long waves are important with regards to beach and dune erosion and are able to reproduce realistic erosion patterns (van Thiel de Vries, 2009). Important coastal processes like undertow are very important during beach erosion and are included in the XBeach model.

The most important modelling processes with regard to beach recovery are related to the short wave run-up and run-down process. This is important in the interaction between the beachface and the sub-aquatic part of the beach. In XBeach, for both the Surfbeat and the stationary mode, the short wave run-up is not included. Only few applications can be found where XBeach is used for modelling beach recovery. A recent study by van Dam (2019) shows that the standard XBeach model is not able to accurately reproduce the effects of beach recovery due to the lack of representation of the complex swash processes. An often found solution to this problem is the use of the Bermslope model which forces the beach slope in the swash zone to predefined slope to compensate for the effects of the non-included complex swash zone processes.

Model validation:

The model validation is performed for both the model hydronamics and morphodynamics. The model hydronamics are validated using two physical wave buoy records located within the model domain. One buoy is used as model input at the offshore boundary and the other buoy is compared with the model output at a similar location. For the erosion simulation no changes needed to be made to the wave direction input showing good model performance in terms of wave refraction in Surfbeat mode. The wave height input for both the recovery and erosion simulation needed to be increased to match the wave buoy measurements. There is no indication of any loss of wave energy within the model domain that results in this decreased wave energy. This decreased wave energy is most probably caused by the transformation of the stationary wave input to a spectral type.

The validation of the morphodynamics is performed with the use of the *facua* and bermslope parameters. This results in accurate erosion quantities. For the recovery simulation the use of the Bermslope model does not result in an accurate representation of the beach recovery as observed

on the satellite images. The interaction between the beachface and sub-aquatic part of the beach is limited especially in the Southern part of the bay where the deposition of sediment occurs further offshore creating a sandbank along the coast which is not observed in the available satellite images. With the use of the Van Rijn and Kampuis alongshore transport formulations the alongshore transport quantities are compared with the model output. The model shows similar behavior in terms of alongshore transport quantities with a North to South directed transport during the erosion simulation. The alongshore transport formulations show minimal alongshore interaction with the two most Southern beach sections. The model output deviates from this trend showing a high increase in sediment quantities due to alongshore transport in this part of the beach. This causes an underestimation of the erosion quantities in the South of the beach. Reason for this could be the diffraction process not taken into account in XBeach resulting in unrealistic wave patterns in the South of the beach.

Sensitivity analysis:

A sensitivity analysis is performed for 2 different parameters which are the wave spreading parameter and the sediment size. These parameters are chosen for the sensitivity analysis because of the limited availability of data with regards to these data sources. As the vulnerability assessment is performed by comparison of the modelling scenarios to a single base case the uncertainties related to the parameters are close to equal in all different scenarios which does not significantly influence the results of the vulnerability assessment.

5.10.2 Conclusion

After discussion of the performance of the model for both the erosion and recovery simulation the main question of this part of the study is answered:

Can a numerical model be used to assess the current vulnerability of the beach?

The use of the Surfbeat model for the erosion part of the simulation shows good model applicability with the wave-averaged approach including the long wave motion. The wave patterns include the wave convergence in the South which is an important factor in determining the vulnerability of the beach. One shortcoming of the model is the deviant behavior in the South of the beach in terms of alongshore transport resulting in an underestimation of the erosion in this part of the beach. This is most likely because of the diffraction process not being included in the XBeach Surbeat mode. Overall it can be concluded that the vulnerability of the beach can be assessed with the use of an numerical model for the erosion part of the beach cycle by use of scenario modelling.

In the case of beach recovery the complex swash zone processes become more important. These are not represented in the XBeach stationary mode but to compensate for these effects the additional Bermslope model can be used. In the case of the Copacabana recovery simulation the use of the Bermslope model did not result in a realistic recovery pattern. High amounts of recovery is visible in the South extending the further offshore than its original beach width which shows the lack of interaction between the beachface and sub-aquatic part of the beach which is important in the case of beach recovery. From this it is concluded that for the recovery part of the beach cycle simulation it is not possible to assess the vulnerability of the beach with the use of XBeach stationary mode including the Bermslope model.

Part 3: The future of Copacabana beach

6 The future of Copacabana beach

This chapter starts with the long term climate trends potentially affecting Copacabana beach. These climate trends can be extracted from different long-term datasets of parameters related to the wave climate. Listed below are the wave parameters which are investigated in this chapter with the use of multiple data sources:

- Average significant wave height
- Extreme significant wave height
- Wave direction
- Frequency of extreme events
- Sea Level Rise

Hereafter, these long term climate trends are put into perspective of the results of the first two parts of this study related to the beach vulnerability. The main findings are discussed in the last section of this chapter including possible strategies for future interventions.

6.1 Long term climate trends

When it comes to the identification of long term trends the properties of the data used are very important because these climate trends are often minor trends. For the analysis the following data sources are used:

COWCLIP2.0:

This dataset is the first multivariate global dataset where there is more standardization between different datasets in terms of for example, wave variables, spatial coverage, resolution and the time-slices used for present and future simulations. This recently released public dataset consists of 155 global wave climate simulations performed according to CMIP5-based structure, which is a is a collaborative framework created by the IPCC for performing global climate models. The modelling is done by 10 different research institutes.

Annual, seasonal and monthly data is available for 2 different time slices: 1979-2004 and 2081-2099. The future time slice is simulated under 2 different emission scenarios: RCP4.5 and RCP8.5, which respectively define a medium stabilization - and a very high emission scenario up to 2100 (Morim et al., 2020). The data used in this chapter is located at -24º latitude and -43º longitude which is approximately 100 kilometers South of Copacabana beach.

ERA5 offshore wave dataset:

This offshore dataset is used in earlier chapter in order to characterize the offshore wave climate. Data spans from 1979 to present and can be used to identify historical trends. The ERA5 wave hindcast is the 4th big scale reanalysis done by the European Centre for Medium-Range Weather Forecasts (ECMWF). As this is a recently published dataset more research is done using the prequal of ERA5: ERA40 (Hennerrmann, 2016). In identifying long term trends from hindcast datasets the homogeneity of this data is very important. Studies into the homogeneity of the ERA40 dataset 1957-2002 show that the data, especially in the Southern hemisphere, shows a lack of data coverage before 1980. This could cause the reanalysis model to create its own

variability and lead to inadequate trends (Sterl, 2004). As ERA5 is a more recent reanalysis created by the same research project and the data of the reanalysis does not include the period before 1980, the dataset is expected not to contain any inhomogeneities which makes identification of long term trends from this data more reliable.

This dataset can be used to identify historical trends in wave data which already exist in present time. Extrapolation of this trend to the future can give insight in future trends.

IPCC:

The existing literature on future climate trend data used in this chapter is from an analysis made by the United Nations about the influence of climate change on the coasts of Latin America and the Caribbean (Barcena et al., 2015). The wave data used in this study is from 1948 to 2010 and with an extrapolation of the trends found in this dataset the future trends of the data from 2010 onwards are predicted for wave heights and wave direction. The source of the data is the Global Ocean Wave (GOW) reanalysis. The data is calibrated to correct the numerical reanalysis data for the instrumental measurements, which includes both wave buoys and satellite images. For the studies into South American climate variability performed by Barcena et al. (2015) the calibration could only be performed for the significant wave height. It is noted that the wave buoys showed an adequate correlation with the wave direction.

Table 15: Characteristics of the different data used in defining long term wave climate trends.

	Data range	Number of data sources	Longitude	Latitude	Future prediction method
COWCLIP 2.0	1979-2004 and 2081-2099	10	-43°	-24°	Simulations using RCP emission scenarios 4.5 and 8.5
ERA5	1979-2020	1	-43°	-23.5°	Linear trend extrapolation
IPCC	1958-2010	1	-	-	Trend extrapolation

The most reliable source of data in terms of future trends is considered to be the COWCLIP2.0 data because it consists of a large amount of different global wave modelling studies, all processed in the same way. This makes the data directly comparable to each other making it easier to obtain clear consensus in observable trends of different parameters. Experts recommend the use of a more systematic framework for future climate projections like the COWCLIP2.0 data framework (Morim et al., 2018).

6.1.1 Mean Hs

The mean wave height tells something about the average wave energy that influences the beach. Under mean conditions the beach, in most cases, moves towards an equilibrium profile. This is also visible at Copacabana beach where the coastline position in the last 10's of years shows minor changes. So possible future changes of the mean wave height can influence the equilibrium state of the beach.

Below, the normal distribution of the mean yearly significant wave height is shown for 2 different time slices of the COWCLIP dataset: 1979-2004 and 2081-2099. It is clearly visible that all the different simulations show an increase in mean significant wave height. The average increase of all 9 different simulations is equal to 0.06m over the period of 100 years which results in a trend of +0.0006m/year. This corresponds to an average increase in wave height of 3% in 100 years.

a) COWCLIP2.0

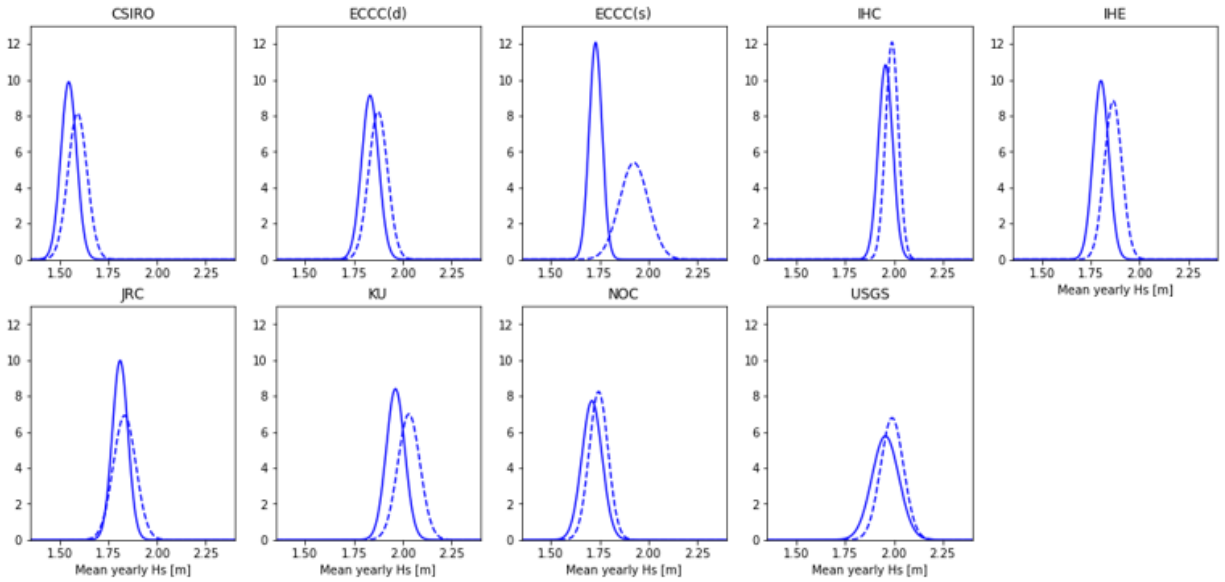

b) IPCC

	Trend 2010-2070	2040	2070
H_{smean} increase	+0.0027 m/year	0.081m	0.162m
H_{smean} 95% interval	-	0.02m	0.044m

c) ERA5

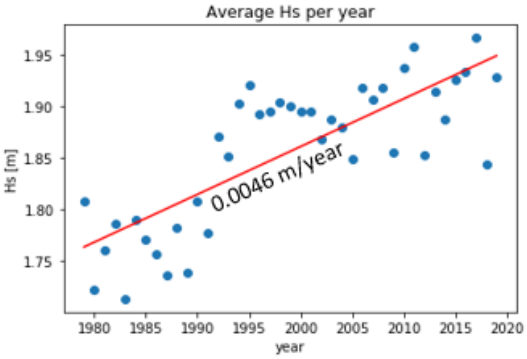

Figure 63: a) COWCLIP2.0: 6 different plots showing the standard deviation of the mean annual Hs for two time periods: 1979-2004 (solid line) and 2081-2099 RCP8.5 (dashed line). b) IPCC: Extrapolated trend in mean Hs between 2010 and 2070. c) ERA5: Mean Hs per year between 1979 and 2020 resulting in a slight negative linear regression fit.

IPCC reports also show a positive trend equal to 0.0027±25% m/year. With an average reported yearly mean wave height of about 1.6m, the increase of mean significant wave height in 2070 is expected to be about 10%. Lastly, when analyzing the ERA5 dataset a positive trend can be found in the data from 1979 until 2019 equal to 0.0046 m/year. However, the data shows a large scatter and a seemingly sudden increase in wave height around 1992. Comparing this data with the 9 datasets from the COWCLIP2.0 this sudden increase in wave height can't be observed. This could imply that inhomogeneities in the ERA5 datasets cause non-realistic trends. This however can't be caused by a lack of data causing the dataset to create its own variabilities as stated at the start of this chapter.

6.1.2 Wave direction

The influence of the wave direction on Copacabana beach became clear in previous chapters. With the orientation of the beach, different wave directions cause different coastal processes to be dominant. Say for example the amount of alongshore transport. Most wave related climate trend studies focus on the trends in mean significant wave height and there is a clear lack of

research related to future wave direction climate trends (Morim et al., 2018). This makes it harder to obtain a clear consensus among different data sources.

The COWCLIP2.0 data shows changes in future wave direction in both directions for model simulations of different wave groups. Also a significant scatter around the mean value can be seen. The most significant trend is found in the IPCC report where a clockwise rotation (Southward) is expected of around 0.17^0/year which would lead to a change in mean wave direction of around 10 degrees in 2070. In contradiction to this, the ERA5 dataset shows a negative trend in the anti-clockwise direction (eastward) of -0.023^0/year. The scatter in the data is large and the goodness-of-fit is low.

a) COWCLIP2.0

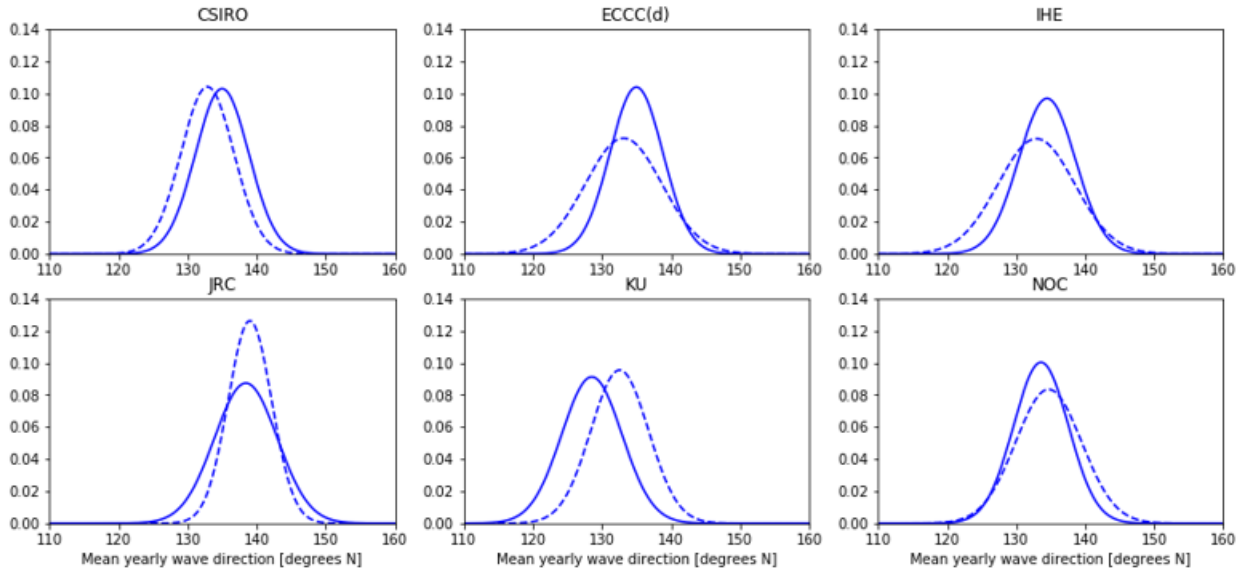

b) IPCC

	Trend 2010-2070	2040	2070
Increase in mean energy flow	+0.17°/year clockwise	5° clockwise	10° clockwise
Mean energy flow 95% interval	-	2.5°	4.9°

c) ERA5

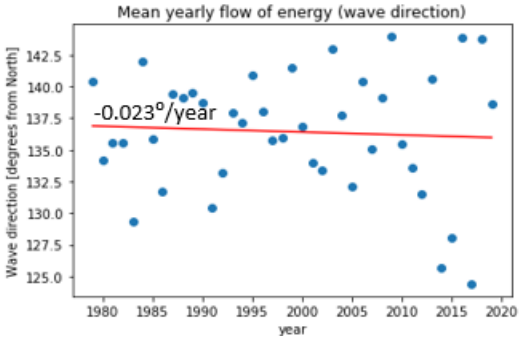

Figure 64: a) COWCLIP2.0: 6 different modelling studies showing the standard deviation of the mean annual wave direction for two time periods: 1979-2004 (solid line) and 2081-2099 RCP8.5 (dashed line). b) IPCC: Extrapolated trend in mean wave energy direction between 2010 and 2070. c) ERA5: Mean yearly energy flow direction resulting in a slight negative linear regression fit.

Concluding from the trends from 3 different data sources there is no clear consensus to be found in the future trends in mean wave direction. In order to test the future effects both the an eastward as a Southward change of wave direction needs to be taken into account.

6.1.3 Extreme events

After extreme events the beach is often found to be in a vulnerable state due to erosion. Hereafter the beach needs time to recover and reach its equilibrium state again. If sequential storms hit the 'not yet recovered' beach, or the storms increase in severeness, consequences of such an event could be even higher. That's why potential changes in both storm frequency and severeness in the future need to be taken into account.

Research has been done into the occurrence of storms reported by a local Brazilian newspaper from 1979 to 2013 for the state of Rio de Janeiro. Most data reported in the news articles was related to damage on streets, houses and bars near the coastline. A total amount of 120 days with damage due to storms is recorded (see Figure 65), from which 29 days are storm damage reports related to Copacabana beach. So roughly once a year there are news reports of storm damage/impact on Copacabana beach. When fitting a linear regression curve to the data a slight negative curve is visible which indicates a decrease in extreme event occurrence. Due to the source of the data, which is the newspaper O'Globo, there could be irregularities in the news reports over time (Lins-de-barros & Klumb-oliveira, 2018).

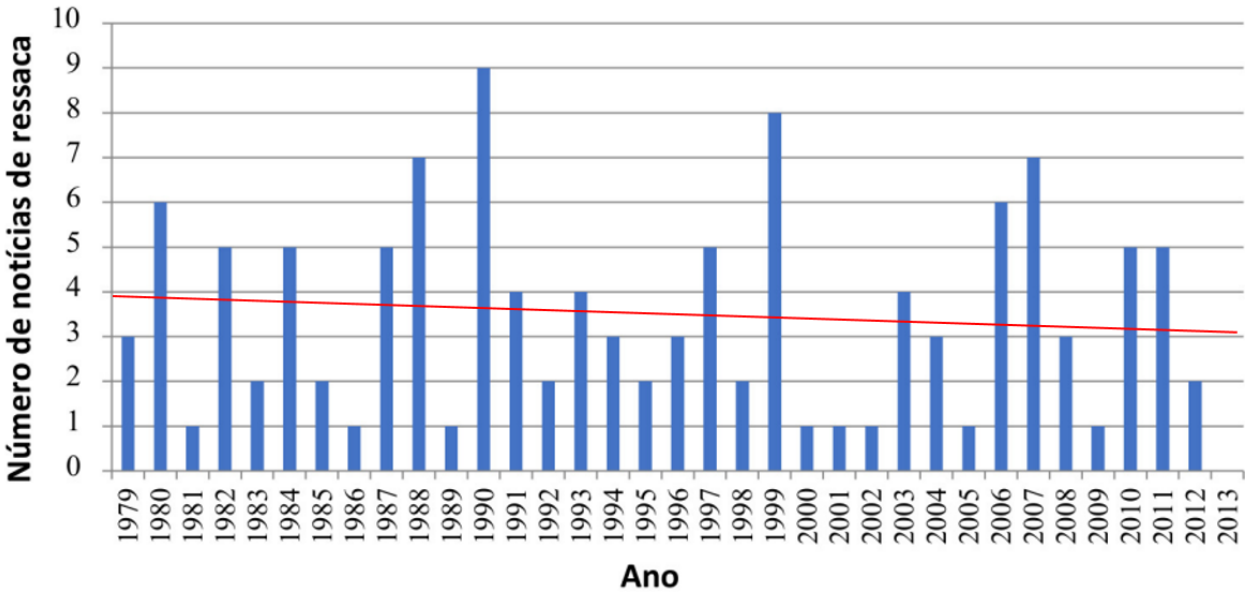

Figure 65: Number of storm news per year in the state of Rio de Janeiro as per survey of the newspaper O'Globo (Lins-de-barros & Klumb-oliveira, 2018).

The COWCLIP2.0 dataset does not include parameters directly giving insight into extreme wave event return periods or severeness but it does include a parameter stating the number of days per year where the significant wave height exceeds 2.5m. The correlation between this parameter and for example the frequency and severeness of extreme events can assumed to be positive. All 6 different modelling studies show a positive trend and thus an increase in 'rough' wave days indicating an increase in extreme wave event severeness and frequency (see Figure 66).

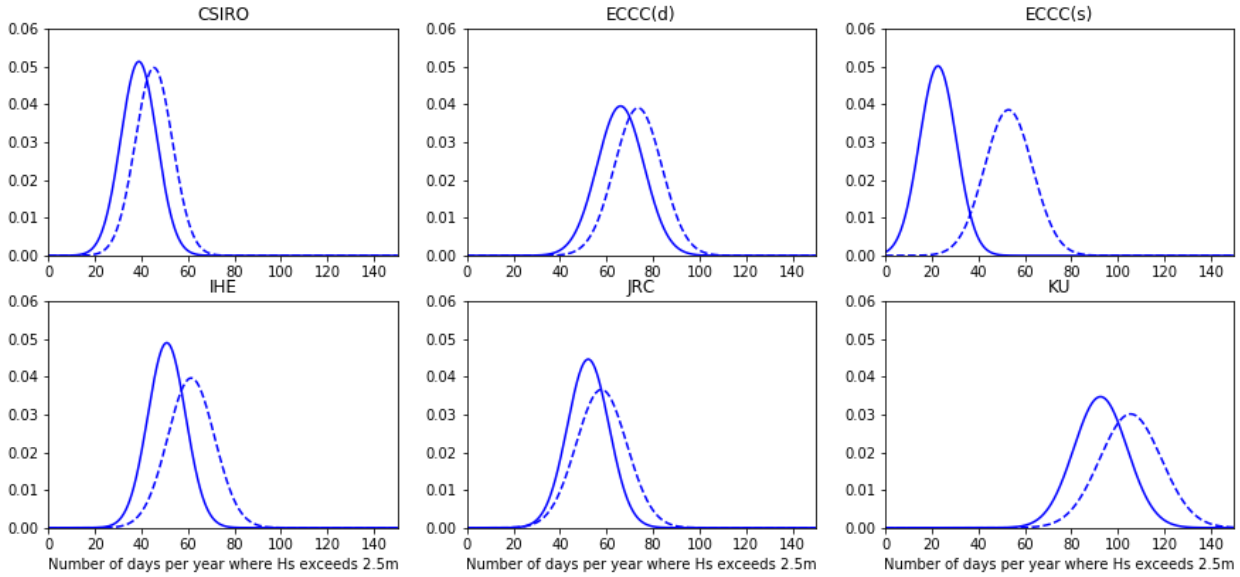

Figure 66: 6 different modelling studies from the COWCLIP2.0 dataset showing the standard deviation of the number of days per year where Hs exceeds 2.5m for 2 different time slices: 1979-2004 (solid line) and 2081-2099 RCP8.5 (dashed line).

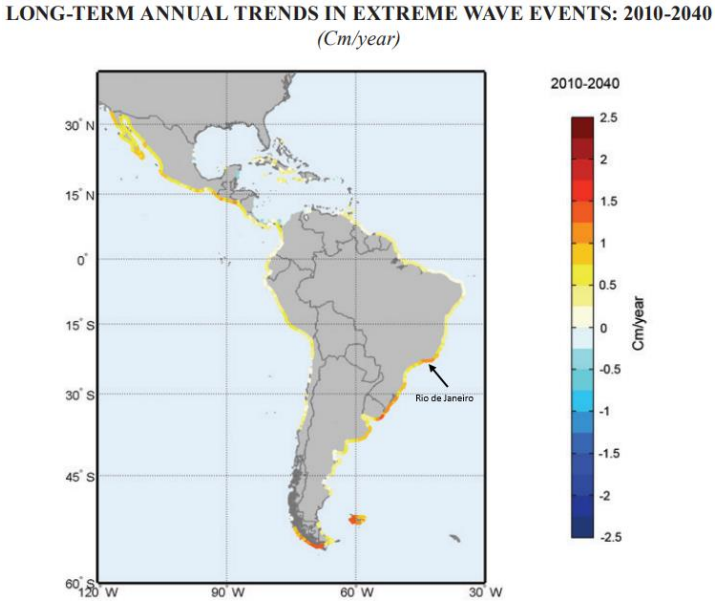

Figure 67: Long-term annual trends in yearly maximum recorded extreme wave height for the continent of South-America and Central America (Barcena et al., 2015).

For the extreme wave events there is also a positive trend found in the IPCC data from 1958 to 2010. This is shown for the annual extreme wave height where at Rio de Janeiro the approximated increase of this wave height is equal to 1.12 cm/year. It is visible that the whole continent of South-America shows a positive trend in extreme wave events which can be considered as a common effect of climate change on weather extremes. When looking at the trends for each of the 4 seasons the most significant trend is in the winter months (March to August). In these months the average trend shows an increase of 1.6 cm/year in the seasonal extreme wave height.

This same trend is found when looking at the 50 year return period significant wave height in 2010. The same wave height in 2040 and 2070 respectively have a return period of 17.21 years and 6.8 years. This confirms the positive trend for extreme wave heights (Barcena et al., 2015).

Concluding from all the different data sources is that both the ERA5 data and study related to the O'Globo news reports suggest a future decrease in frequency and severeness of extreme wave events. This is based on trends derived from historically available information wave and news report data. COWCLIP2.0 data and IPCC shows a positive trend in storm frequency and severeness. Where, as noted at the start of this section, the COWCLIP2.0 data uses multiple climate modelling analyses these results are considered to be most reliable. Testing the possible

consequences of a future increase in extreme event severeness and frequency is therefore most important in predicting future behavior of Copacabana beach.

6.1.4 Sea Level Rise

In terms of Sea Level Rise the most recent IPCC report shows the trends in the figure below. This figure shows a likely range of sea level rise for the 21st century based on all publications to date. The trend clearly shows a persistent increase in sea level rise from now onwards.

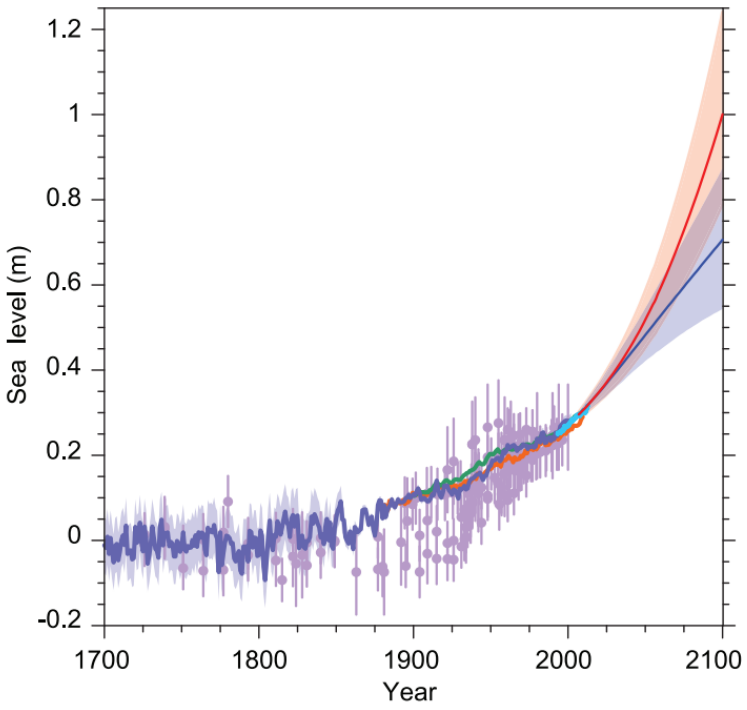

Figure 68: Combination of sea level data, tide gauge data, altimeter data and likely ranges for global mean sea level rise from RCP2.6 (blue) and RCP8.5 (red) scenarios (Church & Gregory, 2019).

In this study our interest lies with the 'worst case scenario' sea level rise. This is considered to be the upper limit of the high emission scenario RCP8.5 visible in the figure above. In the table below the sea level rise values relative to 2020 are shown for 2040, 2070 and 2100.

Table 16: Future 'worst case' sea level rise levels relative to 2020.

Year	Sea level rise [m] (relative to 2020)
2040	0.17
2070	0.47
2100	0.90

6.1.5 Summary

With the use of various data sets long term trends of important climate parameters are analyzed. The COWCLIP2.0 data is considered to be the most reliable data source because it includes multiple different global climate simulations all processed in the same way, making it easy to compare. The use of more systematic data framework like COWCLIP 2.0 is also recommended by different experts (Morim et al., 2018). The following trends result from this data analysis:

Mean Hs:

Clear consensus is found between the different data sources that show a future increase of the mean yearly significant wave height. For 2070 the percentual increase in mean wave height is expected to be in the range of 2 to 10% judging from the different datasets.

Wave direction:

No clear consensus can be found when predicting the future change of wave direction. According to Morim et al. (2018) a lack of research with regards of future wave direction is available as of now. The datasets show both an eastward and Southward possible change of wave direction in the future relative to the mean wave direction approximately from the SE. For 2070 the expected range of wave direction change judging from the datasets is between a Southward direction change of 10% and a eastward directed change of 2%.

Extreme events:

The severeness and frequency of extreme events are closely related. With an increase in extreme event severeness more frequent extreme events of higher magnitude occur. According to the IPCC reports and COWCLIP2.0 future emission scenarios an increase in extreme event severeness is expected which increases the frequency of high magnitude extreme events. These outcomes are contradicted by a research into storm occurrences in the state of Rio de Janeiro using local news reports. Where between 1970 and 2013 the trend shows a minor decrease in extreme event occurrence. Testing the future increase in both severeness and frequency of extreme events is however still of high importance also considering COWCLIP 2.0 being the most reliable data source.

Sea Level Rise:

Based on all different publications related to sea level rise, the IPCC concluded that in the case of a high emission scenario (RCP8.5) sea level rise relative to present-day could be up to 0.17m in 2040, 0.47m in 2070 and 0.9m in 2100.

6.2 Future vulnerability assessment

In the previous chapters especially the cyclic behavior of the beach was accentuated and analyzed with erosion events occurring in the winter months followed up by periods of beach recovery. The long-term dynamics (10's of years) of the beach shows minor changes with a stable equilibrium beach shape which is narrower in the South compared to the North. Up to the occurrence of the July 2019 extreme erosion event there seemed to be a sustainable beach behavior. The recent July 2019 extreme wave event showed an extreme morphological impact which has not occurred in 10's of years, followed up by rapid recovery rates in terms of beach width limiting the exposure of the beach. Erosion on the backbeach, which showed significant decrease in vertical elevation in the South part of the beach, has not yet been followed up by recovery as of 16 months after the erosion. This structural loss of sediment on the backbeach negatively impacts the vulnerability of the beach against similar extreme wave impact in the future. This section discusses the results of part 1 and part 2 of this study in terms of beach vulnerability in the context of future climate change with the use of the long term climate trends. This is discussed for the following future climate trends: Sea Level Rise, extreme event characteristics and frequency and the recovery characteristics.

6.2.1 Sea Level Rise

To estimate the effect of Sea Level Rise the theory of Bruun is used. This theory is based on the assumption of an equilibrium beach profile that matches the water level. With Sea Level Rise a

new equilibrium profile is formed which causes an erosion of material from the upper beach being deposited in the offshore direction (Bruun, 1962). This is visible in Figure 69 below:

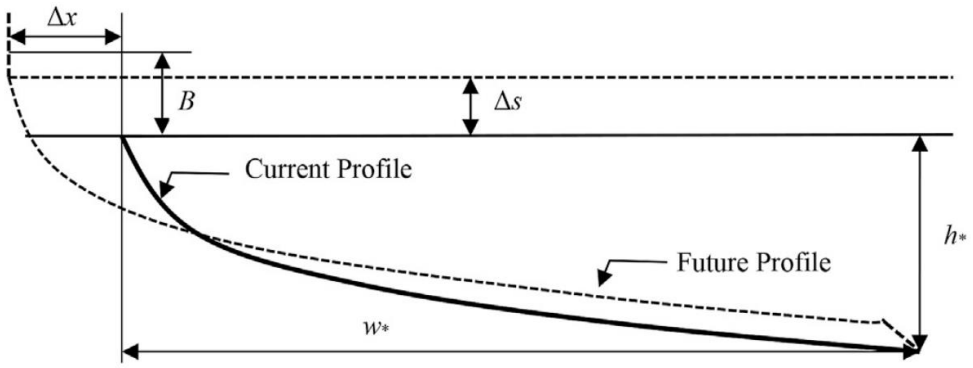

Figure 69: Schematics of the Bruun rule showing the current and future equilibrium profile due to sea level rise by Karunarathna et al. (2018).

The Bruun rule is given by:

$$\Delta x = -\Delta S\left(\frac{W_*}{h_* + B}\right)$$

With;

- Δx = Shoreline recession due to sea level rise [m]
- ΔS = Sea level rise [m]
- h_* = Closure depth [m]
- W_* = Total horizontal distance of the active part of the profile [m]
- B = Maximum vertical elevation of the beach [m]

The figure below shows two cross sections along Copacabana beach taken from the initial bathymetry of the XBeach model. Cross section 5 is located in the South of the beach and Cross Section 15 in the North of the beach (see the exact location of the Cross Sections in Figure 17):

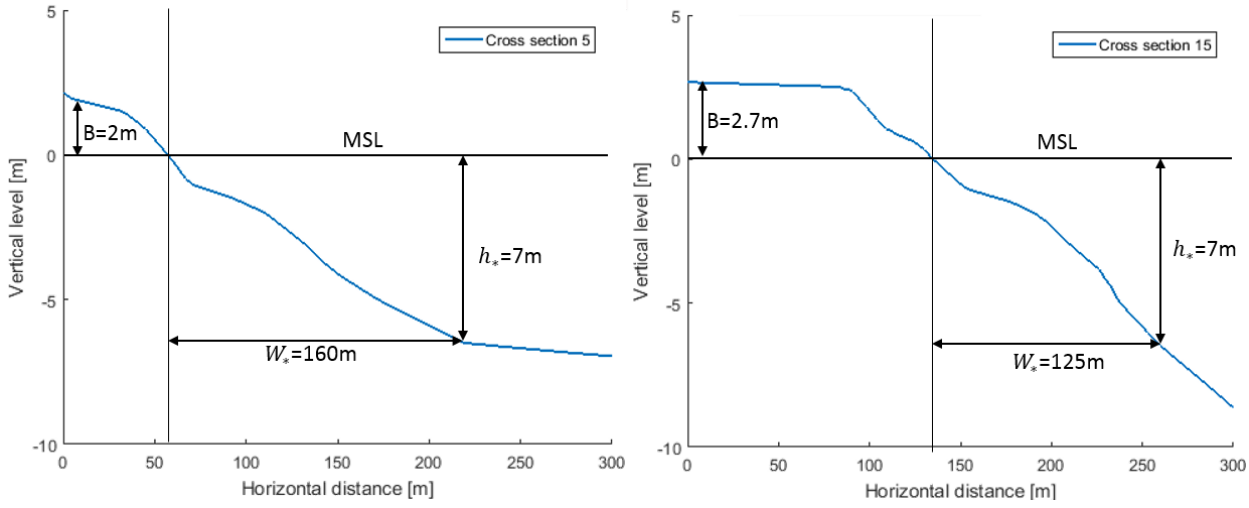

Figure 70: Cross section 5 and 15 including the input parameters for the Bruun rule.

The results of the Bruun rule giving the coastal regression for each cross section are given in Table 17 below:

Table 17: Coastal regression for cross section 5 and 15 for different levels of Sea Level Rise using the Bruun rule.

Year	Sea level rise [m] (relative to 2020)	Coastline regression CS5 [m]	Coastline regression CS15 [m]
2040	0.17	-3.0	-2.2
2070	0.47	-8.4	-6.1
2100	0.90	-16.0	-11.6

What can be concluded from this analysis is that the Northern part of the beach the beach is less sensitive to Sea Level Rise. The Southern part of the beach is more sensitive to sea level rise due to the lower maximum vertical elevation of the beach and the smaller active zone. A maximum coastal regression of 16 meter can be expected to occur in the Southern part of the beach in the case of a high emission sea level rise scenario for 2100. This causes this part of the beach to be more vulnerable to future erosion events because of the smaller buffer in beach width and volume.

6.2.2 Extreme event impact

As concluded in the previous two parts of this a SE wave direction during storm events results in the highest impact in the South of the beach due to a local convergence of wave energy. In combination with the South part of the beach being of smaller equilibrium width this is the most vulnerable part of the beach. This was the main reason for the high impact of the July 2019 erosion event. Within the ranges of long term climate trends the following changes in extreme event characteristics can negatively impact the vulnerability in the beach. For each climate trend the possible changes are discussed using the knowledge obtained from part one and part two of this study:

A change of mean wave direction towards the east of up to 2 degrees in 2070:

With the mean wave direction rotating towards the east there is higher probability of periods of energetic waves originating from the SE. It is shown that the highest variability in beach width is observed in the South of the beach under SE wave direction, this is also confirmed by the model results. This does not occur often but in the future can be expected to occur more. This eventually results in higher beach vulnerability in the South.

The mean significant wave height is bound to increase in the range of 2 to 10% in 2070:

An example of the possible impact of an increase in mean wave height on the erosional impact of extreme wave event is given in part two of this study. Judging from the XBeach model results, a 10% increase of the significant wave height resulted in an increase in total erosional volume of 22% for the July 2019 erosion event, which is significant. For the Southern two beach sections the erosional volume increased with 9%. In the case of the July 2019 erosion event this could cause a significant increase in damage with a high probability that the beach gets fully washed away in the South resulting in possible damage to the hard structures along the beach (see Figure 14b).

An increase in extreme event severeness is expected which increases the frequency of high magnitude extreme events:

Besides the increase in extreme event severeness, which is also the result of an increase in mean wave height, the frequency of high magnitude extreme events is expected to increase in the future. This results in a more frequent erosional impact on the beach resulting in increased beach vulnerability over time. The chance of two or multiple events occurring in close sequence increases as well. This could cause a high beach impact if the second extreme wave event occurs without the beach having returned to its original state during the recovery period.

6.2.3 Post storm recovery

In chapter 3 the recovery characteristics were discussed using the available data and literature on this subject. The conclusion was drawn that Copacabana beach shows very rapid recovery rates in terms of beach width, but in the case of the July 2019 erosion event there was a structural loss in terms of sediment volume on the backbeach in the South negatively impacting future vulnerability. The process of beach recovery occurs on the timescale of months/years according to literature and is the result of high waves overwashing the beach. At Copacabana beach there is one available picture showing such conditions from which is concluded that the possible backbeach recovery occurs on the timescale of years, or does not occur at all.

Total decrease in beach width after an extreme event:

The future wave climate is expected to include a higher extreme event frequency and more severe extreme events. In this case the recovery process becomes more important in determining the beach vulnerability. There is a strong indication that storm severeness is increasing which causes a higher decrease in beach width after extreme events. This, with similar recovery rates, increases the recovery time before the beach reaches its original state and leaves the beach in a vulnerable state for a longer period of time.

Structural erosion on the backbeach:

The long-term behavior of the beach shows a stable equilibrium shape meaning that for most of the erosion event the recovery process has been very effective in fully recovering the beach. The more recent July 2019 erosion event shows that in the case of a very high beach impact significantly impacting the backbeach (which is not seen to have occurred in the last 10's of years) results in structural erosion on the backbeach. This occurred on a small stretch of beach in the South. With increasing extreme event severeness and higher frequency this is expected to occur more often. With an increase in extreme event severeness the impact of extreme events on the backbeach can increase and possibly cause a larger beach stretch to have a structural loss of sediment on the backbeach.

Wave steepness:

With the future increase of mean wave height, the wave steepness during moderate yearly-averaged conditions is likely to increase. The wave steepness is proven to be negatively related to the recovery rate of the beach. This increased wave steepness is expected to slow down recovery rates. On the other hand the model results from the recovery simulation show that with an increased wave height the recovery rates increases. Due to poor model performance (see the outcomes of chapter 5) this result is not reliable. So there is not enough evidence to draw conclusions about the influence of an increase in mean wave height on the rate of recovery.

6.2.4 Storm interval

The interval in between storms is very important in determining the vulnerability of the coastal system of Copacabana beach. The long-term climate trends show that there is evidence from multiple data sources that a future increase in storm severeness can occur, this causes a higher frequency of heavier storms. The relation between storm severeness and beach impact is studied in the previous section which lead to a clear increase in erosion volumes in the case of the July 2019 extreme wave event. The combination of a higher interval of storm and an increase in storm severeness makes the beach more vulnerable. Scenarios where beach recovery from a previous extreme event did not yet fully recover the beach until the time that the next extreme event occurs could lead to a high increase in morphological impact.

6.3 Discussion

Future climate trends are derived from multiple available datasets ranging from hindcast wave data, IPCC reports and a multivariate climate parameter database. The various datasets do not always show the same trends in terms of magnitude, direction and positive or negative trends. The COWCLIP 2.0 is considered to be most reliable because of the use of multiple global climate simulation processed in a similar way for easy comparison. In terms of mean increase in wave height the various datasets show a similar positive trend. For the other climate parameters like the extreme wave heights and especially the wave direction a wide range of trends can be found often showing both positive and negative trends.

When projecting the future climate trends on the results of the first two parts of this study in terms of beach vulnerability it is concluded that within the range of trends there are significant indications that the beach vulnerability is bound to increase. The focus is on the Southern stretch of beach which in the present day is the most vulnerable part of the beach due to the effects of wave convergence under SE directed waves, the relatively low equilibrium width of the beach and the structural backbeach erosion due to the July 2019 extreme erosion event. Especially the influence of a future increase in Sea Level, mean wave height, extreme wave height and a possible eastward rotation of the average wave direction are expected to increase the beach vulnerability in the South of the beach. The impacts of Sea Level Rise is relatively highest in this part of the beach with beach decay predictions being 8.4 meters as of 2070.

6.3.1 Possible interventions

With the results of the future vulnerability assessment the possible future need for interventions is discussed in this section with some examples and possible strategies. The history of Copacabana beach is marked by one major human intervention in 1970 where 3.5 million cubes of sand was nourished at Copacabana beach resulting in an average total shoreline advance of 90 meters. The beach width increased with 35 meters and the beach parallel avenue was widened with 55 meters. Two different nourishment strategies were used with direct sand placement on the beach and the offshore placement off sand within the active zone of the coastal profile. The natural wave forcing was able to transport this offshore placed sediment to the beach being very effective in widening the beach. From 1970 onwards the South part of the beach showed a smaller beach width which is explained by a lack of sediment placement in this part of the beach due to poor accessibility by both dredging vessel and pipeline. Long-term beach dynamics show minor variations in coastline position from which it is concluded that the nourishment in 1970 was very effective in widening the beach and the Copacabana bay behaves like a closed sediment cell. More information on the nourishment in 1970 can be found in Chapter 2.2.

Future interventions should focus on the decrease in vulnerability in the South part of the beach. There is no reason for any interventions in the Northern part of the beach in the next 50 years. With an average beach width of around 120 meters there is sufficient beach area for recreation purposes and the hard structures along the beach are well protected by the wide stretch of beach. Besides the backbeach of this part of the beach shows no signs of structural erosion. The Northern part of the beach is less vulnerable to Sea Level Rise with beach width decrease expected to be not more than 6.1 meters in 2070. Even in the case of storm erosion when beach width decreases up to 40 meters can occur there is still a sustainable beach cycle with rapid recovery rates and sufficient beach width that remains providing sufficient coastal protection in this part of the beach.

Beach interventions can consist of hard structures and/or soft structures (sandy). It is important to take into account the different important values of the beach and how these are either positively

or negatively affected by interventions. The impact of an intervention related to the following need to be taken into account:

- Beach vulnerability
- Ecology
- Safety of beach user / swimmer safety
- Beach recreation
- Water sports (e.g. surfing)
- Impact during construction

With regards to the future interventions two different changes in equilibrium beach state and beach behavior could be considered resulting in an improved beach vulnerability in the South part of the beach with future changing conditions:

- Widening of the beach increasing both the beach area for recreation purposes and the protection of the inland limiting damage to hard structures along the beach.
- Intervening with the results of a decrease in wave energy in the most vulnerable parts of the beach. The convergence zone in the South of the beach is the main cause of vulnerability. Decreasing the nearshore wave energy limits the erosion impact under extreme conditions causing less variations in coastline position.

For both an increased beach width as a decrease in wave energy some examples are given below for possible future intervention strategies and their impact on the beach. It must be noted that before deciding if a strategy is effective, further research is needed into the specific behavior of the beach including the effects of the interventions.

Widening of the South part of the beach:

The widening of the beach has shown to be very effective during the 1970 nourishment. With the Copacabana bay being a closed sediment cell any sediment that is nourished within the embayments is expected not to be lost. Both from the model results and the analysis of the wave buoys measurements there is no indication of any alongshore transport components transporting sediment from the South part to the North part of the beach. From this it is very likely that a possible nourishment in the South remains in place. Besides this, when adding large amounts of sediment it can be expected that the sediment gets lost around the headlands. With the length of especially the Southern headland and the closure depth in this part of the beach judging from the model results, the amount of sediment to be added before there are significant losses is high and a possible nourishment is considered to be well within the safe range of resulting in minimal losses. Sediment placement can be done from both the landside as the seaside. In the case of landside sediment placement there is high hindrance to the beach usage where the beach might be temporarily inaccessible. This is why sand nourishment from the seaside seems is considered to be the best option. The system behavior shows minor influence of alongshore transport and shows a stable beach shape on the long term. It is expected that placement of sand in the South part of the beach is not bound to be transported in the Northern direction looking at typical wave patterns (see Figure 27)

In the case of the 1970 beach nourishment the offshore dumping of sand was performed using a dredging vessel which equally distributed the sand around the -5 meters bottom contour which is within the active zone of the beach profile. The sediment needs to be deposited within the active zone of the beach profile in order to enable cross-shore interaction and transport of sediment towards the beach. A similar strategy can be used in future interventions with the placement of sand equally distributed in the alongshore direction in the South part of the beach (see Figure 71a). During construction the implications for the beach are limited as construction occurs not

directly on the beach and after the nourishment is completed there are minor implications for swimmer safety due to small alongshore differences. As the nourishment stretches over a large area, the underwater ecology could be affected due to it being covered with a thick layer of new sediment. There is however no signs of any reefs or water plant mobilization in the nearshore zone of the coastal area which limits this impact.

A second strategy could be to perform a more concentrated nourishment which allows for lateral spreading of sediment on the timescale of months to years. This could be compared to the sand motor (on a smaller scale) in The Netherlands where the sediment placement is performed on a smaller stretch of beach resulting in less hindrance during construction. Under wave forcing the nourished sand laterally spreads along the beach on the timescale of months/years. This results in more initial alongshore differences and potentially currents which are dangerous for swimming. The alongshore difference however creates opportunities for potential new surf breaks in the first months/years after construction with the alongshore differences eventually diminishing due to lateral spreading and the equilibrium shape of the beach being of a parabolic shape.

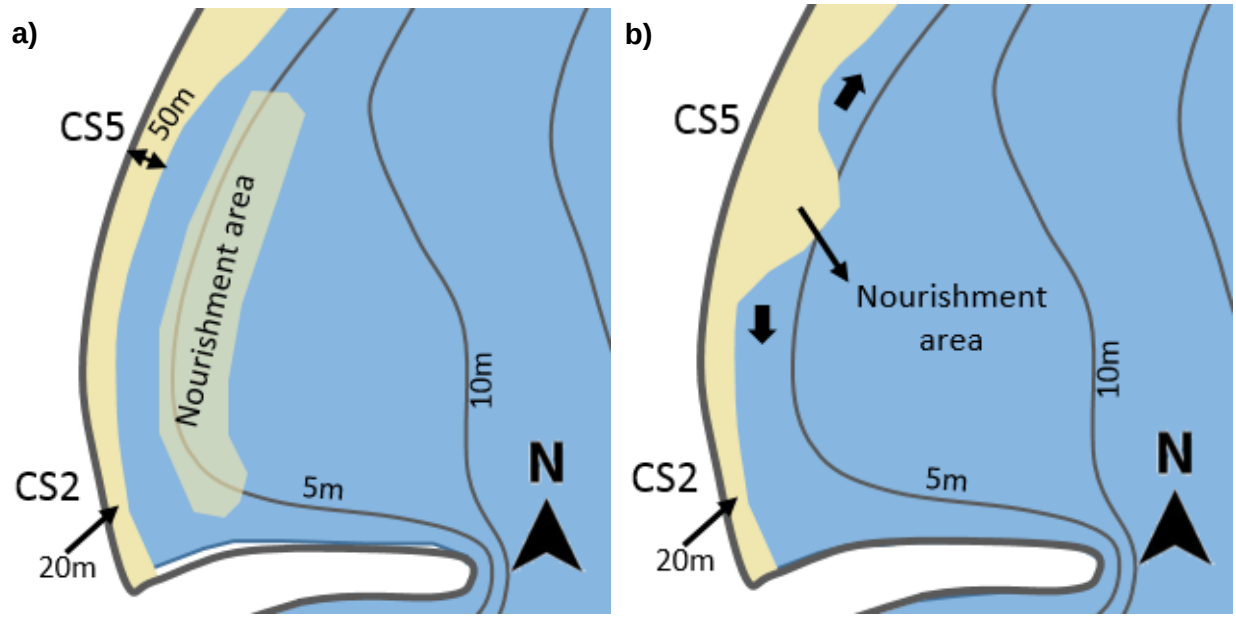

Figure 71: 2 possible nourishment strategies. a) alongshore equally distributed nourishment. b) concentrated nourishment which over time results in lateral spreading of the sediment (indicated with the black arrows).

During the nourishment in 1970 a total of 3.5 million cubes of sediment was needed for an average advance in coastline position of 90 meters over a total beach length of 4 kms. With this information a prediction can be made for the amount of sediment needed for a widening of the South part of the beach. To reach an average widening in the South of 40 meters over 1200 meters of coastline (coastline length of the Southern narrow stretch of beach) an expected amount of 500.000 cubic meters of sediment is needed.

Wave energy decrease in the South part of the beach:

For this case a more innovative intervention can be thought of in the form of a submerged artificial reef structure causing waves to break and limit the wave energy in the nearshore area. The structure needs to be able to withstand the wave impact during storm conditions. This makes that a solution of this form can become more expensive. This form of hard structure adds value to the Copacabana beach system in creating a new ecosystem with the possible growth of a reef and other water plants and a place for fishing. Besides this, the artificial reef can enhance the quality of surfing at Copacabana beach which could be included in the design of the structure to create

a good shorebreak for surfing purposes. The location of such a structure would be best to coincide with the local convergence of wave energy under SE waves in the South of the beach (see Figure 72a for an example). The specific orientation and shape of the artificial reef needs to be determined with the help of more advanced numerical model or physical model studies resulting in a clear overview of the changes of wave patterns, currents and sediment transport due to the structure. An example of such a structure is shown in Figure 72b which shows an artificial reef at Palm beach along the Gold Coast in Australia. This structure is designed for both coastal protection and enhancement of the surf conditions.

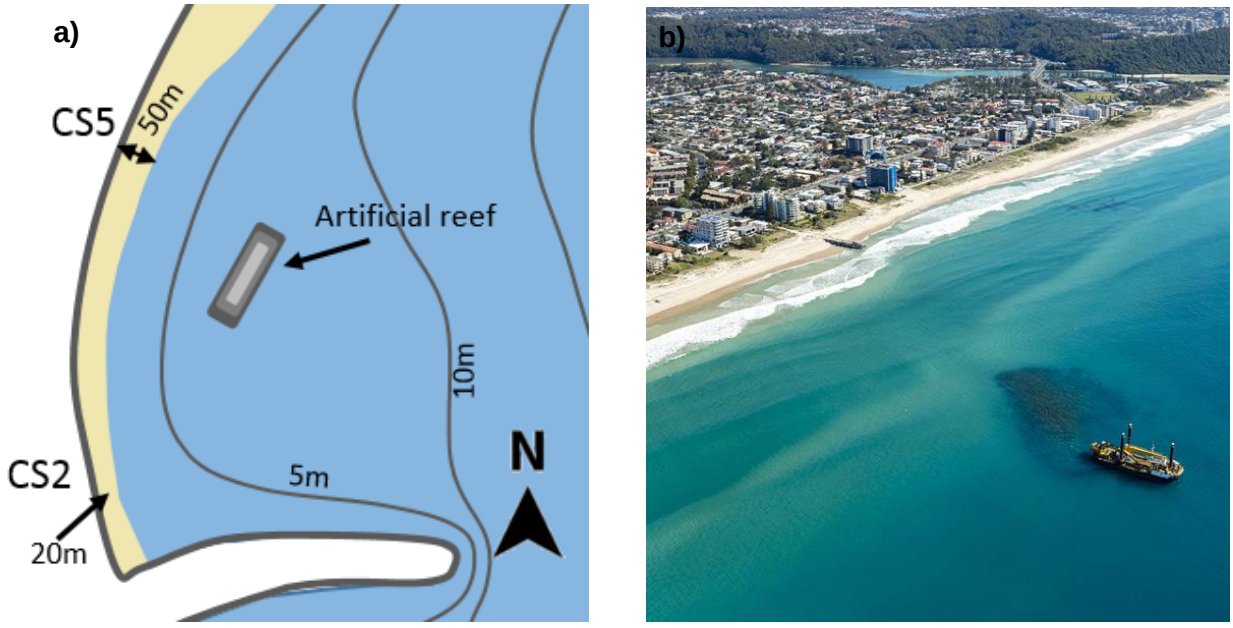

Figure 72: a) An overview of a possible location and orientation of an artificial reef at Copacabana beach. b) This is an example of an artificial reef constructed at Palm beach in Australia where this multifunctional structure functions also functions as a coastal protection. Courtesy of City of Goldcoast.

7 Conclusions and recommendations

7.1 Introduction

The main goal of this thesis was to look into the morphodynamic behavior of Copacbana beach in Rio de Janeiro. After seeing the impact of a recent erosion event in July 2019 this research was instigated raising the questions about the health of the beach. The morphodynamic behavior is looked into for both the current and future beach behavior under the influence of climate change. This lead to the following main research question:

> **What are the current morphodynamic system characteristics of Copacabana beach and how is this possibly changing in the future under changing climate conditions?**

In the section 7.2 the conclusions are given by answering the 3 sub-questions. Hereafter in section 7.3 recommendations are given for further research.

7.2 Conclusion

1. **What are the natural dynamics of the Copacabana beach?**
    a. **What are the typical characteristics of storm events and how does this relate to the July 2019 erosion event?**
    b. **What causes the alongshore difference in storm impact and vulnerability within Copacabana bay?**
    c. **What are the typical beach recovery timescales on Copacabana beach?**

The history of Copacabana beach is marked by one major human intervention 1970 which resulted in an on average 35 meters widening of the beach. From this moment onwards the beach shows stable behavior in terms of coastline position with no observable long-term erosional or accretional trends. Large variations in coastline position are however visible in the short-term which are mostly the result of storm impact with erosion up to 40 meters followed up by recovery of the beach often quickly turning back to its equilibrium state. The erosion and recovery cycle is therefore the main focus in understanding the natural dynamics of the beach.

Storm events are characterized by a 2 to 7 day period of energetic swell-dominated waves (Hs higher than 2m) with a common wave direction in between South and SE. These events are most often the result of cyclones moving over the South-Atlantic ocean from west to east. The July 2019 extreme erosion event was the result of seven-day period of swell waves originating from the SE. Beach erosion occurred up to 40 meters with the highest impact in the South of the beach. From local perspectives and satellite images it can be concluded that this erosion event had an extreme impact which was never seen before. In terms of maximum wave height this event has a return period of 1 year which does not match the erosional impact. The combination of an extraordinary wave direction from the SE in combination with an above average duration of seven days were the main reasons for the high erosional impact.

Under SE wave direction there is a clear convergence of wave energy in the South part of the beach due to refraction around local bottom contours which is reason for the high erosional impact in this part of the beach near Cross Section 5 (see Figure 30). Furthermore, alongshore

differences in extreme event impact are the result of a sheltered zone behind the Southern headland increasing with Southward rotation of the wave direction. Lastly, the equilibrium state of the beach in terms of beach width shows large alongshore variations where the Southern 1200 meters of beach has an average beach width ranging in between 20 and 60 meters. For the Northern 2800 meters the equilibrium beach width ranges in between 100 and 130 meters. The combined effects of the abovementioned alongshore differences results in the South part of the beach to be most vulnerable to extreme event impact. This is confirmed by a satellite image analysis showing the higher variability of this part of the coastline.

Extreme erosion is followed up by a period of beach recovery characterized by rapid recovery rates. A distinction is made between beachface accretion and backbeach aggradation (Morton et al., 1994). Beachface accretion, responsible for an increase in beach width, is clearly observed after extreme erosion with rapid rates up to 1.4m/day. Full recovery in terms of beach width often occurs on the timescale of weeks. This low timescale of recovery limits the beach vulnerability and impact of successive erosion events. Reason for the rapid recovery rates is the swell-dominated wave climate resulting in mild wave steepness in combination with the equilibrium beach state being of an intermediate type with an attached sandbar. Both these system characteristics are positively related to the recovery rates (Phillips et al., 2017). In the case of extreme erosion, the backbeach elevation shows a significant decrease in elevation (e.g. erosion event July 2019 near cross section 5). Backbeach aggradation usually occurs on the timescale of years due to waves overflowing the beach or does not occur at all. As of 16 months after the July 2019 erosion event the backbeach shows no signs of recovery from which it is concluded that there is structural erosion on the backbeach resulting in an increase beach vulnerability near Cross Section 5.

2. Can a numerical model be used to assess the current vulnerability of the beach?

For vulnerability assessment it is important to next to the erosional impact include the successive recovery process. The use of XBeach Surfbeat for erosion modelling shows good model applicability resulting in realistic erosion patterns where the convergence in wave energy under SE waves is clearly observed. A shortcoming of the model is the behavior in the Southern stretch of beach where the model likely overestimates positive alongshore transport quantities (concluded from validation with the use of theoretical alongshore transport formulations) which results in an underestimation of erosion quantities in this part of the beach. This is most likely because of the diffraction process not being included in the model hydronamics. With the use of modelling scenarios the vulnerability of the beach can be assessed judging from relative differences in model results which causes the model sensitivity due to a lack of data to be limited. Overall it can be concluded that the vulnerability of the beach under influence of the erosion process can be assessed using a numerical model. The results from the modelling scenarios confirm that the beach vulnerability is highest in the South under SE wave directions (similar direction as to the July 2019 storm event). The influence of an increased wave height is most significant along the whole beach where an increased extreme event duration has a limited effect on beach vulnerability.

For simulation of the beach recovery the XBeach stationary mode is used. The complex swash zone processes are very important during beach recovery and are responsible for the interaction between the beachface (where accretion takes place during recovery) and the sub-aquatic part of the beach. These processes are not well represented in XBeach but the Bermslope model can be used to compensate for these effects (Roelvink & Costas, 2017). In the case of the 2DH modelling of the Copacabana bay this slightly improved the model results but did not eventually result in realistic recovery patterns. Sediment deposition occurred further offshore than observed in reality. This still shows the lack of interaction between the beachface and sub-aquatic part of

the beach. From this it is concluded that with the use of XBeach stationary mode including the Bermslope model the vulnerability assessment is not possible.

Using a numerical model for a beach vulnerability assessment can be performed using XBeach with regards to the erosion process. In order to assess the full vulnerability of the beach it is very important to take into account the recovery process to for example test the effect of various wave characteristics on recovery rates and the impact of a sequence of erosion events with a partial recovery.

3. **What are the potential likely effects of climate change on the future vulnerability of the beach?**

The local long term climate trends, which are derived from multiple datasets, result in a wide range of trends. For the mean wave height a positive future trend is observed in all datasets between a 2% and 10% increase as of 2070. For both the extreme wave direction as extreme wave heights both a positive and negative trend is found among the available data. Predictions for the wave direction are within the range of a 10% Southward rotation and a 2% eastward rotation. For the extreme wave heights the most reliable dataset concludes an increased return period for major storm events (higher storm frequency). It can be concluded that within the range of trends there are significant indications that the beach vulnerability is bound to increase. The focus is on the Southern stretch of beach which in the present day is the most vulnerable part of the beach. Especially the influence of a future increase in Sea Level Rise, mean wave height, extreme wave height and a possible eastward rotation of the average wave direction (convergence of wave energy with a SE wave direction) are expected to increase the beach vulnerability in the South of the beach. Both the effects of an increase in mean wave height and extreme wave height are visible in the XBeach model scenario results where a 10% increase in extreme wave heights results in a 22% increase in the erosion rates. The impact of Sea Level Rise is relatively highest in this part of the beach with beach erosion predictions up to 8.4 meters as of 2070. Future interventions with the goal of an improvement in beach vulnerability should focus on either widening or further protecting the South part of the beach.

7.3 Recommendations

Additional measurements:

- A first priority would be to have more detailed cross-shore profiles measurements including the sub-aquatic part of the beach. In the currently available cross-section and bathymetry measurements the part of the profile with low water depths (MSL 0m to -3m) could not be included. It is advised to frequently repeat the measurements during a longer period of time including the winter period and to capture the effects of an erosion event preferably capturing pre-storm, post-storm and post recovery beach profiles. This can give important information related to beach behavior during the erosion and recovery cycle. Measurements can be performed at multiple alongshore locations preferably at equal locations as the measurements performed for this study (as visible in Appendix C). The modelling simulation in this study only includes the July 2019 erosion and subsequent recovery period because of the limited availability for other erosion events. This additional data can lead to improved accuracy of both the model input and the validation of the model and allow for modelling of other erosion and recovery events besides the July 2019 event.
- The currently available full bathymetry used as input for the XBeach model is based on a combination of an openly available navigation map with a coarse grid and self-made single-beam bathymetry measurements for a limited part of the beach not including the intertidal area (MSL 0m to -3m). For better model accuracy it is recommended to perform

a single, more detailed bathymetry measurement for example with the use of an echo sounder or multi-beam survey.

- The available information related to the sediment characteristics dates back to the nourishment in 1970 and only includes the grain size. It is recommended to perform more detailed sediment measurements including the sediment density. Surveys are advised to be performed in multiple locations in both the cross-shore and alongshore direction to take into account differences in sediment characteristics.

Data analysis:

- The analysis of the short-term beach dynamics are performed with the use of satellite images by manually measuring the beach width for 5 cross sections with the use of GIS software during a 4-year period. The interface between the saturated and non-saturated part of the beach is taken as the coastline for the beach width measurements including a correction for the tidal height. The momentary wave height affects these measurement as they affect the location of the interface between the saturated and non-saturated part of the beach due to the wave run-up process. For future research, automation of the coastline position extraction can be considered in order to speed-up the process of extracting beach width from satellite image. Correcting for the effects of wave run-up can result in more accurate beach width extraction with the use of theoretical formulations to estimate the wave run-up knowing the local beach slope and momentary wave conditions.

Beach recovery:

- This thesis shows the importance of the recovery process in defining the vulnerability and health of the beach. Most research focuses on beach erosion when equal emphasis for both erosion and recovery is advisable. This could help accelerating the ability of numerical models to simulate beach recovery. The same thing holds for literature studies related to beach recovery for which it would be beneficial to obtain more general knowledge on beach recovery with for example a more general method in defining local recovery rates.

Further steps needed towards the engineering of interventions:

The insights from this thesis made it possible to discuss a range of intervention strategies and some of their expected advantages and disadvantages. The main outcomes related to the intervention strategy is that the focus should be on the South part of the beach which is the most vulnerable to storm impact and the effects of climate change. In order to be able to choose specific intervention strategies and being able to look into the effectiveness of those interventions some further research steps are recommended below:

- In the case of engineering a hard structures like for example an artificial reef it is important to look into the possible negative effects such a structure can have on the beach. As the focus is on the South zone of the beach comprehensive wave patterns need to be taken into account including the process of diffraction. This starts with accurately modelling the hydronamic patterns around such a structure. The XBeach model that is setup during this thesis would in its current state not be suitable for simulating this. One of the main shortcomings of the XBeach model is the diffraction process not being included. This is especially important in the Southern part of the bay where the diffraction patterns are an important part of the hydronamics. Accurately modelling the diffraction pattern is an essential step in obtaining accurate hydronamic patterns around hard structures. The currently available modelling tools that include processes like diffraction and also are able to simulate accurate morphodynamics as a results of these patterns are limited. This is

why it is recommended to focus on the modelling of accurate hydronamic patterns around structures.

- Accurately modelling the hydronamics around structures could be performed with a modelling tool like SWASH. SWASH provides a general basis for deep water to beach including the wave diffraction.
- This thesis gives insight into the relation between the wave characteristics and their possible impact on the beach while also taking into account the alongshore differences. Some clear examples are given of the difference and characteristics of erosive and recovery wave conditions. This can help in providing the link between the hydronamics around structures and their possible morphological impact. The goal of engineering a hard structure should be to limit the erosive conditions in the most vulnerable parts of the beach while still allowing for the recovery conditions to persevere, as beach recovery is an essential part in sustaining a healthy beach state. One could think of a submerged structure that allows for moderate sized waves (recovery conditions) to be able to reach the beach and stronger waves to be partly dissipated.
- As discussed in the beginning of this section, some additional measurements can result in a more accurate representation of especially the bathymetry in future hydronamic model studies which would further decrease uncertainty.
- Another viable option is to apply a sand nourishment in the South part of the beach. A sand nourishment has proven to be very effective in the past looking at the nourishment in 1970. Two essential things that need to be checked is if the sand, when nourished in the South, stays in the this part of the beach where it is most needed and doesn't get lost either to the North part of the beach or around the headland in the South. The model studies in this thesis suggests that there are no losses of sediment both on the North and South side. However with the shortcomings of the model in the South part of the beach this needs to be confirmed by further analysis. For further analysis it could be recommended to move towards the physical modelling of the South part of the beach. Another option, which might me more economic, is to perform some current measurements in the nearshore zone in the South part of the beach. From this, more insights can be obtained with regards to alongshore current directions under varying wave heights and wave directions. This can confirm if the sediment that is possibly nourished in the South will remain in this part of the beach.

References

Barcena, A., Prado, A., Samaniego, J., & Perez, R. (2015). The effect of climate change on the coasts of Latin America and the Caribbean. In *United Nations*.

Brocchini, M., & Baldock, T. E. (2008). Recent advances in modeling swash zone dynamics: Influence of surf-swash interaction on nearshore hydrodynamics and morphodynamics. *Reviews of Geophysics*, *46*(3), 1–21. https://doi.org/10.1029/2006RG000215

Bruun, P. (1962). Sea-level rise as a cause of shore erosion. *Journal of the Waterways and Harbors Division*, *88*(1), 117–132.

Bugajny, N., Furmańczyk, K., Dudzińska-Nowak, J., & Paplińska-Swerpel, B. (2013). Modelling morphological changes of beach and dune induced by storm on the Southern Baltic coast using XBeach (case study: Dziwnow Spit). *Journal of Coastal Research*, *65*(January), 672–677. https://doi.org/10.2112/si65-114.1

Butt, T., Russell, P., & Turner, I. (2001). The influence of swash infiltration–exfiltration on beach face sediment transport: onshore or offshore? *Coastal Engineering*, *42*(1), 35–52. https://doi.org/https://doi.org/10.1016/S0378-3839(00)00046-6

Chrzastowski, M. J. (2005). Beach Features. In M. L. Schwartz (Ed.), *Encyclopedia of Coastal Science* (pp. 145–147). Springer Netherlands. https://doi.org/10.1007/1-4020-3880-1_34

Church, J. A., & Gregory, J. M. (2019). Sea level change. *Encyclopedia of Ocean Sciences*, 493–499. https://doi.org/10.1016/B978-0-12-409548-9.10820-6

Coco, G., Senechal, N., Rejas, A., Bryan, K. R., Capo, S., Parisot, J. P., Brown, J. A., & MacMahan, J. H. M. (2014). Beach response to a sequence of extreme storms. *Geomorphology*, *204*, 493–501. https://doi.org/10.1016/j.geomorph.2013.08.028

Eichentopf, S., Karunarathna, H., & Alsina, J. M. (2019). Morphodynamics of sandy beaches under the influence of storm sequences: Current research status and future needs. *Water Science and Engineering*, *12*(3), 221–234. https://doi.org/10.1016/j.wse.2019.09.007

Elsayed, S. M., & Oumeraci, H. (2017). Effect of beach slope and grain-stabilization on coastal sediment transport: An attempt to overcome the erosion overestimation by XBeach. *Coastal Engineering*, *121*(June 2016), 179–196. https://doi.org/10.1016/j.coastaleng.2016.12.009

Fernández-Mora, A., Calvete, D., Falqués, A., & De Swart, H. E. (2015). Onshore sandbar migration in the surf zone: New insights into the wave-induced sediment transport mechanisms. *Geophysical Research Letters*, *42*(8), 2869–2877. https://doi.org/10.1002/2014GL063004

Gan, M. A., & Rao, V. B. (1990). Surface Cyclogenesis over South America. *Monthly Weather Review*, *119*(5), 1293–1302. https://doi.org/10.1175/1520-0493(1991)119<1293:SCOSA>2.0.CO;2

Garcia, C. A. E., Pereira, E. S., & Copertino, M. (2016). *The Brazilian Coastal Monitoring System (SiMCosta) for Climate Studies*. *July 2017*.

Hennerrmann, K. (2016). *ERA5 hourly data on single levels from 1979 to present*. https://cds.climate.copernicus.eu/cdsapp#!/dataset/reanalysis-era5-single-

levels?tab=overview

Holthuijsen, L. H., Booij, N., & Herbers, T. H. C. (1989). A prediction model for stationary, short-crested waves in shallow water with ambient currents. *Coastal Engineering*, *13*(1), 23–54. https://doi.org/10.1016/0378-3839(89)90031-8

Hopkins, J. (2018). *Storm Impact on Morphological Evolution of a Sandy Inlet*. 5751–5762. https://doi.org/10.1029/2017JC013708

Jongedijk, C. E. (2017). Improving XBeach non-hydrostatic model predictions of the swash morphodynamics of intermediate-reflective beaches. *TU Delft*, MSc Thesis.

Kamphuis, J. W. (1993). Alongshore sediment transport rate. *Journal of Waterway, Port, Coastal and Ocean Engineering*, *119*(3), 344–346. https://doi.org/10.1061/(ASCE)0733-950X(1993)119:3(344)

Karambas, T. V. (2003). Modelling of Infiltration-Exfiltration Effects of Cross-Shore Sediment Transport in the Swash Zone. *Coastal Engineering Journal*, *45*(1), 63–82. https://doi.org/10.1142/S057856340300066X

Karunarathna, H., Brown, J., Chatzirodou, A., & Dissanayake, P. (2018). Multi-timescale morphological modelling of a dune-fronted sandy beach Multi-timescale morphological modelling of a dune-fronted sandy beach. *Coastal Engineering*, *136*(June), 161–171. https://doi.org/10.1016/j.coastaleng.2018.03.005

Kowsmann, R. (1970). variações de curto e longo prazo de um perfil de praia de copacabana rio de janeiro. *Instituto de Pesquisas Da Marinha*, *039*, 16.

Lins-de-barros, F. M., & Klumb-oliveira, L. A. (2018). *Avaliação histórica da ocorrência de ressacas marinhas e danos associados entre os anos de 1979 e 2013 no litoral do estado do Rio de Janeiro (Brasil) Historical evaluation of marine storm occurrence and associated*. *November*. https://doi.org/10.5894/rgci-n146

Lins-de-Barros, F. M., Sauzeau, T., & Varela Guerra, J. (2019). Historical evolution of seafront occupation in France (Bay of Biscay) and Brazil (Rio de Janeiro) face to coastal erosion vulnerability and risks (19th - 21th centuries). *Confins*, *39*. https://journals.openedition.org/confins/18175

List, J. H., Farris, A. S., & Sullivan, C. (2006). Reversing storm hotspots on sandy beaches: Spatial and temporal characteristics. *Marine Geology*, *226*(3–4), 261–279. https://doi.org/10.1016/j.margeo.2005.10.003

Luijendijk, A., Hagenaars, G., Ranasinghe, R., Baart, F., Donchyts, G., & Aarninkhof, S. (2018). *The State of the World ' s Beaches*. 1–11. https://doi.org/10.1038/s41598-018-24630-6

McCall, R. T., Van Thiel de Vries, J. S. M., Plant, N. G., Van Dongeren, A. R., Roelvink, J. A., Thompson, D. M., & Reniers, A. J. H. M. (2010). Two-dimensional time dependent hurricane overwash and erosion modeling at Santa Rosa Island. *Coastal Engineering*, *57*(7), 668–683. https://doi.org/10.1016/j.coastaleng.2010.02.006

Mil-Homens, J., Ranasinghe, R., van Thiel de Vries, J. S. M., & Stive, M. J. F. (2013). Re-evaluation and improvement of three commonly used bulk longshore sediment transport formulas. *Coastal Engineering*, *75*, 29–39. https://doi.org/10.1016/j.coastaleng.2013.01.004

Morim, J., Hemer, M., Cartwright, N., Strauss, D., & Andutta, F. (2018). On the concordance of 21st century wind-wave climate projections. *Global and Planetary Change*, *167*(May), 160–

171. https://doi.org/10.1016/j.gloplacha.2018.05.005

Morim, J., Trenham, C., Hemer, M., Wang, X. L., Mori, N., Prat, M. C., Semedo, A., Shim, T., Timmermans, B., & Cam, P. (2020). *A global ensemble of ocean wave climate projections from CMIP5- driven models*. 1–10. https://doi.org/10.1038/s41597-020-0446-2

Morton, R. A., Paine, J. G., & Gibeaut, J. C. (1994). Stages and durations of post-storm beach recovery, southeastern Texas coast, USA. *Journal of Coastal Research*, 884–908.

Nederhoff, C. M., Lodder, Q. J., Boers, M., Bieman, J. P. Den, & Miller, J. K. (2015). Modelling the effects of hard structures on dune erosion and overwadh: a case study of the impact of Hurricane Sandy on the New Jersey coast. *Proceedings Coastal Sediments, San Diego, CA*, *January 2017*, 1–17.

Otvos, E. G. (2004). Beach aggradation following hurricane landfall: Impact comparisons from two contrasting hurricanes, northern Gulf of Mexico. *Journal of Coastal Research*, *20*(1), 326–339. https://doi.org/10.2112/1551-5036(2004)20[326:bafhli]2.0.co;2

Parise, C. K., Calliari, L. J., & Krusche, N. (2009). Extreme storm surges in the south of Brazil: atmospheric conditions and shore erosion. *Brazilian Journal of Oceanography*, *57*(3), 175–188.

Phillips, M. S., Harley, M. D., Turner, I. L., Splinter, K. D., & Cox, R. J. (2017). Shoreline recovery on wave-dominated sandy coastlines: the role of sandbar morphodynamics and nearshore wave parameters. *Marine Geology*, *385*, 146–159. https://doi.org/10.1016/j.margeo.2017.01.005

Puleo, J. A., Beach, R. A., Holman, R., & Allen, J. (2000). Swash zone sediment suspension and transport and the importance of bore-generated turbulence. *Journal of Geophysical Research Atmospheres*, *105*. https://doi.org/10.1029/2000JC900024

Rangel, S. (2016, June 12). *Mar invade duas obras olímpicas em Copacabana*. https://www1.folha.uol.com.br/esporte/olimpiada-no-rio/2016/06/1780944-mar-invade-duas-obras-olimpicas-em-copacabana.shtml

Roelvink, D., & Costas, S. (2019). Coupling nearshore and aeolian processes: XBeach and duna process-based models. *Environmental Modelling and Software*, *115*(March), 98–112. https://doi.org/10.1016/j.envsoft.2019.02.010

Roelvink, D. J. A., & Costas, S. (2017). *Beach berms as an essential link between subaqueous and subaerial beach/dune profiles*.

Roelvink, D., McCall, R., Mehvar, S., Nederhoff, K., & Dastgheib, A. (2018). Improving predictions of swash dynamics in XBeach: The role of groupiness and incident-band runup. *Coastal Engineering*, *134*(February 2017), 103–123. https://doi.org/10.1016/j.coastaleng.2017.07.004

Roelvink, D., Reniers, A., van Dongeren, A., van Thiel de Vries, J., McCall, R., & Lescinski, J. (2009). Modelling storm impacts on beaches, dunes and barrier islands. *Coastal Engineering*, *56*(11–12), 1133–1152. https://doi.org/10.1016/j.coastaleng.2009.08.006

Roelvink, J. A. (1993). Dissipation in random wave groups incident on a beach. *Coastal Engineering*, *19*(1–2), 127–150. https://doi.org/10.1016/0378-3839(93)90021-Y

Roelvink, J. A., & Stive, M. F. J. (1989). Bar-generating cross-shore flow mechanisms on a beach. *Journal of Geophysical Research*, *94*(C4), 4785–4800.

https://doi.org/10.1029/JC094iC04p04785

Sá-Pires, C., Ferreira, Ó., & Dias, J. A. (2003). Beach recovery rates after a storm event and their association to different morphodynamic characteristics. *Proceedings of Coastal Sediments 2003*, *January*, CD publication.

Sallenger, J. (2000). Storm impact scale for barrier islands. *Journal of Coastal Research*, *16*(3), 890–895.

Senechal, N., Coco, G., Castelle, B., & Marieu, V. (2015). Storm impact on the seasonal shoreline dynamics of a meso- to macrotidal open sandy beach (Biscarrosse, France). *Geomorphology*, *228*, 448–461. https://doi.org/10.1016/j.geomorph.2014.09.025

Short, A. D. (1999). *Handbook of beach and shoreface morphodynamics* (Issue 551.468 HAN).

Steetzel, H. J. (1991). Cross-Shore Transport during Storm Surges. In *Coastal Engineering 1990* (pp. 1922–1934). https://doi.org/10.1061/9780872627765.147

Sterl, A. (2004). On the (in)homogeneity of reanalysis products. *Journal of Climate*, *17*(19), 3866–3873. https://doi.org/10.1175/1520-0442(2004)017<3866:OTIORP>2.0.CO;2

Turner, I. L., & Masselink, G. (1998). Swash infiltration-exfiltration and sediment transport cal flow rates of net. *Journal of Geophysical Research*, *103*(C13), 30813–30824.

van Dam, T. (2019). *NUMERICAL MODELLING OF BEACH RECOVERY*. TU Delft.

van Dijken, W. (2012). *R. Boltje & Zonen NV: de Friese baggeraar uit Zwolle*. W. van Dijken. https://books.google.nl/books?id=C5p9MwEACAAJ

van Rijn, L. C. (1993). *Principles of sediment transport in rivers, estuaries and coastal seas*.

Van Rijn, L. C. (2014). A simple general expression for longshore transport of sand, gravel and shingle. *Coastal Engineering*, *90*, 23–39. https://doi.org/10.1016/j.coastaleng.2014.04.008

van Thiel de Vries, J. S. M. (2009). *Dune erosion during storm surges*.

Vera-cruz, D. (1972). *Artificial nourishment of Copacabana beach*. 14.

Vousdoukas, M. I., Ferreira, Ó., Almeida, L. P., & Pacheco, A. (2012). Toward reliable storm-hazard forecasts: XBeach calibration and its potential application in an operational early-warning system. *Ocean Dynamics*, *62*(7), 1001–1015. https://doi.org/10.1007/s10236-012-0544-6

Wright, L. D., & Short, A. D. (1984). Morphodynamic variability of surf zones and beaches: A synthesis. *Marine Geology*, *56*(1–4), 93–118. https://doi.org/10.1016/0025-3227(84)90008-2

Appendix A. Theoretical background

In this appendix the essential theoretical background is given in relation to wave generation, wave transformation and cross-shore sediment transport.

A.1 Coastal zone definitions

The image below shows an overview of the main features of the beach. In this thesis these definitions are used.

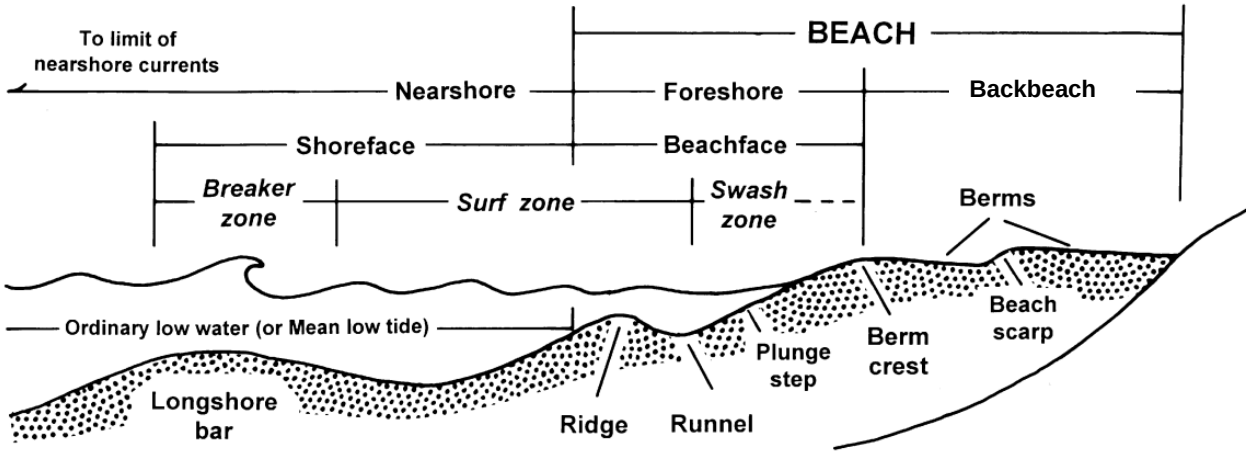

Figure 73: The main features of the beach as defined by (Chrzastowski, 2005).

A.2 Wave generation and transformation

Propagation of waves is influenced by the bottom depth. Deep water is defined as the region where the water depth is bigger than half the wave length ($\frac{1}{2}L \leq h$). In the case of deep water there is no influence of the bottom on the propagation of waves. Shallow water is defined as the region where the water depth is smaller than 1/20th of the wave length ($\frac{1}{20}L \geq h$). The region in between is called the intermediate zone. When waves enter the intermediate region there is a considerable influence of the bed on the propagation of waves.

The relation between the wave propagation speed and the water depth and the wave period is given by the wave dispersion relation:

$$c = \frac{g * T}{2 * \pi} * \tanh(k * h)$$

With:

- c = Wave propagation speed [m/s]
- T = Wave period [s]
- k = Wave number [1/m]
- h = Local water depth [m]

In the image below the dispersion relation is visualized and the different regions of the coastal zone are also denoted:

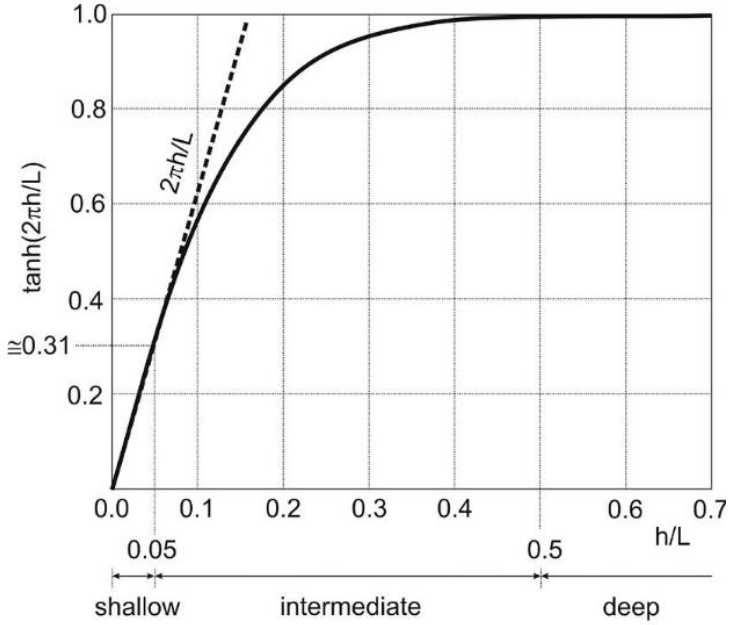

Figure 74: Wave dispersion relation.

A.2.1 Refraction

When waves approach the underwater bottom contours at an angle there is a difference in wave velocity along the wave crest due to differences in water depth along the wave crests (see the dispersion relation). This causes the wave crests to align with the local bottom contours. With different bottom shapes refraction can cause bot a convergence and divergence of wave energy in shallow and intermediate water depths. This change in direction can be approximated using Snell's law:

$$\frac{\sin(\varphi_2)}{c_2} = \frac{\sin(\varphi_1)}{c_1}$$

With:

- φ = angle between the local wave direction relative to the local bathymetry contours [degrees]
- c = wave phase speed [m/s]

A.2.2 Diffraction

In the case of obstructions in the direction of wave propagation occurs or a sudden change in bottom contours, diffraction can occur. This sudden change causes the transfer of wave energy along the wave crests. This results in the bending of waves around structure which results in a circular shaped wave pattern.

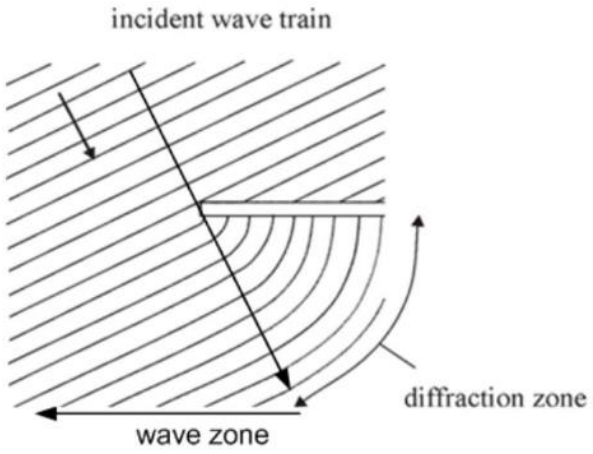

Figure 75: Diffraction of an incident wave train due to a hard structure.

A.2.3 Shoaling

The process of shoaling is caused by the dependency of the group velocity of the waves on the water depth. When waves enter shallow water depths the waves slow down. This can be concluded from the wave dispersion equation which shows the relation between the wave velocity and the water depth. With the wave frequency remaining constant and assuming no dissipation of energy the wave energy per area increases and causes higher wave heights. This process, which is basically the increase in wave height when waves enter intermediate/shallow water depths, is called wave shoaling.

A.2.4 Wave breaking

The theory of shoaling which is dependent on the dispersion relation mathematically shows that when the water depth is approaching zero the wave height would increase until infinity. However, there is a physical limit of the wave height where wave breaking starts to occur. Wave breaking occurs when the particle velocity of the wave crest exceeds the velocity of the wave crest. When waves shoal the wave height increases and the Based on the Stokes wave theory a limit for wave breaking, also called the wave breaking parameter, is found to be the following:

$$\gamma = \frac{H_b}{h_b} \approx 0.88$$

With:

- H_b = Wave height when breaking [m]
- h_b = Water depth when breaking [m]

The process of wave breaking can occur in various ways, which is mainly dependent on the properties of the waves and the bed slope. The wave breaking process is guided by the Iribarren parameter. This parameter relates the bed slope to the wave steepness:

$$\xi = \frac{\tan(\alpha)}{\sqrt{\frac{H_0}{L_0}}}$$

With:

- ξ = Iribarren parameter
- α = Slope [-]

- H_0 = Deep water wave height [m]
- L_0 = Deep water wave length [m]

A distinction is made between surging, collapsing, plunging and spilling waves. In the image below these different wave breaking modes are shown with an indication for corresponding values of the Iribarren parameter. The transition between these different modes is gradual.

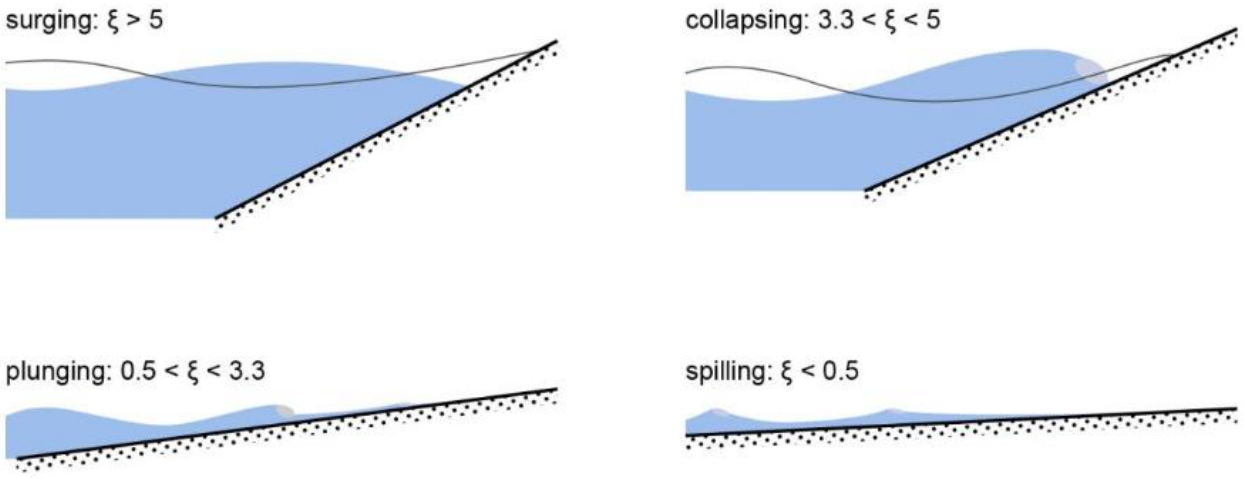

Figure 76: Different breaking modes with an indication of corresponding Iribarren parameters.

Surging breakers occur on steep shores with relatively long swell waves. The waves surge up and down the coast with a small breaker zone. A big part of the wave energy reflects. Plunging waves cause the typical curling top waves where most of the wave energy is dissipated and only a small amount reflects. Spilling breakers occur along flat coasts where a typical foam line develops with the incoming waves. Practically all wave energy is dissipated and very little reflection occurs.

A.2.5 Wave asymmetry and skewness

Wave shoaling was explained in the previous section using linear wave theory. This doesn't fully hold in shallow water depths due to the non-linear effects being an important factor in determining the wave-induced transport. The two main non-linear wave characteristics are the skewness and asymmetry of the wave.

Wave skewness:

Wave skewness is the gradual peaking of the wave crest and the flattening of the wave through. This can be considered as a horizontal asymmetry in wave shape. An example of the superposition of two wave signals shows a positively skewed wave shape in Figure 77 below: Besides influencing the local surface elevation, the wave skewness influences the orbital velocities. This means that the onshore directed velocity increases (due to the peaking of the crest) and the offshore directed velocity decreases (due to the flattening of the wave through). Due to continuity, this automatically means that the duration of the onshore directed flow is decreasing and increasing for the offshore directed flow.

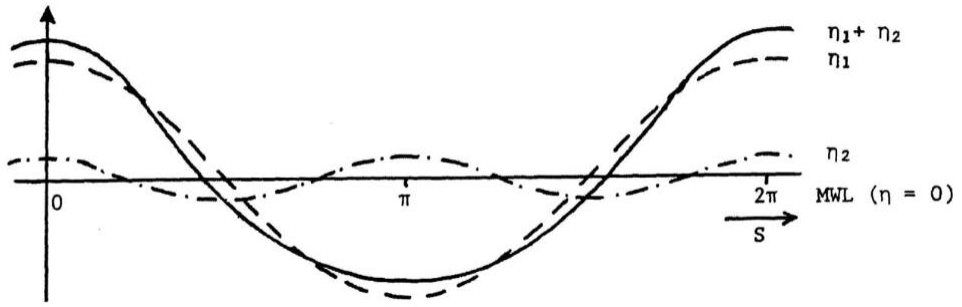

Figure 77: An example of a positively skewed wave by the superposition of two wave signals.

Wave asymmetry:

Wave asymmetry is characterized by a pitched forward wave shape. This occurs due to the difference in propagation speed of the crest compared to the trough. For non-linear waves the propagation speed is described by the following equation:

$$c = \sqrt{g * (h + \eta)}$$

With:

- c = Wave propagation speed [m/s]
- g = Gravitational acceleration [m^2/s]
- h = Water depth [m]
- η = Surface elevation [m]

So with wave amplitude a the propagation velocity of the crest is equal to $\sqrt{g * (h + a)}$ and the propagation velocity of the trough is equal to $\sqrt{g * (h + a)}$. This causes a pitched forward wave shape like shown in the image below which is also called

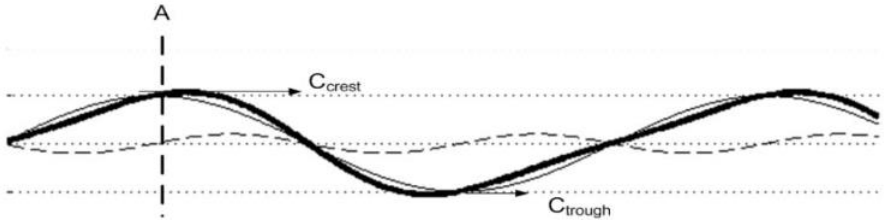

Figure 78: An example of an pitched forward asymmetric wave as a result of the superposition of two single wave signals.

A.2.6 Wave set-up and set-down

The theory of wave set-up and set-down is to do with the variations in the radiation stress component perpendicular to the shoreline. This is considered as the total wave averaged transport of momentum perpendicular to the shore. The radiation stress is defined as:

$$S_{xx} = \left(2n - \frac{1}{2}\right) * E$$

With:

- S_{xx} = Radiation stress x-component [N/m]

- n = Ratio of group velocity and phase velocity [-]
- E = Wave energy in the water column per m^2 [J/m^2]

With an increase in wave height due to shoaling the radiation stress increases which causes a positive gradient in the direction of the coastline. This is then compensated by an in coastward direction decrease in water level which is called set-down. When waves start to break the radiation stress rapidly decreases in shoreward direction due to the dissipation of energy. This is compensated by an increase in water level (wave set-up) in the shoreward direction which causes an offshore directed pressure force that compensates the decrease in radiation stress (which creates a force in shoreward direction).

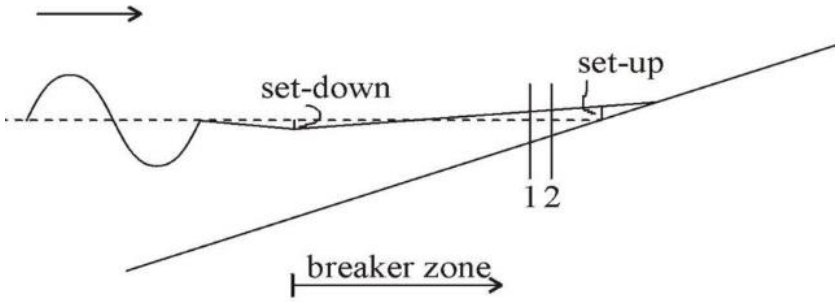

Figure 79: Visualization of wave set-up and wave set-down.

A.2.7 Swash zone

The swash zone is a very dynamic zone where the waves swash up and down the beachface. Figure 80 and Figure 81 show a visualization of the hydronamics in the swash zone made by Brocchini & Baldock (2008). Figure 80 shows the run-up part of the swash motion where the bore collapses on the beach and the run-up is increasing when the bore collapses on the beach. This causes infiltration of sediment under the bore.

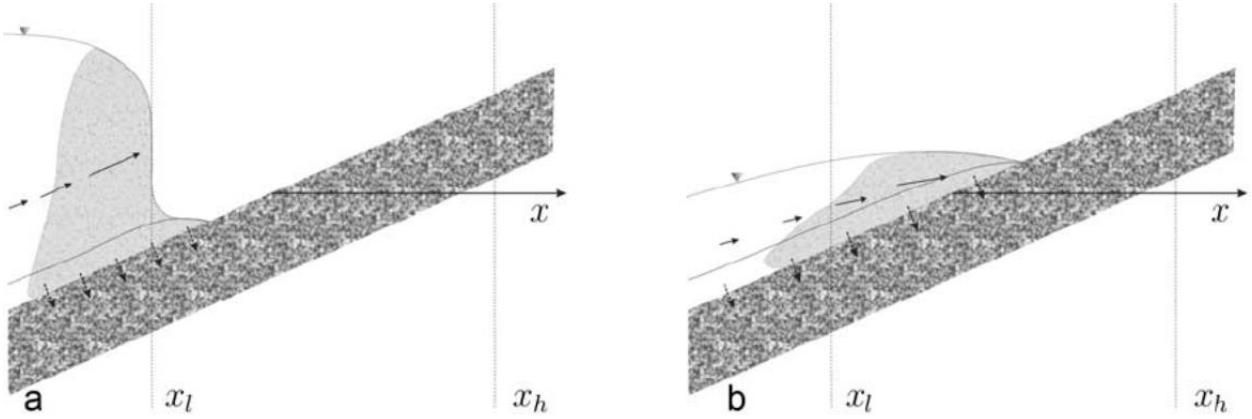

Figure 80: The run-up phase of the swash cycle. The collapse of the bore is visible where the arrows in the water columns denote the flow velocities and the arrows on the bed show the infiltration of water.

In Figure 81 the run-down phase of the swash cycle is shown where in image a) there is a diverging flow where the maximum run-up height is reached. This maximum run-up height is a combination of the upward swash motion combined with the wave set-up. This marks the end point of the run-up. Exfiltration occurs during this phase and the flow is reversed. This flow often reaches supercritical flow velocity. During run-down the acceleration of the flow is more gradual compared to the rundown. When the next waves comes in the swash cycle starts over.

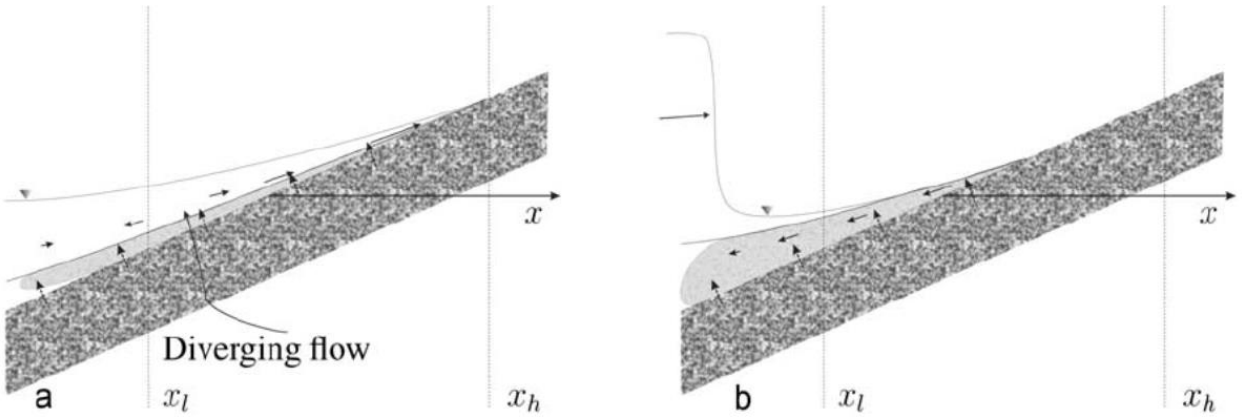

Figure 81: The run-down phase of the swash cycle. a) End of the run-up phase. b) Run-down where the next incoming wave is visible.

A.2.8 Long waves

Long waves are lower frequency wave that act on the wave group timescale. Within wave groups there is a variation in wave height, which also leads to a variation in radiation stresses. The radiation stress increases under the highest waves, causing a water level set-sown. The radiation stress decreases under the lowest waves causing a set-up of the water level. This kind of long wave is called the bound long wave that has the length of the wave group and travels with the group.

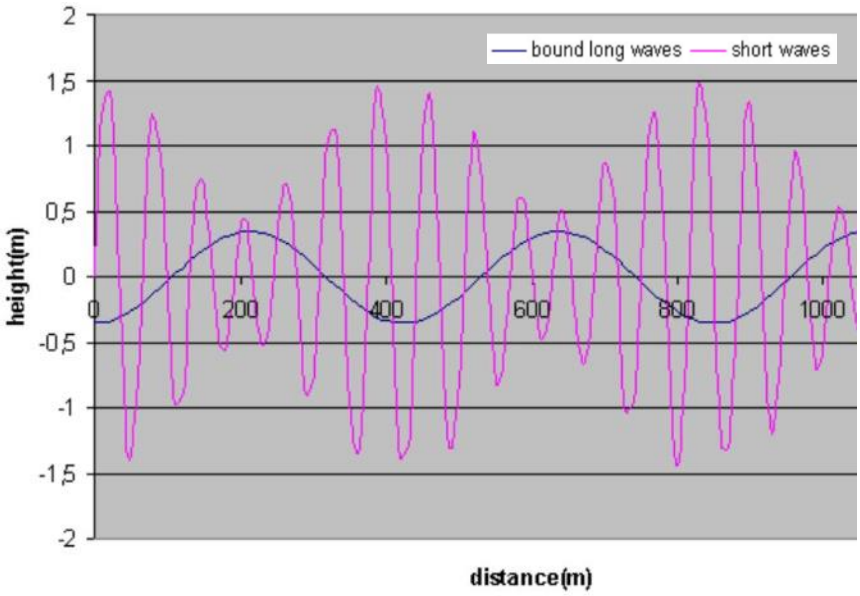

Figure 82: Bound long wave with a 180 degrees phase difference with the short-wave envelope.

In reality however, the long wave do not have a perfect correlation with the wave group. It is observed that the long wave are no longer moving at the speed of the wave group especially after the breaker line. The bound long wave is no longer bound at this point and is released from the group after the point of breaking. The negative correlation offshore of the breaker line changes to a positive correlation in the breaker zone.

A.3 Cross-shore transport

The cross-shore transport consists of a mix of bed transport and suspended transport. Different coastal processes are encountered in the surf zone. The main factors that influence the cross-shore transport quantities are undertow, wave asymmetry and skewness, bound and free long waves, in combination with the breaking induced turbulence (J. A. Roelvink & Stive, 1989):

Undertow is the return current under the waves that occurs especially in the surf zone. The undertow is visible in Figure 83 below. The undertow is considered as the main process that results in transport in the offshore direction. Especially during extreme conditions the undertow is mainly responsible for the beach erosion (Steetzel, 1991).

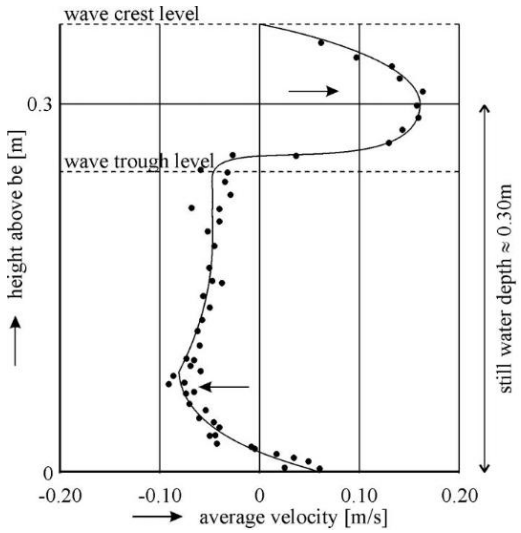

Figure 83: Measured wave cycle averaged flow velocities in a wave flume. The return current, also called undertow, is clearly visible in the image.

The relative contribution of the different processes to the cross-shore sediment transport is investigated by J. A. Roelvink & Stive (1989). In Figure 84 below, this relative contribution is shown for both the suspended transport as the bed load transport. It is visible that the return flow (undertow) is responsible for the biggest part of the offshore directed sediment transport. Wave asymmetry and wave skewness cause an onshore transport component. Long waves result in both an offshore and offshore transport component dependent on the location. Within the breaker zone, where the long waves are unbound and the high flow velocities (meaning more suspended sediment) within the wave group match with the crest of the long waves the net cross-shore transport is onshore directed. Before the breakerline, where the long waves are bound to the wave groups, the trough of the long waves coincides with the high flow velocities within the wave group which causes an offshore directed cross-shore transport. The role of long waves in extreme conditions and especially in dune erosion is very important (van Thiel de Vries, 2009).

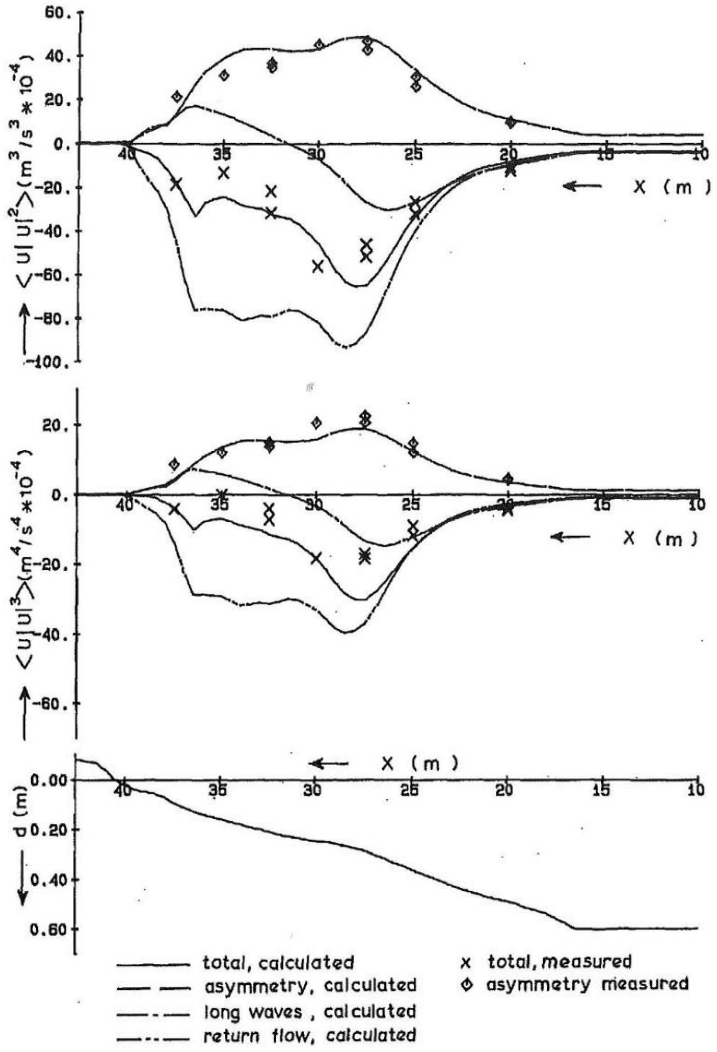

Figure 84: Overview of the relative contributions of the third (bed transport) and fourth (suspended transport) odd moments and their relative calculated contributions in combination with the measured values of wave flume tests from Roelvink & Stive (1989).

A distinction can be made between the velocity skewness and the acceleration skewness. Both these processes result in onshore directed transport. In the shoaling zone the velocity skewness results in an onshore directed bed shear transport due to the pitched forward shape of the waves. In the surf zone the acceleration skewness becomes more dominant resulting in onshore directed transport due to pressure gradients. Taking into account both the velocity skewness as the acceleration skewness is essential to accurately model the onshore direct sediment transport (Fernández-Mora et al., 2015).

A.4 Morphodynamics of the swash zone

In the previous section it was concluded that the main onshore directed cross-shore transport component is related to wave asymmetry and skewness. The placement of the onshore transported sediment is most often on the beachface due to sediment transport processes within the swash zone. As discussed before, the swash zone is very dynamic with high turbulence and flow velocities. For the transfer of sediment from the more subaqueous parts of the surfzone to the beachface, the swash zone processes are most important. Especially for beach recovery

where this transfer of sediment is important. Van Dam (2019) identified 4 key swash zone processes that are most important in the onshore sediment transport:

Bore turbulence:

With the use of field measurements it is shown that the bore turbulence enhances the suspension of sediment in the swash zone (see Figure 80a for a visualization of the bore). This may influence sediment transport due to big suspended sediment gradients in the cross-shore direction (Puleo et al., 2000).

Settling and scouring lag:

As said before, the flow characteristics during the run-up differ from the run-down. Especially related to the acceleration of the flow, which is more gradual at the beginning of the run-down. When taking into account the settling lag of the sediment this could lead to a onshore transport component. Due to the more gradual acceleration in the top part of the swash zone, the mobilization of bed sediment is smaller. During run-up where there is high initial acceleration the mobilized sediment during this acceleration settles higher up the beach due to the settling lag. Hereafter due to the gradual acceleration at the start of the run-down is not mobilized again. This phenomena is also called scour lag.

Infiltration and exfiltration:

The swash in- and exfiltration changes the thickness of the boundary layer, this directly influences the degree of sediment mobilization due to the changing velocity profile. Next to that the sediment stabilizes due to the seepage during infiltration and destabilizes during exfiltration. During run-up infiltration occurs but the boundary layer is decreasing in thickness. The opposite occurs during run-down where the exfiltration destabilizes the sediment and the thickening of the boundary layer destabilizes the sediment.

Different field experiments are performed that show different dominant cross-shore transport directions due to the influence of in- and exfiltration. Turner & Masselink (1998) performed field measurements under calm conditions (Hs = 0.5m and Tp = 14s) with a sediment size of 0.5mm and a beach slope of 7 degrees. This resulted in a clear enhancement of the onshore sediment transport due to the effects of in- and exfiltration. Butt et al. (2001) performed similar tests under higher energy conditions at a dissipative beach (Hs = 2m and Tp = 8s) with a bed slope of about 1 degrees and a sediment size of 0.24 mm. This resulted in an enhancement of the offshore directed transport due to the effects of in- and exfiltration. The use of sensitivity tests suggest the existence of a critical grain size at which the influence of in- and exfiltration change from onshore to offshore. This is confirmed by a numerical model study performed by Karambas (2003) who estimates the critical ‘changeover’ grain size to be in between 0.4 and 0.6mm where the higher grain sizes result in an onshore transport component.

A.5 Beach states

Wright & Short (1984) did extensive investigations from 1979 to 1982 into different beaches along the coast of Australia. This analysis focused on the nearshore morphological properties of beaches under the influence of different hydraulic conditions. They concluded that a beach can go through different states. The two extreme beach states are fully reflective and fully dissipative. Fully reflective beaches have a steep slope and a small sand storage. And on the other side, dissipative beaches are more shallow and approach an almost flat slope with high sand storage. In between the two extreme beach states 4 intermediate beach states that include combinations of reflective and dissipative aspects are defined. The range of 6 beach states is visible in the images below:

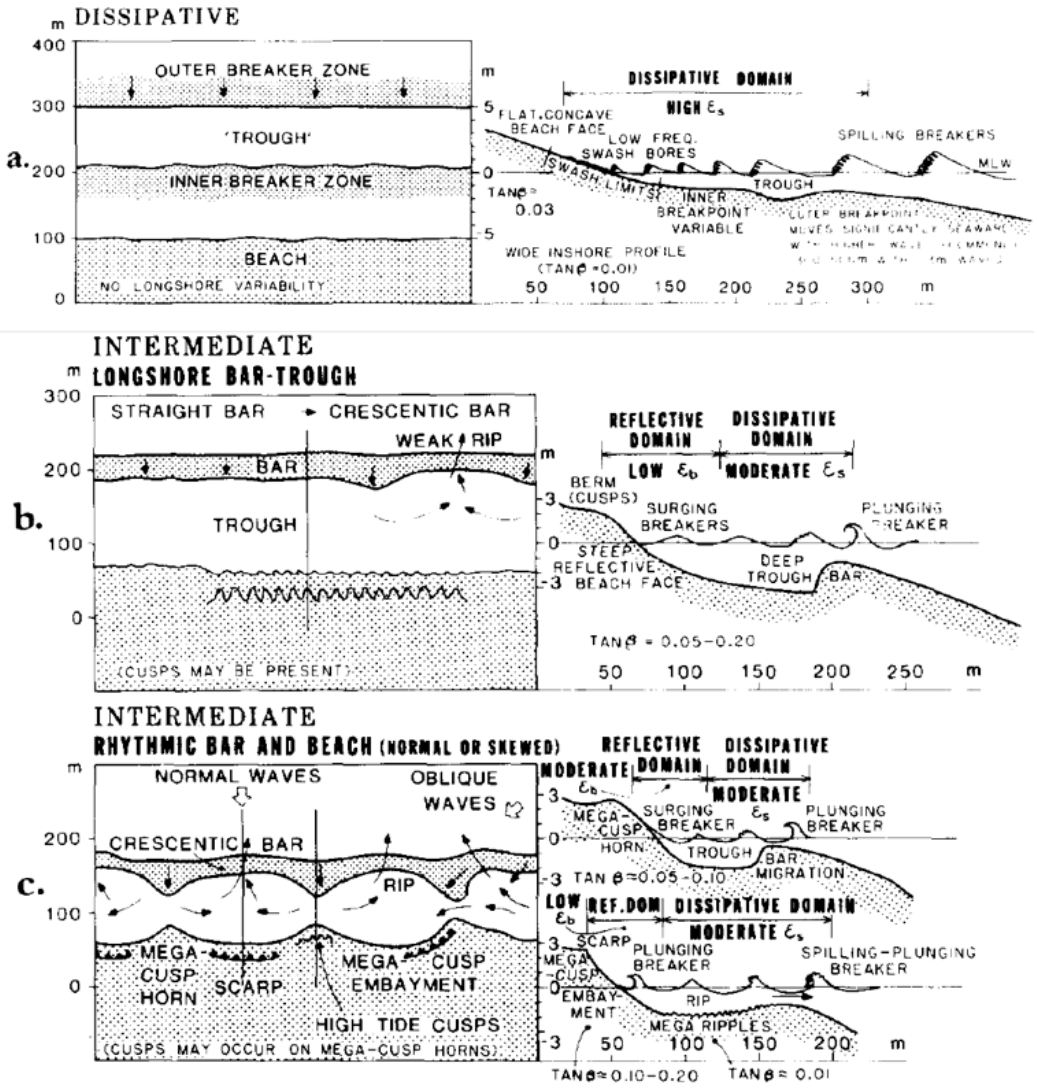
DISSIPATIVE
OUTER BREAKER ZONE
'TROUGH'
INNER BREAKER ZONE
BEACH
NO LONGSHORE VARIABILITY
a.
DISSIPATIVE DOMAIN
HIGH ε_s
FLAT-CONCAVE BEACH FACE
LOW FREQ. SWASH BORES
SWASH LIMITS
SPILLING BREAKERS
MLW
TROUGH
INNER BREAKPOINT VARIABLE
TANβ = 0.03
WIDE INSHORE PROFILE (TANβ = 0.01)
INTERMEDIATE
LONGSHORE BAR-TROUGH
STRAIGHT BAR
CRESCENTIC BAR
WEAK RIP
BAR
TROUGH
(CUSPS MAY BE PRESENT)
b.
REFLECTIVE DOMAIN
DISSIPATIVE DOMAIN
LOW ε_b
MODERATE ε_s
BERM (CUSPS)
SURGING BREAKERS
PLUNGING BREAKER
STEEP REFLECTIVE BEACH FACE
DEEP TROUGH
BAR
TANβ = 0.05–0.20
INTERMEDIATE
RHYTHMIC BAR AND BEACH (NORMAL OR SKEWED)
NORMAL WAVES
OBLIQUE WAVES
CRESCENTIC BAR
RIP
MEGA-CUSP HORN
SCARP
MEGA CUSP EMBAYMENT
HIGH TIDE CUSPS
(CUSPS MAY OCCUR ON MEGA-CUSP HORNS)
c.
MODERATE
REFLECTIVE DOMAIN
DISSIPATIVE DOMAIN
MEGA-CUSP HORN
SURGING BREAKER
PLUNGING BREAKER
TROUGH
BAR MIGRATION
TANβ=0.05-0.10
LOW
REF.DOM
DISSIPATIVE DOMAIN
SCARP
PLUNGING BREAKER
SPILLING-PLUNGING BREAKER
MEGA-CUSP EMBAY-MENT
RIP
MEGA RIPPLES
TANβ≈0.10-0.20
TANβ≈0.01

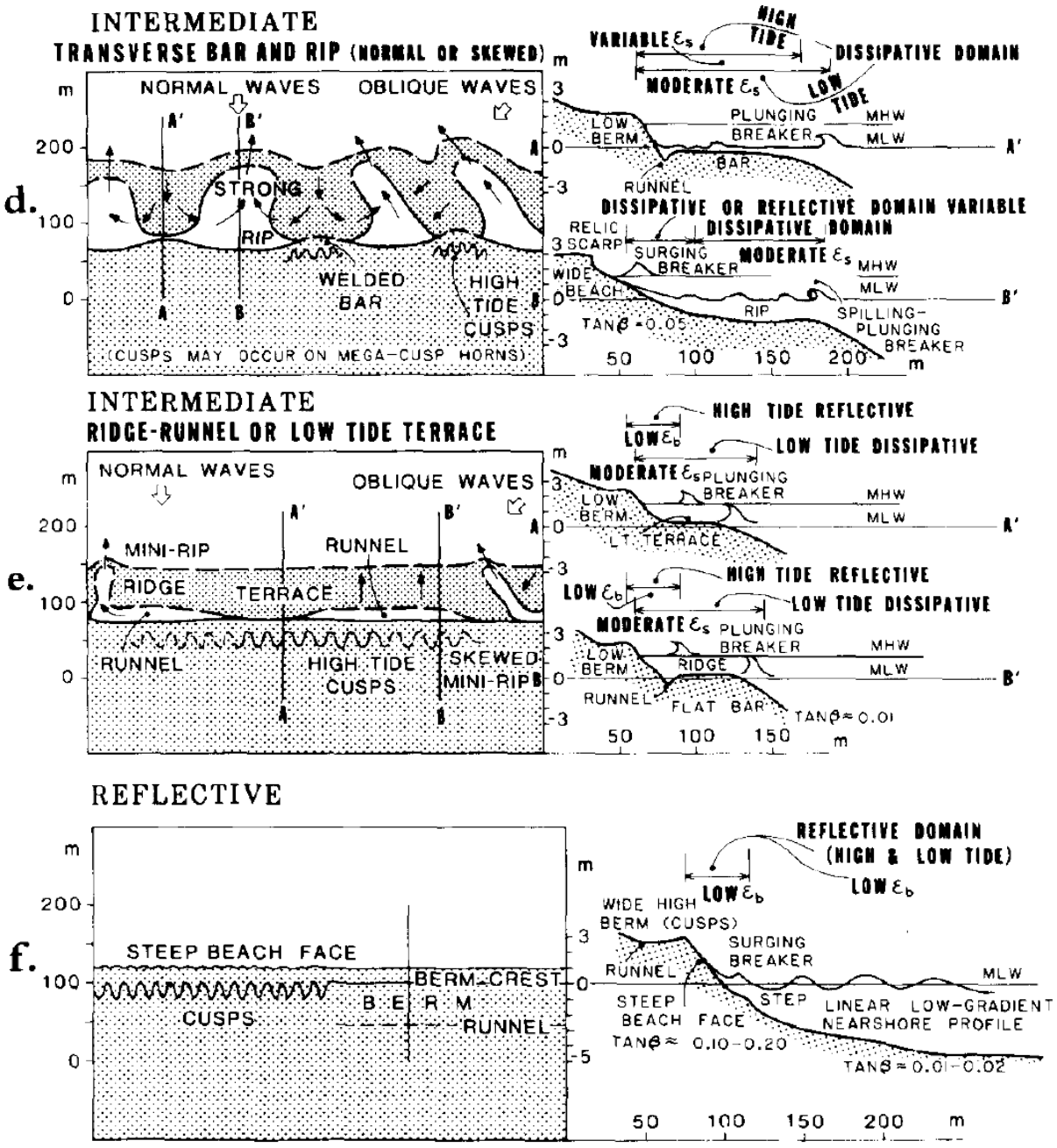

Figure 85: 6 different beach states as defined by Wright and Short (1984)

The beach state at any particular time is dependent on sediment characteristics, immediate and antecedent wave conditions, tide, wind conditions and the antecedent beach state. Studying the beach state on the longer timescale a modal or most frequently occurring beach state can be observed. This beach state is determined by the modal incident wave conditions of a certain beach. The extent of the variations on wave conditions around the modal conditions determine the mobility of a beach (rate of change and variability in beach states). High waves and a high availability of fine sands result in the full dissipative state. Reflective beaches occur with low swell conditions or in more sheltered coastal areas and most of the time come with coarser sediments.

To create a more universal framework a dimensionless parameter Ω can be used:

$$\Omega = \frac{H_s}{\omega_s * T_p}$$

With:

- H_s = Significant wave height [m]
- ω_s = Sediment fall velocity [m/s]
- T_p = Peak wave period [s]

With $1 < \Omega < 6$ the beach state is in the intermediate regime. A value of 1 is considered to be the threshold between reflective and intermediate conditions. So for example when a beach is already in the reflective state and Ω is lower than 1, the beach remains in the reflective state and if the beach is not yet reflective the beach starts moving to the reflective state. The threshold between intermediate and dissipative beach states is for values of Ω around 6 (Wright & Short, 1984).

Appendix B. Wave data

This appendix includes additional information related to the wave data including monthly wave roses, offshore wave characteristics, a more detailed description of the offshore to nearshore wave transformation and details on the extreme value analysis.

B.1 Monthly wave roses

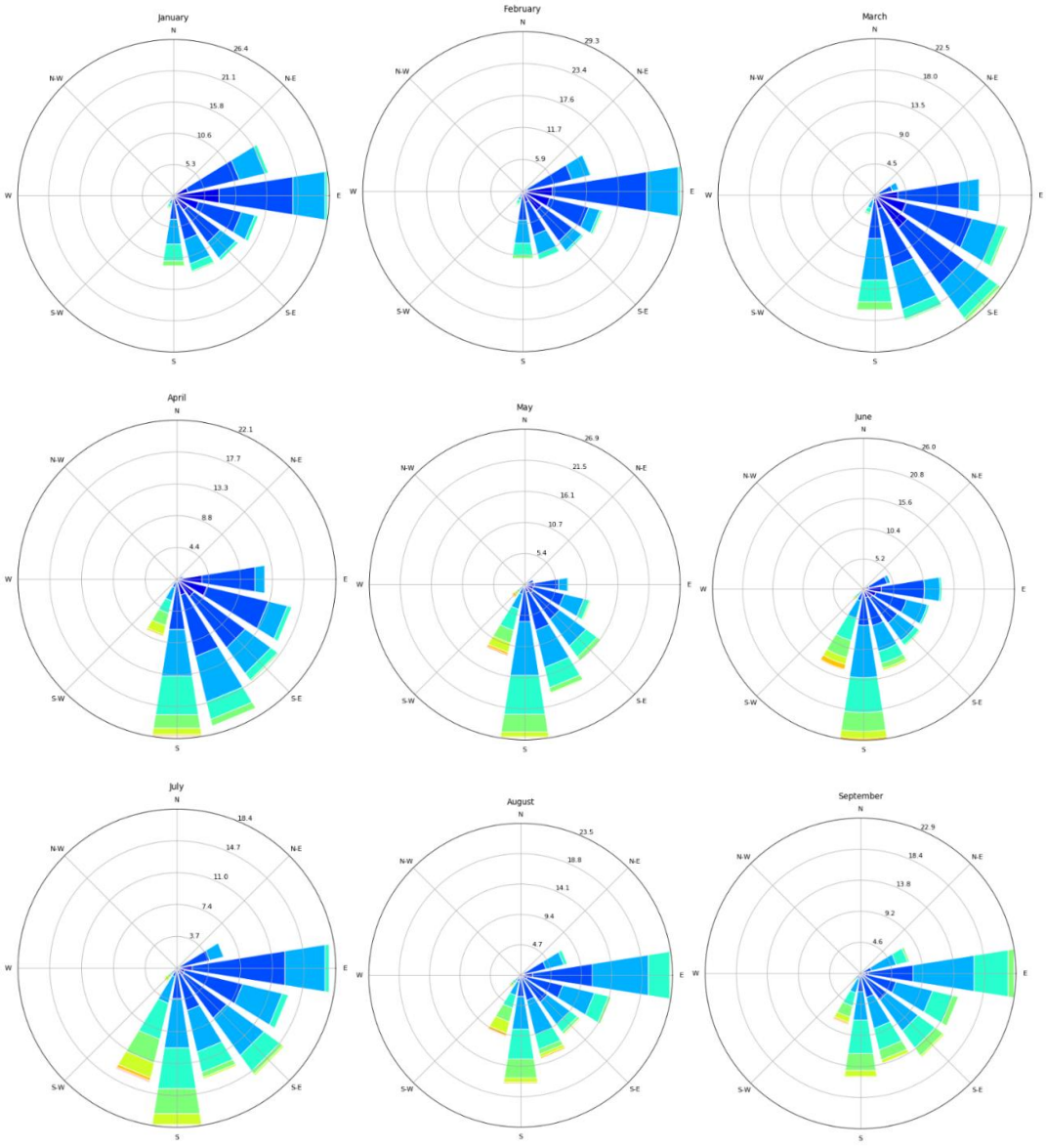

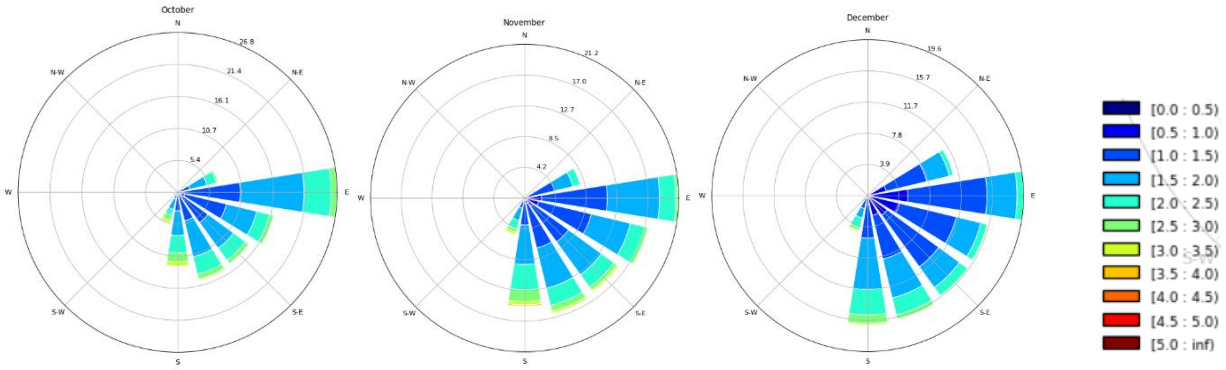

Figure 86: Monthly offshore wave roses.

B.2 Offshore wave characteristics

There are 2 different available datapoints of offshore wave data located in different offshore locations. In the figure below a graph is shown of the wave height during one month of the nearshore wave height and the offshore wave height of the 2 available offshore datapoints. It can be seen that the wave height for both offshore data points shows a very similar trend over time compared to the nearshore dataset. This indicates that the offshore wave data points are both representative for the nearshore wave climate. For further analysis of the offshore wave characteristics, the datapoint located closest to the Copacabana bay is chosen. This point is located 60 km South of Copacabana beach on latitude -23.5 and longitude -43.

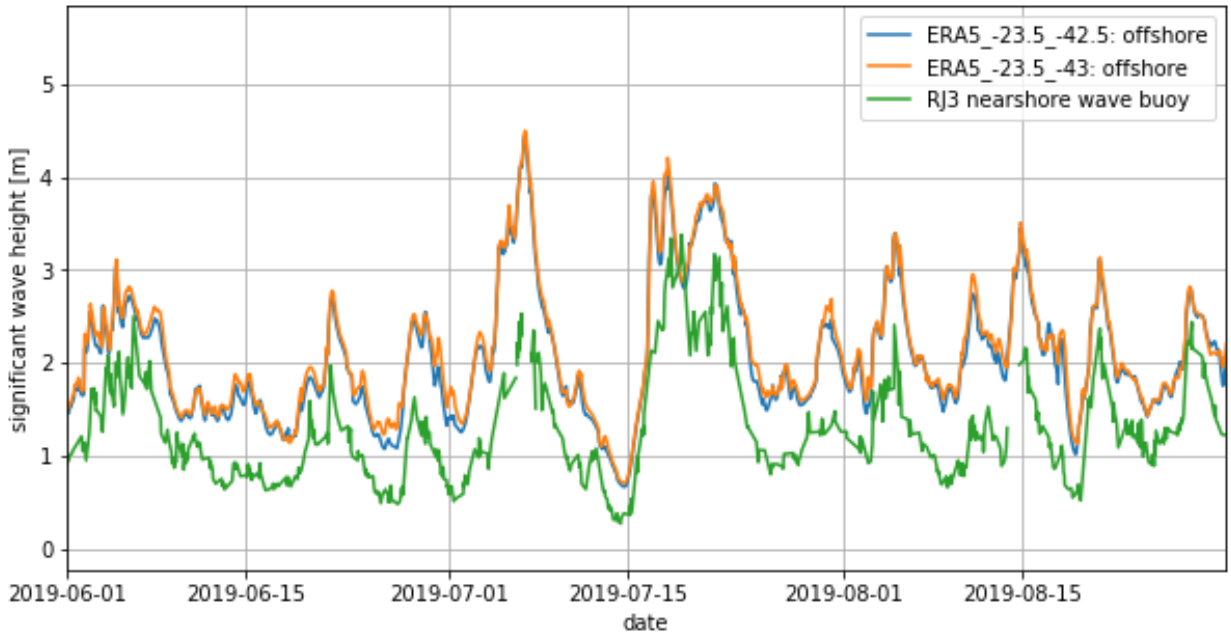

Figure 87: Significant wave height during 2 months of the nearshore RJ3 datapoint and the 2 available offshore datapoints.

The full wave climate is shown in the figure below. The main offshore wave direction is from the east with an average significant wave height between 1 and 2 meters and a peak period of 7 to 12 seconds. This hindcast dataset has a swell partition and a wind wave partition. These partitions are plotted separately. It must be noted that the significant wave heights for the swell and wind partitions are plotted against the mean period instead of the peak period. In contrast to the nearshore wave dataset, there is a clear wind wave partition visible. The main direction for the

wind waves is from the ENE. This offshore wave direction is not prone to reach the Copacabana bay because of the Southern orientation of the coast.

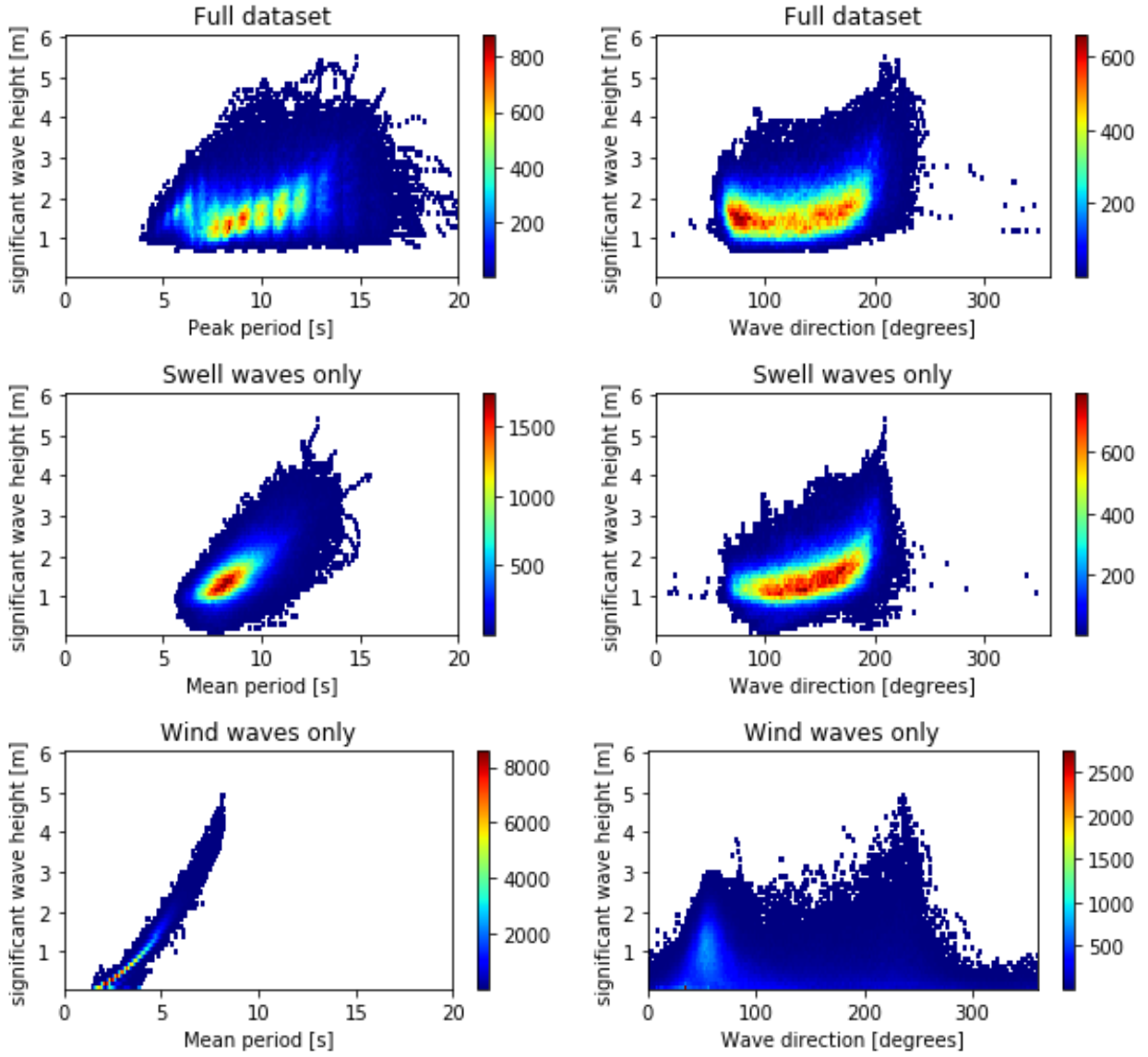

Figure 88: Significant offshore wave height compared to the peak period and wave direction for the full wave spectrum, the swell waves and the wind waves.

The full wave rose is visible in the figure below. The waves origin from in between 50 and 200 degrees. The extreme wave direction (H_s > 2.0m) is mainly from the South and calmer waves tend to origin from the east.

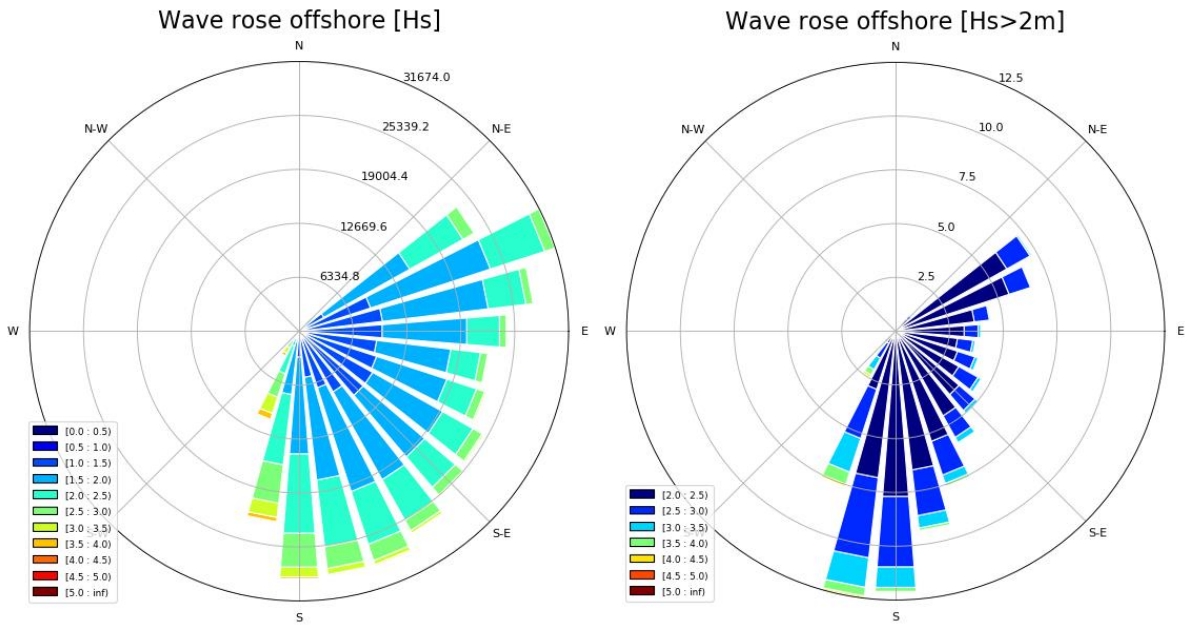

Figure 89: Normal and extreme offshore wave rose of the full data set.

B.3 Offshore to nearshore wave propagation

The image below shows an overview of the offshore and nearshore area of Copacabana beach. A wave envelope is drawn from both sides of Copacabana beach indicating the direction range with the most frequent wave directions. This is between 120 and 170 degrees (SE). 83 percent of the time the wave direction is within this range. Waves propagating from offshore to nearshore within this wave envelope have minimal hindrance of islands, structures or headlands before they reach the Copacabana bay. Furthermore, the local bathymetry and topography shows that in the range of S to SW there is no direct propagation possible of the offshore wave to the beach due to the existence of islands off the coast. This is similar for waves in the range of 110 to 90 degrees (ESE).

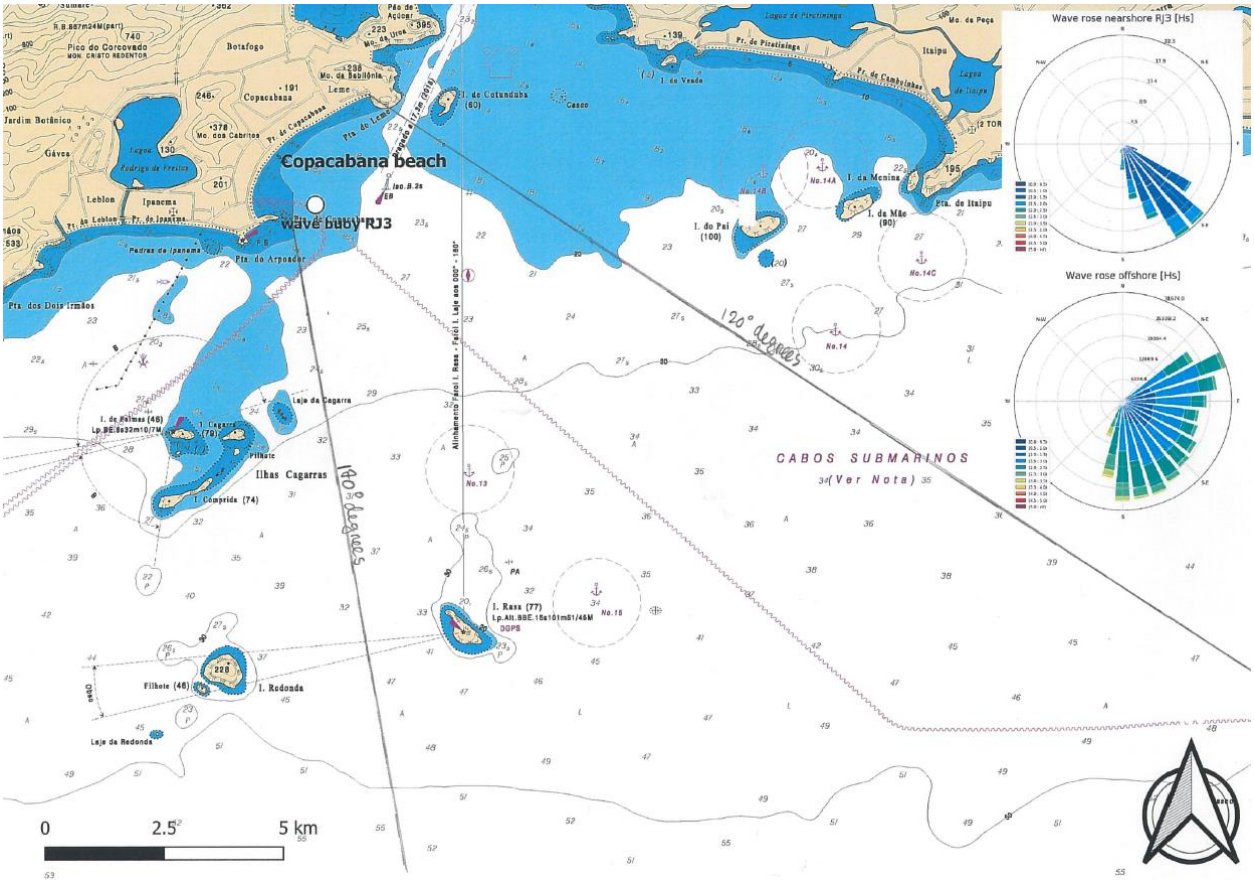

Figure 90: Bathymetry of nearshore and offshore area including the most frequent wave envelope.

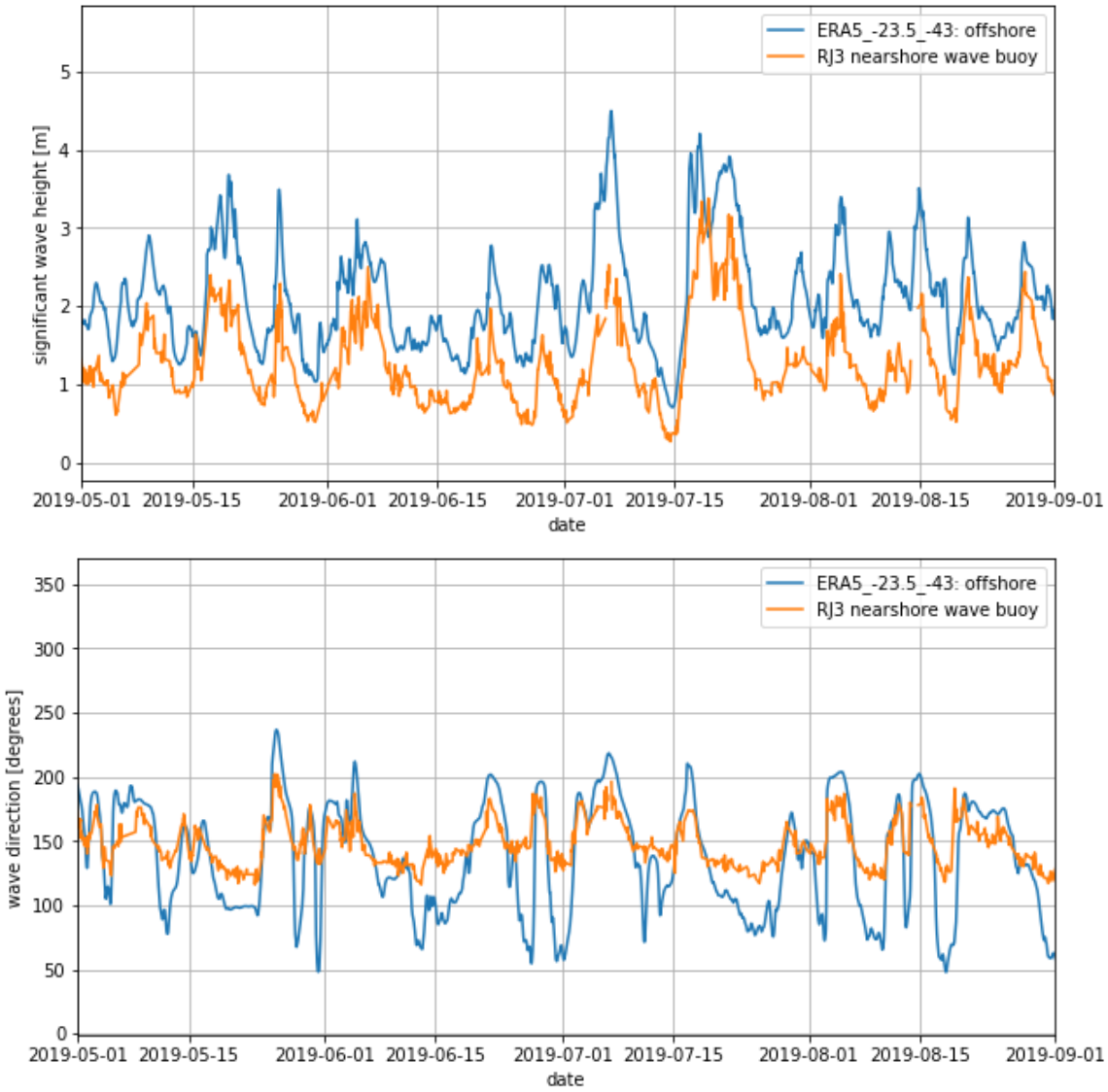

Figure 91: Time series for the significant wave height and the wave direction for both the nearshore and offshore datapoint.

In the image above the time series is shown for both the offshore and nearshore for the mean wave direction and the significant wave height for the 4 month winter period. It is visible that for the nearshore waves the wave direction is within the envelope drawn in Figure 90 between 120 and 170 degrees with some exceptions. As observed before, the extreme waves with significant wave heights higher than 2 meters origin from the South and the more calm conditions are from the SE for the nearshore dataset and from the east in the offshore dataset. A wave direction between 140 and 170 degrees seems to result in minimal change of direction of the waves when propagating from offshore to nearshore. In this direction range the wave crests are almost aligned with the local bathymetry contours, so no refraction is occurring (see Figure 90). When offshore waves origin from directions in between 180 and 230 degrees (SE) waves diffract around the islands located directly South of Copacabana beach resulting in a nearshore wave direction from the South. Offshore waves in the direction range of 100 to 140 degrees propagate to nearshore with a change in direction more to the South. This can be explained by the orientation of the beach with respect to the east to SE wave direction which is more sheltered by local topography and islands off the coast (see Figure 90). Next to that, the bathymetry gradient along the wave crests

of the incoming waves from this direction can cause refraction of waves with a clockwise change of direction.

Refraction is caused by depth variation along the wave crests causing a difference in phase speed along the crest resulting in change of wave direction. This direction change can be estimated using Snell's law:

$$\frac{\sin(\varphi_2)}{c_2} = \frac{\sin(\varphi_1)}{c_1}$$

With:

- φ = angle of the wave direction to the local bathymetry contours [degrees]
- c = wave phase speed

According to linear wave theory the following theories hold for the wave length and wave phase speed.

$$L = g * \frac{T^2}{2 * \pi} * \tanh\left(\frac{2 * \pi * d}{L}\right) \quad and \quad c = L/T$$

With:

- c = wave phase speed [m/s]
- k = $\frac{2*\pi}{L}$ = wave number [1/m]
- L = wave length [m]
- d = local water depth [m]
- g = 9.81 [m/s^2]

To confirm the influence of the local bathymetry on the wave direction when waves propagate from offshore to nearshore the linear wave theory equations can be used as a first indication. Using the knowledge gained from the nearshore wave analysis, the peak wave period is most frequently between 10 and 15 seconds. The figure below shows a plot of the wave phase speed over depth relative to the deep water wave phase speed using linear wave theory. With the offshore wave buoy being in deep water (depth of about 100 meters) there is minimal influence of the sea bottom, this is confirmed by linear wave theory. But during propagation to the nearshore datapoint, at a depth of 17 meters, there is significant influence of the bathymetry and the wave phase speed for waves with a peak period of 15 seconds is about half the deep water phase speed.

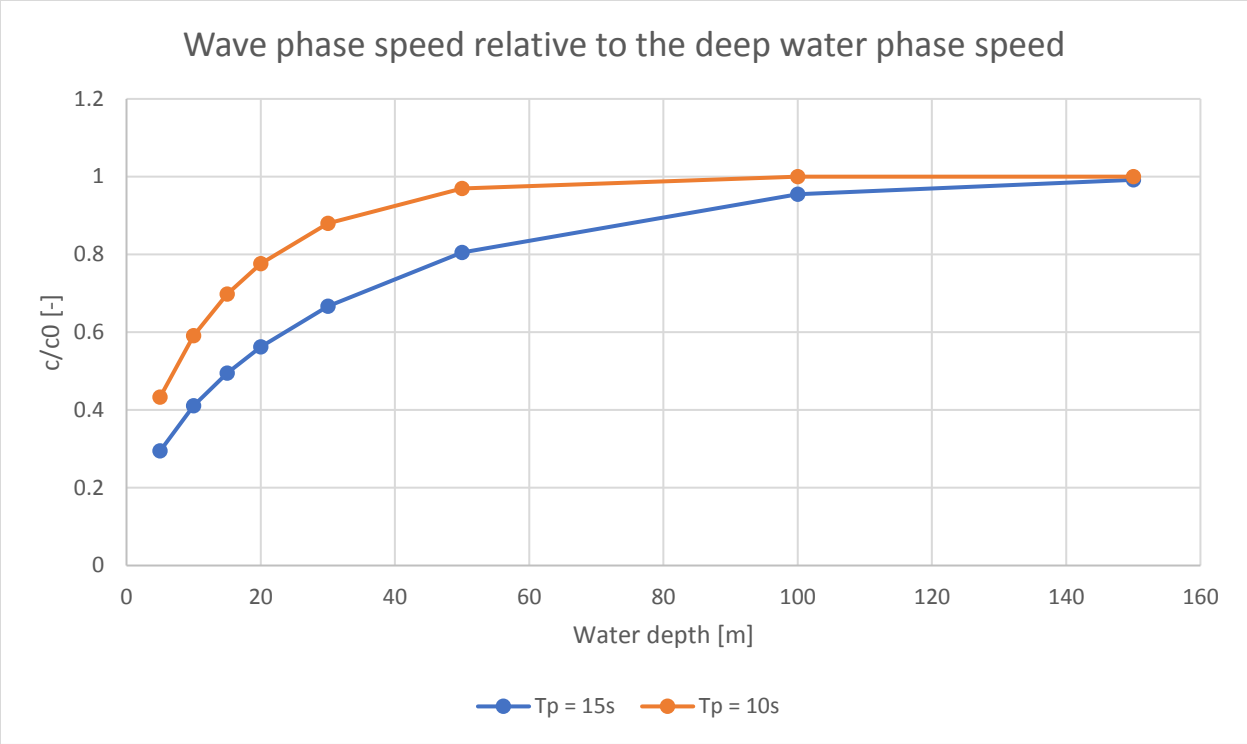

Figure 92: Plot of the wave speed relative to deep water against the water depth for typical wave periods occurring at Copacabana beach.

B.4 Extreme Value Analysis

An extreme value analysis is done to find out what the return time is of specific wave heights. For this, the Peak-over-threshold method is used. In this method the maximum recorded significant wave height per storm is taken into account. A storm is defined as a uninterrupted sequence of values above a certain threshold. The offshore dataset from 1979 to 2019 is used for this analysis as the nearshore dataset only contains 2 years of wave data which is not long enough to perform an Extreme Value Analysis. A threshold of 4 meters is chosen and using the peak-over-threshold method, every storm with significant wave heights surpassing 4 meters is recorded. In the figure below the dataset is shown including the selected peaks above 4 meters. Two peaks of 4 meters within a period of two days are considered to be part of the same storm to avoid two different recorded peaks within a single storm event.

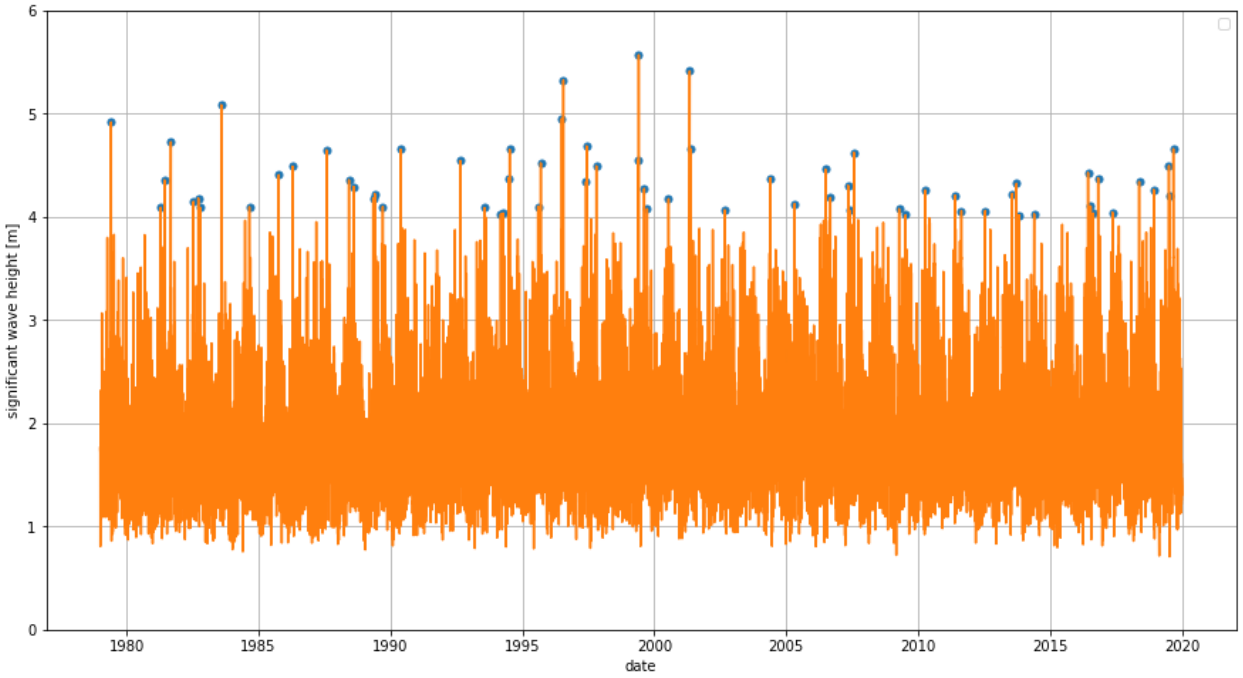

Figure 93: Selected peaks in the offshore dataset using the peak-over-threshold method.

A total of 66 peaks are found and ranked from low to high and assigned with a probability of exceedance. This is the cumulative distribution function of the ranked peaks:

$$P\left(H_{s,peak} < H_{s,peak,i}\right) = \frac{i-1}{66}$$

Then the return period for each peak can be found using the following formula:

$$RP\left(H_{s,peak,i}\right) = \frac{\Delta T_{storm}}{1 - P\left(H_{s,peak,i}\right)}$$

Where the average storm interval is equal to: $\Delta T_{storm} = \frac{41 years}{66} = 0.621\ years$. The data is then plotted on the horizontally logarithmic scale with a shifted exponential distribution to be able to extrapolate to higher return periods if needed:

$$P\left(H_{s,peak} < H_{s,peak,i}\right) = 1 - \exp\left(-\frac{H_{s,peak} - A}{B}\right)$$

With A=4 and B=0.375 the best fit was obtained which is visible in Figure 94 below.

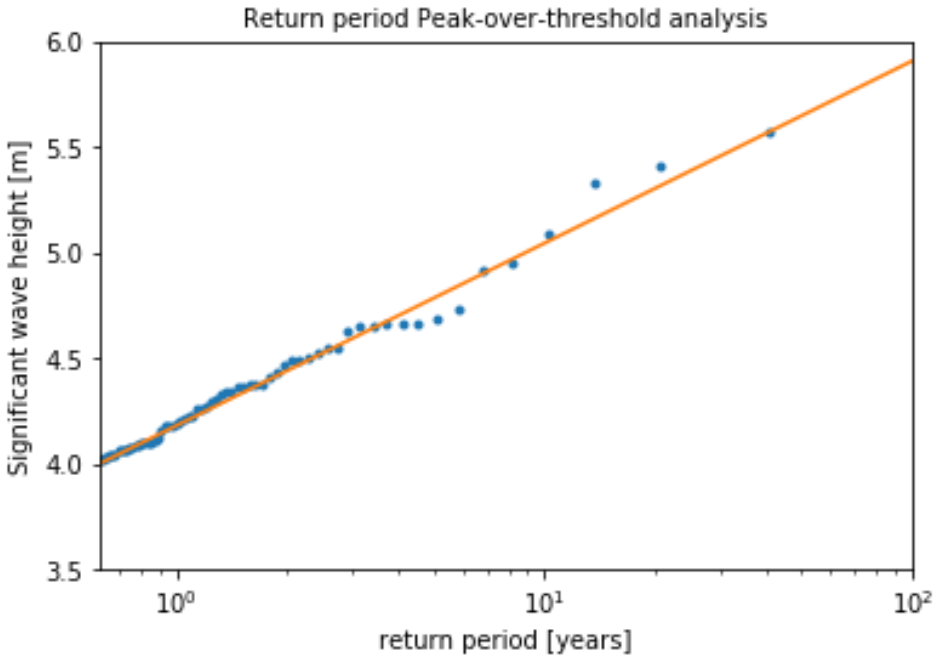

Figure 94: The long term distribution of the peak-over-threshold significant wave height fitted by a shifted exponential distribution with A=4 and B=0.375.

Appendix C. Beach profile measurements

The measurements related to the topography of the beach and bathymetry measurements are listed below:

- DGPS beach profile measurements
- Total station beach profile measurements
- Bathymetry measurements using sonar transducer

In total 19 different cross sections are allocated to the beach. They are visible in Figure 95 below:

Figure 95: Overview of the different allocated cross sections along Copacabana beach.

The coordinates shown in Table 18 are the starting points for the profile measurements. The profiles are measured perpendicular to the promenade at every location.

Table 18: Longitude and latitude for all 19 cross sections along the beach.

Longitude	Latitude	Cross section
-43.18876143	-22.98558217	CS1
-43.18911056	-22.98449484	CS2
-43.1895056	-22.98272978	CS3
-43.18937439	-22.98092915	CS4
-43.18883645	-22.97895855	CS5
-43.18835383	-22.97768123	CS6
-43.18779676	-22.97653294	CS7
-43.187353	-22.97574287	CS8
-43.18694843	-22.97509382	CS9
-43.18600338	-22.97379125	CS10
-43.18453545	-22.97217477	CS11
-43.18287282	-22.97073876	CS12
-43.17965155	-22.96859581	CS13
-43.17633782	-22.96676489	CS14
-43.17346306	-22.96541954	CS15
-43.17132531	-22.96451194	CS16
-43.16921283	-22.96364966	CS17
-43.16666869	-22.96277772	CS18
-43.16543669	-22.96262826	CS19

C.1 DGPS measurements

The DGPS measurements were carried out on 04-12-2019 from 10:12 to 16:33 UTC-3. The 19 profiles like listed above have been measured. The tidal levels during the measurements are shown below:

Table 19: Tidal levels during the DGPS cross section measurements.

Local time	Tidal elevation [m]
9:00:00 AM UTC-3	0.22
10:57:00 AM UTC-3	0.19
11:42:00 PM UTC-3	0.2
2:00:00 PM UTC-3	0.08
4:22:00 PM UTC-3	0.02

For the DGPS measurements two different GPS instruments were used simultaneously. One was set up in a 3 different fixed location on the edge of the beach promenade during the day of the measurements. This is visible in the image below. When turned on, the instrument records it's horizontal and vertical location every second.

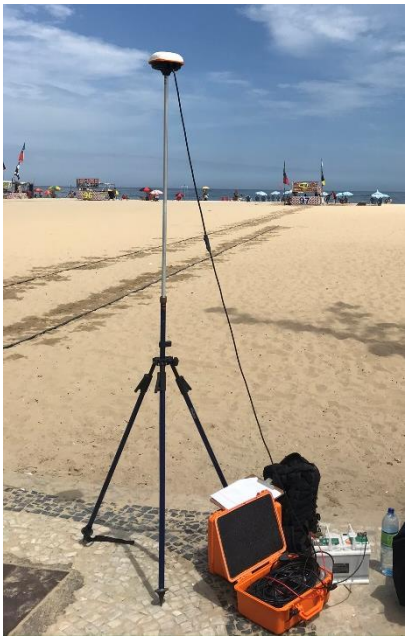

Figure 96: DGPS instrument used for the profile measurements.

The second DGPS instrument was used to measure the profiles. In total 19 different cross sections are measured. Every cross section was measured twice. After the measurements there were some problems with the data and the connection of the DGPS was not good during part of the measurements. After obtaining the raw log files and putting the GPGGA elevation measurements in excel the following cross sections measurements resulted to be inaccurate:

Table 20: Accurateness of the DGPS measurements for each cross section.

	a	b
CS1	x	x
CS2	x	x
CS3	x	x
CS4	x	x
CS5	x	x
CS6	good	good
CS7	x	x
CS8	good	good
CS9	x	good
CS10	x	x
CS11	x	good
CS12	good	good
CS13	good	good
CS14	x	x
CS15	good	x
CS16	good	good
CS17	x	good
CS18	good	good
CS19	good	good

C.1.1 Base stations

There were 3 different base stations. They were located respectively on points CS2, CS12 and CS18. The average elevation of these base points with respect to mean sea level (geoid) was:

Table 21: Elevation of the base stations.

Base station	Elevation [m]
CS2 base	2.75
CS12 base	2.9
CS18 base	2.85

As can be seen there is a small variation in the elevation of the different base stations. This variation is due to the accuracy of the DGPS measuring station and the small irregularities in the position of the base station on the edge of the promenade. **From this point onwards the assumption is made that the promenade has a constant height along the whole beach perimeter. This level is set equal to the average of the 3 base stations: 2.83m.**

C.1.2 Cross sections

The cross sections are measured perpendicular to the promenade. The measurements are started at the edge of the promenade and ended approximately 0.6 meters below the water level. It was not possible to go further in the water because the risk of the equipment getting wet was too high. So for every cross sections measured, the location of the momentary water level is approximated at the point which is 0.6 meters above the lowest measured vertical position per cross section. This table lists the approximate position of the water level and the DGPS position of the promenade:

Table 22: Overview of the DGPS measurements

Cross section	Promenade height [m]	Momentary water level [m]	Tidal level [m]	Difference promenade and water level [m]	Difference promenade and water level [m] (with tidal correction to MSL)	Momentary water level with tide correction [m]
CS6a	2.9	0.5	0.2	2.4	2.6	0.3
CS6b	2.9	0.5	0.2	2.4	2.6	0.3
CS8a	3.1	0.8	0.2	2.3	2.5	0.6
CS8b	3.1	0.0	0.2	3.1	3.3	-0.2
CS9b	3.0	0.4	0.2	2.6	2.8	0.2
CS11b	2.9	0.2	0.1	2.7	2.8	0.1
CS12a	2.7	-0.1	0.1	2.8	2.9	-0.1
CS12b	2.8	0.1	0.1	2.9	2.9	0.0
CS13a	3.0	0.3	0.0	2.7	2.7	0.3
CS13b	3.0	0.3	0.0	2.7	2.7	0.3
CS15a	3.2	0.2	0.0	3.0	3.0	0.2
CS16a	2.9	0.0	0.0	2.9	2.9	0.0
CS16b	3.2	0.2	0.0	3.0	3.0	0.2
CS17b	2.8	0.0	0.0	2.8	2.8	0.0
CS18a	2.8	0.1	0.0	2.7	2.7	0.1
CS18b	2.8	0.2	0.0	2.6	2.6	0.2
CS19a	2.7	0.1	0.0	2.6	2.6	0.1
CS19b	2.7	0.1	0.0	2.6	2.6	0.1
Average	**2.92**	**0.22**	**-**	**2.71**	**2.78**	**0.15**

Taking the average of the both the promenade height and the water level in the DGPS vertical coordinate system, which is 0m when a vertical point is located on the earths geoid, results in **+0.15m for the Mean Sea level**. **For the promenade height, as said before, the average of the elevation of the base stations is taken. This was equal to +2.83m.** The accuracy of the

base station is expected to be better than the accuracy of the other DGPS device which measured the cross sections. This is because of the fixed position of the base stations.

C.2 Total station measurements

The total station measurements were carried out on 18-12-2019 from 8:50 to 15:10 UTC-3. During the measurements profiles 1 to 17 were able to be measured. The last two profiles were not able to be measured because of a failure of the equipment. The tidal levels ranged between -0.05m and 0.05 meter with respect to Mean Sea Level. So the tidal difference is neglected for the total station measurements.

Figure 97: Total station used to perform cross section measurements on the beach.

When configuring the total station the North direction of the coordinate system is perpendicular to the promenade. The height of the total station above the ground is entered and also the height of the prism pole, taking into account the sinking of the pole in the sand when setting it up. This makes it that the location of the total station on the edge of the promenade is at a level of 0 meter.

Table 23: Vertical elevation of the Mean Sea Level for each cross section during the total station measurements.

Cross section	Mean Sea Level [m]	Tidal height [m]
CS1	-2.6	0.0
CS2	-2.6	0.0
CS3	-2.4	0.0
CS4	-2.6	0.0
CS5	X	0.0
CS6	X	0.0
CS7	-2.7	0.0
CS8	-2.6	0.0
CS9	-2.7	0.0
CS10	-2.9	0.0
CS11	-2.9	0.0
CS12	-2.6	0.0
CS13	-2.6	0.0
CS14	X	0.0
CS15	-2.6	0.0
CS16	X	0.0
CS17	-2.7	0.0
Average	**-2.68**	**-**

C.3 Results

From both the total station measurements and the DGPS measurements the average distance between the edge of the promenade and the Mean Sea Level (taken from the tidal charts) is known. For both the DGPS measurements and the total station measurements this distance was equal to 2.68 meters. To compare the measurements done with both methods the Mean Sea Level is set equal to 0m and the promenade level equal to +2.68m. For both methods the starting point of the measurements was the edge of the promenade which is in all cases set equal to +2.68 meters.

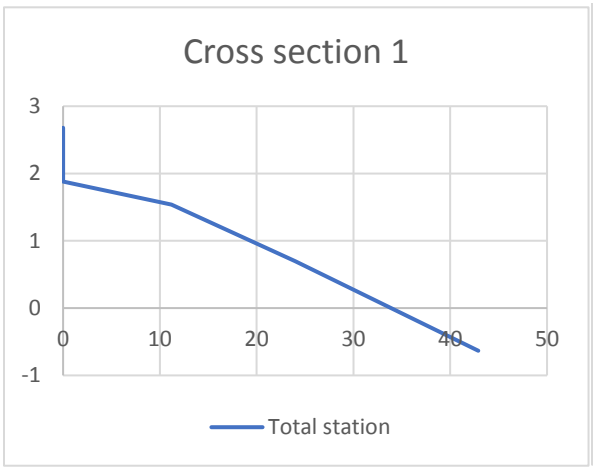

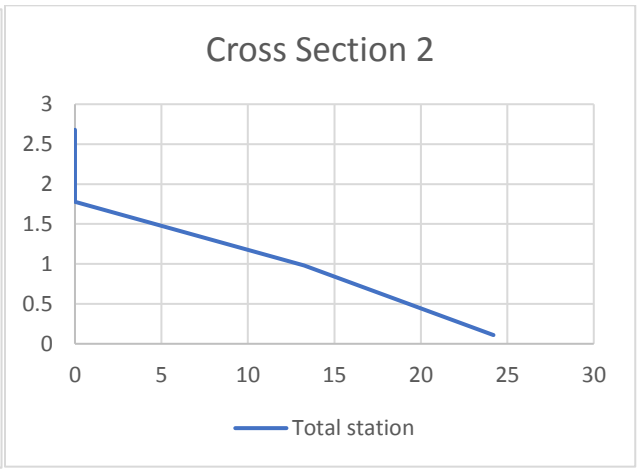

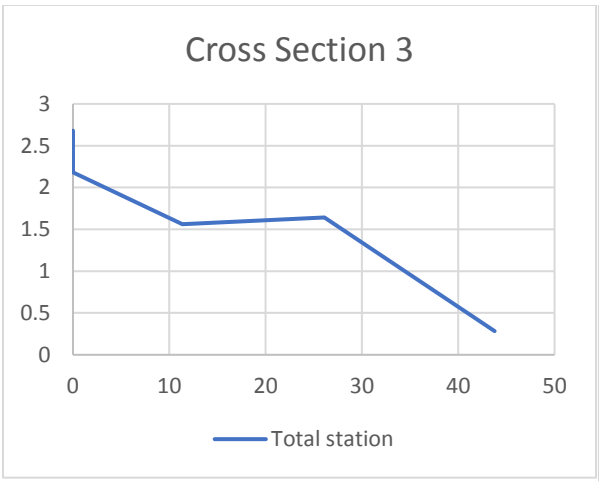
Cross Section 3
3
2.5
2
1.5
1
0.5
0
0
10
20
30
40
50
Total station

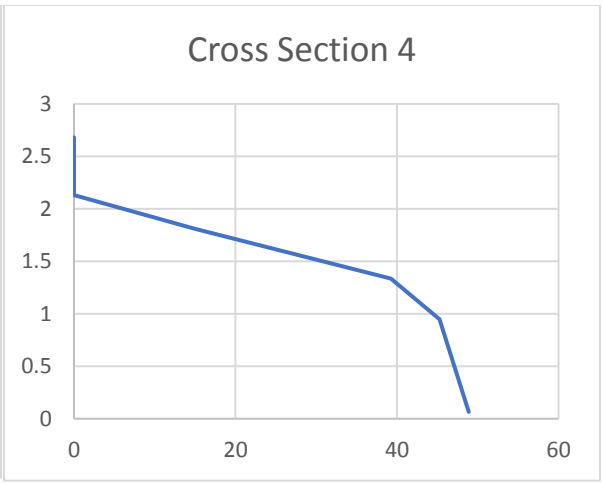
Cross Section 4
3
2.5
2
1.5
1
0.5
0
0
20
40
60

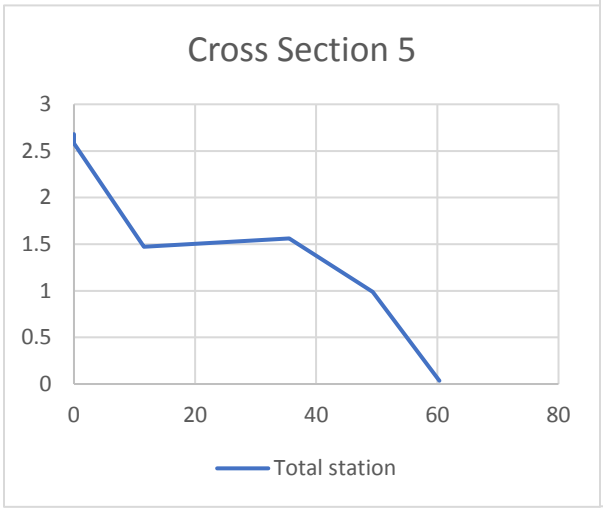
Cross Section 5
3
2.5
2
1.5
1
0.5
0
0
20
40
60
80
Total station

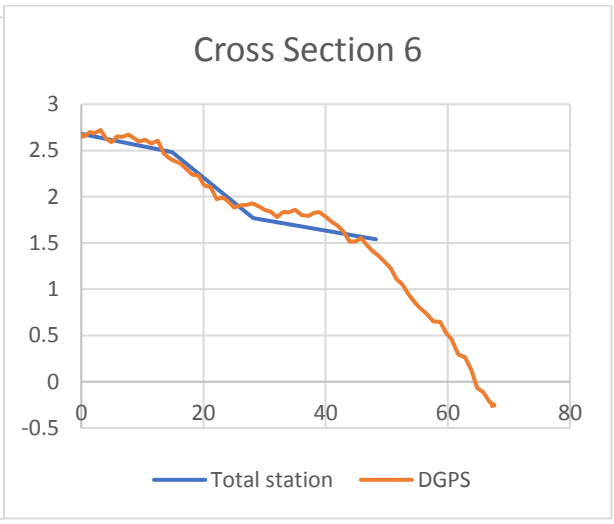
Cross Section 6
3
2.5
2
1.5
1
0.5
0
-0.5
0
20
40
60
80
Total station
DGPS

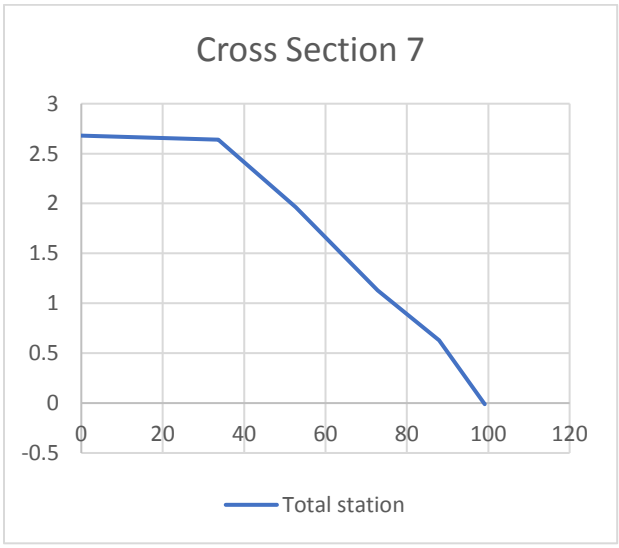
Cross Section 7
3
2.5
2
1.5
1
0.5
0
-0.5
0
20
40
60
80
100
120
Total station

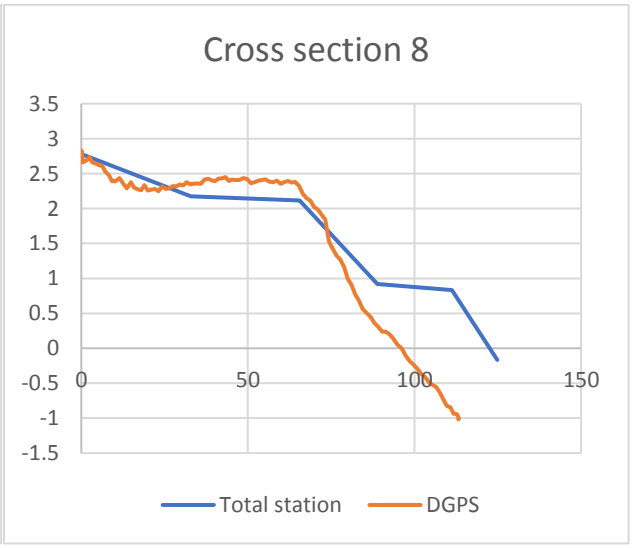
Cross section 8
3.5
3
2.5
2
1.5
1
0.5
0
-0.5
-1
-1.5
0
50
100
150
Total station
DGPS

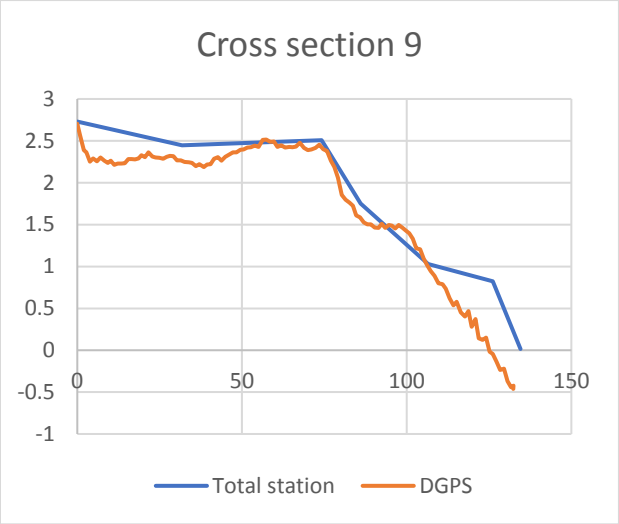
Cross section 9
3
2.5
2
1.5
1
0.5
0
-0.5
-1
0
50
100
150
Total station
DGPS

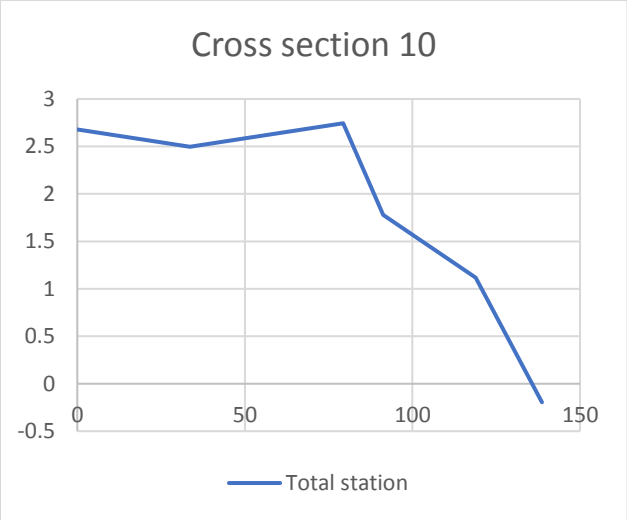
Cross section 10
3
2.5
2
1.5
1
0.5
0
-0.5
0
50
100
150
Total station

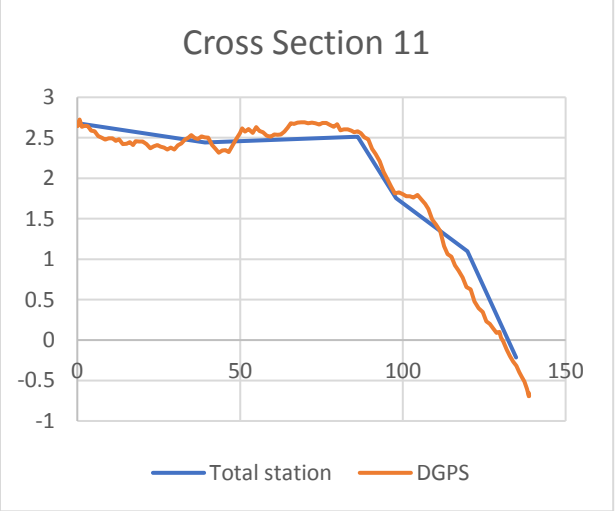
Cross Section 11
3
2.5
2
1.5
1
0.5
0
-0.5
-1
0
50
100
150
Total station
DGPS

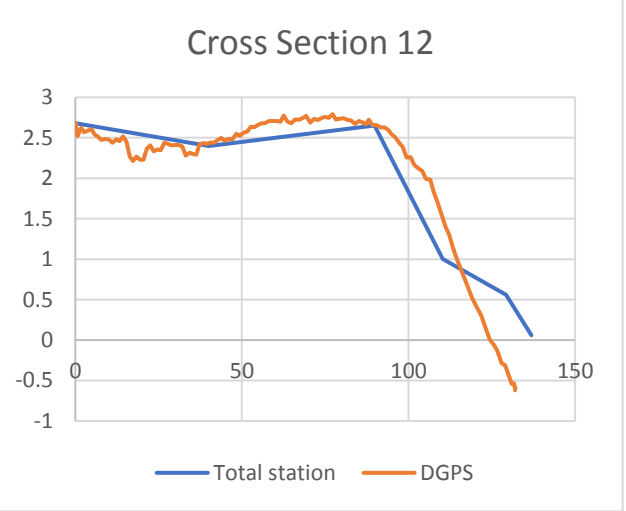
Cross Section 12
3
2.5
2
1.5
1
0.5
0
-0.5
-1
0
50
100
150
Total station
DGPS

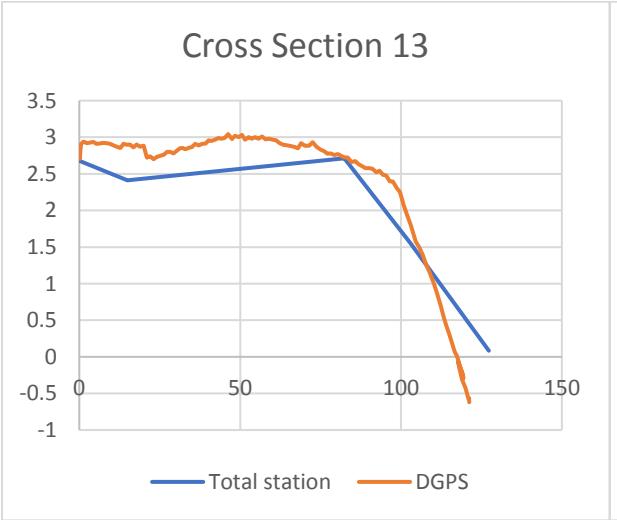
Cross Section 13
3.5
3
2.5
2
1.5
1
0.5
0
-0.5
-1
0
50
100
150
Total station
DGPS

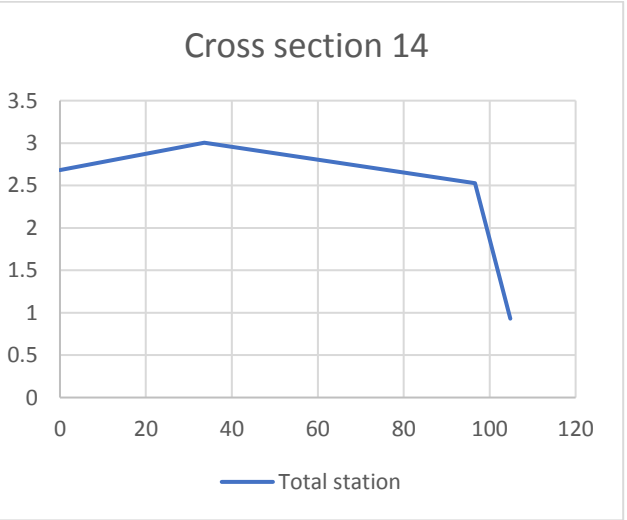
Cross section 14
3.5
3
2.5
2
1.5
1
0.5
0
0
20
40
60
80
100
120
Total station

Figure 98: 19 different cross section measurements performed with a total station on 18-12-2019 and with a DGPS device on 04-12-2019. Mean Sea Level is at 0 meters on the vertical axis.

Appendix D. Extreme wave event analysis

This appendix includes the full analysis of the characteristics of extreme wave events which are captured in terms of changes in beach width in the image below.

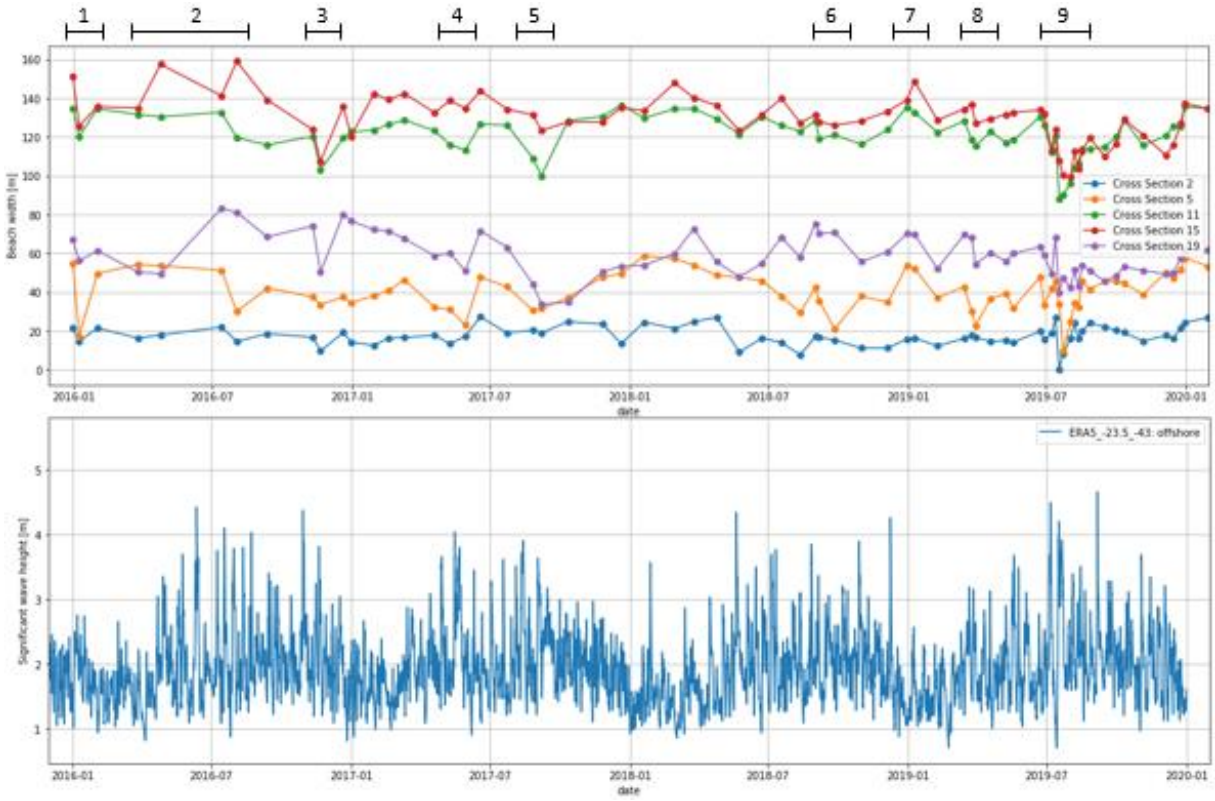

Figure 99: Sentinel 2 beach width measurements for 5 cross sections along the beach.

D.1 January 2016 (1)

It must be noted that the wave data used in this case is from the offshore datapoint. In the other recorded extreme events the nearshore buoys are used. In this case this was not possible because for this period there is no nearshore wave data available. This results in somewhat higher wave heights on average and the transformation of the waves to the nearshore is not fully included. In the nearshore it is expected that the wave direction turns more towards the SE (see Appendix B.3)

- Extreme event duration: 5 days
- Maximum significant wave height: 2.8m (offshore)
- Mean wave direction during erosion: ESE (offshore)
- Mean wave direction during accretion: SSE (offshore)
- Erosion cross section 5: 37m

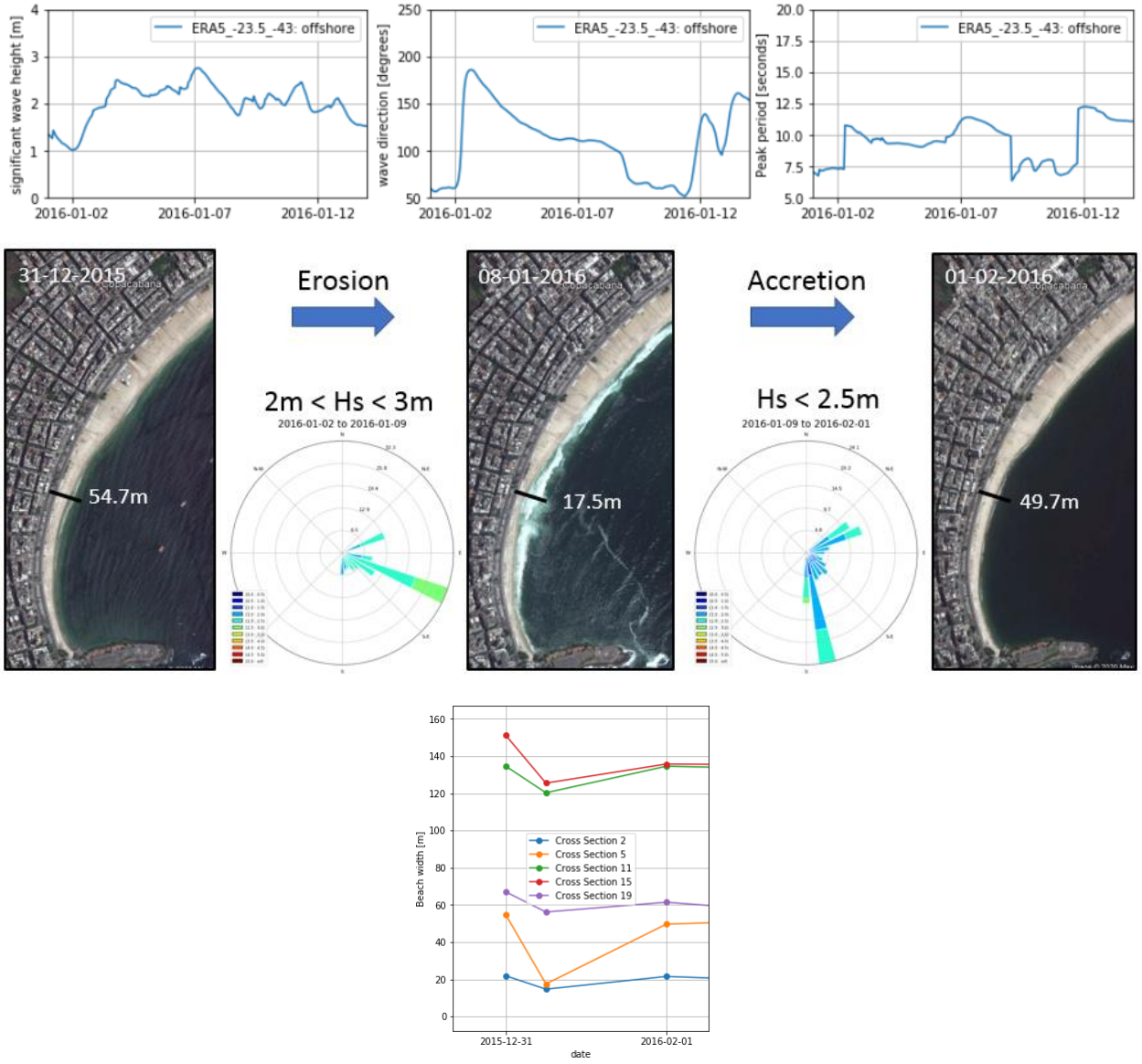

Figure 100: Characteristics of the January 2016 extreme wave event.

D.2 May 2017 (4)

- Extreme event duration: 8 days
- Maximum significant wave height: 2.9m
- Mean wave direction during erosion: SE
- Mean wave direction during accretion: SSE
- Erosion Cross Section 5: 8m

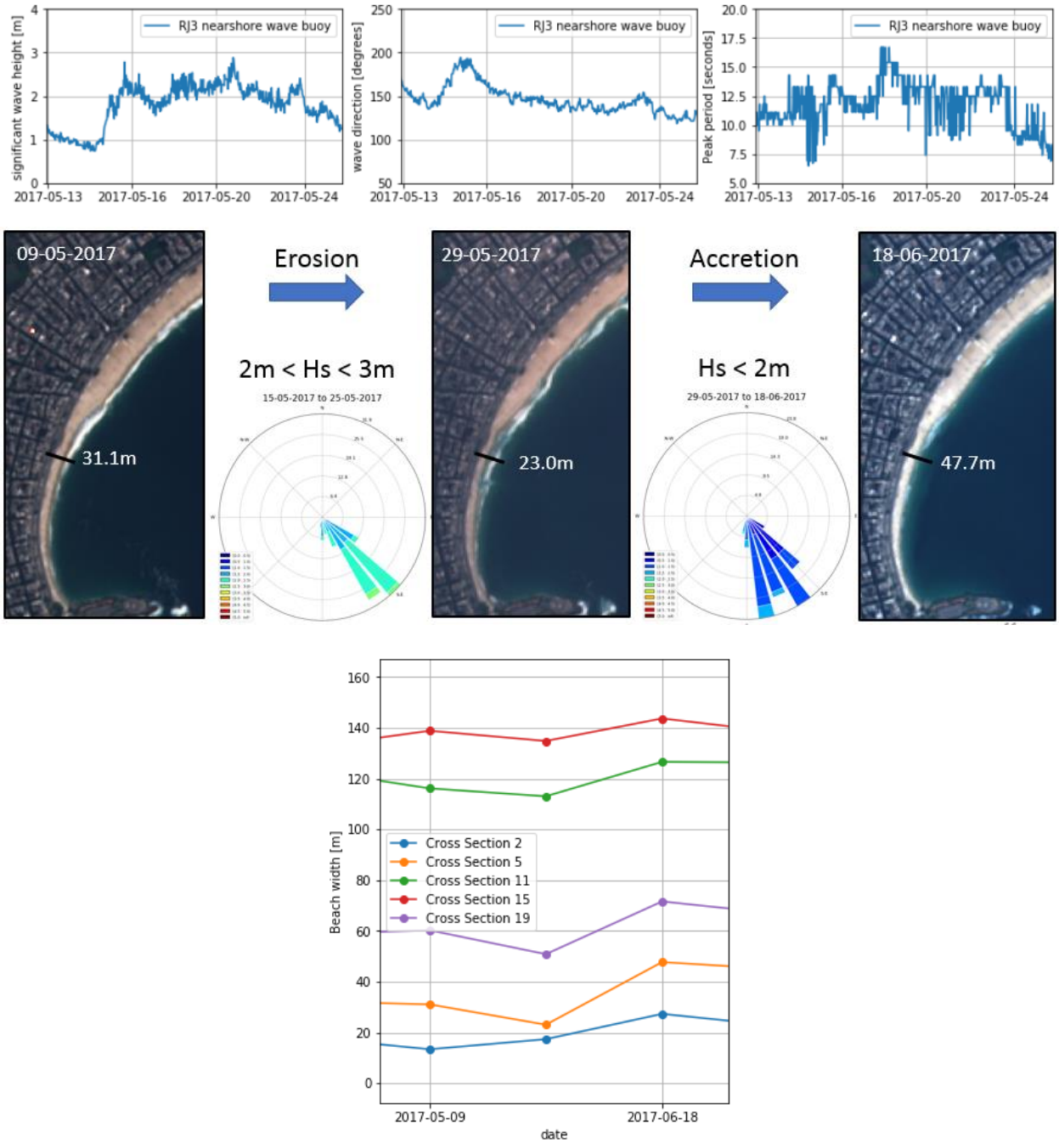

Figure 101: Characteristics of the May 2017 extreme wave event.

D.3 August 2017 (5)

The available satellite images during the time of this event is limited and the image showing the erosion is about 2 weeks after the extreme waves which could cause the image to already include part of the recovery and not show the full erosion.

- Extreme event duration: 5 days
- Maximum significant wave height: 3.6m
- Mean wave direction during erosion: SE
- Mean wave direction during accretion: SE
- Erosion Cross Section 5: 12m

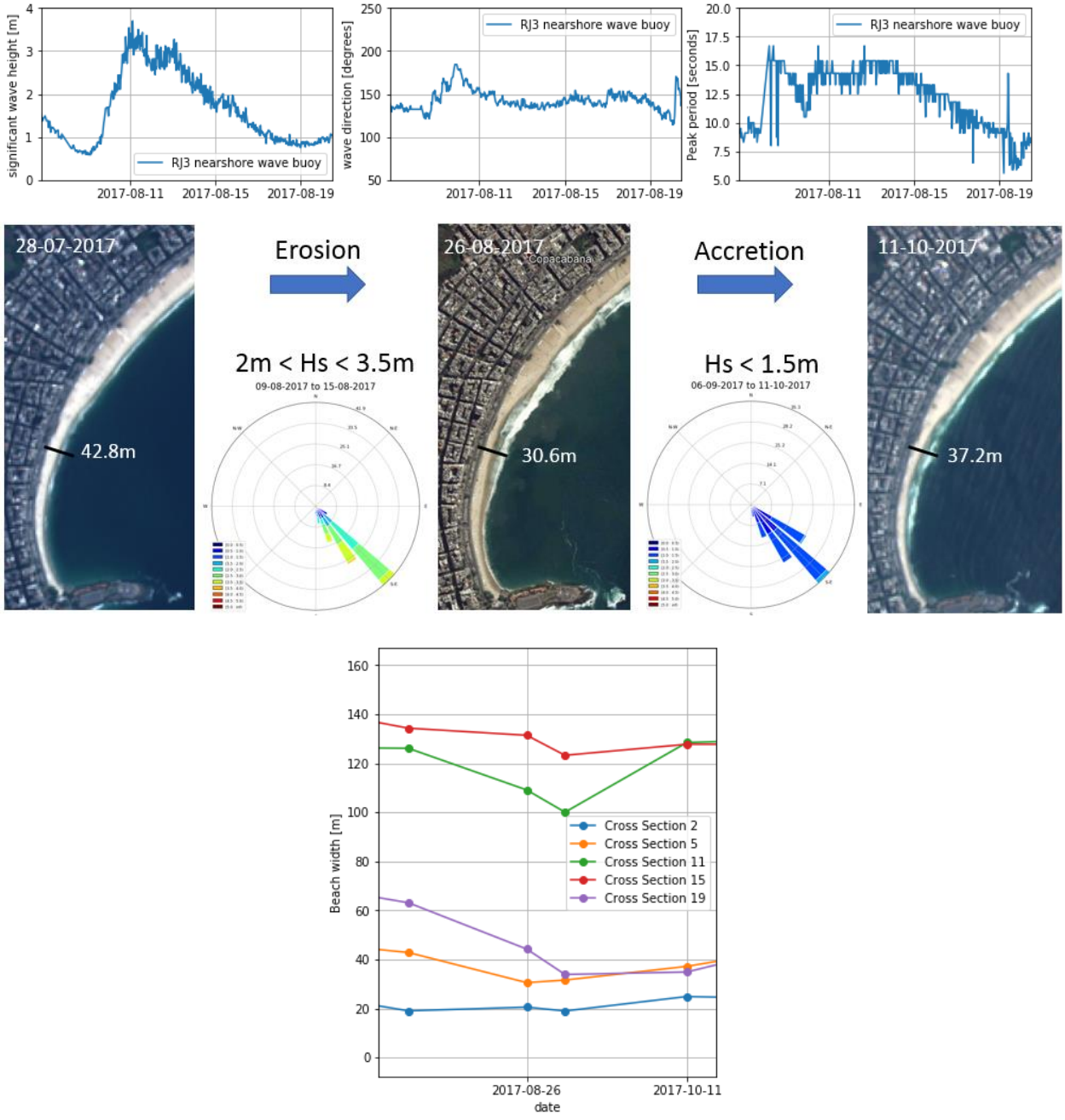

Figure 102: Characteristics of the August 2017 extreme wave event.

D.4 September 2018 (6)

- Extreme event duration: 4 days
- Maximum significant wave height: 2.4m
- Mean wave direction during erosion: SSE
- Mean wave direction during accretion: SSE
- Erosion cross section 5: 22m

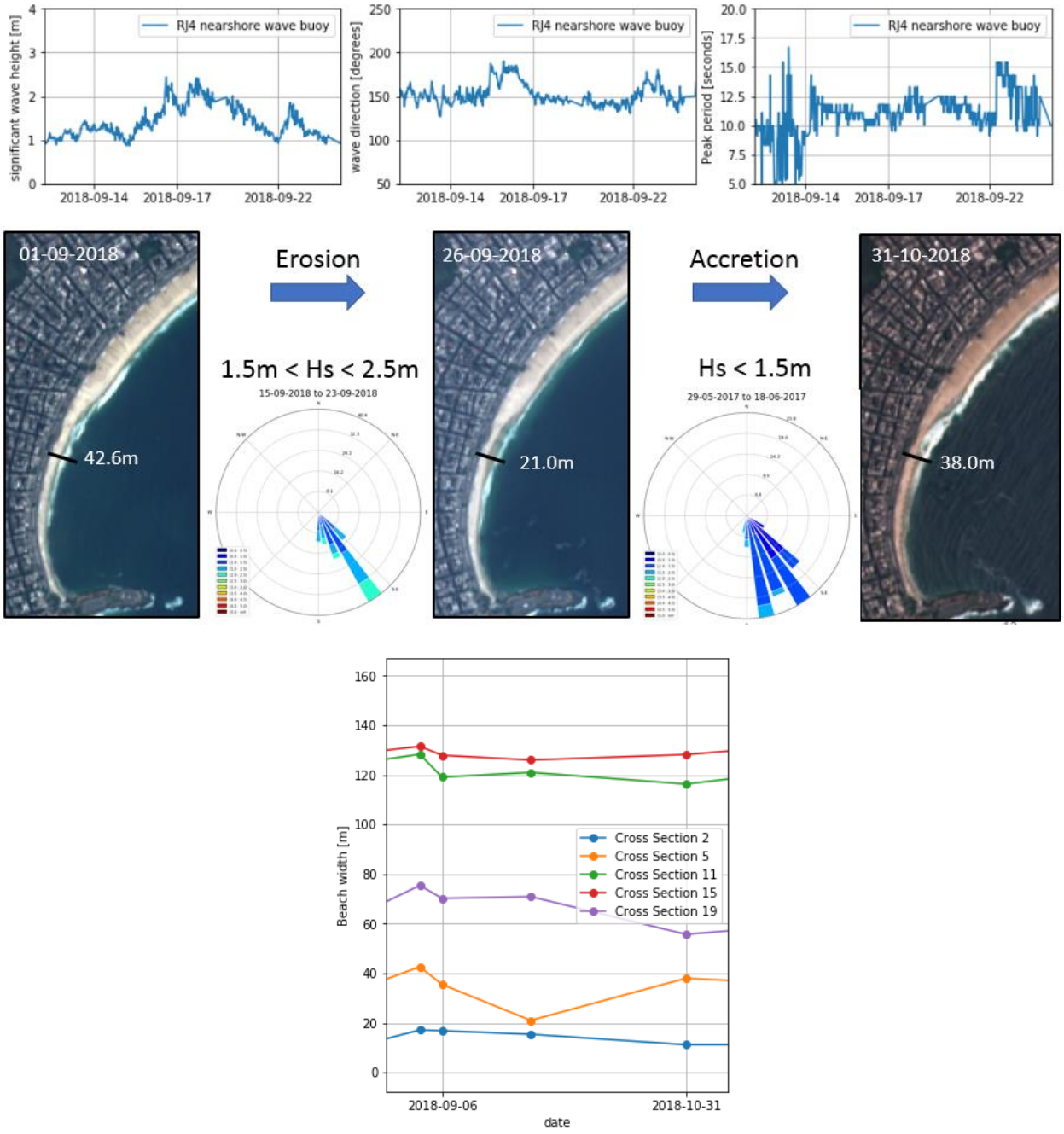

Figure 103: Characteristics of the September 2018 extreme wave event.

D.5 March 2019 (8)

- Extreme event duration: 4 days
- Maximum wave height: 2.6m
- Mean wave direction during erosion: SE
- Mean wave direction during accretion: SE
- Erosion cross section 5: 20m

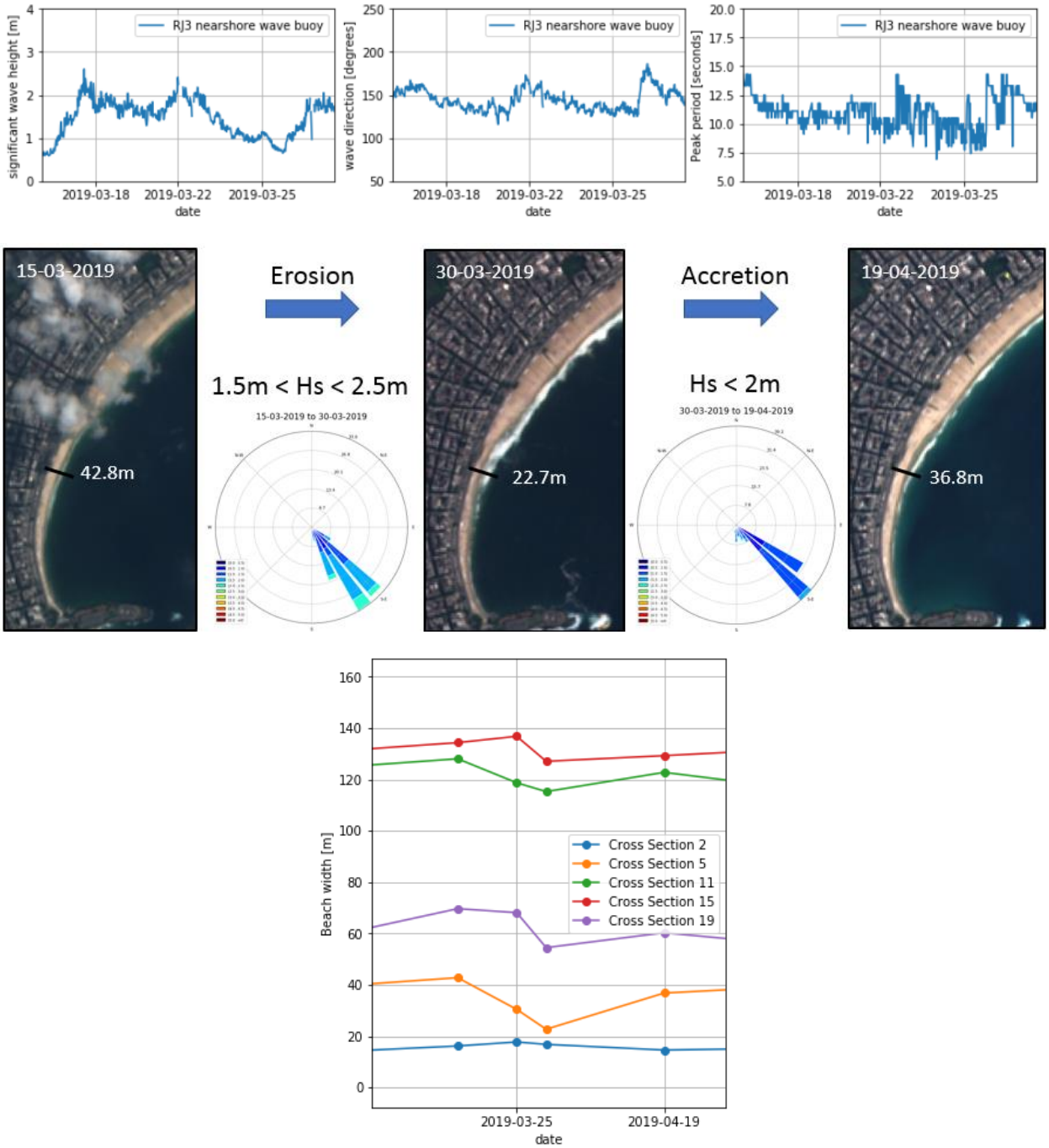

Figure 104: Characteristics of the March 2019 extreme wave event.

D.6 July 2019 (9)

- Extreme event duration: 6 days
- Maximum wave height: 3.4m
- Mean wave direction during erosion: SE
- Mean wave direction during accretion: SSE
- Erosion cross section 5: 36m

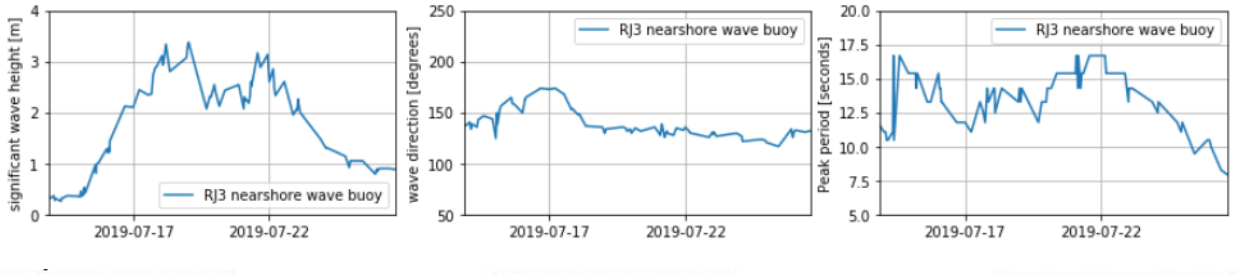

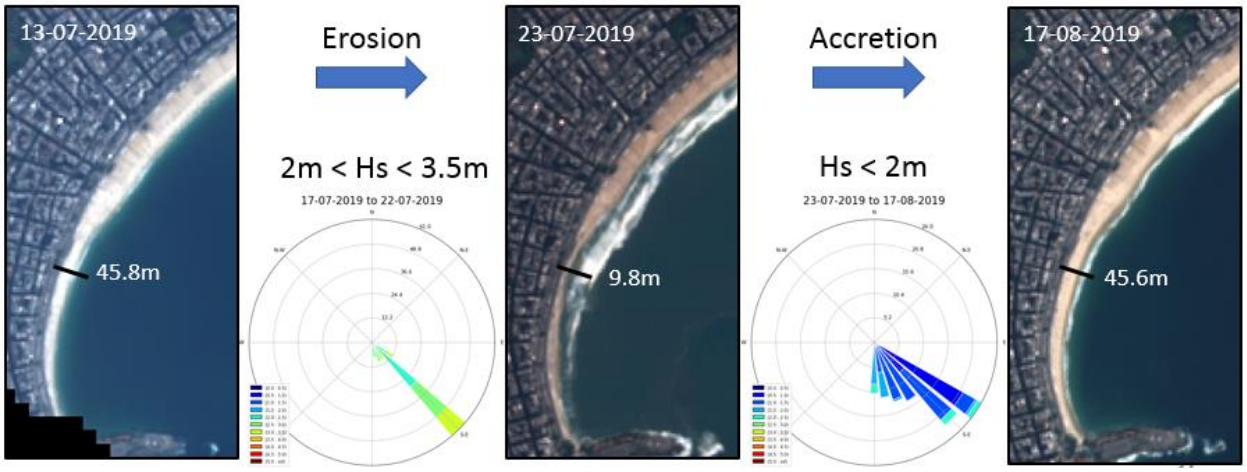

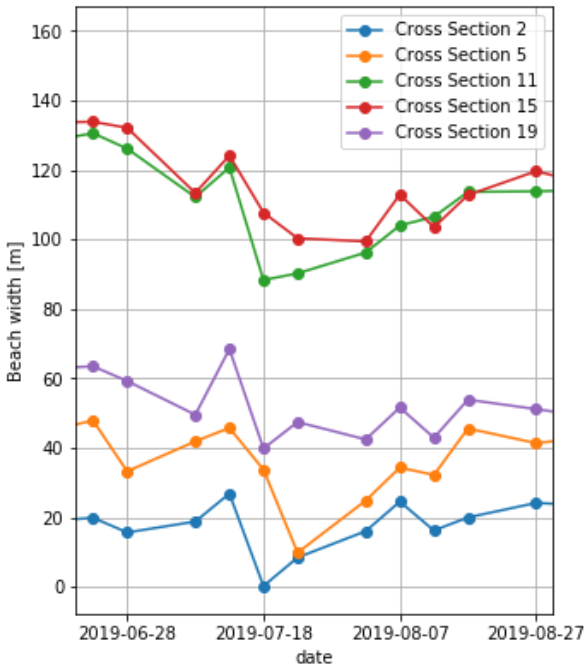

Appendix E. Additional model results

This appendix contains additional visualizations of the model results of some of the model runs carried out in chapter 5.

E.1 Recovery simulation: validation

For the validation of the recovery simulation the following model runs are made:

Table 24: Overview of the different model runs made for the validation of the recovery simulation.

	facua	Bermslope depth [m]
Run 1:	0.15	1
Run 2:	0.225	1
Run 3:	0.3	1
Run 4:	0.15	0.5
Run 5:	0.15	0.15
Run 6:	0.15	Without bermslope model

E.1.1 Model run 1

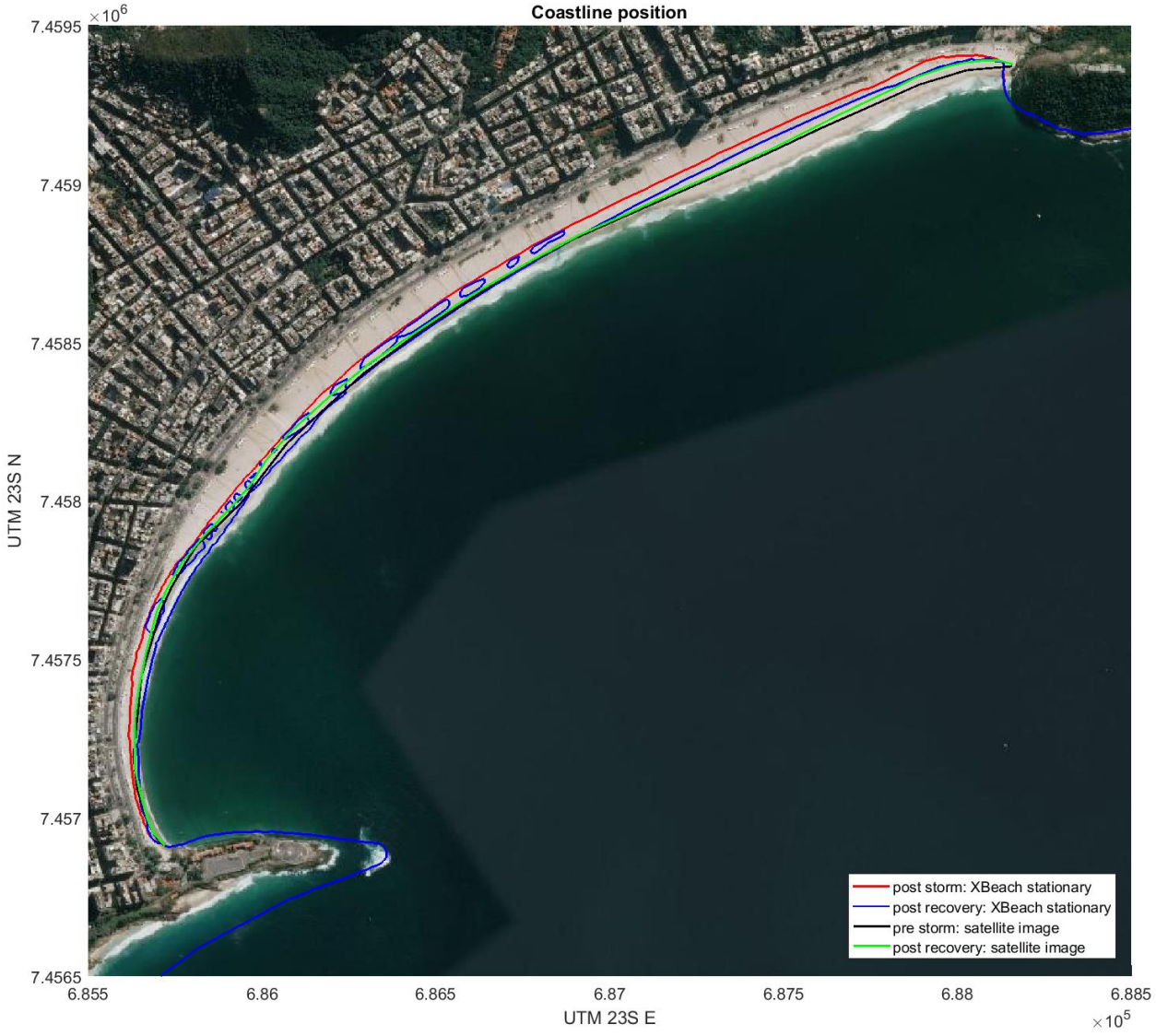

Figure 105: Coastline position for model run 1.

E.1.2 Model run 2

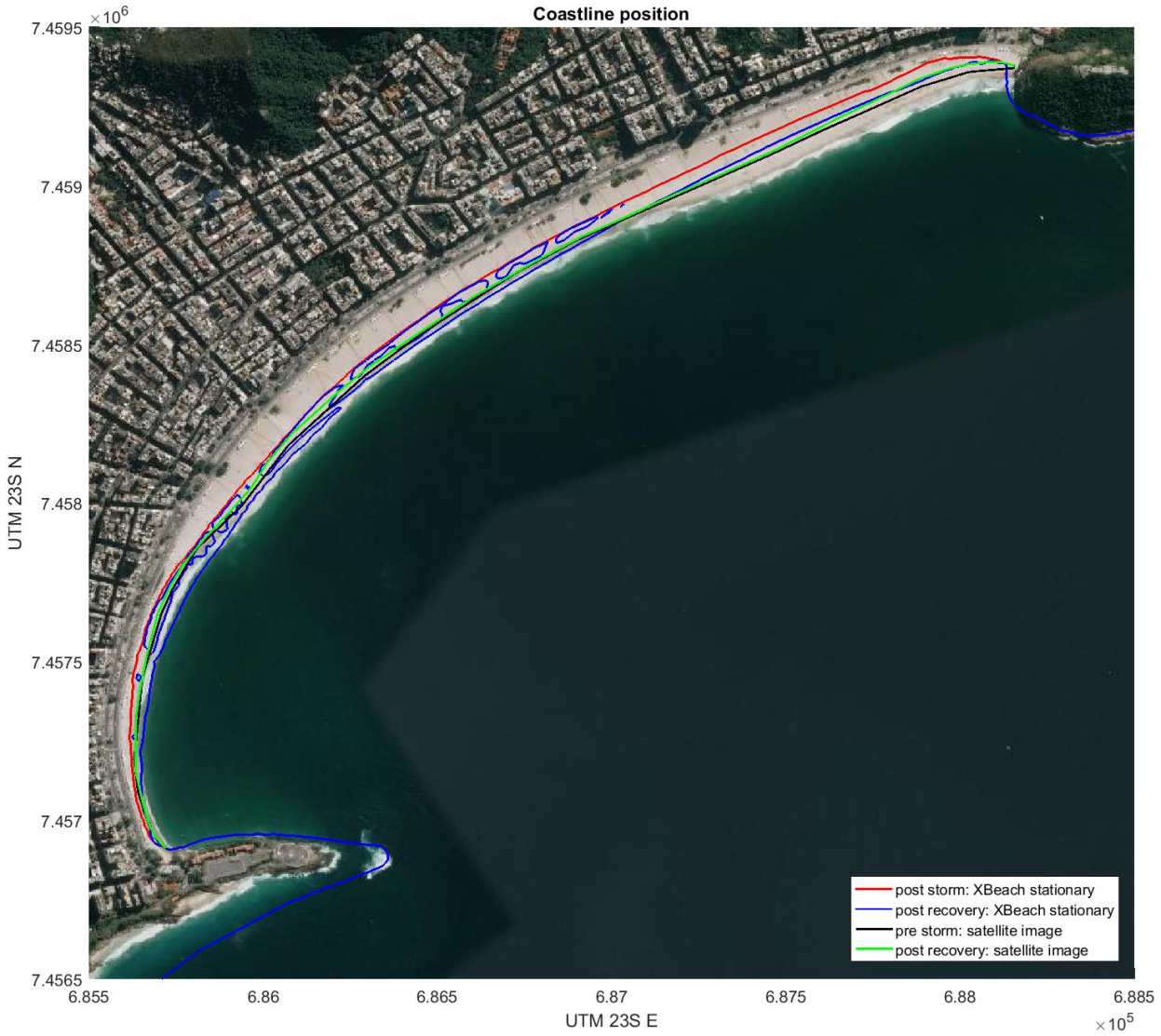

Figure 106: Coastline position for model run 2.

E.1.3 Model run 3

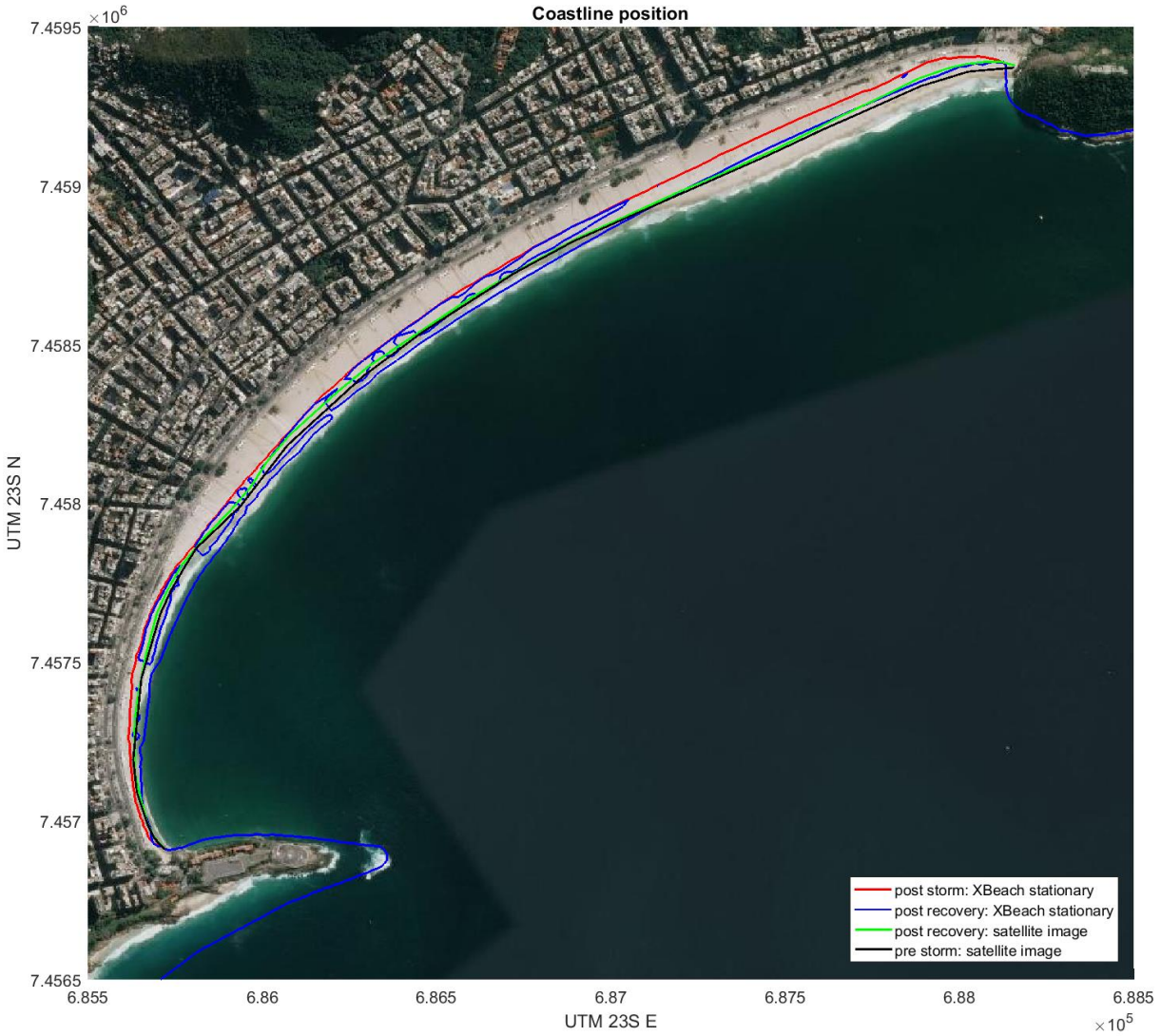

Figure 107: Coastline position for model run 3.

E.1.4 Model run 4

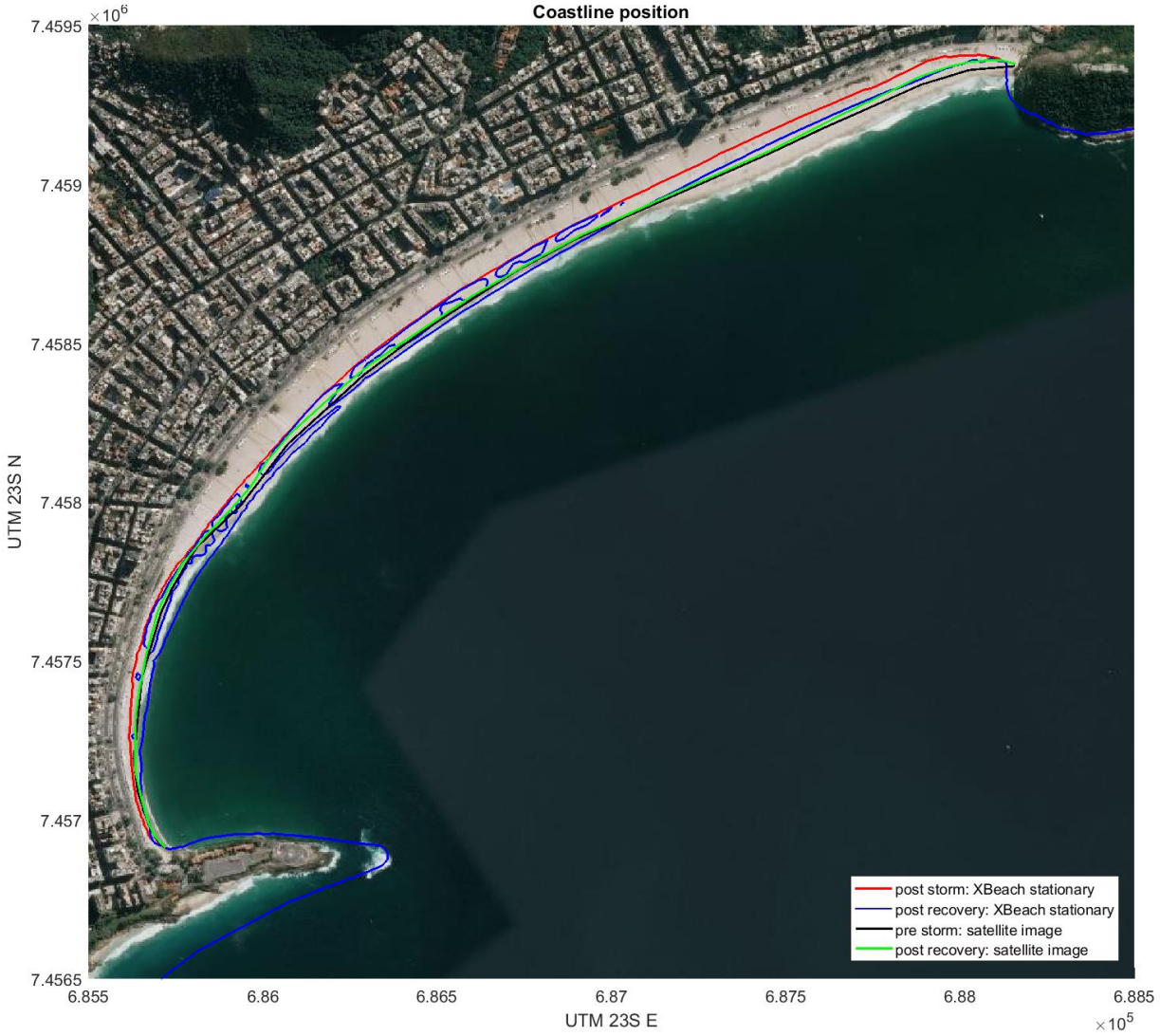

Figure 108: Coastline position for model run 4.

E.1.5 Model run 5

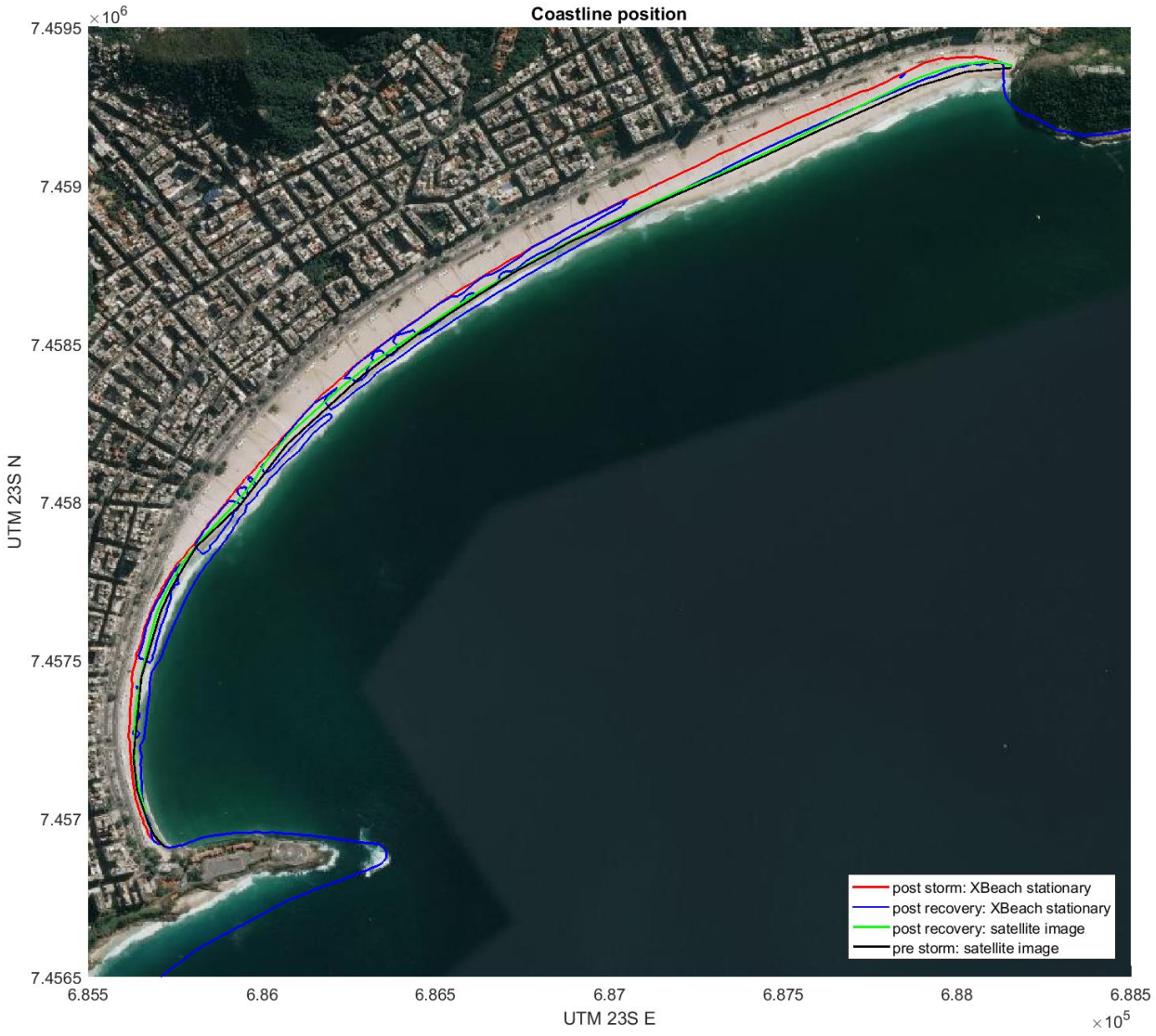

Figure 109: Coastline position for model run 5.

E.1.6 Model run 6

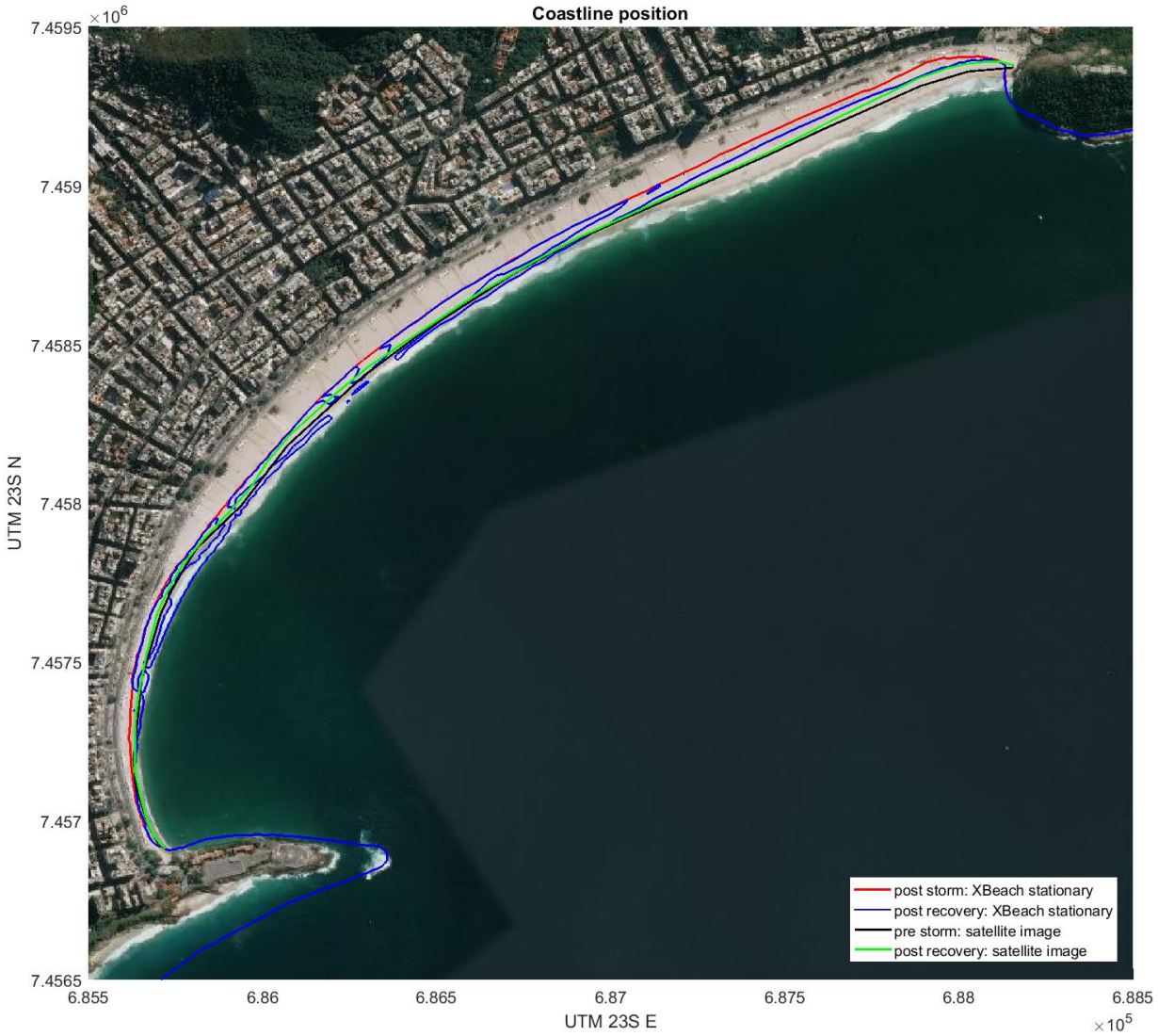

Figure 110: Coastline position for model run 6.